Justus-Liebig-Universität Gießen

Fachbereich Medizin

Campus Kerckhoff, Bad Nauheim; Abteilung für Kardiologie

Direktor: Prof. Dr. med. C. W. Hamm

Beurteilung der Relevanz von Koronarstenosen anhand anatomischer und funktioneller Informationen durch die koronare computertomografische Angiografie

Habilitationsschrift

zur Erlangung der Venia legendi

für das Fach Innere Medizin

im Fachbereich Medizin der Justus-Liebig-Universität Gießen

vorgelegt von

Dr. med. Matthias Renker

Bad Nauheim, 2021

Inhaltsverzeichnis

1 Publikationsbasis der vorliegenden kumulativen Habilitationsschrift

PUBLIKATION 1:

Renker M, Ramachandra A, Schoepf UJ, Raupach R, Apfaltrer P, Rowe GW, Vogt S, Flohr TG, Kerl MJ, Bauer RW, Fink C, Henzler T. Iterative image reconstruction techniques: Applications for cardiac CT. J Cardiovasc Comput Tomogr. 2011;5(4):225-30. DOI: https://doi.org/10.1016/j.jcct.2011.05.002

PUBLIKATION 2:

Renker M, Nance JW, Schoepf UJ, O'Brien TX, Zwerner PL, Meyer M, Kerl JM, Bauer RW, Fink C, Vogl TJ, Henzler T. Evaluation of Heavily Calcified Vessels with Coronary CT Angiography: Comparison of Iterative and Filtered Back Projection Image Reconstruction. Radiology. 2011;260(2):390-9. DOI: https://doi.org/10.1148/radiol.11103574

PUBLIKATION 3:

Wang R, Baumann S, Schoepf UJ, Meinel FG, Rier JD, Morris JZ, Moellmann H, Hamm CW, Steinberg DH, **Renker M**. Comparison of quantitative stenosis characteristics at routine coronary computed tomography angiography with invasive fractional flow reserve for assessing lesion-specific ischemia. J Cardiovasc Comput Tomogr. 2015;9(6):546-52. DOI: https://doi.org/10.1016/j.jcct.2015.08.003

PUBLIKATION 4:

Baumann S, Wang R, Schoepf UJ, Steinberg DH, Spearman JV, Bayer RR 2nd, Hamm CW, **Renker M**. Coronary CT Angiography-Derived Fractional Flow Reserve Correlated with Invasive Fractional Flow Reserve Measurements - Initial Experience with a Novel Physician-Driven Algorithm. Eur Radiol. 2015;25(4):1201-7. DOI: https://doi.org/10.1007/s00330-014-3482-5

PUBLIKATION 5:

Renker M, Schoepf UJ, Wang R, Meinel FG, Rier JD, Bayer RR 2nd, Moellmann H, Hamm CW, Steinberg DH, Baumann S. Comparison of diagnostic value of a novel noninvasive coronary computed tomography angiography method versus standard coronary angiography for assessing fractional flow reserve. Am J Cardiol. 2014;114(9):1303-8. DOI: https://doi.org/10.1016/j.amjcard.2014.07.064

PUBLIKATION 6:

Baumann S*, **Renker M***, Hetjens S, Fuller SR, Becher T, Loßnitzer D, Lehmann R, Akin I, Borggrefe M, Lang S, Wichmann JL, Schoepf UJ. Comparison of Coronary Computed Tomography Angiography-Derived vs Invasive Fractional Flow Reserve Assessment: Meta-Analysis with Subgroup Evaluation of Intermediate Stenosis. Acad Radiol. 2016;23(11):1402-11. DOI: http://dx.doi.org/10.1016/j.acra.2016.07.007

* contributed equally

PUBLIKATION 7:

Renker M, Baumann S, Hamm CW, Tesche C, Kim W, Savage RH Coenen A, Nieman K, De Geer J, Persson A, Kruk M, Kepka C, Yang DH, Schoepf UJ. Influence of Coronary Stenosis Location on Diagnostic Performance of Machine Learning-based Fractional Flow Reserve from CT Angiography. J Cardiovasc Comput Tomogr. 2021;15(6):492-498. DOI: 10.1016/j.jcct.2021.05.005.

2 Einleitung und Zielsetzung

Bei der koronaren Herzerkrankung (KHK) handelt es sich um eine prävalente Erkrankung, die auf atherosklerotischen Veränderungen der epikardialen Herzkranzgefäße beruht und die Todesursachenstatistik in Deutschland nach wie vor anführt (1). Im Frühstadium verläuft die Erkrankung oftmals oligo- bis asymptomatisch, sodass das akute Koronarsyndrom als plötzliche Insuffizienz der Koronarperfusion die Erstmanifestation darstellen kann. Eine frühzeitige Diagnostik spielt daher eine entscheidende Rolle. Hierfür steht ein breitgefächertes Instrumentarium zur Verfügung. An erster Stelle steht jedoch die anamnestische Erhebung des kardiovaskulären Risikoprofils und der genauen Symptome. Zur Basisdiagnostik gehören die Echokardiografie und das Elektrokardiogramm (EKG). Beide Untersuchungsverfahren können sowohl in Ruhe als auch unter Belastung durchgeführt werden. Die Myokardszintigrafie und die kardiale Magnetresonanztomografie sind kostenintensivere und technisch anspruchsvollere Stress-Tests.

Unter den nichtinvasiven Methoden nimmt darüber hinaus die Computertomografie (CT) eine wichtige Rolle ein. Bei der koronaren CT-Angiografie wird jodhaltiges Kontrastmittel (KM) intravenös appliziert und unter Anwendung von Röntgenstrahlung im Schichtaufnahmeverfahren in den Herzkranzgefäßen dargestellt. Dieses Untersuchungsverfahren ist für den Ausschluss einer KHK bei Patientinnen und Patienten mit niedrigem bis intermediärem Risiko etabliert (2-4). Zudem ist die prognostische Aussagekraft der koronaren CT-Angiografie erwiesen (5).

Der diagnostische Wert der koronaren CT-Angiografie bemisst sich traditionell an der invasiven Koronarangiografie, dem Goldstandard für den Nachweis einer KHK. Die invasive Koronarangiografie, bei der via arteriellem Gefäßzugang mittels Katheter selektiv KM in die Herzkranzgefäße injiziert und dann mithilfe von Röntgenstrahlung dargestellt wird, erlebte innerhalb der letzten Jahre einen Paradigmenwechsel. Neben einer rein visuellen Einschätzung der

Obstruktion eines Koronargefäßes erlaubt die Methode nun auch eine hämodynamische Beurteilung von Stenosen. Hintergrund dessen ist, dass einerseits akute Koronarsyndrome häufig nicht auf dem Boden einer hochgradigen Stenose entstehen und andererseits der Stenosierungsgrad eines Koronargefäßes allein kein geeignetes Behandlungssubstrat darstellt (6-8). Als Indikator hämodynamischer Relevanz ist inzwischen die katheterbasierte Druckdrahtmessung proximal und distal einer Koronarstenose zur Bestimmung der fraktionellen Flussreserve (FFR) anerkannt (9-12). An dieser Entwicklung muss sich somit auch die koronare CT-Angiografie messen.

Ziel dieser kumulativen Habilitationsschrift ist es, wichtige Entwicklungsschritte der koronaren CT-Angiografie anhand einer Auswahl der eigenen Publikationen darzustellen. Im Fokus steht hierbei die Transformation von einem rein visuell-anatomischen Verfahren über die Erfassung quantitativer Stenosenmarker und koronarer Kontrastgradienten bis hin zur Anwendung von Prinzipien der numerischen Strömungsmechanik sowie maschinellen Lernverfahren zur Beurteilung der funktionellen Relevanz von Koronarstenosen.

3 Technische Grundlagen

Bei der CT gewinnt die Einheit aus Röntgenröhre und gegenüberliegendem Detektor durch Rotation um die zu untersuchende Person Projektionen der abgeschwächten Röntgenstrahlen. Alle modernen CT-Systeme verwenden die Spiralaufnahmetechnik, die eine zeitlich wie räumlich entlang der Körperlängsachse (z-Achse) fortlaufende Untersuchung von Patientinnen und Patienten ermöglicht. Die Mehrschicht-Technik (Multidetektor-CT, MDCT) basiert auf paralleler Anordnung multipler Detektorreihen, wodurch heutzutage bis zu 384 (2 x 192) Schichten in der z-Achse gleichzeitig erfassbar sind. Diese und weitere Entwicklungen resultieren in einer hohen räumlichen Auflösung. Das kleinste in allen Raumrichtungen darstellbare Volumenelement (isotropes Voxel) beträgt hierbei deutlich unter 1 mm^3. Ferner kann die Rotationszeit der Röntgenröhren-Detektor-Einheit z. B. durch das Dual-Source Prinzip auf bis zu 0,25 s verkürzt werden, was zu einer hohen zeitlichen Auflösung führt.

Die Bildakquisition erfolgt bei der CT-Angiografie der Koronararterien synchronisiert mit dem EKG-Signal und erlaubt eine phasenkonsistente Darstellung z. B. in der Diastole des Herzzyklus. Es ist zwischen retrospektiver und prospektiver Aufnahmetechnik zu unterscheiden. Für Patientinnen und Patienten mit niedriger Herzfrequenz sowie rhythmischer Herzaktion ist die prospektive, EKG-getriggerte Sequenzaufnahme geeignet. Als spezielle prospektive Untersuchungsform mit noch geringerer Strahlendosis ist die EKG-getriggerte Spiraluntersuchung innerhalb eines Bruchteils einer Herzaktion mit sehr hoher Tischvorschubgeschwindigkeit zu nennen (13). Die retrospektiv EKG-gegatete Spiraluntersuchung ist mit höherer Strahlendosis verbunden, aber flexibler einsetzbar.

Mithilfe von Rekonstruktionsverfahren werden die primären Messdaten, also die eindimensionalen Projektionen der abgeschwächten Röntgenstrahlen, computergestützt in verwertbare Bilddaten umgerechnet. Algebraische Methoden wurden durch den Rekonstruktionsalgorithmus der gefilterten

Rückprojektion (*Filtered Back Projection*, FBP) abgelöst. Die FBP erfordert relativ wenig Rechenleistung und erlaubt eine schnelle Rekonstruktion. Bei dieser digitalen Bildverarbeitung werden die Projektionen zunächst durch Faltungskerne mathematisch gefiltert und dann in die Bildebene zurückprojiziert (14).

Die bei der CT angewandte Röntgenstrahlung zählt zu den ionisierenden Strahlungen und kann Materie verändern. Dies wurde 2007 in einer vielbeachteten Publikation von Brenner und Hall thematisiert (15). Mittels Risikoschätzung führten sie bis zu 2 % aller Malignome bei Menschen in den USA auf die klinische Anwendung der CT zurück (15). Strahlendosis und Bildqualität sind eng miteinander verknüpft. Nach Brooks und Di Chiro besteht prinzipiell eine inverse Korrelation zwischen Strahlendosis und Bildrauschen (16). Jedoch ist es aufgrund verschiedener Errungenschaften möglich, die Strahlendosis bei vergleichbar hoher Bildqualität zu reduzieren (17). Die Anwendung ionisierender Strahlung beim Menschen erfolgt gemäß den Vorgaben des Strahlenschutzes nach dem Prinzip ALARA (*As Low As Reasonably Achievable*). In einer prospektiven Multicenter-Studie untersuchten Stocker et al. die mit der koronaren CT-Angiografie assoziierte effektive Strahlendosis (Einheit: Sievert) (18). Diese ist ein Maß für die Strahlenexposition der untersuchten Person unter Berücksichtigung der unterschiedlichen Empfindlichkeit von Organen. Im Jahre 2017 lag die effektive Dosis im Durchschnitt bei 2,7 mSv (18). Bemerkenswert ist, dass die Entwicklungen im Bereich der koronaren CT-Angiografie von 2007 bis 2017 in einer Reduktion der Strahlenbelastung um ca. 78 % resultierten, ohne jedoch zu einer höheren Anzahl an nichtauswertbaren Untersuchungen zu führen (18).

Trotz der technischen Entwicklungen ist die koronare CT-Angiografie nicht für alle Personen gleichermaßen gut geeignet. Eingeschränkte Bildqualität kann bei Arrhythmien, Adipositas oder Bewegung der zu untersuchenden Patientinnen und Patienten auftreten.

4 Anatomische Informationen durch die koronare CT-Angiografie

4.1 Visuelle Stenosenbeurteilung und deren Limitationen

Die koronare CT-Angiografie zeichnet sich durch eine schnelle, nichtinvasive Visualisierung der Koronararterien inklusive der umgebenden Strukturen aus. Haupteinsatzgebiet der koronaren CT-Angiografie ist der Verdacht auf KHK bei stabilen Patientinnen und Patienten mit niedriger bis intermediärer Vortestwahrscheinlichkeit, also der Wahrscheinlichkeit des Vorliegens der Erkrankung vor Anwendung eines Tests. Hierfür erreicht sie bei Verwendung von 64-zeiligen MDCT-Systemen gemessen an der invasiven Koronarangiografie eine Sensitivität von 95–99 % und einen als Trennschärfe verstandenen negativ prädiktiven Wert von 97–99 % (19-21). Sie übertrifft damit alle anderen nichtinvasiven Verfahren bei geeigneten Patientenkollektiven mit niedrigem bis intermediärem Risiko. Die diagnostische Genauigkeit der koronaren CT-Angiografie ist daneben durch eine Spezifität von 64–90 % und einen positiv prädiktiven Wert, d. h. Testaussagewert, von 64–91 % gekennzeichnet (19, 20, 22). Die weite Spanne der eher mäßigen Spezifität kann auf eine unterschiedlich gute Eignung der untersuchten Patientinnen und Patienten für eine koronare CT-Angiografie einerseits und unterschiedliche Erkrankungsprävalenz andererseits zurückgeführt werden. Während die in der hohen Sensitivität und dem positiven prädiktiven Wert begründete Stärke der koronaren CT-Angiografie darin liegt, eine KHK auszuschließen, nimmt die diagnostische Genauigkeit in Patientenkollektiven mit höherer Erkrankungsprävalenz typischerweise ab. Eine Publikation von Meijboom et al. dient als Beispiel einer Studie, die diesen Sachverhalt demonstrierte (23). So gibt es einige bekannte Szenarien, die sich negativ auf eine visuelle Einschätzung des Stenosierungsgrades anhand der koronaren CT-Angiografie auswirken können. Als Beispiele dienen kalzifizierte Plaques und positives Remodeling, also eine atherosklerotische Veränderung mit kompensatorischer Gefäßerweiterung. In diesen Fällen besteht die Gefahr einer Überschätzung des Stenosierungsgrades. Insbesondere für einen hohen

Verkalkungsgrad der Koronararterien wurde die Gefahr falsch-positiver Interpretation der Koronarläsionen nachgewiesen (Abb. 1) (24, 25). Daher definierten viele Studien einen oberen Grenzwert der koronaren Kalklast als Kriterium für die nachfolgende Durchführung einer koronaren CT-Angiografie. Diese koronare Kalklast wird im nativen CT ohne KM nach der Agatston-Methode auf der Skala der Abschwächung von Röntgenstrahlung durch unterschiedliche Gewebe in Hounsfield-Einheiten (HE) angegeben (26). Zudem wurde gezeigt, dass das Vorhandensein von Stents, also implantiertem Fremdmaterial zur Offenhaltung der Koronararterien, Artefakte in der Bildgebung bedingt und die diagnostische Genauigkeit der CT-Angiografie negativ beeinflusst (27).

Abb. 1: Überstrahlungsartefakte durch überwiegend kalzifizierte Plaques (Quelle: eigene Darstellung) Die koronare CT-Angiografie (links) zeigt überwiegend kalzifizierte Plaques mit Überstrahlungsartefakten im Ramus interventricularis anterior. Hierdurch besteht eine Tendenz zur Überschätzung des Stenosierungsgrades, wie der Vergleich zur invasiven Koronarangiografie (rechts) zeigt.

4.1.1 Einfluss iterativer Rekonstruktion auf Bildqualität und Volumen von Koronarkalk sowie Stents (PUBLIKATION 1)

Zur Verarbeitung von CT-Rohdatensätzen wurde lange das Rekonstruktionsverfahren der FBP verwendet. Allerdings ist die bei diesem Verfahren höhere räumliche Auflösung direkt mit vermehrtem Bildrauschen assoziiert (28). Kompensatorisch ist eine höhere Röhrenspannung erforderlich, was sich in höherer Strahlenbelastung auswirkt. Zudem werden Überstrahlungseffekte durch Koronarkalk und Strahlhärtungsartefakte durch Stents unzureichend supprimiert. Diese können eine exakte Koronarbeurteilung empfindlich einschränken und zu einer Überschätzungstendenz von Koronarstenosen und Stents führen (24). Iterative Rekonstruktionsverfahren wurden bereits vor mehreren Jahrzenten als Alternative vorgestellt, deren Anwendung im klinischen Alltag wurde jedoch erst durch technische Verbesserungen im Bereich der Rechnerleistung ermöglicht (29). Nachdem Min et al. für die iterative Rekonstruktion eine bessere Beurteilung des Innenraumes von Stents (i. e. Stentlumen) ex vivo aufgezeigt hatten (30), verfolgte die eigene hier vorgestellte Publikation das Ziel, mögliche Vorteile der iterativen Bildrekonstruktionstechnik in vivo zu untersuchen. Hierfür wurde ein iterativer Rekonstruktionsalgorithmus (*Iterative Reconstruction in Image Space*, IRIS; Siemens, Forchheim, Deutschland) additiv zum vormaligen Standardrekonstruktionsverfahren FBP in 24 Patientinnen und Patienten angewendet. Darüber hinaus wurden in einer Matched-Pair-Analyse weitere 24 Personen eingeschlossen. Die eine Hälfte dieses Patientenkollektivs wurde mit regulärer Strahlenbelastung und FBP untersucht, während die andere Hälfte mit iterativer Rekonstruktion und reduzierter Strahlenbelastung untersucht wurde.

Es konnte gezeigt werden, dass das Bildrauschen durch Anwendung des iterativen Rekonstruktionsverfahrens im Vergleich zur FBP statistisch signifikant ($p < 0,02$) geringer war (Abb. 2). Diese Beobachtung traf auch für unterschiedliche Faltungskerne zu. In der subjektiven Bildqualitätsanalyse, die auf der Klassifizierung der CT-Datensätze durch zwei erfahrene Untersucher

anhand einer 5-Punkt-Skala von 1 (= ungenügende diagnostische Aussagekraft) bis 5 (= exzellent ohne diagnostische Einschränkung) hinsichtlich Bildrauschen, Strahlhärtungsartefakten und Überstrahlungseffekten basierte, ergab sich eine ebenfalls signifikante Verbesserung zugunsten der Anwendung von iterativer Rekonstruktion. Dieses Ergebnis war wiederum für verschiedene Faltungskerne konstant. Das semiautomatisch gemessene Volumen des vorhandenen Stentmaterials und Koronarkalks war bei Anwendung des iterativen Verfahrens signifikant ($p < 0,05$) geringer (Abb. 3). In der Matched-Pair-Analyse fand sich bei gleichem Bildrauschen in den beiden Gruppen aufgrund der geringeren Strahlenbelastung in der mit iterativer Rekonstruktion untersuchten Patientenhälfte ein Einsparpotential bei der effektiven Strahlendosis von mehr als 60 %.

Schlussfolgernd ergaben sich durch PUBLIKATION 1 Arbeit Hinweise auf Vorteile für das Verfahren der iterativen Rekonstruktion im Vergleich zur traditionellen Rohdatenrekonstruktion mittels FBP: quantitativ geringeres Bildrauschen, subjektiv bessere Bildqualität, geringeres Volumen von koronaren Stents und Kalk sowie Einsparpotential hinsichtlich der Strahlendosis. Für eine Implementierung der iterativen Rekonstruktion in die klinische Routine war noch weitere Evidenz erforderlich. Aus diesem Grund widmete sich PUBLIKATION 2 mit prospektivem Studiendesign dem Einfluss der Rekonstruktionsweise auf die diagnostische Genauigkeit der koronaren CT-Angiografie.

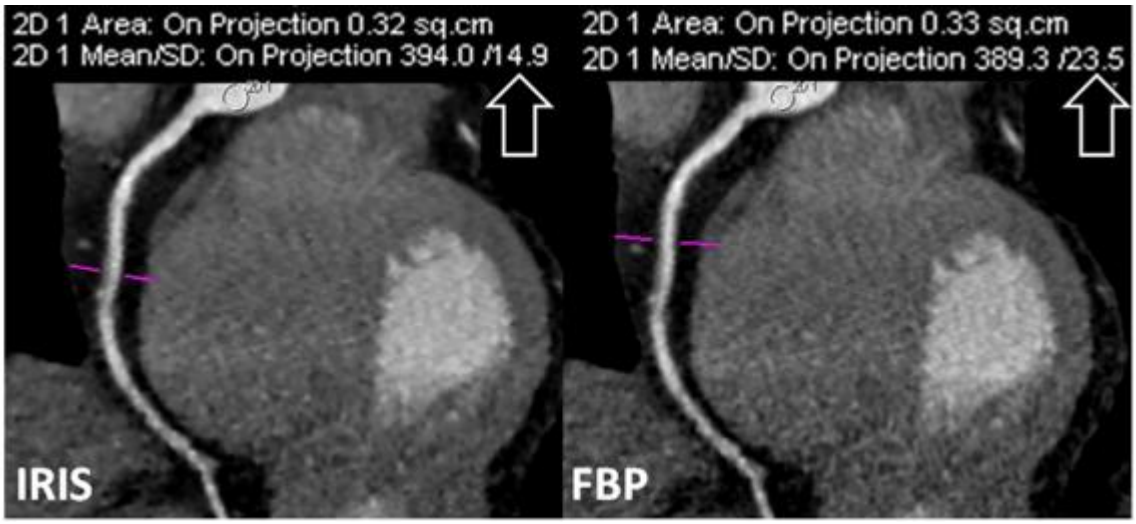

Abb. 2: Bildrauschen bei iterativer Rekonstruktion und FBP (Quelle: PUBLIKATION 1, mit Genehmigung)

Koronare CT-Angiografie einer adipösen Patientin (Körpermaßindex 37 kg/m^2), welche mit dem iterativen Verfahren (links) und dem herkömmlichen Verfahren FBP (rechts) rekonstruiert wurde. Anhand der Standardabweichung der Abschwächung im ausgewählten Messbereich in der Aorta lässt sich das deutlich geringere Bildrauschen bei iterativer Rekonstruktion erkennen.

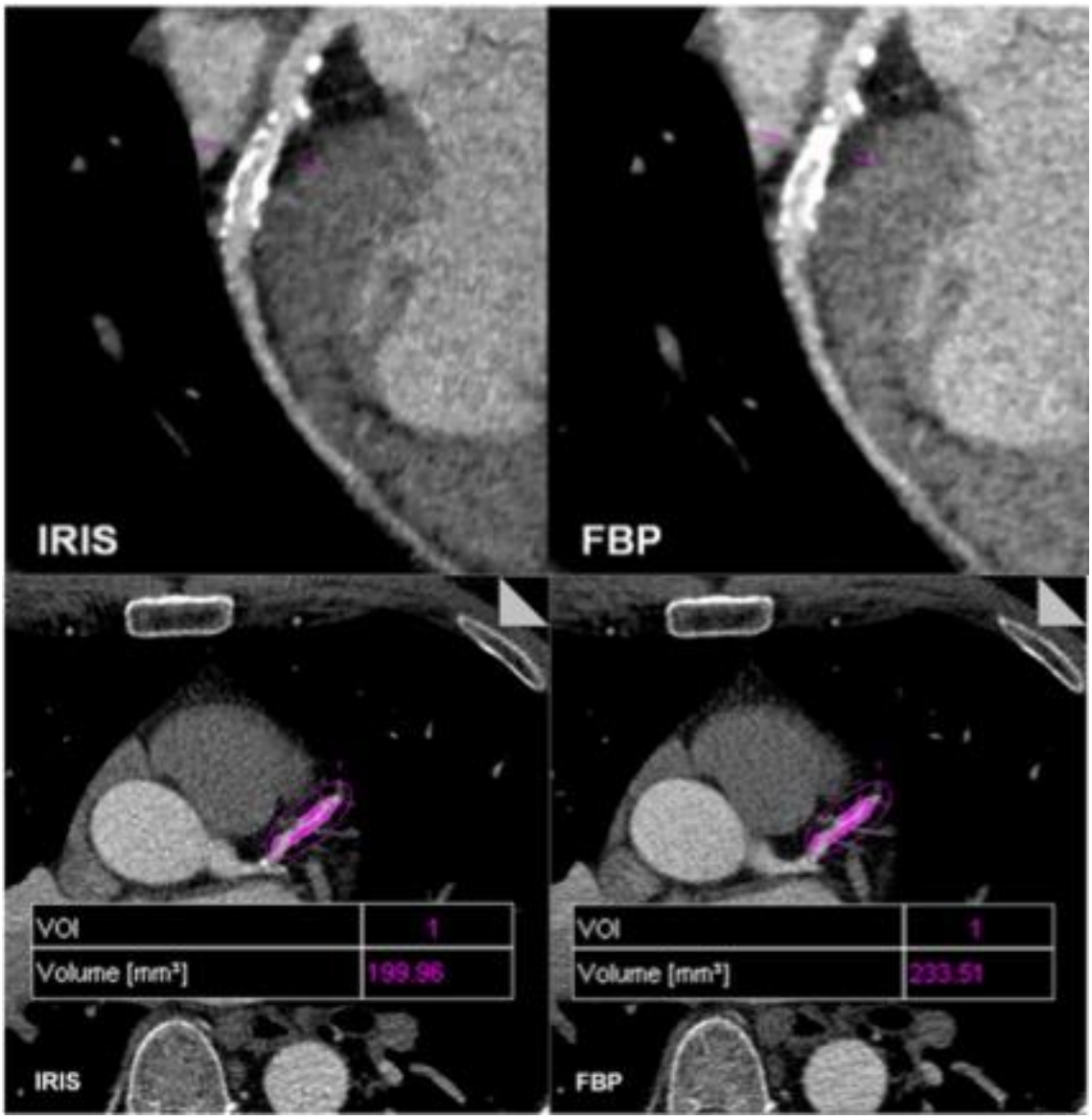

Abb. 3: Beurteilbarkeit des Koronarlumens sowie Kalkvolumen bei iterativer Rekonstruktion und FBP (Quelle: PUBLIKATION 1, mit Genehmigung)

Koronare CT-Angiografie eines 63-jährigen männlichen Patienten mit schwer kalzifizierten Plaques im Ramus interventricularis anterior. Überstrahlungsartefakte durch Kalk schränken die Beurteilbarkeit in der FBP-Rekonstruktion (rechts) stark ein und suggerieren eine relevante Stenosierung. Mittels iterativer Rekonstruktion „IRIS“ (links) ist die Beurteilbarkeit des Koronarlumens besser gegeben. Auch das gemessene Volumen des Kalks ist geringer in der Rekonstruktion mit IRIS im Vergleich zu FBP.

4.1.2 Diagnostische Genauigkeit der koronaren CT-Angiografie mit iterativer Rekonstruktion (PUBLIKATION 2)

Iterative Rekonstruktionsverfahren hatten sich als vorteilhaft für CT-Untersuchungen verschiedenster Organe erwiesen (31-35). Da fortgeschrittene Gefäßverkalkungen eine der wichtigsten Limitationen der koronaren CT-Angiografie darstellen, schloss sich aufbauend auf PUBLIKATION 1 die Evaluation der diagnostischen Genauigkeit der iterativen Rekonstruktion an (36). Eine schematische Darstellung des verwendeten Rekonstruktionsverfahrens findet sich in Abb. 4. In dieser zweiten Arbeit wurden die CT-Datensätze von 55 prospektiv eingeschlossenen Personen (35 männlich, 20 weiblich; mittleres Alter 58 ± 12 Jahre) mit schwerer Koronarverkalkung (Agatston-Score > 400) herangezogen (Abb. 5). Von allen Rohdatensätzen wurde sowohl eine Rekonstruktion mit FBP, als auch eine mit dem iterativen Algorithmus IRIS erstellt.

Die Hauptaussage dieser zweiten Studie liegt in der besseren diagnostischen Genauigkeit von iterativer Rekonstruktion gegenüber FBP für den Nachweis von Koronarstenosen mit > 50 % Verminderung des Lumens im Vergleich zur invasiven Koronarangiografie als Referenz (Abb. 6 und Abb. 7). Auf der Ebene der Koronarsegmente wie auch auf Patientenebene ergab sich eine signifikante Verbesserung insbesondere der Spezifität und des positiv prädiktiven Wertes. Insgesamt wurden 825 Segmente mittels invasiver Koronarangiografie und koronarer CT-Angiografie evaluiert, wovon sich invasiv bei 31 Patientinnen und Patienten mit insgesamt 104 Läsionen relevante Stenosen fanden. Daneben zeigte sich auch in dieser Studie mit dem iterativen Verfahren ein signifikant geringeres Bildrauschen, ein signifikant geringeres Kalkvolumen in semiautomatischer Analyse sowie eine von zwei Spezialisten der kardialen Bildgebung signifikant besser beurteilte subjektive Bildqualität.

Schlussfolgernd ließ sich die in PUBLIKATION 1 bereits angedeutete bessere Bildqualität, das geringere Bildrauschen und das geringere Volumen

kalzifizierter Koronarläsionen durch iterative Rekonstruktion gegenüber FBP in dieser prospektiven Studie bestätigen und in eine signifikante Verbesserung der diagnostischen Genauigkeit übersetzen. Dieser Auswertungsvorteil für die visuelle Beurteilung der koronaren CT-Angiografie ergibt sich vornehmlich durch eine signifikante Steigerung von Spezifität und positiv prädiktivem Wert.

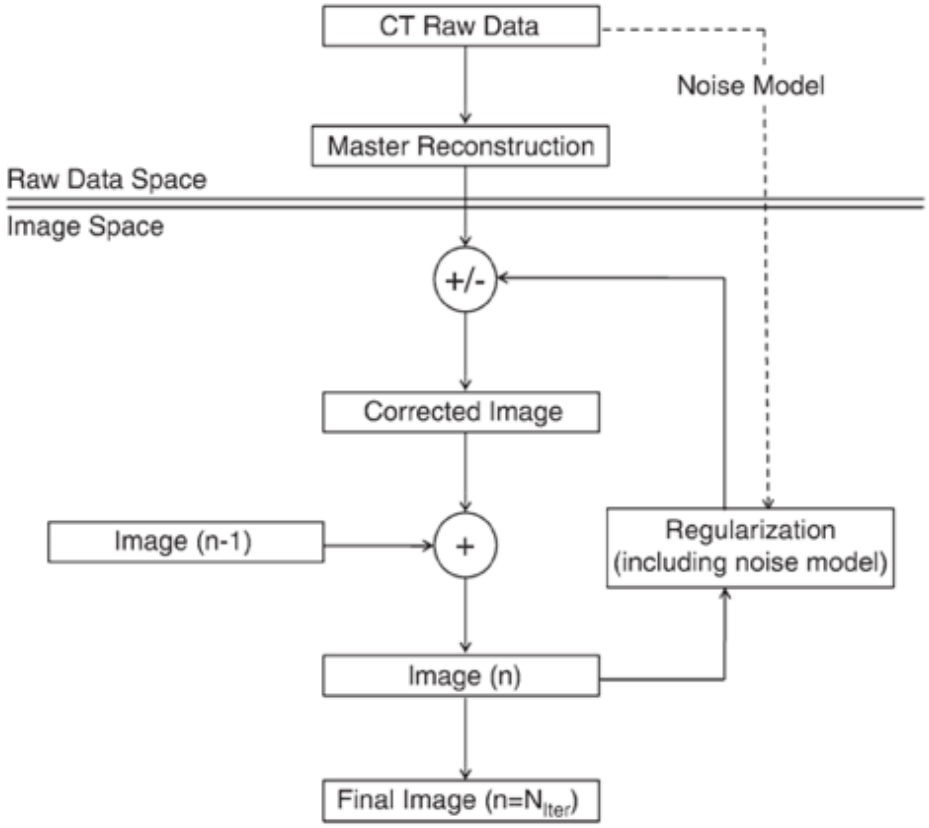

Abb. 4: Schematische Darstellung des verwendeten iterativen Rekonstruktionsverfahrens (Quelle: PUBLIKATION 2, mit Genehmigung)

Eine einzelne FBP-Rekonstruktion findet initial im Rohdatenspeicher statt, um die Master-Rekonstruktion zu erstellen. Alle weiteren Schritte folgen im Bildspeicher und umfassen eine Regulierungsschleife anhand der Vorinformation mit dem Ziel, Artefakte und Bildrauschen zu reduzieren.

+: Modellierung des Bildrauschens und Validierung der Korrekturen

−: Subtraktion des erfassten Bildrauschens

n: Bildnummer innerhalb der Iterationsschleife

n -1: Bild der vorherigen Iterationsschleife

N_{Iter}: Anzahl an Iterationen

Parameter	Datum
Age (y)	58.2 ± 12.0
Male-to-female ratio	35:20
Height (cm)	170.4 ± 10.3
Weight (kg)	92.2 ± 20.7
Body mass index (kg/m^2)	31.6 ± 5.8
Heart rate (beats per minute)*	63.1 ± 8.0 (53–72)
Agatston score*	710 ± 289 (466–2934)
No. of patients at each tube potential	
80 kVp	1
100 kVp	10
120 kVp	44
Tube current–time product (mAs)	331.4 ± 22.9
CT dose index volume (mGy)	35.0 ± 21.2
Dose-length product (mGy · cm)	609.1 ± 394.3
Scan length (cm)	12.9 ± 1.8
Effective dose (mSv)	
Retrospective ECG gated (n = 35)	10.5 ± 4.2
Prospective ECG triggered (n = 11)	6.6 ± 3.1
High pitch spiral (n = 9)	2.3 ± 1.4

Abb. 5: Demografie des Patientenkollektivs sowie Parameter des CT-Protokolls (Quelle: PUBLIKATION 2, mit Genehmigung*)*

Sofern nicht anders gekennzeichnet, handelt es sich um Mittelwerte ± Standardabweichung.

** In Klammern ist der Wertebereich angegeben.*

Parameter	Per Segment			Per Patient		
	FBP	Iterative Reconstruction	*P* Value	FBP	Iterative Reconstruction	*P* Value
Accuracy (%)*	91.8 (71.7, 91.1)	95.9 (78.2, 94.9)	.0001	83.6 (89.7, 93.5)	89.1 (94.3, 97.0)	NS
Sensitivity (%)*	95.2 (83.8, 99.4)	96.2 (83.8, 99.4)	NS	96.7 (89.2, 97.9)	96.7 (90.5, 98.5)	NS
Specificity (%)	91.2 (46.7, 82.0)	95.8 (59.5, 90.8)	.0001	66.7 (89.0, 93.1)	79.2 (94.1, 97.1)	.0189
Negative predictive value (%)*	99.2 (69.2, 99.7)	99.4 (73.1, 99.7)	NS	94.1 (98.1, 99.7)	95.0 (98.4, 99.8)	NS
PPV (%)*	61.1 (62.2, 89.9)	76.9 (69.0, 94.6)	.0001	78.9 (53.1, 68.6)	85.7 (68.6, 83.7)	.0403
No. of true-positive findings	99	100	NS	30	30	NS
No. of false-positive findings	63	30	.0001	8	5	NS
No. of true-negative findings	658	691	.0001	16	19	NS
No. of false-negative findings	5	4	NS	1	1	NS

Abb. 6: Diagnostische Genauigkeit von FBP und iterativer Rekonstruktion für den Nachweis von Koronarstenosen > 50 % im Vergleich zur invasiven Koronarangiografie, die als Referenz diente (Quelle: PUBLIKATION 2, mit Genehmigung)

NS: Nicht signifikant

PPV: Positiv prädiktiver Wert

** Daten in Klammern entsprechen dem 95 % Konfidenzintervall.*

Abb. 7: Beurteilbarkeit des Koronarlumens bei iterativer Rekonstruktion und FBP im Vergleich zur Koronarangiografie (Quelle: PUBLIKATION 2, mit Genehmigung)

Koronare CT-Angiografie eines 55-jährigen männlichen Patienten mit Angina pectoris. Es zeigen sich schwere Kalzifizierungen des medialen Ramus interventricularis anterior. Überstrahlungsartefakte durch die kalzifizierten Anteile erschweren die Beurteilbarkeit des Koronarlumens mit FBP und ergaben den Verdacht auf eine relevante Stenose (a). Anhand der iterativen Rekonstruktion sind die Artefakte reduziert und die Plaque konnte als exzentrisch mit nur leichtgradiger Stenosierung klassifiziert werden, was sich in der nachfolgenden invasiven Koronarangiografie als korrekt herausstellte.

4.2 Morphologische Plaque-Kriterien und transkoronarer Kontrast

In der koronaren CT-Angiografie unterliegt nicht nur die visuelle Stenosengraduierung Limitationen. Im Vergleich zu Verfahren zur Bestimmung des Blutflusses im Herzmuskelgewebe, sprich Myokardperfusions-Bildgebung, zeigte sich auch die Vorhersage myokardialer Ischämie wenig verlässlich (37). So lag der positiv prädiktive Wert der koronaren CT-Angiografie für myokardiale Ischämie bei nur 24–31 % (38-41). Als Referenz dienten hierbei z. B. die Myokardszintigrafie und die Positronen-Emissions-Tomografie. Zwecks verbesserter Erfassung myokardialer Ischämie wurden von verschiedenen Arbeitsgruppen zunächst morphologische Plaque-Kriterien sowie quantitative Stenosemarker und später transkoronare KM-Messungen untersucht. Diese Entwicklung wird im Folgenden anhand ausgewählter Publikationen zusammengefasst.

Lin et al. untersuchten die Zusammensetzung, das Ausmaß, die Lokalisation und das Verteilungsmuster von Koronarplaques hinsichtlich deren Assoziation mit Perfusionsdefiziten in der Myokardszintigrafie (42). Nakazato et al. beschäftigten sich unter anderem mit dem prozentualen aggregierten Plaquevolumen (% APV), gemessen als Gesamtvolumen einer Koronarplaque dividiert durch die Summe des Gefäßvolumens vom Ostium bis zum distalen Gefäßabschnitt (43). Li et al. stellten einen von der Hagen-Poiseuille´schen Gleichung abgeleiteten morphologischen Stenosen-Index (Läsionslänge/minimaler Lumendurchmesser^4; LL/MLD^4) vor (44). Daneben untersuchten Voros et al. neben weiteren Parametern den prozentualen Stenosendurchmesser, die prozentuale Stenosenfläche, den minimalen Lumendurchmesser (MLD) und die minimale Lumenfläche (MLA) (45). Dass eine Assoziation zwischen Plaque-Charakteristika in der koronaren CT-Angiografie mit zukünftiger Instabilität bzw. Ruptur besteht, konnten Motoyama et al. in einer prospektiven Studie an mehr als 1000 Patientinnen und Patienten sowohl für positives Remodeling, als auch für niedrige CT-Zahlen der Plaques (< 30 HE) zeigen (46). In einer darauf aufbauenden Arbeit lieferten Park et al. Hinweise

dafür, dass diese und einzelne weitere Plaque-Charakteristika auch mit myokardialer Ischämie in der invasiven FFR korrelieren (47).

Basierend auf dem Konzept, dass die KM-Anreicherung in einer Koronararterie mit dem intrakoronaren Blutfluss korreliert, konnte eine linear abnehmende KM-Anreicherung im Koronargefäß nachgewiesen werden (48). Bei Vorliegen einer Stenose zeigte sich distal hiervon eine stärkere lineare Abnahme der Kontrastierung je hochgradiger die Stenose war (48). Die Ableitung der sogenannten transluminalen Abschwächungsgradienten (TAG) fußte letztlich auf einer Weiterentwicklung der MDCT-Technik, da mit bis zu 320 Detektor-Reihen das gesamte Herzvolumen innerhalb eines Herzschlages erfasst werden kann. Mit dieser Technologie erlangten Choi et al. vielversprechende Ergebnisse zur Beurteilbarkeit hämodynamischer Relevanz von Koronarstenosen mittels TAG (49). Auch für eine schrittweise Erfassung des Herzvolumens über mehrere Herzschläge hinweg, wurde eine Technik entwickelt, um transkoronare KM-Gradienten bestimmen zu können: Chow et al. stellten eine Korrektur für die zeitlich versetzte Darstellung des KM im Koronarverlauf vor (*Coronary Contrast Opacification*, CCO) (50). Hierbei wird eine Normalisierung der KM-Abschwächung entlang des Koronargefäßes jeweils anhand der aortalen Kontrastierung im selben Transversalschnitt vorgenommen (50).

4.2.1 Prädiktion myokardialer Ischämie durch quantitative Stenosenmarker und Kontrastmittelgradienten (PUBLIKATION 3)

Als Grundlage für diese eigene Arbeit dienten die oben aufgeführten, meist separat und mit teils divergenten Ergebnissen vorgestellten morphologischen Plaque-Kriterien und quantitativen Stenosenmarker sowie koronaren KM-Gradientenmessungen. Ziel war es, hiervon eine sinnvolle Auswahl zu treffen und in einem Patientenkollektiv umfassend hinsichtlich Trennschärfe zwischen Läsionen mit und ohne hämodynamische Relevanz zu vergleichen. Aus den Jahren 2008 bis 2014 wurden 49 Patientinnen und Patienten mit insgesamt 56 Koronarstenosen retrospektiv in die Studie eingeschlossen (Abb. 8). Alle Patienten hatten zunächst eine koronare CT-Angiografie und mit einer zeitlichen Latenz von maximal drei Monaten eine Koronarangiografie mit invasiver FFR-Messung. Hiervon waren 13 Läsionen signifikant, die restlichen Koronarstenosen verursachten keine Myokardischämie. Ausschlusskriterien waren eine stattgehabte Revaskularisation, eine ungenügende Bildqualität der koronaren CT-Angiografie und Bifurkationsstenosen.

Die in dieser Studie miteinander verglichenen quantitativen Stenosencharakteristika umfassten LL, MLA, MLD, LL/MLD^4, Remodeling-Index, % APV und CCO. In einer initialen univariaten Analyse wurde gesondert die Trennschärfe der einzelnen Parameter hinsichtlich hämodynamischer Relevanz von Koronarstenosen untersucht (Abb. 9). Für die Parameter, die sich in der univariaten Analyse signifikant gezeigt hatten (LL, MLD, LL/MLD^4, CCO), wurde die jeweilige Fläche unter der Kurve (*Area Under the Curve*, AUC) der Operationscharakteristik eines Beobachters berechnet und miteinander verglichen. In diesem direkten Vergleich zeigte sich die AUC des morphologischen Index LL/MLD^4 (0,909) signifikant größer als die des MLD ($p = 0,014$) und der LL ($p = 0,041$). Hierbei wurde zudem der optimale Grenzwert für diese Parameter erfasst (Abb. 10). Obwohl die AUC des Index LL/MLD^4 auch größer als die AUC von CCO war (0,809), war dieser Unterschied nicht signifikant ($p = 0,175$). Bei der multivariaten Analyse zur Untersuchung der Beziehung

mehrerer Variablen untereinander verblieb LL/MLD^4 jedoch als einziger unabhängiger Prädiktor für hämodynamische Relevanz (Quotenverhältnis 2,021; 95 %-Konfidenzintervall (KI) 1,331–3,069; p = 0.001). Weiterhin wurde die AUC dieses Prädiktors der AUC der rein visuellen Interpretation der koronaren CT-Angiografie gegenübergestellt (*Abb. 11*). Hierbei war die AUC des Index LL/MLD^4 (0,909) im Vergleich zur AUC einer rein visuellen Interpretation der koronaren CT-Angiografie (0,678) signifikant (p = 0,004) größer.

Schlussfolgernd zeigte sich in dieser Studie, dass die quantitativen Parameter LL, MLA, MLD, LL/MLD^4, Remodeling-Index, % APV und CCO aus Routinedatensätzen der koronaren CT-Angiografie ohne zusätzliche Strahlenbelastung und KM-Anwendung erhoben werden können. Ferner zeigten die Ergebnisse, dass diese quantitativen Parameter die diagnostische Genauigkeit der koronaren CT-Angiografie für den Nachweis hämodynamischer Relevanz von Stenosen verbessern können. Der Index LL/MLD^4 war hierbei den anderen untersuchten Parametern überlegen.

Characteristic	Datum
No. of patients	49
Age, yrs	62.1 ± 11.4
No. of males[a]	33 (67%)
Height, cm	171.5 ± 11.9
Weight, kg	90.0 ± 21.3
Body-mass index, kg/m^2	30.8 ± 7.9
Left ventricular function, %	61.3 ± 10.6
Vital signs	
Systolic blood pressure, mmHg	132.6 ± 20.9
Diastolic blood pressure, mmHg	71.5 ± 11.1
Heart rate, beats per minute	72.4 ± 14.0
Cardiovascular risk factors[a]	
Diabetes mellitus	13 (26%)
Hypertension	24 (49%)
Dyslipidemia	23 (47%)
Smoking	5 (11%)
Agatston score[b]	810 ± 747
Range	0 – 2595
No. of patients ≥400	24 (49%)
No. of coronary artery stenoses	56
Spatial distribution of lesions of interest[a]	
Left anterior descending	38 (68%)
Left circumflex	8 (14%)
Right coronary artery	10 (18%)

Abb. 8: Demografische Patienteninformation (Quelle: PUBLIKATION 3, mit Genehmigung)

Sofern nicht anders spezifiziert, handelt es sich um Mittelwerte ± Standardabweichung.

[a]: Werte entsprechen der Anzahl mit Prozentangabe in Klammern.

[b]: Der Agatston-Score wurde in 42 Patientinnen und Patienten erhoben.

Parameter	All lesions (N = 56)	Lesions with FFR ≥ 0.80 (N = 43)	Lesions with FFR < 0.80 (N = 13)	*P* Value	Odds ratio	95% Confidence interval of odds ratio
Lesion length, mm	25.5 ± 12.9	23.5 ± 12.7	32.4 ± 11.5	0.036	1.054	1.004 – 1.107
Minimal lumen diameter, mm	1.9 ± 0.5	2.1 ± 0.5	1.5 ± 0.2	0.004	0.026	0.002 – 0.322
Minimal lumen area, mm^2	5.4 ± 2.8	5.6 ± 2.8	5.0 ± 2.6	0.521	0.921	0.716 – 1.184
Lesion length/minimal lumen diameter[4]	3.5 ± 4.5	2.1 ± 1.8	8.0 ± 7.2	0.001	2.021	1.331 – 3.069
Remodeling index	1.0 ± 0.3	1.0 ± 0.3	1.0 ± 0.3	0.893	1.152	0.146 – 9.114
Percentage aggregate plaque volume, %	41.0 ± 14.5	40.6 ± 13.4	42.1 ± 18.5	0.750	2.036	0.026 – 162.283
Coronary contrast opacification	0.1 ± 0.2	0.1 ± 0.1	0.2 ± 0.1	0.014	933.237	4.100 – 212436.233

Abb. 9: Univariate Analyse der Parameter der koronaren CT-Angiografie zur Prädiktion hämodynamischer Relevanz von Stenosen in der FFR als invasive Referenz (Quelle: PUBLIKATION 3, mit Genehmigung)

Parameter	AUC (95% confidence interval)	*P* Value	Optimal cut-off value
Lesion length, mm	0.739 (0.604 – 0.847)	0.0012	20.4
Minimal lumen diameter, mm	0.802 (0.674 – 0.897)	<0.0001	1.8
Lesion length/minimal lumen diameter[4]	0.909 (0.801 – 0.969)	<0.0001	3.54
Coronary contrast opacification	0.809 (0.681 – 0.901)	<0.0001	0.18

Abb. 10: AUC der Parameter LL, MLD, LL/MLD4 und CCO für deren optimalen Grenzwert (Quelle: PUBLIKATION 3, mit Genehmigung)

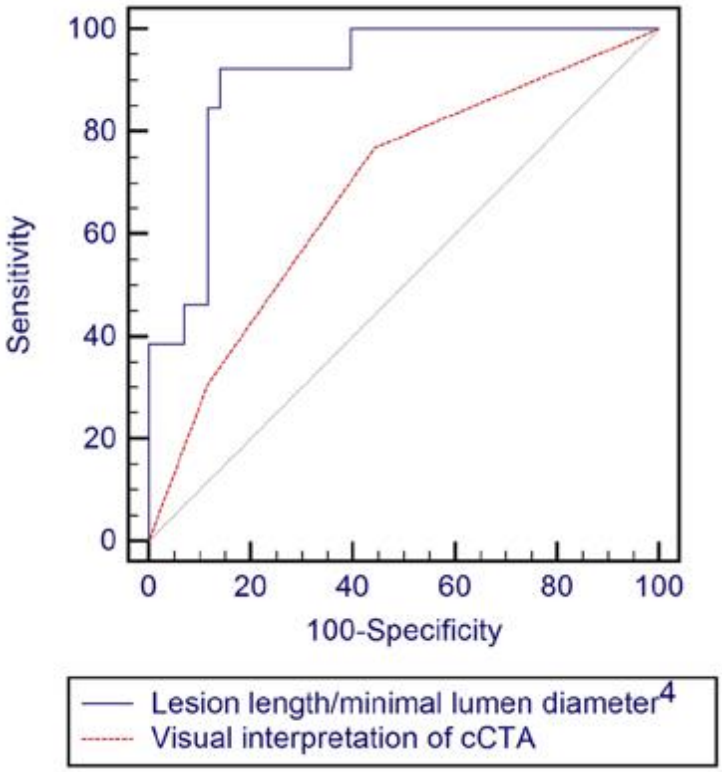

Abb. 11: AUC des morphologischen Stenosen-Index LL/MLD⁴ im Vergleich zur AUC einer rein visuellen Interpretation der koronaren CT-Angiografie (Quelle: PUBLIKATION 3, mit Genehmigung)

5 Funktionelle Informationen durch die koronare CT-Angiografie

5.1 Myokardiale Perfusionsbildgebung

Die CT-basierte myokardiale Perfusionsbildgebung (CTMP) ist ein weiteres Verfahren, um durch die koronare CT-Angiografie neben anatomischen auch funktionelle Informationen zur hämodynamischen Relevanz einer KHK zu erhalten. Die Anfänge der CTMP datieren zurück bis in das Jahr 1987 (51). Lange schränkten allerdings technische Limitationen die klinische Anwendung der CTMP ein. Erst mit den jüngeren Entwicklungen im Bereich der CT-Technologie, welche zu verbesserter räumlicher und zeitlicher Auflösung führten, konnte diese Methode weiterentwickelt werden. Mittlerweile haben eine Reihe von Publikationen den Nachweis der Durchführbarkeit der CTMP erbracht (52-56). Als Beispiel sei hier die multizentrische CORE320-Studie erwähnt, welche Hinweise auf eine verbesserte diagnostische Genauigkeit durch die Kombination von koronarer CT-Angiografie mit CTMP lieferte (57).

Die CTMP fußt auf dem Prinzip, dass die KM-Verteilung im Myokard ein Indikator für den koronaren Blutfluss darstellt (58). Ganz im Gegensatz zu gesundem Myokard, zeigen ischämische Areale eine verzögerte KM-Aufnahme und eine verminderte maximale KM-Anreicherung in der sogenannten First-Pass-Phase, während die KM-Abnahme normal ist. In infarziertem Myokard kann man eine verzögerte KM-Verteilung beobachten, eine verminderte maximale KM-Anreicherung in der First-Pass-Phase sowie eine langsamere KM-Abnahme. Reduzierte KM-Anreicherungen in allen Myokardarealen sind gleichbedeutend mit einem Perfusionsdefizit (Abb. 12).

Ganz ähnlich wie bei den nuklearmedizinischen Stress-Tests, beinhalten CTMP-Akquisitionsprotokolle nicht nur eine Untersuchung in Ruhe, sondern eine zusätzliche Untersuchung unter pharmakologisch induziertem Stress, welche allerdings auch eine weitere KM-Applikation und Strahlenbelastung für die untersuchte Person bedeutet. Da reversible Perfusionsdefizite im Allgemeinen

vor fixierten Perfusionsdefiziten auftreten (59), kann die Stress-Untersuchung die Sensitivität der CTMP erhöhen. Die zeitliche Reihenfolge von Ruhe- und Stress-Akquisition ist dabei variabel. Allerdings kann bei zuerst durchgeführter Ruhe-Akquisition mittels koronarer CT-Angiografie eine KHK theoretisch ausgeschlossen werden, sodass eine Stress-Akquisition dann nicht erforderlich wäre. Daher ist diese Reihenfolge der Akquisitionen bei der CTMP zu bevorzugen. Weiterhin kann bei der Untersuchungstechnik zwischen statischer und dynamischer CTMP unterschieden werden. Während die statische Erfassung der KM-Anreicherung im Myokard einer Momentaufnahme der Verteilung gleichzusetzen ist, wird bei der deutlich strahlenintensiveren, dynamischen Technik zu verschiedenen Zeitpunkten die KM-Anreicherung erfasst.

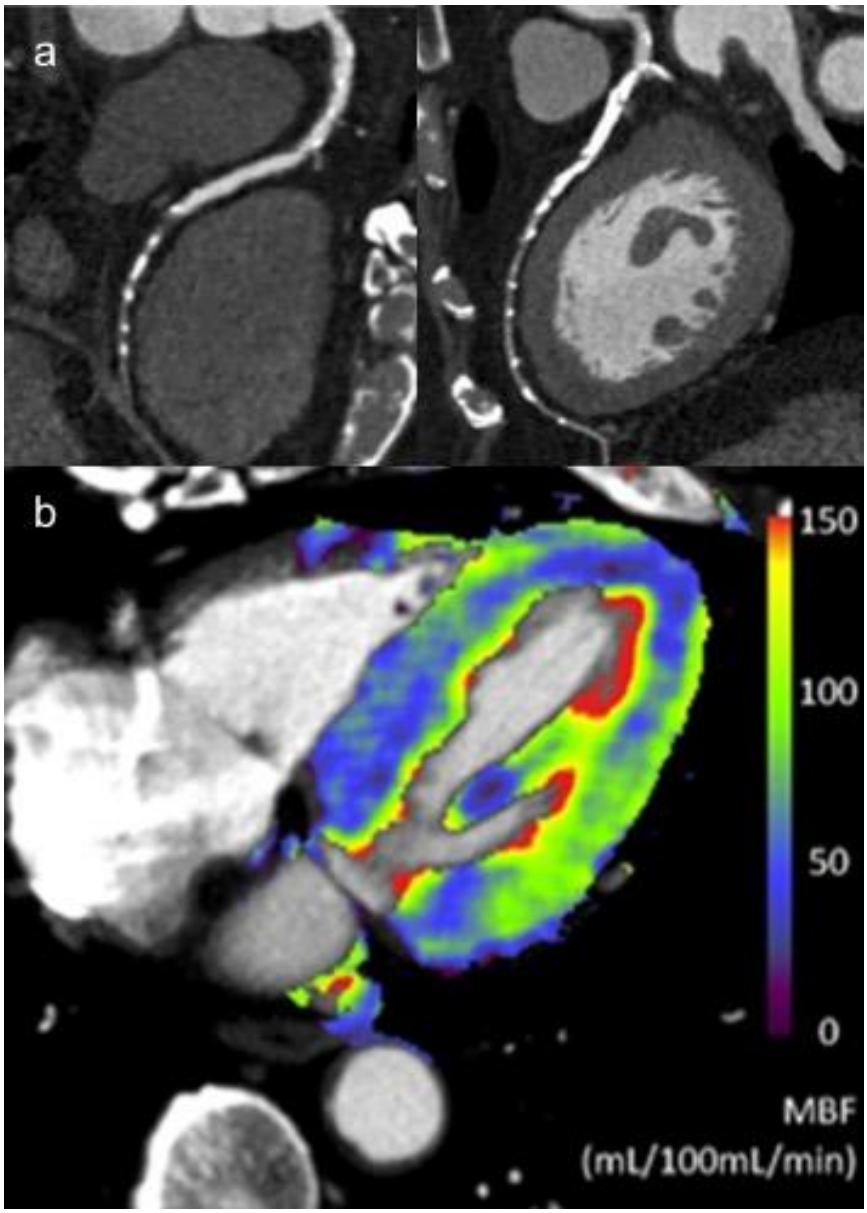

Abb. 12: Beispiel einer CTMP-Untersuchung (Quelle: eigene Darstellung)

Zunächst wird bei der CT-Akquisition in Ruhe eine koronare Zweigefäßerkrankung unter Beteiligung des Ramus interventricularis anterior und des Ramus circumflexus nachgewiesen (a). Basierend auf der nachfolgenden Stress-Akquisition kann eine farbkodierte Kartierung des linken Ventrikels auf das diffuse Perfusionsdefizit insbesondere des gesamten Interventrikularseptums und des Apex sowie basal lateral hinweisen, wobei der myokardiale Blutfluss (MBF) anhand der Farbskala rechts im Bild definiert ist (b).

5.2 Anwendung computerbasierter Flussdynamikmodelle

Die wissenschaftliche Basis der Berechnungen des koronaren Blutflusses zur Erlangung der CT-basierten FFR wurde durch Taylor et al. beschrieben (60). Es sind dabei drei Prinzipien maßgeblich: die Assoziation zwischen der im CT-Datensatz messbaren Myokardmasse und dem koronaren Blutfluss, die Adaptation des Durchmessers eines Koronargefäßes an die Perfusionsrate im nachgeschalteten myokardialen Versorgungsareal und eine inverse Korrelation zwischen Größe des Koronargefäßes und dem vorhandenen Flusswiderstand (60, 61). Die CT-basierte FFR beruht letztlich darauf, dass die patientenspezifischen, anatomischen Informationen des CT-Datensatzes Rückschlüsse auf die zirkulatorischen Eigenschaften des Koronarsystems in Ruhe zulassen, welche im nächsten Schritt auf andere physiologische Zustände (z. B. Belastung) angewendet werden können.

Der CT-Datensatz wird herangezogen, um ein möglichst getreues anatomisches Modell des koronaren Gefäßbaumes zu generieren. Hierbei werden wandständige atherosklerotische Plaques und Stenosen bereits berücksichtigt. Im nächsten Schritt wird dann ein patientenspezifisches physiologisches Modell der Koronarzirkulation erstellt (60, 62). Es werden dabei standardisierte Umgebungsbedingungen angenommen. Gepaart mit bekannten Informationen wird der koronare Blutfluss zusammen mit den Flusswiderständen unter Simulation maximaler Hyperämie berechnet (60, 63, 64). Hierfür werden computerbasierte Flussdynamikmodelle herangezogen. Die computerbasierte Flussdynamik nutzt als Teildisziplin der Strömungsmechanik Algorithmen, um Flüssigkeitsbewegungen in virtuellen Modellen nachzuvollziehen. Bekanntere Anwendungsgebiete der computerbasierten Flussdynamik finden sich im Flugzeug- und Rennwagendesign. Aktuelle technische Entwicklungen im Feld der bildbasierten Modellierung und der numerischen Strömungsmechanik erlauben eine Simulation des koronaren Blutflusses sowohl im Ruhezustand, als auch unter Hyperämie anhand dreidimensionaler Bilddatensätze der koronaren CT-Angiografie. Anders als bei der CTMP werden hier Datensätze aus der klinischen Routine verwendet, ohne dass zusätzliche Akquisitionen mit

Strahlenbelastung oder KM-Anwendung erforderlich sind. Auch eine pharmakologische Belastung ist für die nichtinvasive Bestimmung der FFR nicht erforderlich.

Da für weite Teile des koronaren Gefäßbetts mathematisch komplexe Rechenoperationen durch den initialen Ansatz der CT-basierten FFR (FFR_{CT}; HeartFlow, Inc., Redwood City, California, USA) angewendet werden, ist eine enorme Rechnerleistung erforderlich (60, 65-68). Hierzu werden parallel geschaltete Supercomputer verwendet, deren Inanspruchnahme einen kommerziell verfügbaren, kostenpflichtigen externen Service bedeutet. Datensätze koronarer CT-Angiografie müssen bei dieser 2011 in Europa und 2014 in USA zugelassenen Methode für CT-basierte FFR in ein entsprechendes externes Zentrum transferiert werden. Nach wie vor ist je nach Qualität des Datensatzes eine Bearbeitungszeit von 1–4 Stunden zu veranschlagen (Abb. 13) (69).

In klinischen Studien konnte gezeigt werden, dass dieser oben beschriebene Ansatz FFR_{CT} vorteilhaft gegenüber einer rein anatomischen Beurteilung der koronaren CT-Angiografie abschneidet, wenn die invasive FFR als Referenz herangezogen wird. In der monozentrischen Studie namens DISCOVER-FLOW (Diagnosis of Ischemia-Causing Stenoses Obtained Via Noninvasive Fractional Flow Reserve) von Koo et al. ergab der Vergleich von CT-basierter FFR mit der invasiven FFR eine Sensitivität von 82 %, eine Spezifität von 82 %, einen positiv prädiktiven Wert von 85 % und einen negativ prädiktiven Wert von 91 % auf Patientenebene (65). Darüber hinaus ergab die FFR_{CT} hinsichtlich der Identifikation ischämieverursachender Koronarstenosen eine signifikant bessere diagnostische Genauigkeit als die koronare CT-Angiografie mit einer AUC von 0,90 versus 0,75 ($p < 0,001$).

Die von Min et al. publizierte internationale multizentrische Studie DeFACTO (Determination of Fractional Flow Reserve by Anatomic Computed Tomographic Angiography) bestimmte den diagnostischen Wert der FFR_{CT}

anhand von insgesamt 252 Patientinnen und Patienten (70). Die FFR_{CT} ergab für die Detektion funktionell relevanter Koronarstenosen eine bessere diagnostische Genauigkeit als die koronare CT-Angiografie (90 % vs. 84 % Sensitivität, 54 % vs. 42 % Spezifität, 67 % vs. 61 % positiv prädiktiver Wert, 84 % vs. 72 % negativ prädiktiver Wert). Auch hier zeigte sich für die FFR_{CT} eine gute Trennschärfe für stenosenassoziierte Myokardischämie (AUC 0,81). Auch die Sensitivität gerade von intermediären Stenosen (hier definiert als 30–70 % Lumenobstruktion) verdoppelte sich von der koronaren CT-Angiografie im Vergleich zur FFR_{CT} (37 % vs. 82 %) ohne Einbußen bei der Spezifität (66 % vs. 66 %) (70).

Die von Nørgaard et al. zur diagnostischen Wertigkeit der FFR_{CT} vorgestellte internationale Multicenter-Studie NXT (Analysis of Coronary Blood Flow Using CT Angiography: Next Steps) umfasste 484 Gefäße von 251 untersuchten Personen und demonstrierte ebenfalls Überlegenheit gegenüber der koronaren CT-Angiografie (AUC 0,90 vs. 0,81 pro untersuchter Person und AUC 0,93 vs. 0,79 pro Gefäß) (69). Im Vergleich zur koronaren CT-Angiografie erlaubte FFR_{CT} eine korrekte Reklassifizierung von 67 % der falsch-positiven Ergebnisse in der Analyse auf Gefäßebene. Auch wurde bei der koronaren CT-Angiografie als Grenzwert der binären Einteilung von Stenosen in obstruktiv und nichtobstruktiv zusätzlich zu 50 % auch 70 % luminale Stenosierung untersucht. Hierbei zeigte sich zwar eine höhere Spezifität (84 % vs. 79 %) der koronaren CT-Angiografie, allerdings bei einer deutlich verminderten Sensitivität (70 % vs. 86 %).

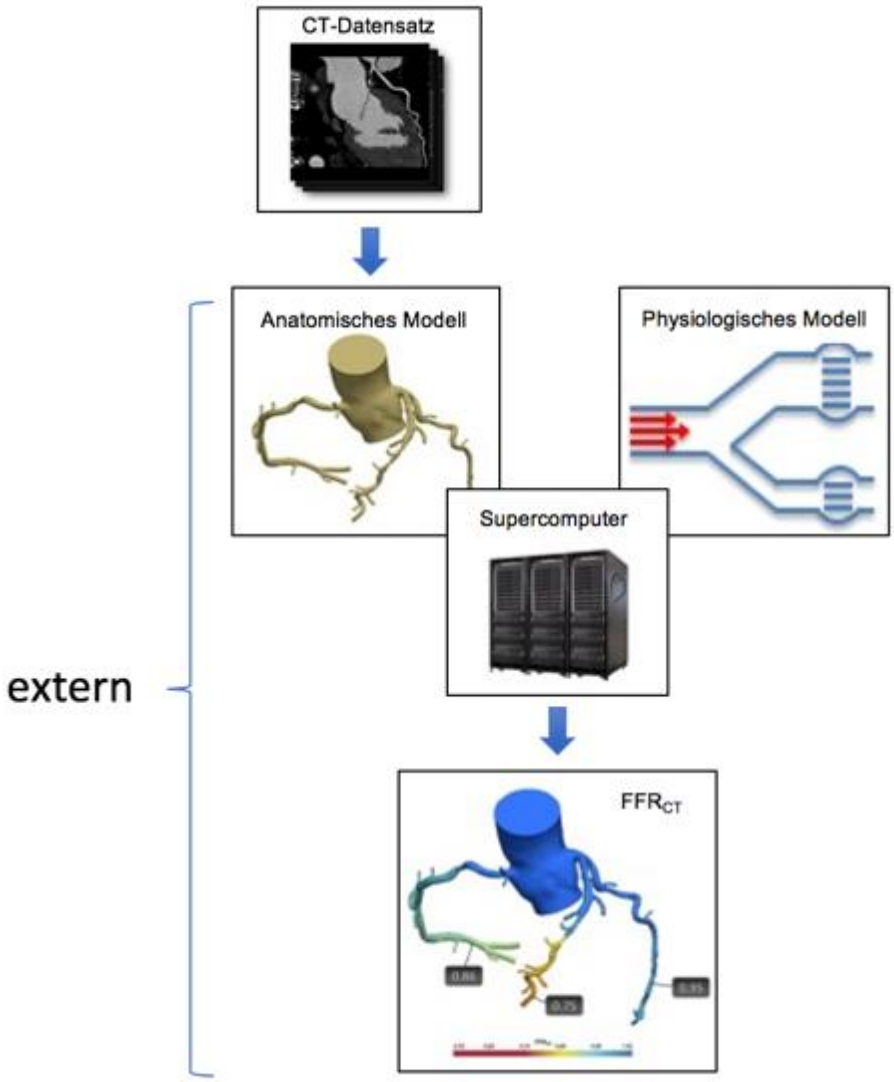

Abb. 13: CT-basierte FFR mit Datentransfer nach extern (Quelle: Verwendung von Teilen der Abbildung aus Nørgaard BL et al. (69), mit Genehmigung)

Der reguläre koronare CT-angiografische Datensatz wird zum Anbieter nach extern transferiert, wo ein dreidimensionales anatomisches Modell des Gefäßbaumes erstellt wird. Gepaart mit patientenspezifischer Information wird parallel ein physiologisches Modell der Mikrozirkulation erstellt. Unter Inanspruchnahme höherer Rechnerleistung werden physikalische Gesetze der Strömungsmechanik angewendet, um aus diesen Informationen den koronaren Blutfluss und für jede Stelle des Koronarbaumes die CT-basierte FFR zu berechnen (FFR_{CT}; HeartFlow, Inc., Redwood City, California, USA).

5.2.1 Initiale Erfahrungen mit einem neuen CT-Algorithmus basierend auf computerbasierter Flussdynamik (PUBLIKATION 4)

Neben dem oben vorgestellten CT-basierten FFR-Verfahren FFR_{CT}, wurde ein weiterer, auf computerbasierter Flussdynamik beruhender Algorithmus zur Erfassung hämodynamischer Relevanz von Koronarstenosen entwickelt (cFFR, Siemens, Forchheim, Deutschland; derzeit kommerziell nicht verfügbar). Dieser CT-Algorithmus stand als Prototyp zur Verfügung. Wesentlicher Unterschied zu FFR_{CT} ist bei cFFR die intrahospitale Anwendung durch den Untersucher. Ein Transfer der CT-Datensätze nach extern zur Auswertung beim Anbieter ist somit nicht erforderlich (Abb. 14). In dieser Publikation wurde der neue CT-basierte FFR-Ansatz cFFR erstmalig vorgestellt und aus klinischer Perspektive im Hinblick auf die Anwendbarkeit und Handhabung charakterisiert.

Hervorzuheben ist zunächst, dass für den intrahospitalen CT-Algorithmus cFFR – wie auch für die FFR_{CT} – keine zusätzlichen CT-Akquisitionen erforderlich waren. Es wurden also CT-Datensätze aus der klinischen Routine verwendet. Bei dem intrahospitalen Verfahren erstellte die Software automatisch eine zentrale Gefäßachse, die der Anwender dann anpassen konnte. Dann wurde mittels semiautomatischer Segmentierung ein dreidimensionales, geometrisches Modell des koronaren Gefäßbaumes erstellt. Die Software erstellte hierbei Konturvorschläge aller Gefäßabschnitte, die der Anwender entsprechend korrigieren oder akzeptieren konnte. In einem weiteren Schritt wurden durch den Anwender dann alle Koronarstenosen gekennzeichnet (Abb. 15). Des Weiteren wurden computerbasierte Flussdynamikmodelle durch die Software angewendet, um zusammen mit einem patientenindividuellen, physiologischen Modell den koronaren Blutfluss zu simulieren (64). Ein Hybrid-Verfahren ermöglichte hierbei die zeiteffiziente und patientennahe Diagnostik durch Kopplung von Rechenmodellen höherer und niedrigerer Ordnung. Eine Modellordnungsreduktion war die hier zugrundeliegende Technik, um Rechenoperationen zu vereinfachen und auf geringere Computerleistung zurückgreifen zu können. Die im Vergleich zum initial vorgestellten externen

Verfahren FFR_{CT} weniger umfangreichen Rechenoperationen bei cFFR können mit einem regulären Befundungsrechner gemäß Herstellereinschätzung innerhalb von maximal ca. 10 Minuten erfolgen.

Bei 28 Patientinnen und Patienten mit insgesamt 36 Koronarstenosen wurde die zu veranschlagende mittlere Dauer von der Erstellung des dreidimensionalen Modells des koronaren Gefäßbaumes zusammen mit der Berechnungsdauer des Algorithmus untersucht. In den ersten Erfahrungen mit dem intrahospitalen Algorithmus zur Erfassung der CT-basierten FFR ergab sich eine mittlere Zeit von 51,9 $\pm$ 9,0 min. Da eine gewisse Lernkurve im Umgang mit dem Algorithmus zu veranschlagen ist, erscheint die Erfassungszeit im Vergleich zum extern zu transferierenden Verfahren (1-4 h in der aktuellen Version) vorteilhaft (69). Der Großteil der Zeit wurde für den semiautomatischen Segmentierungsprozess des koronaren Gefäßbaumes verwendet (48,0 ± 8,6 min). Als finale Berechnungszeit für die CT-basierten FFR-Werte wurden 3,9 ± 0,8 min gemessen. Auf Grundlage der für alle eingeschlossenen Koronarstenosen vorliegenden Referenzergebnisse der invasiven FFR wurde die Korrelation zwischen CT-basierter und invasiver FFR in verblindeter Art und Weise untersucht. Der mittlere cFFR-Wert betrug 0,85 und der mittlere invasive FFR-Wert ergab 0,87. Auf Gefäßebene konnte zwischen CT-basierter FFR und invasiver FFR eine gute direkte Korrelation nach Pearson erfasst werden ($r = 0,74$; $p < 0,0001$) (Abb. 16 und Abb. 17).

Schlussfolgernd konnten in dieser Studie erste vielversprechende Ergebnisse des auf computerbasierten Flussdynamiken beruhenden Prototyp-Algorithmus cFFR zur intrahospitalen Berechnung von CT-basierter FFR an einem regulären Befundungsrechner vorgestellt werden. Die Ergebnisse sprechen für eine zeiteffiziente und praktikable Anwendung. Zudem suggerieren die Ergebnisse eine gute Trennschärfe hinsichtlich stenosenassoziierter Myokardischämie aufgrund der Korrelation mit dem invasiven Referenzstandard.

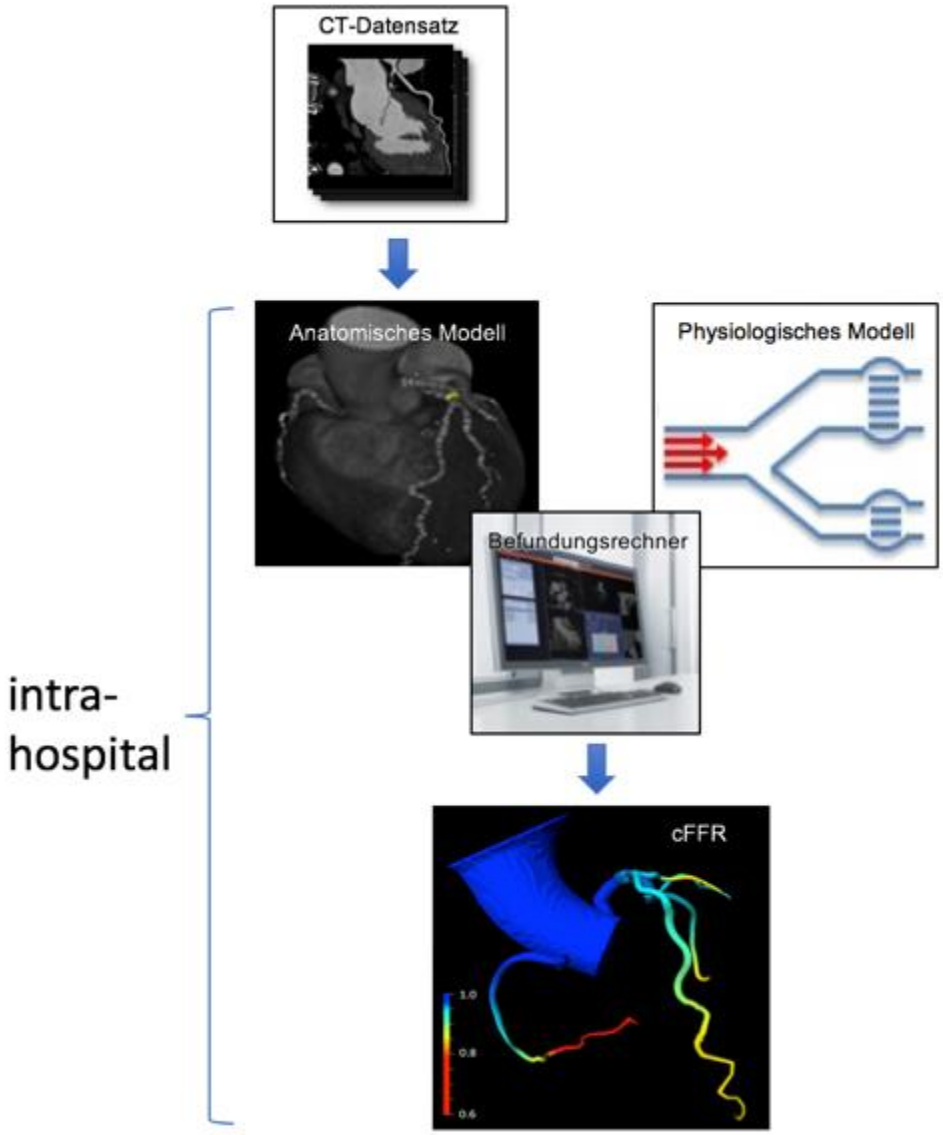

Abb. 14: Intrahospitale CT-basierte FFR (Quelle: eigene Darstellung)

Der reguläre CT-Datensatz verbleibt intrahospital an einem Befundungsrechner, wo mittels semiautomatischer Segmentierung ein dreidimensionales anatomisches Modell des koronaren Gefäßbaumes erstellt wird. Gepaart mit patientenspezifischer Information wird parallel ein physiologisches Modell der Mikrozirkulation erstellt. Mittels Kopplung von Rechenoperationen höherer und niedrigerer Ordnung, wird aus diesen Informationen der koronare Blutfluss berechnet. Daraus ergibt sich für jede Stelle des Koronarbaumes die CT-basierte FFR (cFFR, Prototyp-Version 1.4, Siemens, Forchheim, Deutschland; derzeit kommerziell nicht verfügbar).

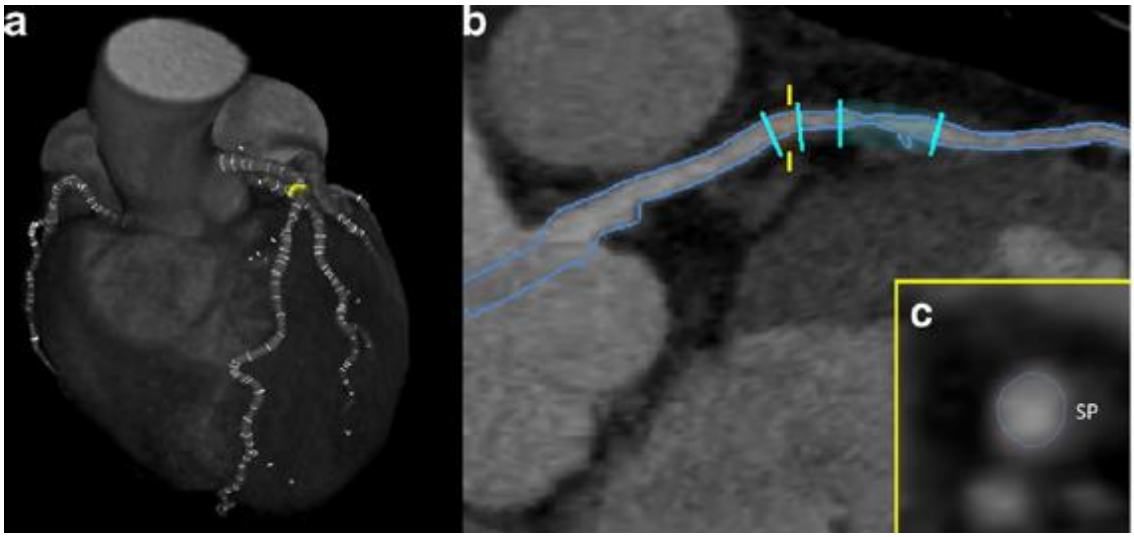

Abb. 15: Arbeitsschritte bei der intrahospitalen CT-basierten FFR (Quelle: PUBLIKATION 4, mit Genehmigung)

Ein dreidimensionales geometrisches Modell des koronaren Gefäßbaumes wird erstellt (a). In der multiplanaren Darstellung (b) kann der Anwender Stenosen (hervorgehoben in türkis) definieren, wobei die blauen Linien die Gefäßwände repräsentieren. In der perpendikularen Gefäßansicht (c) lässt sich eine mit „SP" gekennzeichnete, nichtkalzifizierte Plaque erkennen. Die rot gestrichelte Linie entspricht dem Gefäßkonturvorschlag durch die Software.

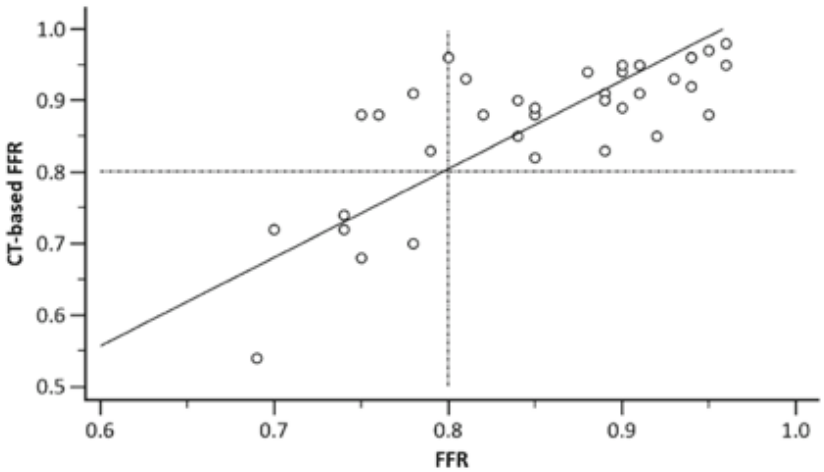

Abb. 16: Streudiagramm zur Korrelation zwischen CT-basierter und invasiver FFR (Quelle: PUBLIKATION 4, mit Genehmigung)

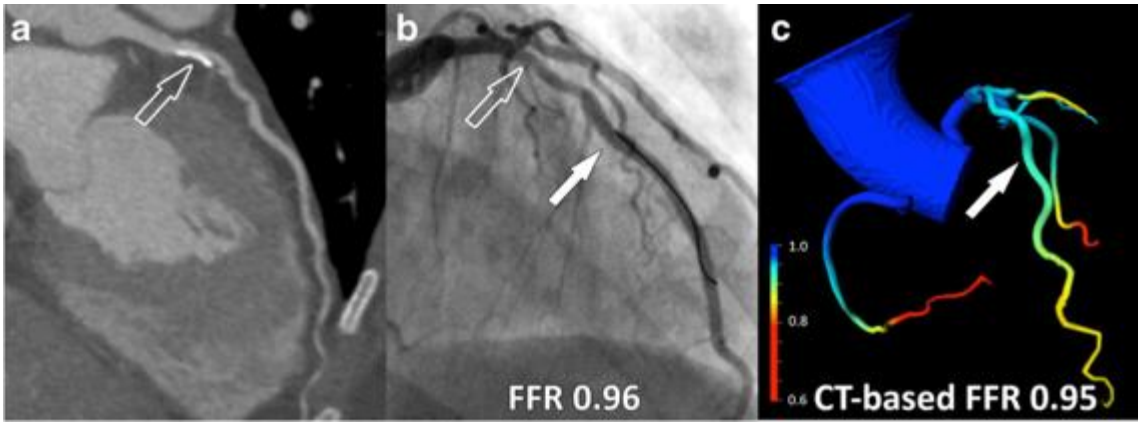

Abb. 17: Erstes Fallbeispiel intrahospitale CT-basierte FFR (Quelle: PUBLIKATION 4, mit Genehmigung)

Bei einer 53-jährigen Patientin mit intermediärem Risiko für eine KHK wurde aufgrund von atypischen pektanginösen Beschwerden eine koronare CT-Angiografie durchgeführt (a). Hierbei zeigte sich eine intermediäre Stenose im Ramus interventricularis anterior auf dem Boden einer gemischten Plaque (offener Pfeil). In der nachfolgenden invasiven Koronarangiografie (b) konnte diese Stenose (offener Pfeil) herabgestuft werden. Die Druckdrahtmessung (geschlossener Pfeil) ergab keine funktionelle Relevanz (FFR = 0,96). Die post-hoc bestimmte cFFR (c) ergab mit 0,95 ebenfalls keine funktionelle Relevanz (geschlossener Pfeil kennzeichnet Messstelle).

5.2.2 Diagnostische Genauigkeit eines intrahospital anwendbaren CT-basierten FFR-Algorithmus (PUBLIKATION 5)

Aufbauend auf PUBLIKATION 4 zielte diese eigene Arbeit auf eine umfassende Analyse der diagnostischen Wertigkeit der intrahospital anwendbaren CT-basierten FFR-Methode cFFR ab. Zwischen 02/2014 und 09/2018 wurden retrospektiv Patientinnen und Patienten, die nach klinisch indizierter koronarer CT-Angiografie innerhalb von drei Monaten eine invasive Koronarangiografie mit FFR erhalten hatten, eingeschlossen. Ausschlusskriterien waren größerer Zeitabstand oder schwere kardiale Komplikationen (Tod, Myokardinfarkt oder myokardiale Revaskularisation) zwischen CT und Koronarangiografie, hochgradig reduzierte systolische Funktion des linken Ventrikels, vorherige interventionelle oder chirurgische Revaskularisation, Bifurkationsstenosen Typ D und G (nach der SYNTAX-Klassifikation (71)), hochgradige Stenosen des linken Hauptstammes oder der ostialen rechten Koronararterie, Vorhandensein einer chronischen Totalokklusion und ungenügende Bildqualität des CT-Datensatzes.

Die Interpretation der koronaren CT-Angiografie erfolgte durch einen Untersucher mit siebenjähriger Erfahrung in kardialer Bildgebung. Die Stenosengraduierung erfolgte visuell anhand der anatomischen Informationen. Weiterhin wurde eine subjektive Einschätzung der Bildqualität anhand einer 5-Punkt-Skala vorgenommen. Die Erfassung der CT-basierten FFR erfolgte anhand regulärer Datensätze der koronaren CT-Angiografie ohne ergänzende Akquisitionen, ohne Modifikation des CT-Protokolls und ohne pharmakologisch induzierte Hyperämie. Der für Forschungszwecke entworfene Prototyp-Algorithmus (cFFR, Version 1.4, Siemens, Forchheim, Deutschland; derzeit kommerziell nicht verfügbar) wurde auf einem regulären Befundungsrechner verwendet. Es wurde Wert darauf gelegt, dass das cFFR-Ergebnis an der gleichen Position im Koronarsystem erhoben wurde wie die invasive FFR-Messung mittels Druckdrahtsensor. Von den initial 72 infrage kommenden Personen wurden insgesamt 19 ausgeschlossen: aufgrund einer Latenz zwischen koronarer CT-Angiografie und invasiver Koronardiagnostik von mehr

als drei Monaten (n = 11), einer nichtdiagnostischen Bildqualität des CT-Datensatzes (n = 3) und Vorliegen von Bifurkationsstenosen (n = 5). Von den verbliebenen 53 Patientinnen und Patienten sind die demografischen Informationen in Abb. 18 und die Ergebnisse von sowohl invasiver Koronarangiografie als auch koronarer CT-Angiografie in Abb. 19 aufgeführt. Der mediane Wert der subjektiven Bildqualität ergab 4 (Interquartilsabstand 3–4). Es wurde eine mittlere Dauer von $37{,}5 \pm 13{,}8$ min für cFFR inklusive semiautomatischer Datensatzbearbeitung und Berechnung erfasst. Der Rangkoeffizient nach Spearman ($\varphi = 0{,}66$; $p < 0{,}001$) ergab eine gute Korrelation und im Bland-Altman-Diagramm konnte kein systematischer Fehler gefunden werden (Abb. 20 und Abb. 21). Die AUC der CT-basierten FFR für den stenosenspezifischen Ischämienachweis zeigte einen signifikanten Vorteil gegenüber der koronaren CT-Angiografie (Abb. 22). Diese Verbesserung geht hauptsächlich auf die signifikante Steigerung der Spezifität (von 34 % auf 85 % auf Läsionsebene und von 32 % auf 84 % auf Patientenebene) bei nahezu unveränderter Sensitivität zurück (Abb. 23). Repräsentative Patientenbeispiele sind in Abb. 24 und Abb. 25 gegeben.

Schlussfolgernd stellt diese eigene Arbeit erste klinische Ergebnisse aus der Anwendung des neuen CT-basierten FFR-Prototyp-Algorithmus cFFR vor. Es zeigte sich eine zeiteffiziente, intrahospitale Erfassung von nichtinvasiver FFR aus regulären CT-Datensätzen. Zudem fand sich eine gute Korrelation mit der invasiven Referenzmethode. Die Hauptaussage liegt in einer Verbesserung der diagnostischen Genauigkeit im Vergleich zur koronaren CT-Angiografie.

Parameter	Mean ± Standard Deviation or Frequency (%)
Age (years)	61.2 ± 12.0
Men	34 (64%)
Height (cm)	173.2 ± 10.8
Weight (kg)	87.0 ± 21.2
Body-mass index (kg/m^2)	28.9 ± 6.5
Caucasian	44 (77%)
African American	13 (23%)
Hypertension*	31 (54%)
Diabetes mellitus	18 (32%)
Hyperlipidemia†	31 (54%)
Current smoker	8 (14%)
Prior percutaneous coronary intervention	9 (16%)
Prior coronary bypass surgery	0 (0%)
Left ventricular ejection fraction (%)	58.3 ± 9.3
Systolic blood pressure (mm Hg)	136.2 ± 15.7
Diastolic blood pressure (mm Hg)	71.8 ± 9.3
Heart rate (beats per minute)	70.2 ± 12.6
Aspirin	31 (54%)
Clopidogrel	10 (18%)
β blocker	30 (53%)
Statin	35 (61%)
Angiotensin converting enzyme inhibitor	23 (40%)
Calcium-channel blocker	10 (18%)

Abb. 18: Charakteristika des finalen Patientenkollektivs von 53 Personen (Quelle: PUBLIKATION 5, mit Genehmigung)

** Definiert als Blutdruck > 140 mmHg systolisch oder > 90 mmHg diastolisch oder Einnahme antihypertensiver Medikation*

† Definiert als Gesamtcholesterin > 200 mg/dl oder Einnahme von Lipid-senkender Medikation

Coronary Catheter Angiography	Frequency (%)
Luminal stenosis ≥50%	44 (66%)
Luminal stenosis ≥70%	21 (31%)
FFR <0.80	20 (30%)
No. of stenoses of interest per location	
Left anterior descending coronary artery	41 (61%)
Left circumflex coronary artery	15 (22%)
Right coronary artery	11 (16%)
Coronary Computed Tomography Angiography	**Value or Frequency (%)**
Agatston score, mean ± standard deviation*	778.4 ± 731.1
Range*	0–2547
No. of patients ≥400*	19 (36%)
Luminal stenosis ≥50%	55 (82%)
Luminal stenosis ≥70%	27 (40%)
Intermediate grade luminal stenosis (30%–70%)	39 (58%)
CT-based FFR <0.80	24 (36%)

Abb. 19: Ergebnisse der invasiven Koronarangiografie und der koronaren CT-Angiografie (Quelle: PUBLIKATION 5, mit Genehmigung)

** Der Agatston-Score wurde in 46 Patientinnen und Patienten erhoben.*

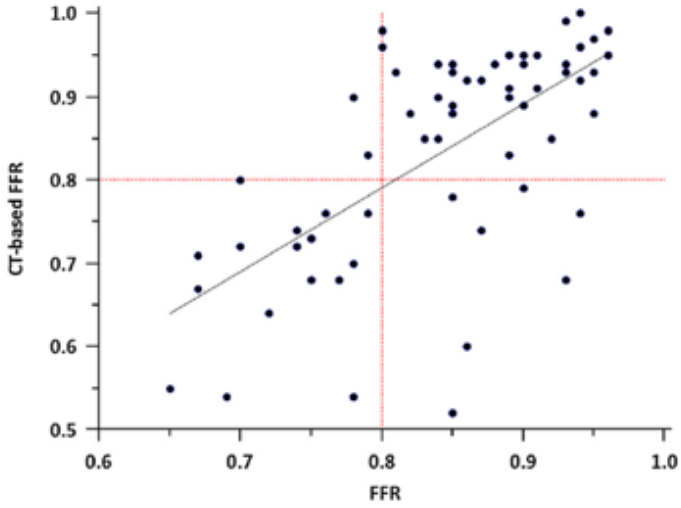

Abb. 20: Streudiagramm der intrahospitalen CT-basierte FFR und der invasiven FFR mit guter Korrelation auf Läsionsebene (Quelle: PUBLIKATION 5, mit Genehmigung)

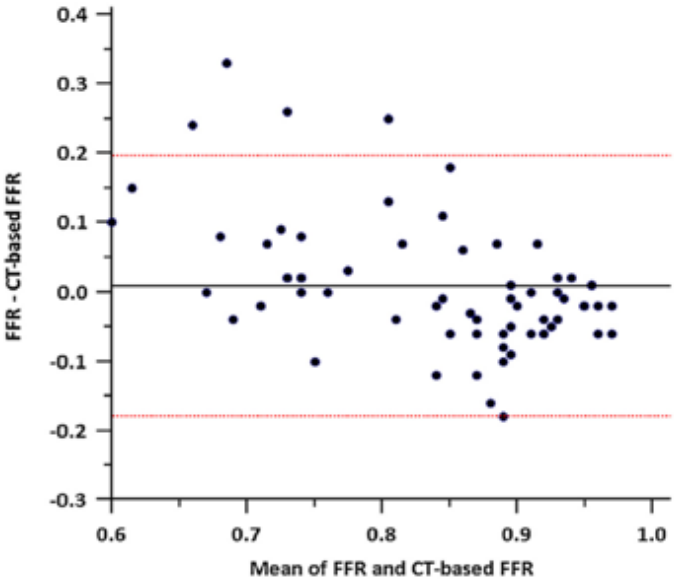

Abb. 21: Punktdiagramm nach Bland-Altmann ohne systematischen Fehler auf Läsionsebene (Quelle: PUBLIKATION 5, mit Genehmigung)

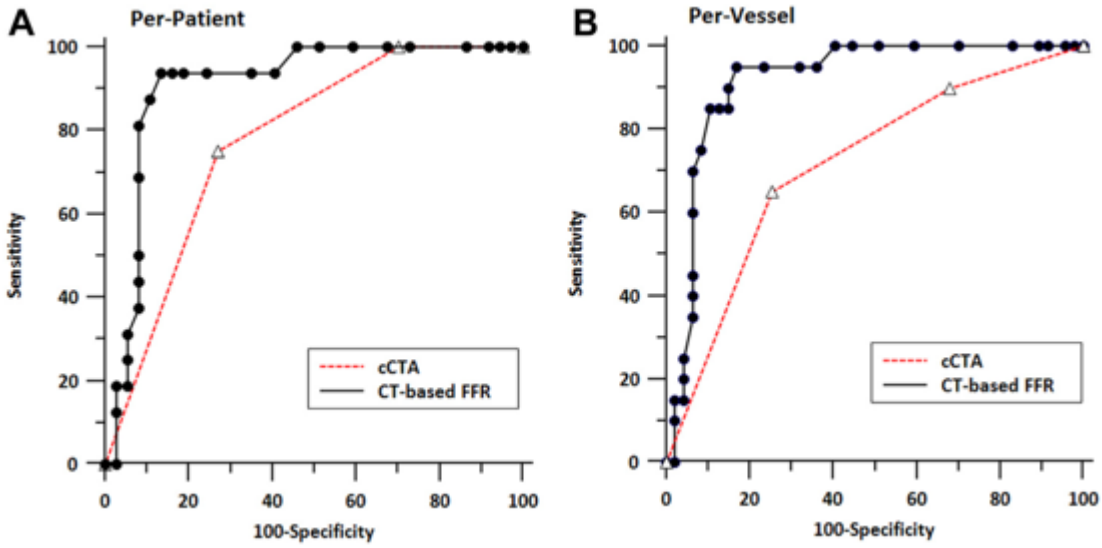

Abb. 22: AUC-Vergleich von koronarer CT-Angiografie und intrahospitaler CT-basierter FFR mit invasiver FFR als Referenz (Quelle: PUBLIKATION 5, mit Genehmigung)

Auf der Patientenebene (A) und Läsionsebene (B) betrug die jeweilige AUC des intrahospitalen CT-basierten FFR-Verfahrens cFFR 0,91 und 0,92. Auf der Patientenebene und Läsionsebene betrug demgegenüber die jeweilige AUC der koronaren CT-Angiografie 0,78 und 0,72. Der AUC-Vergleich erreichte statistische Signifikanz auf der Läsionsebene (p = 0,005), aber nicht auf der Patientenebene (p = 0,078).

	Per-Lesion (n = 67)		Per-Patient (n = 53)	
	CT-Based FFR <0.80 (95% CI)	cCTA Stenosis ≥0.50 (95% CI)	CT-Based FFR <0.80 (95% CI)	cCTA Stenosis ≥0.50 (95% CI)
Sensitivity	85 (62–97)	90 (68–98)	94 (70–99)	94 (70–99)
Specificity	85 (72–94)	34 (21–49)	84 (68–94)	32 (18–50)
PPV	71 (49–87)	37 (23–52)	71 (48–89)	38 (23–54)
NPV	93 (81–98)	89 (65–98)	97 (84–99)	92 (64–99)

Abb. 23: Diagnostische Genauigkeit von intrahospitaler CT-basierter FFR im Vergleich zur koronaren CT-Angiografie auf Läsions- und Patientenebene (Quelle: PUBLIKATION 5, mit Genehmigung)

cCTA: koronare CT-Angiografie

CI: Konfidenzintervall

NPV: negativ prädiktiver Wert

PPV: positiv prädiktiver Wert

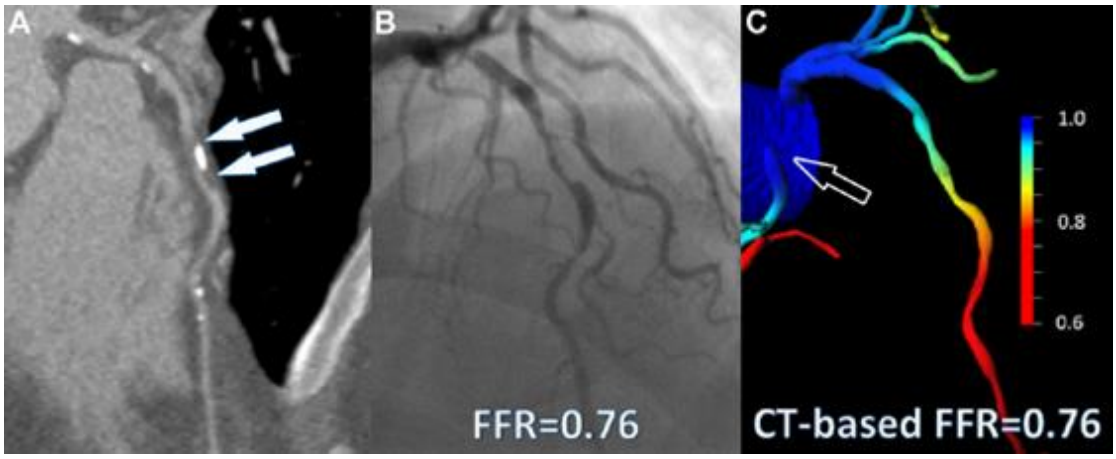

Abb. 24: Zweites Fallbeispiel intrahospitale CT-basierte (Quelle: PUBLIKATION 5, mit Genehmigung)

In der regulären koronaren CT-Angiografie zeigt sich im medialen Ramus interventricularis anterior eine gemischte Plaque mit höhergradiger Stenose (geschlossene Pfeile, A). Die Koronarangiografie mit invasiver FFR zeigt eine hämodynamische Relevanz der Stenose (B). Die intrahospitale CT-basierte FFR „cFFR" ergab einen identischen Wert (C). Nebenbefundlich ist hier ein atypischer Abgang der rechten Koronararterie aus der linkskoronaren Aortenklappentasche zu erkennen (offener Pfeil).

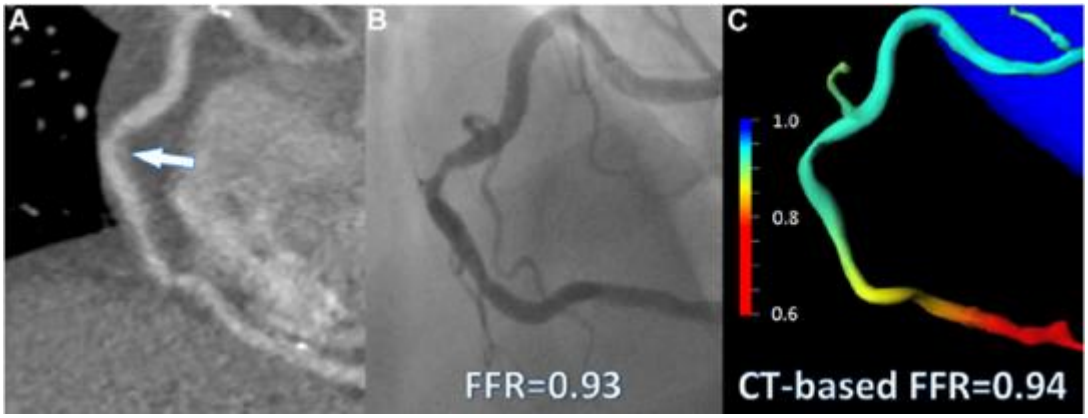

Abb. 25: Drittes Fallbeispiel intrahospitale CT-basierte FFR (Quelle: PUBLIKATION 5, mit Genehmigung)

In der koronaren CT-Angiografie der medialen rechten Koronararterie zeigt sich eine intermediäre Stenose (A). In der Koronarangiografie bestätigte sich diese Stenose, gemäß invasiver FFR jedoch ohne hämodynamische Relevanz (B). Die Bestimmung der CT-basierten FFR ergab mit 0,94 ebenfalls keine

hämodynamische Relevanz dieser Stenose. Es handelt sich um denselben Patienten wie in Abb. 24.

5.2.3 Metaanalyse der CT-basierten FFR mit Subgruppenanalyse intermediärer Stenosen (PUBLIKATION 6)

Ziel dieser Arbeit war es, die Ergebnisse aller bisher veröffentlichten Studien zum Thema CT-basierte FFR in einer Metaanalyse zusammenzuführen. Da gerade intermediäre Stenosen hinsichtlich ihrer funktionellen Relevanz schwer einzuschätzen sind, wurde hier ein Schwerpunkt der Studie gesetzt. Die selektive Literaturrecherche umfasste die Suchbegriffe „CT-based FFR“, „FFR“, „CT“, „noninvasive FFR“, „noninvasive fractional flow reserve“, „non-invasive FFR“, und „non-invasive fractional flow reserve“. Herangezogen wurden die wesentlichsten wissenschaftlichen Datenbanken: Science Citation Index, EMBASE, Cochrane Library, Google Scholar und PubMed. Der Einschluss von Studien in diese Metaanalyse war an die folgenden Kriterien geknüpft: Studiendesign mit Erfassung der diagnostischen Genauigkeit, Alter der Erkrankten ≥ 18 Jahre, Vorstellung der Erkrankten mit Verdacht auf bzw. bekannter KHK, CT-basierte FFR als Index-Untersuchung mit zudem durchgeführter invasiver FFR als Referenzuntersuchung, Mindestanzahl von 50 eingeschlossenen Personen. Duplikate wurden in dieser Metaanalyse ausgeschlossen (Abb. 26).

Es wurden drei multizentrische Studien mit Ergebnissen des Algorithmus FFR_{CT} aus insgesamt 17 Zentren in acht Ländern herangezogen (65, 70, 72). Zudem wurden zwei kleinere retrospektive Arbeiten über den intrahospital anwendbaren Algorithmus cFFR in diese Metaanalyse eingeschlossen (73, 74). Die Ergebnisse zur diagnostischen Genauigkeit der CT-basierten FFR in intermediären Stenosen wurden teils in Substudien publiziert (75, 76). Typische Ausschlusskriterien der herangezogenen Studien waren eine stattgehabte interventionelle oder chirurgische Myokardrevaskularisation, ein akutes Koronarsyndrom und eine ungenügende Bildqualität der koronaren CT-Angiografie. Unterschiede im Studiendesign betrafen den Einschluss von Personen mit Arrhythmien, Bifurkationsstenosen, Körpermaßindizes > 35 kg/m^2 sowie Kontraindikationen gegenüber Betablockern, Nitroglycerin oder Adenosin. Hämodynamisch relevante Stenosen wurden in der visuellen Befundung der

koronaren CT-Angiografie als ≥ 50 % Obstruktion des Koronarlumens definiert. Intermediäre Stenosen wurden – ebenfalls basierend auf visueller Beurteilung der koronaren CT-Angiografie – als 30 bis 70 % Lumenobstruktion definiert. Einzige Ausnahme bildete eine Substudie, bei der intermediäre Stenosen in quantitativer Analyse der invasiven Koronarangiografie als 40 bis 69 % Stenosierung definiert waren (76). Insgesamt wurden in der Metaanalyse 765 Patientinnen und Patienten eingeschlossen. Das mittlere Alter war in den zugrunde liegenden Studien ähnlich verteilt und reichte von 61 ± 12 bis 64 ± 10 Jahren. Von den insgesamt 1306 untersuchten Läsionen waren 386 (29,6 %) gemäß invasiver FFR hämodynamisch relevant. Die demografischen Charakteristika der eingeschlossenen Personen, Informationen zum Design der herangezogenen Studien sowie Ergebnisse der koronaren CT-Angiografie und invasiven Koronarangiografie sind in den Abb. 27 und Abb. 28 aufgeführt. Die gepoolten Ergebnisse für Sensitivität, Spezifität, positiv prädiktiven Wert und negativ prädiktiven Wert der CT-basierten FFR hinsichtlich Detektion hämodynamisch relevanter Stenosen betrugen auf Läsionsebene jeweils 83,7 % (KI: 78,1–89,3 %); 74,7 % (KI: 52,2–97,1 %); 64,8 % (KI: 52,1–77,5 %); und 90,1 % (KI: 80,8–99,3 %). Dahingegen betrugen die gepoolten Ergebnisse für Sensitivität, Spezifität, positiv prädiktiven Wert und negativ prädiktiven Wert bei rein visueller Auswertung der koronaren CT-Angiografie auf Läsionsebene jeweils 84.6 % (KI: 78,1–91,1 %); 49,7 % (KI: 31,1–68,4 %); 39,0 % (KI: 28,0–50,1 %); und 87,3 % (KI: 72,5–100,0 %). Die Ergebnisse sind in Abb. 29 und Abb. 30 zusammengefasst. Sowohl auf Läsions- ($p = 0,0047$) als auch auf Patientenebene ($p = 0,0121$) war die Summations-AUC der CT-basierten FFR signifikant größer als die der rein visuellen Beurteilungen von Stenosen in der koronaren CT-Angiografie (Abb. 31a und Abb. 31b). Von den 1306 in dieser Metaanalyse untersuchten Läsionen waren 634 von intermediärem Stenosengrad. Die gepoolten Ergebnisse für Sensitivität, Spezifität, positiv prädiktiven Wert und negativ prädiktiven Wert der CT-basierten FFR hinsichtlich Detektion hämodynamisch relevanter intermediärer Stenosen betrug auf Läsionsebene jeweils 81,4 % (KI: 70,4–92,9 %); 71,7 % (KI: 54,5–89,0 %); 59,4 % (KI: 35,5–83,4 %); und 89,9 % (KI: 85,0–94,7 %). Die Ergebnisse sind in

Abb. *32* und Abb. 33 zusammengefasst. Die Summations-AUC der CT-basierten FFR war somit signifikant größer ($p = 0{,}0027$), als die der rein visuellen Stenosenbeurteilung in der koronaren CT-Angiografie (Abb. 31c).

Schlussfolgernd lässt sich von der Metaanalyse eine Verbesserung der diagnostischen Genauigkeit für den Nachweis hämodynamisch relevanter Koronarstenosen durch die CT-basierte FFR ableiten. Die CT-basierte FFR schnitt im direkten Vergleich besser ab als die koronare CT-Angiografie allein. Es handelt sich hierbei wahrscheinlich um einen systematischen Effekt, der sowohl für die initial vorgestellte externe CT-basierte FFR-Methode FFR_{CT} als auch für den intrahospital anwendbaren Prototyp-Algorithmus cFFR gilt. Die genannte Verbesserung der diagnostischen Genauigkeit wurde hauptsächlich durch die höhere Spezifität bei praktisch unveränderter Sensitivität getragen. Auch in der gepoolten Subgruppenanalyse der intermediären Stenosen konnte eine signifikant verbesserte diagnostische Genauigkeit der CT-basierten FFR gegenüber der rein visuell interpretierten koronaren CT-Angiografie gezeigt werden.

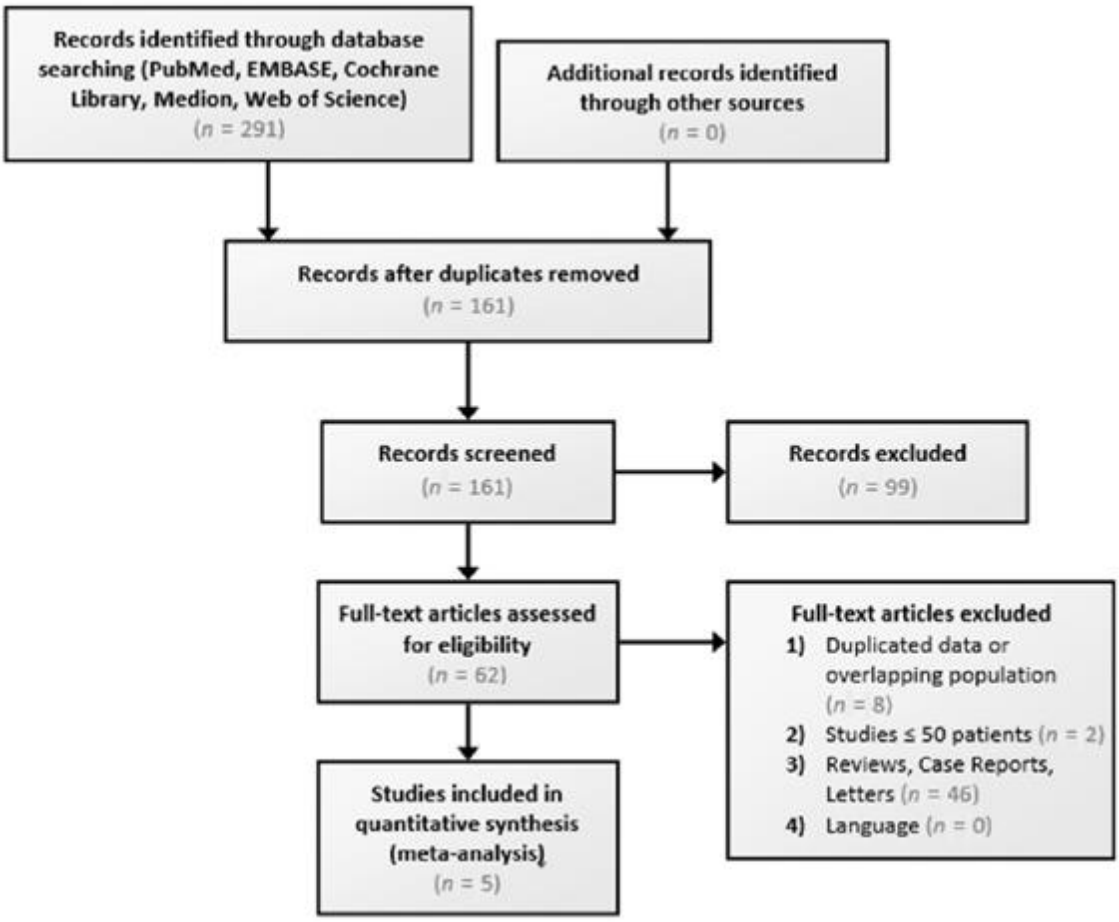

Abb. 26: Flussdiagramm der Metaanalyse (Quelle: PUBLIKATION 6, mit Genehmigung)

	Koo et al. (DISCOVER-FLOW)	Min et al. (DeFACTO)	Nørgaard et al. (NXT Trial)	Renker et al.	Coenen et al.
Journal	J Am Coll Cardiol	JAMA	J Am Coll Cardiol	Am J Cardiol	Radiology
Year	2011	2012	2014	2014	2014
Study design	Multicenter, (4 centers in 3 countries), prospective	Multicenter (17 centers in 5 countries), prospective	Multicenter (10 centers in 8 countries), prospective	Single-center, retrospective	Single-center, retrospective
CT system	64- or 256-detector CT	64- or higher detector CT	64- or higher detector CT	64- or 128-section dual-source CT	64- or 128-section dual-source CT
CT-FFR software (manufacturer)	FFR_{CT} (HeartFlow, Inc., Redwood City, CA), V1.2	FFR_{CT} (HeartFlow, Inc., Redwood City, CA), V1.2	FFR_{CT} (HeartFlow, Inc., Redwood City, CA), V1.4	cFFR (Siemens Healthcare, Forchheim, Germany), V1.4*	cFFR (Siemens Healthcare, Forchheim, Germany), V1.4*
Number of included patients	103	252	251	53	106
Number of excluded patients	NA	33/285 (11.6%)	111/365 (30.4%)	19/64 (29.7%)	16/122 (13.1%)
Number of vessels	159	407	484	67	189
Age (years)	62.7 ± 8.5	62.9 ± 8.7	64 ± 10	61.2 ± 12.0	61.4 ± 9.2
Male (%)	74 (72%)	178 (70.6%)	162 (64%)	34 (64%)	82 (77%)
BMI (kg/m^2)	25.8 ± 3.5	NA	26 ± 3	28.9 ± 6.5	27.2 ± 4.0
Diabetes mellitus (%)	26 (26%)	53 (21.2%)	58 (23%)	18 (32%)	20 (19%)
Hypertension (%)	67 (65%)	179 (71.2%)	174 (69%)	31 (54%)	63 (59%)
Hyperlipidemia (%)	67 (65%)	201 (79.8%)	200 (79%)	21 (54%)	63 (59%)
Current smoker (%)	24 (36%)	44 (17.5%)	46 (18%)	8 (14%)	26 (25%)

Abb. 27: Übersicht der in der Metaanalyse eingeschlossenen Studien (Quelle: PUBLIKATION 6, mit Genehmigung)

Die Werte sind angegeben als Mittelwerte ± Standardabweichung oder Häufigkeit (%).

BMI: Köpermaßindex

CT-FFR: CT-basierte FFR

NA: nicht verfügbar

	Koo et al. (DISCOVER-FLOW)	Min et al. (DeFACTO)	Nørgaard et al. (NXT Trial)	Renker et al.	Coenen et al.
Invasive coronary angiography (ICA)					
ICA stenosis ≥50% (%)	NA	190 (46.5%)	81 (32%)	44 (66%)	87 (46.0%)
FFR ≤0.80 (%)	35 (23%)	151 (37.1%)	100 (21%)	20 (30%)	80 (42.3%)
Coronary computed tomography angiography (cCTA)					
Agatston score (±SD)	NA	381.5 ± 401.0	302 ± 468	778.4 ± 731.1	555 ± 542
cCTA stenosis ≥50% (%)	NA	216 (53.2%)	220 (87%)	55 (82%)	133 (70.4%)
CT-FFR ≤0.80 (%)	NA	216 (53.3%)	135 (28%)	24 (36%)	108 (57.1%)

Abb. 28: Übersicht der Koronarbefunde für die einzelnen Studien der Metaanalyse (Quelle: PUBLIKATION 6, mit Genehmigung)

Die Werte sind angegeben als Mittelwerte ± Standardabweichung oder Häufigkeit (%).

cCTA: koronare CT-Angiografie

CT-FFR: CT-basierte FFR

ICA: invasive Koronarangiografie

NA: nicht verfügbar

	Koo et al. (DISCOVER-FLOW)	Min et al. (DeFACTO)	Nørgaard et al. (NXT Trial)	Renker et al.	Coenen et al.	Pooled
Per-vessel (n = 1306) diagnostic performance of CT-FFR <0.80 (95% CI) and cCTA ≥50% (95% CI) [in brackets]						
Number of vessels	159	407	484	67	189	1306
Sensitivity (%)	87.9 (76.7–95.0) [91.4 (81.0–97.1)]	80 (73–86) [NA]	84 (75–89) [83 (74–89)]	85 (62–97) [90 (68–98)]	87.5 (78.2–93.8) [81.3 (71.0–89.1)]	83.7 (78.1–89.3) [84.6 (78.1–91.1)]
Specificity (%)	82.2 (73.3–89.1) [39.6 (30.0–49.8)]	61 (54–67) [NA]	86 (82–89) [60 (56–65)]	85 (72–94) [34 (21–49)]	65.1 (55.4–74.0] [37.6 (28.5–47.4)]	74.7 (52.2–97.1) [49.7 (31.1–68.4)]
PPV (%)	73.9 (61.9–83.7) [46.5 (37.1–56.1)]	56 (49–62) [NA]	61 (53–69) [33 (27–39)]	71 (49–87) [37 (23–52)]	64.8 (55.0–73.8)] [48.9 (40.1–57.7)]	64.8 (52.1–77.5) [39.0 (28.0–50.1)]
NPV (%)	92.2 (84.6–96.8] [88.9 (75.9–96.3)]	84 (78–89) [NA]	95 (93–97) [92 (88–95)]	93 (81–98) [89 (65–98)]	87.7 (78.5–93.9) [73.2 (59.7–84.2)]	90.1 (80.8–99.3) [87.3 (72.5–100.0)]
Accuracy (%)	84.3 (77.7–90.0) [58.5 (50.4–66.2)]	NA [NA]	86 (83–89) [65 (61–69)]	NA [NA]	74.6 (68.4–80.8) [56.1 (49.0–63.2)]	83.1 (74.0–92.2) [61.7 (56.6–66.9)]
AUC	0.90 (NA) [0.75 (NA)] (P = .001)	NA [NA]	0.93 (0.91–0.95) [0.79 (0.74–0.84)] (P < .001)	0.92 (NA) [0.72(NA)] (P < .005)	0.83 (NA) [0.64 (NA)] (P < .001)	0.90 (0.82–0.98) [0.74 (0.63–0.86)] (P = .0047)
Correlation between CT-FFR and FFR						
Per-vessel correlation	Pearson's correlation coefficient = 0.678 (p < 0.0001)	Pearson correlation coefficient = 0.63 (P = NA)	Pearson correlation coefficient = 0.82 (P < .001)	NA	Pearson correlation coefficient = 0.59 (P = NA)	NA
	Spearman's rank correlation coefficient = 0.717 (p < 0.0001)	NA	NA	Spearman rank correlation coefficient = 0.66 (P < .001)	NA	NA

Abb. 29: Diagnostische Genauigkeit der CT-basierten FFR und koronaren CT-Angiografie auf Läsionsebene, gemessen an invasiver FFR (Quelle: PUBLIKATION 6, mit Genehmigung)

cCTA: koronare CT-Angiografie

CI: Konfidenzintervall

CT-FFR: CT-basierte FFR

NA: nicht verfügbar

NPV: negativ prädiktiver Wert

PPV: positiv prädiktiver Wert

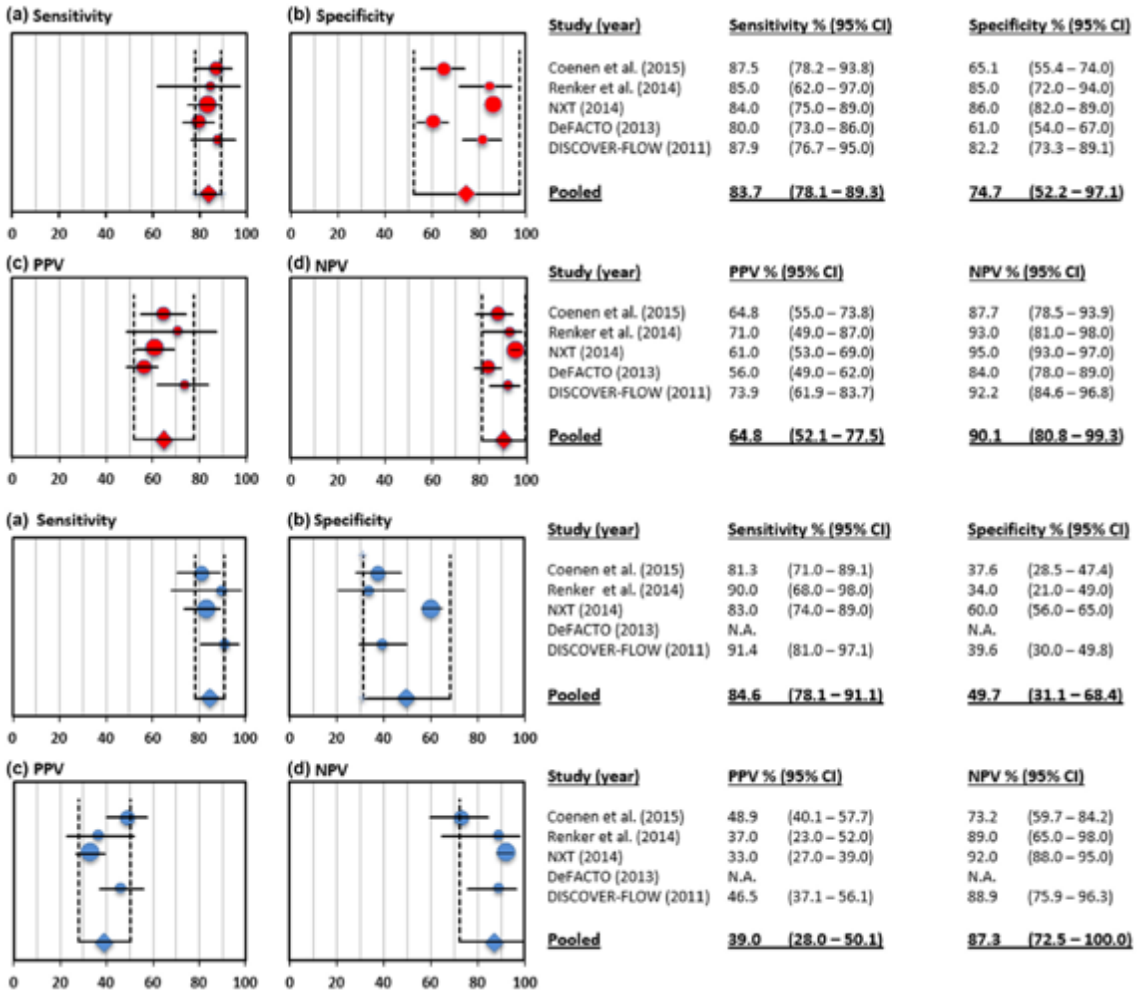

Abb. 30: Wald-Diagramm der gepoolten Ergebnisse der diagnostischen Genauigkeit der CT-basierten FFR (Quelle: PUBLIKATION 6, mit Genehmigung)

Aufgeführt sind die Sensitivität, die Spezifität, der negativ prädiktive Wert und der positiv prädiktive Wert sowohl für die CT-basierten FFR (rote Punkte), als auch die koronare CT-Angiografie (blaue Punkte) auf Läsionsebene, verglichen mit der invasiven FFR als Referenzstandard.

CI: Konfidenzintervall

N.A.: nicht verfügbar

NPV: negativ prädiktiver Wert

PPV: positiv prädiktiver Wert

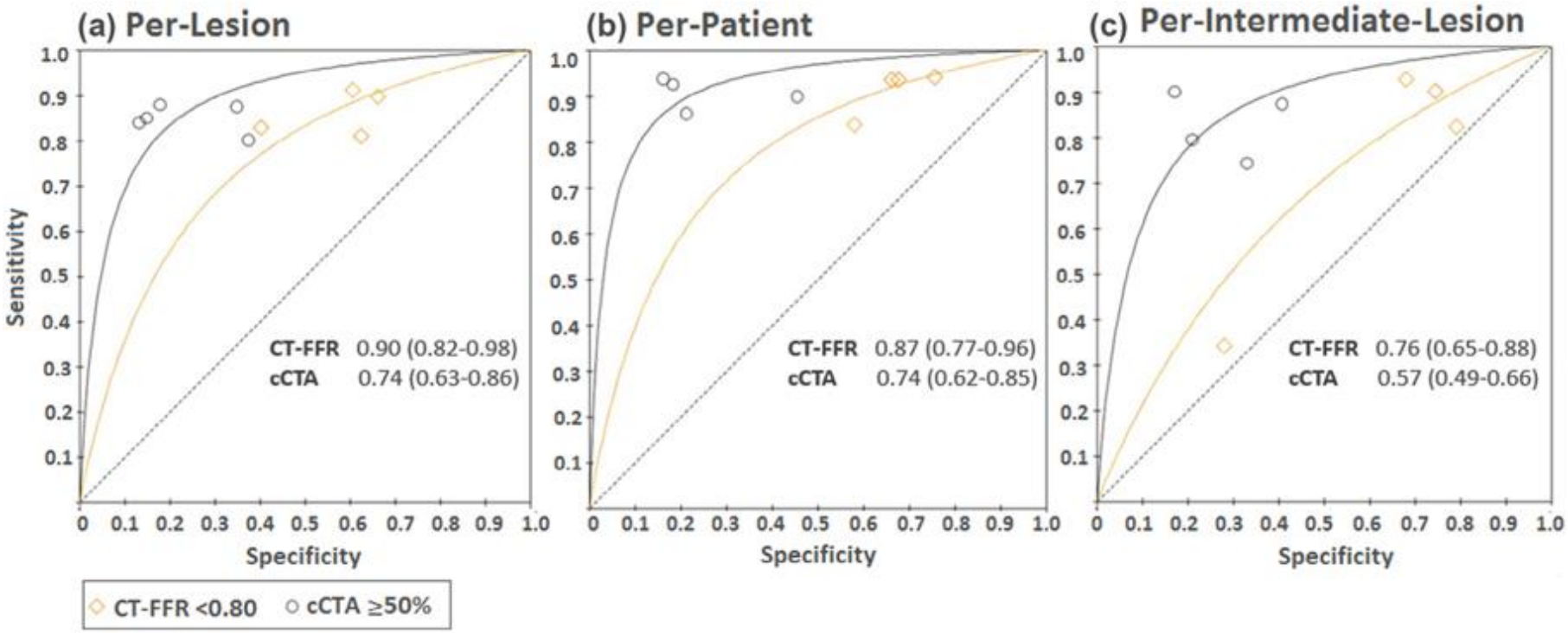

Abb. 31: Summations-AUC der CT-basierten FFR (schwarze Linie) und der koronaren CT-Angiografie (gelbe Linie), gemessen an der invasiven Referenz FFR, auf Patienten- (a) und Läsionsebene (b). Zudem sind die Summations-AUCs der Verfahren separat aufgetragen für intermediäre Stenosen (c) (Quelle: PUBLIKATION 6, mit Genehmigung)

cCTA: koronare CT-Angiografie

CT-FFR: CT-basierte FFR

Substudy	Koo et al. (DISCOVER-FLOW) Min et al. Am J Cardiol 2012	Min et al. (DeFACTO) Nakazato Circ Imaging 2013	Nørgaard et al. (NXT Trial)	Renker et al.	Coenen et al.	Pooled
Number of vessels with intermediate stenosis (30%–70%)	66/159* (41.5%)	150/407 (36.9%)	235/484 (48.6%)	39/67 (58.2%)	144/189 (76.2%)	634/1306 (48.5%)
Sensitivity (%)	90 (28–31) [90 (28–31)]	74 (57–88) [34 (19–52)]	80 (75–85) [93 (85–97)]	NA	87.3 (76.5–94.3) [82.5 (70.9–90.9)]	81.4 (70.4–92.3) [75.3 (27.6–100.0)]
Specificity (%)	83 (29–35) [26 (9–35)]	67 (58–75) [72 (63–80)]	79 (72–84) [32 (26–40)]	NA	59.3 (47.8–70.1) [21.0 (12.7–31.5)]	71.7 (54.3–89.0) [38.8 (25.6–77.5)]
PPV (%)	82 (28–34) [52 (28–54)]	41 (29–54) [27 (15–43)]	63 (53–72) [37 (31–44)]	NA	62.5 (51.5–72.6) [44.8 (35.6–54.3)]	59.4 (35.5–83.4) [38.0 (22.4–53.7)]
NPV (%)	91 (29–32) [75 (9–12)]	90 (81–95) [78 (69–86)]	92 (87–96) [91 (81–96)]	NA	85.7 (73.8–93.6) [60.7 [40.6–78.5)]	89.9 (85.0–94.7) [78.6 (55.4–100.0)]
Accuracy (%)	86 (57–66) [56 (43–68)]	69 (61–76) [63 (55–71)]	80 (75–85) [51 (44–57)]	NA	71.5 (64.2–78.9) [47.9 (39.8–56.1)]	75.9 (62.5–89.2) [55.1 (43.9–66.4)]
AUC	0.86 (0.78–0.95) [0.58 (0.49–0.67)] ($P < .0001$)	0.71 (0.62–0.79) [0.53 (0.44–0.62)] ($P = .0063$)	0.79 (0.74–0.85) [0.63 (0.58–0.67)] ($P < .0001$)	NA NA	0.73 (0.66–0.80) [0.52 (0.45–0.58)] ($P < .0001$)	0.76 (0.65–0.88) [0.57 (0.49–0.66)] ($P = .0027$)

Abb. 32: Diagnostische Genauigkeit der CT-basierten FFR auf Läsionsebene in der Subgruppe der Erkrankten mit intermediärer Stenose (n = 634) (Quelle: PUBLIKATION 6, mit Genehmigung)

cCTA: koronare CT-Angiografie

CT-FFR: CT-basierte FFR

NA: nicht verfügbar

NPV: negativ prädiktiver Wert

PPV: positiv prädiktiver Wert

** Intermediäre Stenosen wurden definiert als 40–69 % luminale Einengung in quantitativer Analyse der Koronarangiografie.*

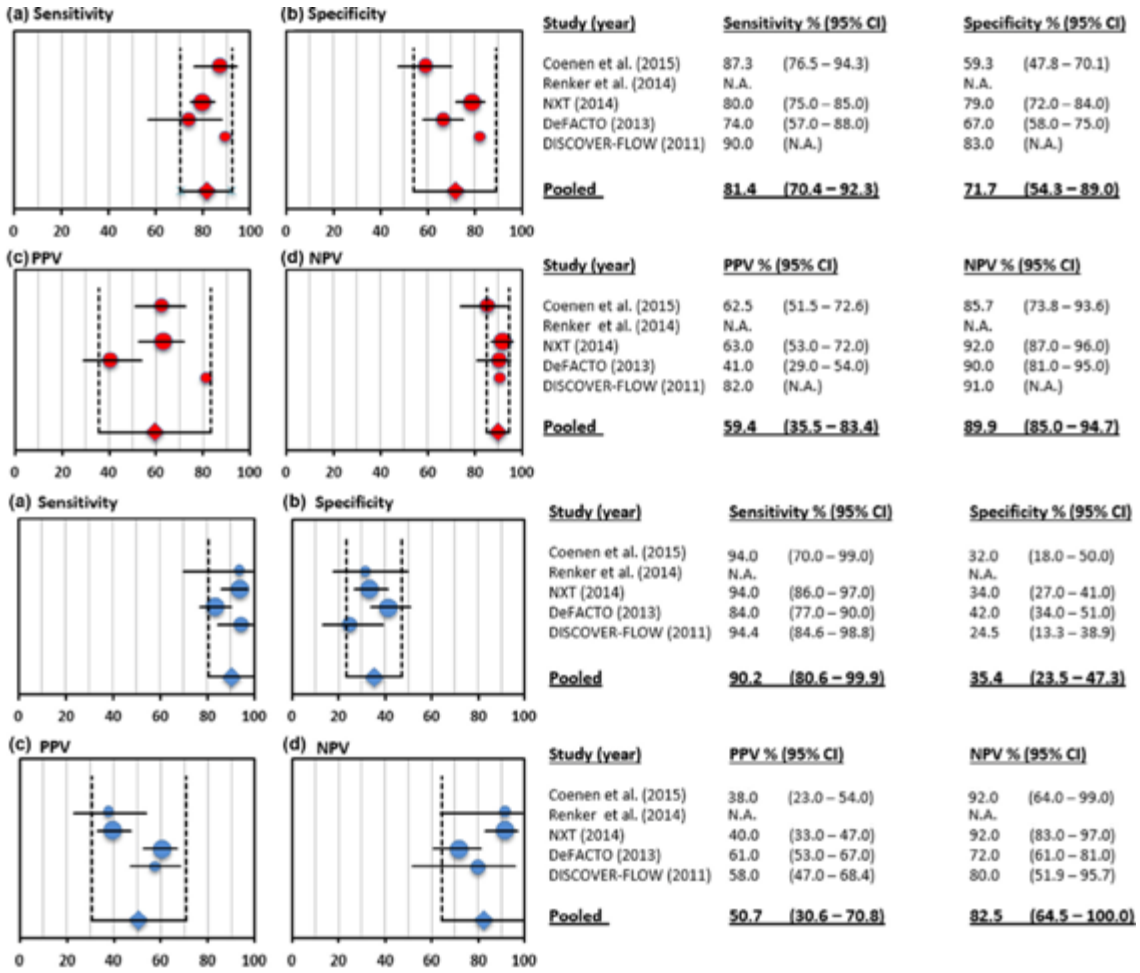

Abb. 33: Wald-Diagramm der gepoolten Ergebnisse der diagnostischen Genauigkeit der CT-basierten FFR in intermediären Stenosen (Quelle: PUBLIKATION 6, mit Genehmigung)

Aufgeführt sind die Sensitivität, die Spezifität, der negativ prädiktive Wert und der positiv prädiktive Wert für die CT-basierte FFR (rote Punkte) und die koronare CT-Angiografie (blaue Punkte) auf Läsionsebene in der Subgruppe intermediärer Stenosen, verglichen mit der invasiven FFR als Referenzstandard.

CI: Konfidenzintervall

N.A.: nicht verfügbar

NPV: negativ prädiktiver Wert

PPV: positiv prädiktiver Wert

5.3 Anwendung maschineller Lernverfahren

Die artifizielle Intelligenz ist ein Teilbereich der Informatik. Im Kern werden hierbei kognitive Fähigkeiten des Menschen nachempfunden. Aus zum Teil umfangreichen Daten filtert und klassifiziert ein Computer-basierter Algorithmus relevante Informationen. Solche Abläufe können entweder programmiert sein, oder aber durch maschinelle Lernverfahren (ML) realisiert werden. Aufgrund der vorhandenen Technologien zur Verarbeitung und Auswertung immer größerer Datenmengen („Big Data“) rückt ML zunehmend in den Vordergrund. Die wesentliche Voraussetzung für artifizielle Intelligenz zur Bearbeitung der Datenmengen ist durch die enorm gesteigerte Rechnerleistung gegeben.

Ein Computer-basierter Algorithmus kann im Rahmen von ML durch Repetition eigenständig Anforderungen erfüllen lernen. Ohne vorgegebenen Lösungsweg richtet sich der Algorithmus zunehmend genau nach definierten Gütekriterien und dem Informationsgehalt der Daten aus und entwickelt ein Modell für die Bearbeitung unbekannter Datensätze (77). Durch ML erfasst der Algorithmus in der Folge die Struktur der eingehenden Daten, klassifiziert Informationen, und erkennt darin Muster (77). Daraus resultiert, dass Algorithmen mithilfe von ML Ergebnisse vorhersagen und fundierte Entscheidungen treffen können. Ein weiterer Vorteil liegt in der Prozessgeschwindigkeit. Die Anwendung erfolgt ohne Zeitverzug durch komplexe Rechenprozesse, sodass Resultate nahezu unmittelbar vorliegen (78). Mittlerweile ist bereits eine Vielzahl an Modellen basierend auf ML bekannt. Zentral für die Wertigkeit eines Modells sind die definierten Gütekriterien. Weiterhin ist sowohl die Qualität, als auch die Quantität der zur Entstehung des Modells eingegebenen Daten entscheidend (77).

Die vorgenannten Eigenschaften von ML sind in der Medizin und insbesondere in der medizinischen Diagnostik aufgrund des zunehmenden Einsatzes bilgebender Verfahren gefragt (79, 80). Auch in der kardiovaskulären Bildgebung haben diese bereits Einzug erhalten (81-83). Beispielsweise konnte in einer prospektiv angelegten multizentrischen Registerstudie von Motwani et al.

(83) gezeigt werden, dass ein Algorithmus mithilfe von ML klinische Patientencharakteristika und Informationen der koronaren CT-Angiografie für Mortalitätsprognosen nutzen konnte. Diese Prognosen waren signifikant genauer, als solche von etablierten Risikokalkulatoren.

Wie durch Itu et al. (78) beschrieben, wurden die Vorteile von ML zudem genutzt, um einen Algorithmus für die instantane Vorhersage CT-basierter FFR zu generieren. Zunächst wurden 12000 synthetische dreidimensionale Koronarmodelle mit vielfältigen Koronaranatomien und unterschiedlichem Ausmaß an KHK verwendet, um den ML-Algorithmus zu trainieren. Hierbei wurde ein sogenanntes „*deep learning*“ Verfahren verwendet, um insgesamt 28 Kriterien für die Vorhersage der errechneten CT-basierten FFR zu extrahieren. An der durch Coenen et al. (84) publizierten Validierungsstudie des ML-Algorithmus (cFFR version 2.1, Siemens Healthineers, Forchheim, Deutschland; derzeit nicht kommerziell verfügbar) nahmen 5 internationale Zentren teil. Diese stellten ihre Ergebnisse mit dem in den PUBLIKATIONEN 4, 5 und 6 beschriebenen CT-basierten FFR-Algorithmus cFFR im Rahmen des MACHINE (*Machine Learning Based CT Angiography Derived FFR: A Multi-Center Registry*) Konsortiums zur Verfügung. Gemessen an invasiver FFR ergab sich für den ML-Algorithmus und den CT-basierten FFR-Algorithmus eine vergleichbar gute diagnostische Genauigkeit. Beide Verfahren schnitten hierbei signifikant besser ab, als die konventionelle koronare CT-Angiografie.

5.3.1 Untersuchung eines maschinellen Lernalgorithmus für CT-basierte FFR mit Fokus auf Stenosenlokalisation (PUBLIKATION 7)

Diese Arbeit stellt eine Substudie des von Coenen et al. (84) beschriebenen multizentrischen MACHINE-Registers dar. Sie zielte auf die Beurteilung der diagnostischen Genauigkeit des ML-Algorithmus für CT-basierte FFR in Abhängigkeit von der Lokalisation der Koronarstenosen ab. Hierbei wurden Patientinnen und Patienten mit invasiver Koronarangiografie inklusive FFR und koronarer CT-Angiografie aus den beteiligten Zentren eingeschlossen. Im Rahmen der Substudie wurden die Ergebnisse des ML-Algorithmus und der koronaren CT-Angiografie unter Beachtung der Stenosenlokalisation mit der invasiven FFR als diagnostischer Referenz verglichen.

Von der Studie ausgeschlossen wurden Personen mit vorheriger Stentimplantation im Zielgefäß, stattgehabter koronarer Bypassoperation, Verdacht auf Vorliegen eines akuten Koronarsyndroms, signifikanten Arrhythmien, Körpermaßindex > 35 kg/m^2 sowie Kontraindikation gegenüber Betablockern, Nitraten oder Adenosin. Die für diese Substudie relevanten Informationen lagen bei 330 (94 %) der insgesamt 351 Patientinnen und Patienten des MACHINE-Registers vor. Diese 330 Patientinnen und Patienten mit insgesamt 502 Stenosen gingen in weiterführende Analysen ein. Die Werte des ML-Algorithmus und der CT-basierten FFR wurden jeweils an der selben Stelle abgelesen, wie die der invasiven FFR. Werte ≤ 0.80 wurden als hämodynamisch relevant definiert. Die Befundung der koronaren CT-Angiografie folgte den Emfehlungen der *Society of Cardiovascular Computed Tomography*; hämodynamisch relevante Stenosen wurden als ≥ 70 % luminale Einengung definiert (85). Die Lage der insgesamt 502 weiterführend zu untersuchenden Läsionen wurde nach Zugehörigkeit zu entweder der rechten Koronararterie, dem Ramus interventricularis anterior oder dem Ramus circumflexus unterteilt. Gemäß invasiver FFR fand sich hämodynamische Relevanz von Läsionen in der rechten Koronararterie in 29/124 (23.4 %) Fällen, im Ramus interventricularis anterior in 138/265 (52.1 %) Fällen und im Ramus circumflexus in 39/113

(34.5 %) Fällen. Weiterhin wurden die Läsionen nach proximaler, medialer oder distaler Lage unterteilt. Gemäß invasiver FFR fand sich hämodynamische Relevanz von Läsionen in den proximalen Koronarsegmenten in 75/163 (46.0 %) Fällen, in den medialen Koronarsegmenten in 95/244 (38.9 %) Fällen und in den distalen Koronarsegmenten in 36/95 (37.9 %) Fällen. Weitere demografische Charakteristika und Untersuchungsergebnisse werden in Abb. 34 gezeigt. Es konnte eine hohe Korrelation zwischen dem ML-Algorithmus und invasiver FFR für alle Stenoselokalisationen nachgewiesen werden. Dies ist in den jeweiligen Streudiagrammen (Abb. 35) nachvollziehbar. In den Punktdiagrammen nach Bland-Altmann fand sich kein systematischer Fehler (Abb. 36). In Bezug auf die Spezifität und den positiv prädiktiven Wert zeigte der ML-Algorithmus eine deutliche Verbesserung im Vergleich zur konventionellen koronaren CT-Angiografie in allen untersuchten Gefäßabschnitten (Abb. 37 und Abb. 38). Auch die AUC des ML-Algorithmus war der der koronaren CT-Angiografie für Stenosen in allen Gefäßabschnitten überlegen (Abb. 39). Einzig für Stenosen in der RCA waren die jeweiligen AUC vergleichbar. Ein repräsentatives Fallbeispiel mit dem ML-Algorithmus ist in Abb. 40 gezeigt.

Schlussfolgernd korreliert der ML-Algorithmus gut mit der invasiven FFR und zeigt verglichen mit der koronaren CT-Angiograpfie eine signifikant bessere diagnostische Genauigkeit zur Erfassung hämodynamisch relevanter Koronarstenosen unabhängig von deren Lokalisation.

Clinical baseline characteristics and procedural results from 330 patients with 502 vessels.

Parameter	Result
Demographic data	
Age [y]	63 (56–69)
Female	82 (24.8%)
Body mass index [kg/m^2][a]	26.8 (24.5–29.1)
Heart rate during cCTA [bpm]	63 (57–70)
Cardiovascular risk factors	
Hypertension	216 (65.5%)
Hyperlipidemia	196 (59.4%)
Family history of coronary artery disease	107 (32.4%)
Current smoker	117 (35.5%)
Diabetes mellitus	72 (21.8%)
Coronary CT angiography	
Image quality, 1–4[b]	3 (3–4)
Tube voltage [kV]	100 (100–120)
Tube current [mA]	246 (165–341)
Dose length product [mGy x cm]	529 (360–784)
Left ventricular mass [g]	163 (144–181)
Agatston-Score[c]	238 (39–676)
Agatston-Score 0	28 (8.9%)
Agatston-Score >400	128 (40.7%)
Patients with cCTA stenosis ≥50%	323 (97.9%)
Patients with cCTA stenosis ≥70%	287 (87.0%)
Vessels with cCTA stenosis ≥50%	435 (86.7%)
Vessels with cCTA stenosis ≥70%	364 (72.5%)
Patients with ML-CT-FFR ≤0.80	237 (71.8%)
Vessels with ML-CT-FFR ≤0.80	236 (47.0%)
Invasive coronary angiography	
Patients with invasive FFR ≤0.80	241 (73.0%)
Vessels with invasive FFR ≤0.80	206 (41.0%)

Values are median (interquartile range) or n (%).

[a] Data was not available in 9 patients.

[b] 1, poor; 2, satisfactory; 3; good; 4, excellent.

[c] Data was not available in 16 patients.

Abb. 34: Klinische Charakteristika des finalen Patientenkollektivs (Quelle: PUBLIKATION 7, mit Genehmigung)

cCTA: koronare CT-Angiografie

ML-CT-FFR: maschineller Lernalgorithmus für CT-basierte FFR

[a] Werte nicht verfügbar in 9 Personen.

[b] Bildqualität: 1, nicht diagnostisch; 2: ausreichend; 3: gut; 4: exzellent.

[c] Werte nicht verfügbar in 16 Personen.

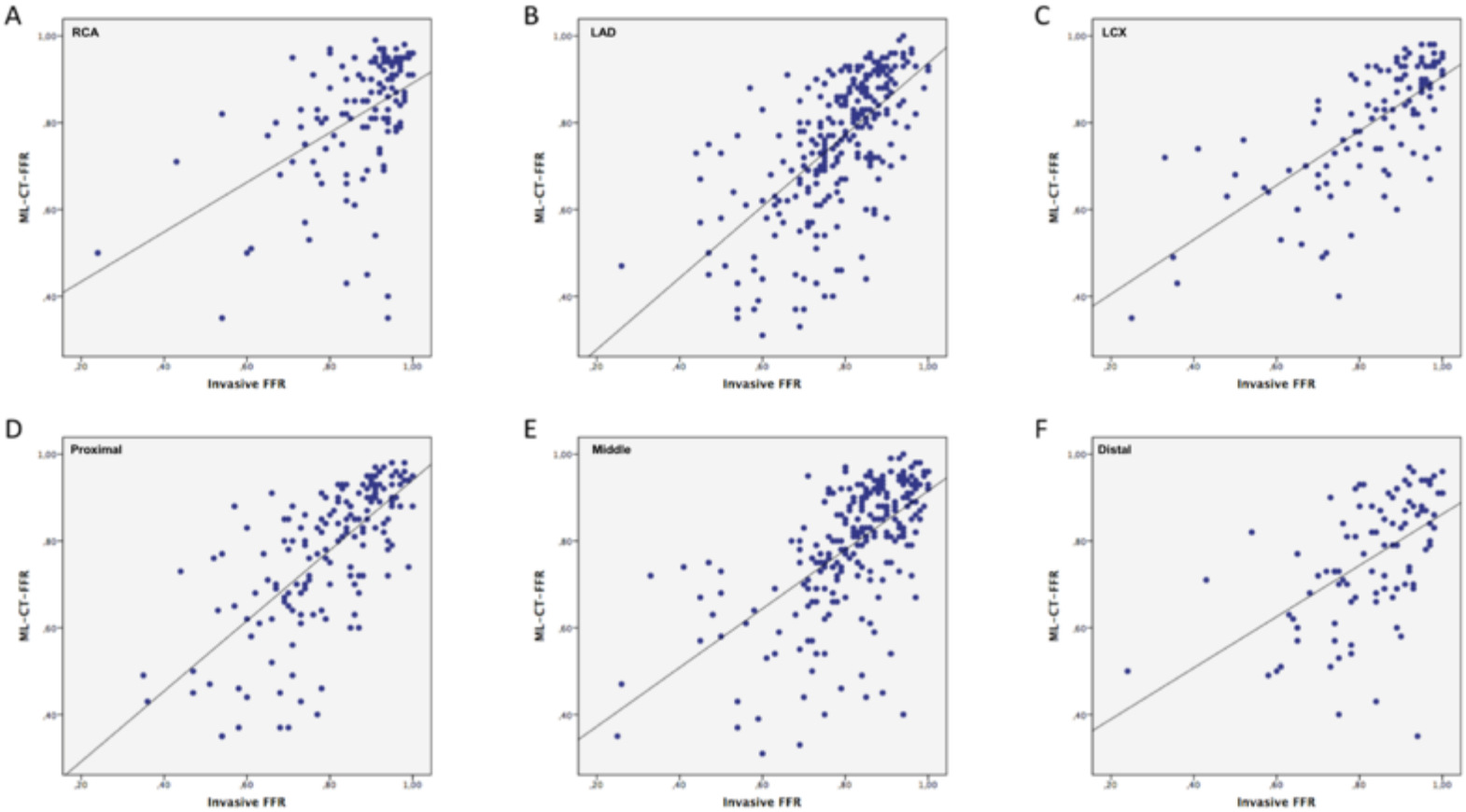

Abb. 35: Korrelation des maschinellen Lernalgorithmus mit der invasiven FFR nach Lage der Stenosen (Quelle: PUBLIKATION 7, mit Genehmigung)

ML-CT-FFR: maschineller Lernalgorithmus für CT-basierte FFR

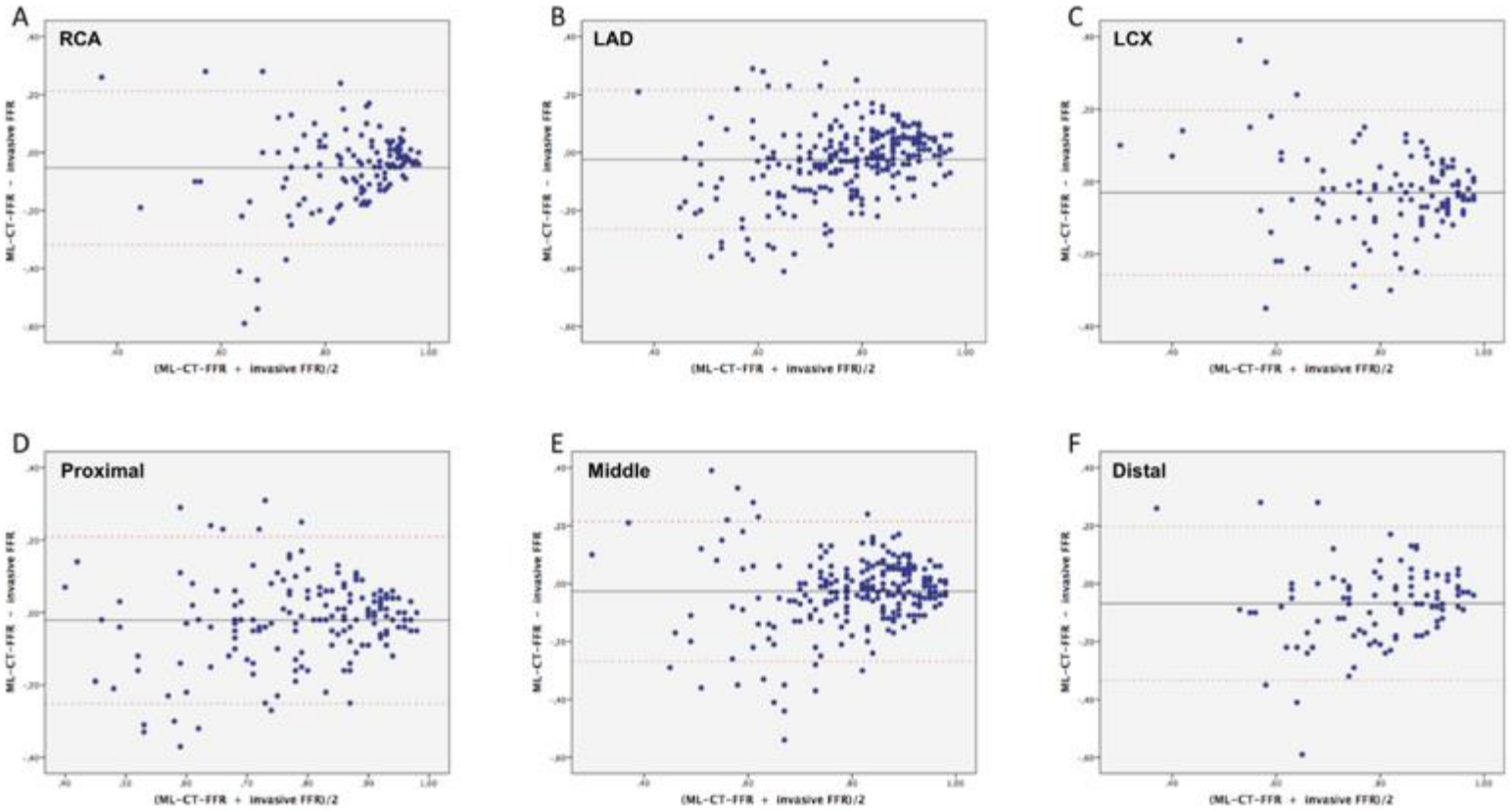

Abb. 36: Punktdiagramm nach Bland-Altman zum Vergleich des maschinellen Lernalgorithmus mit der invasiven FFR nach Lage der Stenosen (Quelle: PUBLIKATION 7, mit Genehmigung)

ML-CT-FFR: maschineller Lernalgorithmus für CT-basierte FFR

Per-vessel diagnostic performance of cCTA and ML-CT-FFR for the detection of hemodynamically relevant stenosis in RCA, LAD, and LCX (n = 502).

	RCA			LAD			LCX		
	cCTA (≥50%)	cCTA (≥70%)	ML-CT-FFR	cCTA (≥50%)	cCTA (≥70%)	ML-CT-FFR	cCTA (≥50%)	cCTA (≥70%)	ML-CT-FFR
Accuracy	45.2 (36.2–54.4)	54.8 (45.7–63.8)	71.8 (63.0–79.5)	54.7 (48.5–60.8)	59.6 (53.5–65.6)	79.3 (73.9–84.0)	54.9 (45.2–64.2)	63.7 (54.1–72.6)	84.1 (76.0–90.3)
Sensitivity	96.6 (82.2–99.9)	89.7 (72.7–97.8)	65.5 (45.7–82.1)	97.8 (93.7–99.6)	90.6 (84.4–94.9)	82.6 (75.2–88.5)	97.4 (86.5–99.9)	82.1 (66.5–92.5)	87.2 (72.6–95.7)
Specificity	29.5 (20.6–39.7)	44.2 (34.0–54.8)	73.7 (63.7–82.2)	8.6 (4.4–14.9)	26.0 (18.6–34.5)	75.6 (67.2–82.8)	32.4 (22.0–44.3)	54.1 (42.1–65.7)	82.4 (71.8–90.3)
PPV	29.5 (26.5–32.6)	32.9 (28.3–37.9)	43.2 (33.1–53.8)	53.4 (51.9–54.9)	57.1 (54.2–59.9)	78.6 (72.8–85.4)	43.2 (39.2–47.3)	48.5 (41.4–55.7)	72.3 (61.1–81.3)
NPV	96.6 (79.9–99.5)	93.3 (82.4–97.7)	87.5 (80.7–92.1)	78.6 (51.1–92.8)	71.7 (58.3–82.2)	80.0 (73.3–85.4)	96.0 (77.1–99.4)	85.1 (73.9–92.0)	92.4 (84.2–96.5)

Values are % (CI). Positive test results are defined as stenosis ≥50% or ≥70% on cCTA, and ML-CT-FFR ≤0.80.

Abb. 37: Diagnostische Genauigkeit des maschinellen Lernalgorithmus verglichen mit der koronaren CT-Angiografie und gemessen an der invasiven FFR (Quelle: PUBLIKATION 7, mit Genehmigung)

ML-CT-FFR: maschineller Lernalgorithmus für CT-basierte FFR

Per-vessel diagnostic performance of cCTA and ML-CT-FFR for the detection of hemodynamically relevant stenosis in proximal, middle, and distal vessel segments (n = 502).

	Proximal			Middle			Distal		
	cCTA (≥50%)	cCTA (≥70%)	ML-CT-FFR	cCTA (≥50%)	cCTA (≥70%)	ML-CT-FFR	cCTA (≥50%)	cCTA (≥70%)	ML-CT-FFR
Accuracy	58.3 (50.3–65.9)	63.8 (55.9–71.2)	81.5 (74.6–87.1)	50.8 (44.4–57.3)	59.4 (53.0–65.6)	81.2 (75.7–85.9)	46.3 (36.0–56.9)	51.6 (41.1–62.0)	67.4 (57.0–76.6)
Sensitivity	100.0 (95.1–100.0)	93.3 (85.1–97.8)	80.0 (69.2–88.4)	96.8 (91.1–99.3)	86.3 (77.7–92.5)	83.2 (74.1–90.1)	94.4 (81.3–99.3)	86.1 (70.5–95.3)	77.8 (60.9–89.9)
Specificity	23.6 (15.2–33.8)	38.6 (28.4–49.6)	82.8 (73.2–90.0)	21.5 (15.2–28.9)	42.3 (34.2–50.6)	79.9 (72.5–86.0)	17.0 (8.4–29.0)	30.5 (19.2–43.9)	61.0 (47.4–73.5)
PPV	45.4 (37.6–53.4)	56.5 (52.1–60.7)	80.0 (71.4–86.5)	38.9 (32.8–45.4)	48.8 (44.9–52.8)	72.5 (65.4–78.6)	41.0 (37.6–44.4)	43.1 (37.9–48.4)	54.9 (45.8–63.7)
NPV	52.1 (49.2–55.0)	87.2 (73.7–94.3)	82.8 (75.1–88.4)	91.4 (77.1–97.1)	82.9 (73.9–89.3)	88.2 (82.5–92.1)	83.3 (53.7–95.6)	78.3 (59.4–89.9)	81.8 (70.3–89.6)

Values are % (CI). Positive test results are defined as stenosis ≥50% or ≥70% on cCTA, and ML-CT-FFR ≤0.80.

Abb. 38: Diagnostische Genauigkeit des maschinellen Lernalgorithmus mit der koronaren CT-Angiografie nach Lage der Stenosen (Quelle: PUBLIKATION 7, mit Genehmigung)

cCTA: koronare CT-Angiografie

ML-CT-FFR: maschineller Lernalgorithmus für CT-basierte FFR

NPV: negativ prädiktiver Wert

PPV: positiv prädiktiver Wert

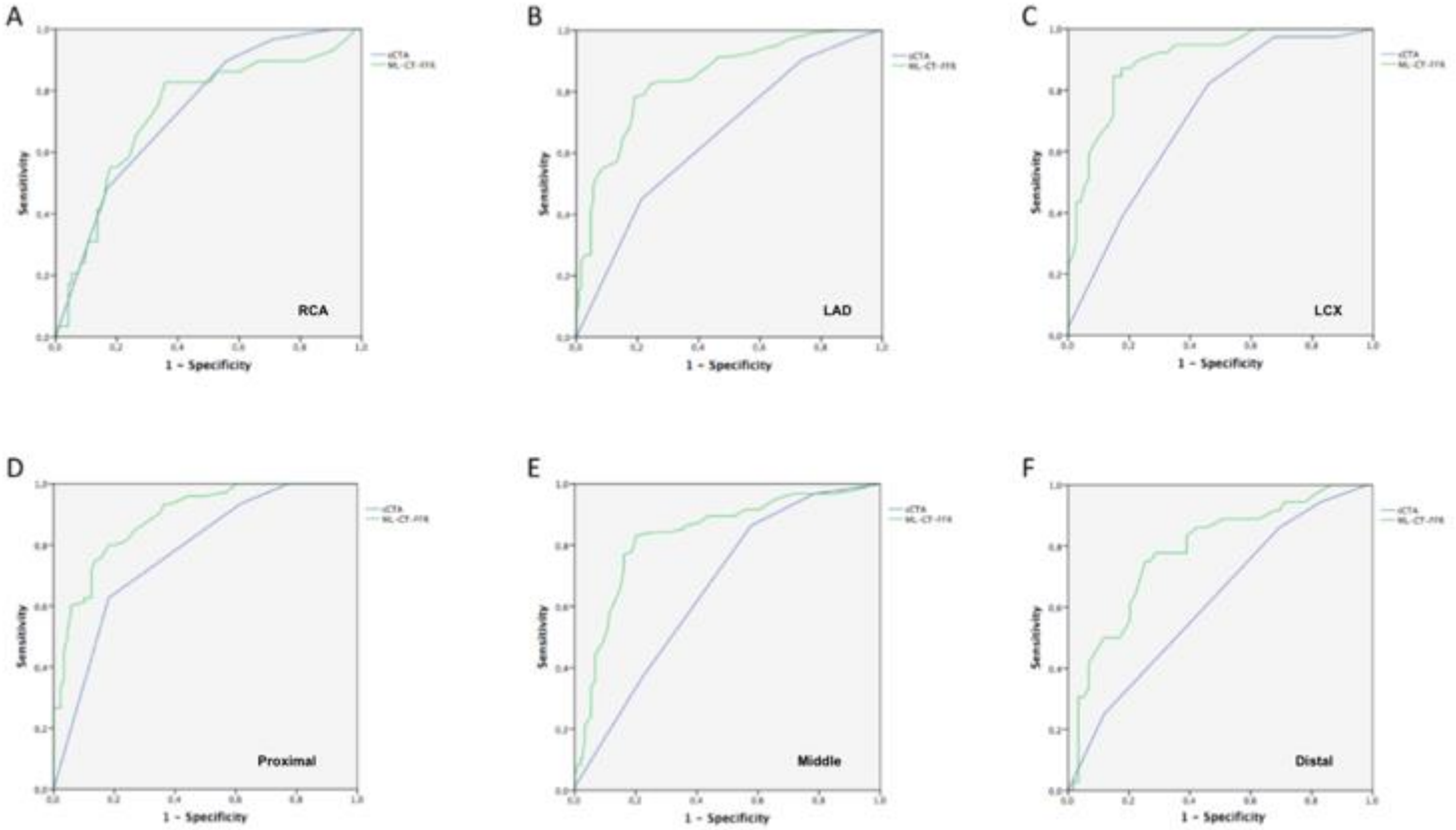

Abb. 39: AUC des maschinellen Lernalgorithmus verglichen mit der koronaren CT-Angiografie nach Lage der Stenosen (Quelle: PUBLIKATION 7, mit Genehmigung)

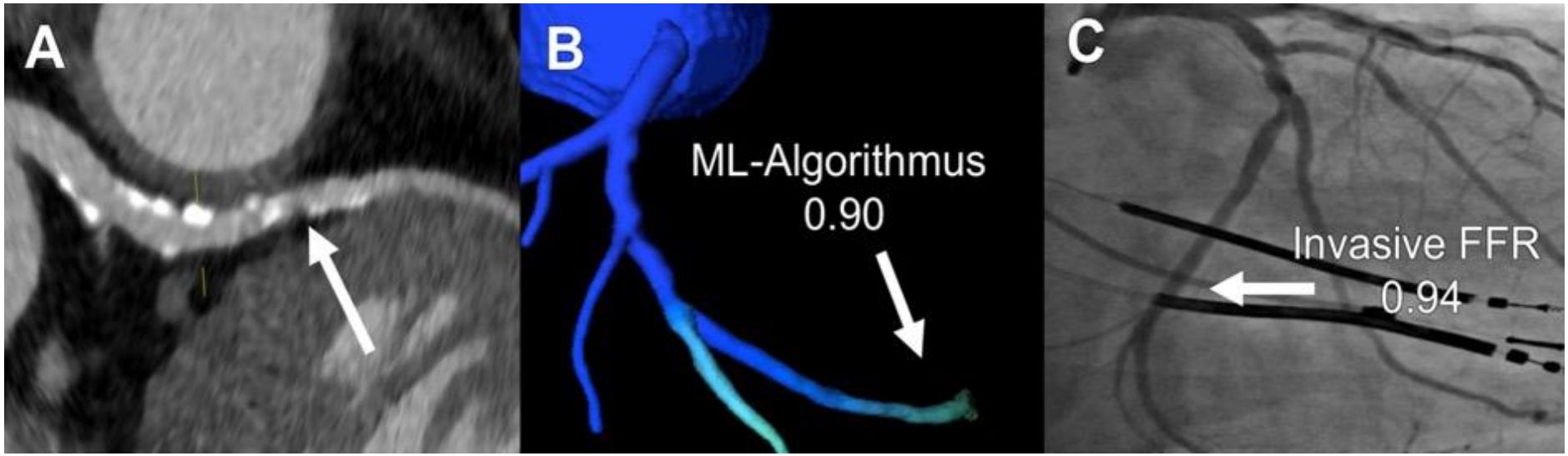

Abb. 40: Fallbeispiel maschineller Lernalgorithmus für CT-basierte FFR (Quelle: PUBLIKATION 7, mit Genehmigung)

Die koronare CT-Angiografie (A) zeigt eine hochgradige (≥ 70 %) Stenose des Ramus circumflexus (Pfeil), während der maschinelle Lernalgorithmus für CT-basierte FFR (B) und die Koronarangiografie mit invasiver FFR (C) keine hämodynamische Relevanz der Stenose anzeigen.

6 Diskussion

Die koronare CT-Angiografie ist mittlerweile fester Bestandteil mehrerer Leitlinien zur Diagnose des chronischen Koronarsyndroms. Dies geht auf eine Vielzahl an Studien mit vorteilhaftem Vergleich zur invasiven Koronarangiografie zurück. Beispielsweise konnte in der multizentrischen SCOT-HEART-Studie von Newby et al. über einen Zeitraum von 5 Jahren erstmalig eine signifikant geringere Sterblichkeit und Herzinfarktrate durch Verwendung koronarer CT-Angiografie zusätzlich zur Standardbehandlung bei Personen mit stabiler Angina pectoris gezeigt werden (4). Die Entwicklungsschritte der koronaren CT-Angiografie von einem visuell-anatomischen Verfahren hin zur Beurteilung der funktionellen Relevanz von Koronarstenosen wurde in der vorliegenden kumulativen Habilitationsschrift anhand einer Auswahl eigener Publikationen erörtert. Ungeachtet der Limitationen einer rein visuellen Einschätzung von Koronarstenosen waren zuvor ausschließlich anatomische Informationen in der koronaren CT-Angiografie maßgeblich. In PUBLIKATION 1 ließ sich zunächst zeigen, dass ein neu entwickeltes iteratives Rekonstruktionsverfahren bei Vorhandensein von Koronarkalk oder Stents Überstrahlungsartefakte reduzieren und die allgemeine Bildqualität günstig beeinflussen kann (36). Dies ließ sich objektivieren durch ein geringeres Volumen von Stents und kalzifizierten Plaques. PUBLIKATION 2 konnte daraufhin den Nachweis erbringen, dass diese neue Rekonstruktionstechnik die diagnostische Genauigkeit der koronaren CT-Angiografie zur Beurteilung von kalzifizierten Koronarstenosen verbessert (86). Mit Einführung der invasiven FFR kam es zu einem Paradigmenwechsel in der invasiven Koronardiagnostik. Dieses Verfahren wurde bald zur diagnostischen Referenz. Parallel hierzu wurde der Fokus auch bei der koronaren CT-Angiografie zunehmend auf eine Bewertung der funktionellen Relevanz von Koronarstenosen gerichtet. In diesem Zusammenhang wurde nachfolgend eine Reihe an morphologischen Plaque-Kriterien und transkoronaren Kontrastgradienten in der Literatur beschrieben. Die vielversprechendsten Parameter wurden in PUBLIKATION 3 vergleichend hinsichtlich deren Prädiktion von Myokardischämie untersucht (87). Des Weiteren wurde die myokardiale

Perfusionsbildgebung mittels CT als Möglichkeit beschrieben, funktionelle Informationen zu erhalten und die hämodynamische Relevanz von Koronarstenosen besser zu erfassen. Die Anwendung neuer Techniken der bildbasierten Modellierung und der numerischen Strömungsmechanik in der koronaren CT-Angiografie stellt einen weiteren Entwicklungsschritt dieses Untersuchungsverfahrens dar, welcher detailliert beschrieben wurde. Initiale Erfahrungen mit einem neuen CT-Algorithmus basierend auf computerbasierter Flussdynamik wurden in PUBLIKATION 4 beschrieben (88). In einer weiterführenden Evaluation konnte PUBLIKATION 5 die verbesserte diagnostische Genauigkeit eines intrahospital anwendbaren CT-basierten FFR-Algorithmus zur Beurteilung der funktionellen Relevanz von Koronarstenosen darlegen (73). Eine Metaanalyse der diagnostischen Genauigkeit der verfügbaren CT-basierten FFR-Algorithmen folgte mit PUBLIKATION 6 und legte einen positiven systematischen Effekt dieses Verfahrens allgemein und bei intermediären Stenosen im Speziellen nahe (89). Als letzter Entwicklungsschritt wurde hier die Einführung künstlicher Intelligenz in der bildgebenden Diagnostik ausgeführt. Die in PUBLIKATION 7 durchgeführte Untersuchung eines maschinellen Lernalgorithmus für CT-basierte FFR mit Fokus auf Stenosenlokalisation konnte Vorteile dieses Verfahrens bei der diagnostischen Genauigkeit im Vergleich zur konventionellen koronaren CT-Angiographie nachweisen (90).

6.1 Kritische Einordnung der eigenen Arbeiten

Iterative Rekonstruktionstechniken, wie in PUBLIKATION 1 und 2 dargelegt, gehören zu den jüngeren technischen Errungenschaften der Untersuchungsmethode (36, 86). Ansatzpunkt für diese beiden eigenen Arbeiten waren die Einschränkungen der koronaren CT-Angiografie mit FBP Bildrekonstruktion insbesondere bei Vorliegen von Stents und fortgeschrittener Koronarkalzifikation. In den Arbeiten von Bittencourt et al. sowie von Leipsic et al. wurden ebenfalls erste Erfahrungen mit unterschiedlichen Verfahren iterativer Rekonstruktion in der koronaren CT-Angiografie beschrieben (33, 91). In Abgrenzung zu diesen anderen Arbeiten, wurde in PUBLIKATION 1 eine Matched-Pair Analyse durchgeführt zwecks Einschätzung der mit iterativer Rekonstruktion möglichen Einsparung von Strahlendosis. Das in PUBLIKATION 1 und 2 semiautomatisch bestimmt Volumen von kalzifizierten Koronarplaques und Stents diente als Surrogatparameter für das Ausmaß an Überstrahlungsartefakten und stellt einen neuen Aspekt dar. Limitationen von PUBLIKATION 1 und 2 sind die monozentrische Datenerhebung, die geringe Fallzahl und eine eingeschränkte Verblindungsmöglichkeit bei der subjektiven Bildqualitätserhebung von iterativer Rekonstruktion gegenüber FBP. Insbesondere die Ergebnisse von PUBLIKATION 1 müssen aufgrund der retrospektiven Auswertung eines kleinen Patientenkollektivs als Hypothesen-generierend angesehen werden. Übereinstimmend konnte in beiden eigenen Publikationen jedoch gezeigt werden, dass die Eigenschaften der iterativen Rekonstruktionstechnik den Anforderungen der Koronarbeurteilung mittels CT besser gerecht werden. Für die Evaluation der kleinkalibrigen Koronargefäße als Zielstrukturen mit zum Teil dicht angrenzenden Strukturen hoher (Stents, Kalzifikationen) und niedriger Röntgendichte (nichtkalzifizierte Plaques) sind sowohl eine optimale Kontrastauflösung als auch eine möglichst hohe räumliche Auflösungskapazität erforderlich. Der Vorteil für die untersuchte iterative Rekonstruktionstechnik ergab sich durch vermindertes Bildrauschen, eine verbesserte Bildqualität, geringeres Volumen von koronaren Stents und Kalk sowie einer signifikanten Verbesserung der diagnostischen Genauigkeit der koronaren CT-Angiografie aufgrund verbesserter Spezifität und positiv

prädiktivem Wert. Daher haben die eigenen Arbeiten (PUBLIKATION 1 und 2) Anteil an der Ablösung des traditionellen Bildrekonstruktionsverfahrens FBP durch die iterative Rekonstruktionstechnik, die heutzutage in allen modernen CT-Systemen standardisiert eingesetzt wird.

Die in PUBLIKATION 3 vergleichend untersuchten quantitativen Plaque-Kriterien und KM-Gradienten können als Zusammenfassung der wesentlichsten zuvor in der Literatur dazu vorgestellten Ansätze zur diagnostischen Verbesserung der koronaren CT-Angiografie angesehen werden (87). Sie stellen den ersten Schritt von der Erfassung rein anatomischer Informationen zur Beurteilung hämodynamischer Relevanz von Koronarstenosen dar. Der morphologische Index LL/MLD^4 ging aus dieser Arbeit als aussagekräftigster Marker hervor, da er am engsten mit der invasiven FFR korrelierte und sich überlegen gegenüber den anderen in dieser Arbeit verglichenen Stenosekriterien bzw. KM-Gradienten zeigte. Die Ergebnisse zeigten einen inkrementellen Wert über die rein anatomische Information aus der koronaren CT-Angiografie hinaus, wenngleich die Spanne des KI der AUC aufgrund des begrenzten Patientenkollektivs relativ groß ist. Darüber hinaus ist bei der Bewertung der Ergebnisse zu beachten, dass es sich um eine retrospektive, monozentrische Studie handelt. Neben weiteren Limitationen erfolgte die Auswertung der Parameter durch einen einzelnen Untersucher. Einige Datensätze mussten aufgrund von Bewegungsartefakten ausgeschlossen werden. Allerdings zeigte der moderate Bildqualitäts-Score, dass die Patientengruppe nicht hochselektioniert für ausschließlich gute oder sehr gute Bildqualität war.

Die PUBLIKATIONEN 4, 5 und 6 befassten sich mit dem neuen Ansatz der CT-basierten FFR (73, 88, 89). Diese CT-Technik konkurriert direkt mit der CTMP als weiterem aussichtsreichen nichtinvasiven Ansatz zur Bestimmung der hämodynamischen Relevanz von Koronarstenosen. Im Vergleich zur CTMP ist jedoch ein großer Vorteil der CT-basierten FFR, dass keine Erweiterung des CT-Protokolls mit zusätzlicher Strahlenbelastung, KM und pharmakologischem Stress erforderlich ist. Nachdem bereits ausführlich der extern anzuwendende

CT-basierte FFR-Algorithmus FFR_{CT} beschrieben wurde, konnten in PUBLIKATION 4 frühe Ergebnisse mit der Methodik der computerbasierten Flussdynamik in Form des intrahospital anwendbaren Prototyp-Algorithmus cFFR dargelegt werden (88). Der Stellenwert dieser Arbeit ergibt sich durch die Erstbeschreibung und Diskussion der technischen Prinzipien in Abgrenzung zum extern anzuwendenden CT-basierten FFR-Algorithmus. Der hier neu vorgestellte Ansatz cFFR zeichnet sich durch seine Verfügbarkeit vor Ort, Zeiteffizienz und Anwendbarkeit auf einem regulären Befundungsrechner aus. Wenngleich es sich um eine retrospektive, monozentrische Studie handelte, lassen die Ergebnisse auf eine deutlich kürzere Bearbeitungs- und Berechnungszeit schließen. Binnen weniger als einer Stunde ließ sich die semiautomatische Segmentation eines dreidimensionalen Koronarmodells mitsamt Berechnung realisieren. Obwohl bei cFFR eine Kopplung von Rechenoperationen unterschiedlicher Ordnung erfolgt, um die Anforderungen an die Rechnerkapazität praktikabel zu halten, war die Korrelation mit der invasiven FFR gut. Aufgrund der limitierten Anzahl an Patientinnen und Patienten konnten hier allerdings keine weiterführenden Schlüsse auf die diagnostische Genauigkeit der Methode gezogen werden.

Eine umfassendere Evaluation des intrahospital anwendbaren Algorithmus cFFR erfolgte in PUBLIKATION 5 basierend auf einem größeren Patientenkollektiv (73). Hier wurden erstmalig Ergebnisse zur diagnostischen Genauigkeit mit dem beschriebenen Algorithmus cFFR vorgestellt. In dieser retrospektiven Studie zeigte sich eine signifikante Verbesserung von Spezifität und positiv prädiktivem Wert auf Läsionsebene, sodass die diagnostische Wertigkeit der intrahospitalen cFFR vergleichbar zu FFR_{CT} schien. Dass der AUC-Vergleich zwischen der koronaren CT-Angiografie und cFFR nur auf Läsions- aber nicht auf Patientenebene einen signifikanten Vorteil zeigte, kann vorrangig auf die Größe des Patientenkollektivs zurückgeführt werden. Wie alle Studien über CT-basierte FFR unterliegt auch PUBLIKATION 5 einem Selektionsbias, da nur Erkrankte mit mindestens einer Koronarstenose eingeschlossen wurden und zur hohen Prävalenz einer KHK im Untersuchungskollektiv führte. Zudem ist eine weitere Selektion zu benennen, da

überwiegend Stenosen unklarer hämodynamischer Signifikanz eingeschlossen wurden und es folglich zu einer Häufung intermediärer Stenosen kam. Nachfolgende Arbeiten umfassten zumeist noch deutlich größere Patientenkollektive und waren teilweise prospektiv angelegt. Ungeachtet dessen hat PUBLIKATION 5 einen hohen Stellenwert in der Entwicklung der CT-basierten FFR. Es handelt sich um eine häufig zitierte Arbeit, da hier die ersten Ergebnisse zur diagnostischen Genauigkeit des neuen intrahospitalen Algorithmus cFFR veröffentlicht werden konnten.

Bei der verbesserten diagnostischen Genauigkeit der CT-basierten FFR im Vergleich zur koronaren CT-Angiografie deutet viel auf einen systematischen Effekt hin. Diese These wurde mit PUBLIKATION 6 im Rahmen einer Metaanalyse untersucht und unterstützt (89). Mit den Studien, die die Einschlusskriterien für diese Metaanalyse erfüllten, konnte ein Überblick über die Ergebnisse mit den beiden CT-basierten FFR-Algorithmen FFR_{CT} und cFFR gegeben werden. Wie bei allen Metaanalysen bedingen Unterschiede der Einzelstudien, z. B. bei den Ein- und Ausschlusskriterien, die Homogenität der Untersuchung. Bei der Einordnung der Ergebnisse dieser Metaanalyse muss zudem berücksichtigt werden, dass insgesamt nur fünf Studien mit limitierter Patientenanzahl herangezogen werden konnten. Dennoch hat diese Arbeit aufgrund der gemeinsamen Betrachtung der beiden CT-basierten FFR-Algorithmen FFR_{CT} und cFFR ihre Berechtigung. Die Subgruppenanalyse der intermediären Koronarstenosen, welche bei konventioneller Beurteilung der koronaren CT-Angiografie besonders schwer hinsichtlich ihrer funktionellen Relevanz einzuschätzen sind, dient hierbei als Alleinstellungsmerkmal. Es zeigte sich in der Gesamtheit wie auch in der Subgruppe der intermediären Stenosen ein Vorteil für die CT-basierte FFR. PUBLIKATION 6 unterstreicht somit die Wertigkeit des neuen Ansatzes CT-basierte FFR für eine genauere Einschätzung der funktionellen Relevanz von Koronarstenosen mittels koronarer CT-Angiografie.

In PUBLIKATION 7 konnte die im Vergleich zur konventionellen koronaren CT-Angiografie verbesserte diagnostische Genauigkeit eines auf künstlicher Intelligenz beruhenden ML-Algorithmus unabhängig von der Lage der Koronarstenosen bestätigt werden (90). Hierbei ist herauszustellen, dass der untersuchte ML-Algorithmus eine praktisch instantane Vorhersage der hämodynamischen Relevanz von Stenosen via Mustererkennung ermöglicht. Die Daten dieser Arbeit stammen zwar aus einem Register und wurden überwiegend retrospektiv erhoben, sodass eine Auswahlverzerrung nicht ausgeschlossen werden kann. Allerdings handelt es sich bei dem MACHINE (Machine Learning Based CT Angiography Derived FFR: A Multi- Center Registry) Register um eine umfangreiche Sammlung multizentrischer und internationaler Daten. Der ML-Algorithmus könnte aufgrund der Vorteile für die Anwendung im klinischen Alltag wegweisend sein. Vorherige Substudien dieses Registers konnten zeigen, dass weder das Geschlecht, noch das Vorliegen eines Diabetes mellitus, noch das Ausmaß an Koronarverkalkung einen negativen Einfluss auf die diagnostische Genauigkeit des ML-Algorithmus haben (92-94). Unsere Ergebnisse unterstützen diesen Trend. Die Lokalisation von Koronarstenosen hatte in dieser eigenen Arbeit keinen nennenswerten Einfluss auf die diagnostische Wertigkeit des ML-Algorithmus für CT-basierte FFR. Obwohl die Gruppengrößen für die unterschiedlichen Stenosenlokalisationen in dieser Substudie variierte, stellte das untersuchte Kollektiv eine realistische Auswahl an Patientinnen und Patienten mit Verdacht auf Vorliegen eines chronischen Koronarsyndroms dar.

6.2 Schlussfolgerung

Diese kumulative Habilitationsschrift zeigt anhand eigener Publikationen auf, wie sich die koronare CT-Angiografie von einem visuell-anatomischen Verfahren über die Erfassung quantitativer Stenosenmarker und koronarer Kontrastgradienten bis hin zur Anwendung von Prinzipien der numerischen Strömungsmechanik sowie maschinellen Lernverfahren zur Beurteilung der funktionellen Relevanz von Koronarstenosen verändert hat. Die Entwicklung ist jedoch nicht abgeschlossen und bestehende Wissenslücken müssen geschlossen werden. Beispielsweise bedürfen die beschriebenen Ansätze zur Berechnung der CT-basierten FFR, deren Prädiktion mittels ML-Algorithmen und die CTMP weiterer Validierung. Belastbare Evidenz aus weniger selektionierten Patientengruppen ist gefragt, um eine breitere Anwendung im klinischen Alltag zu ermöglichen. Erstmals hat die von Douglas et al. veröffentlichte PLATFORM-Studie die Frage der Kosteneffizienz aufgeworfen und diese für den Algorithmus FFR_{CT} positiv beantwortet (95, 96). Allerdings sind weitere, größer angelegte und randomisierte Studien über die klinischen Implikationen und den gesundheitsökonomischen Stellenwert der vorgestellten CT-basierten FFR-Algorithmen erforderlich. Erst kürzlich konnte eine Metaanalyse von Nørgaard et al. über fünf große Studien die hohe prognostische Aussagekraft eines CT-basierten FFR-Algorithmus FFR_{CT}-Wertes >0,80 anhand günstiger Outcomes nach 12 Monaten verdeutlichen. Mit zuverlässiger Bewertung der funktionellen Relevanz von Koronarstenosen könnte sich die koronare CT-Angiografie daher als primäre nichtinvasive Untersuchungsmethode weiter etablieren und andere nichtinvasive Verfahren ersetzen. Schließlich würde hierdurch die Anzahl rein diagnostischer Koronarangiografien weiter reduziert werden. Die invasiven Verfahren wären dann vornehmlich Patientinnen und Patienten vorbehalten, die einer Myokardrevaskularisation bedürfen.

7 Zusammenfassung

Die koronare CT-Angiografie ist ein sehr gut geeignetes nichtinvasives Verfahren zum Ausschluss einer KHK bei ausgewählten Patientinnen und Patienten mit niedrigem bis intermediärem Risiko. Die diagnostische Genauigkeit der Untersuchungsmethode nimmt bei höherer KHK-Prävalenz aufgrund einer Häufung falsch positiver Ergebnisse ab. Ein Grund hierfür sind die Limitationen der subjektiven Interpretation anatomischer CT-Datensätze. Gerade bei kalzifizierten Plaques unterliegt die Stenosenbeurteilung einer Tendenz zur Überschätzung. Indessen hat sich mit der invasiven FFR ein neuer Referenzstandard zur Erfassung hämodynamischer Relevanz von Koronarstenosen durchgesetzt, an dem sich auch die koronare CT-Angiografie messen lassen muss. Zielsetzung der vorliegenden kumulativen Habilitationsschrift war es, anhand einer Auswahl der eigenen Publikationen die Entwicklung der CT-Angiografie von einem visuell-anatomischen Verfahren über quantitative Stenosemarker und transkoronare KM-Abschwächung bis hin zur Anwendung von Prinzipien der numerischen Strömungsmechanik als auch ML-Algorithmen zwecks Beurteilung der funktionellen Relevanz von Koronarstenosen, darzustellen.

Zunächst zeigte sich durch die Einführung iterativer CT-Rekonstruktionsverfahren im Vergleich zur traditionellen Rohdatenrekonstruktion FBP eine bessere Bildqualität und geringere Überstrahlungseffekte von koronaren Stents und Kalk. Dies ließ sich in eine signifikante Verbesserung der diagnostischen Genauigkeit übersetzen, wobei der Auswertungsvorteil vornehmlich auf eine signifikante Steigerung von Spezifität und positiv prädiktivem Wert zurückzuführen war. Im nächsten Schritt wurden verschiedene quantitative Stenosenmarker wie LL, MLD, MLA, %APV, Remodeling-Index, LL/MLD^4 und die KM-Abschwächungsbestimmung CCO aus Routinedatensätzen der koronaren CT-Angiografie erhoben. Es konnte gezeigt werden, dass diese die diagnostische Genauigkeit der koronaren CT-Angiografie für den Nachweis hämodynamischer Relevanz verbessern können. Hierfür erschien der

untersuchte morphologische Stenosen-Index LL/MLD[4] und der transkoronare KM-Gradient CCO geeigneter als die anderen Marker. Des Weiteren wurde die CTMP beleuchtet und deren Potenzial für eine verbesserte Erfassung hämodynamisch relevanter Stenosen beschrieben – wobei hier eine zusätzliche Strahlenbelastung, KM und pharmakologische Stress-Agenzien erforderlich sind. Zudem wurde die CT-basierte FFR vorgestellt. Diese geht auf die Anwendung von Erkenntnissen der numerischen Strömungsmechanik in der computerbasierten Flusssimulation zurück. Hierbei sind zwei unterschiedliche Herangehensweisen zu unterscheiden: der kommerzielle Algorithmus FFR_{CT} (erfordert einen Datentransfer nach extern) und der Prototyp-Algorithmus cFFR (zeiteffizient intrahospital an einem regulären Befundungsrechner anwendbar durch Integration von Rechenoperationen niedrigerer Ordnung). Bezüglich diagnostischer Genauigkeit zeigte sich eine Überlegenheit der CT-basierten FFR im Vergleich zur visuell-anatomisch interpretierten koronaren CT-Angiografie, welche insbesondere auf die verbesserte Spezifität zurückzuführen ist. Hierbei handelt es sich offenbar um einen systematischen Effekt, da sich die Ergebnisse in einer Metaanalyse gleichermaßen für FFR_{CT} und cFFR zeigten. In einer Subgruppenanalyse für die am schwersten hinsichtlich hämodynamischer Relevanz einzuschätzenden intermediären Stenosen konnte eine ebenfalls signifikant verbesserte diagnostische Genauigkeit der CT-basierten FFR gegenüber der koronaren CT-Angiografie gezeigt werden. Zuletzt wurde ein auf artifizieller Intelligenz beruhender ML-Algorithmus zur praktisch instantanen Vorhersage der funktionellen Relevanz von Koronarstenosen untersucht. Hiermit konnte eine im Vergleich zur konventionellen koronaren CT-Angiografie signifikant verbesserte diagnostische Genauigkeit nachgewiesen werden - unabhängig von der Lage der Koronarstenosen.

Die vorgestellten Ergebnisse lassen den Schluss zu, dass sich die koronare CT-Angiografie parallel zur Entwicklung der invasiven Koronardiagnostik von rein visuell-anatomischer Interpretation zu einer umfassenderen Beurteilung der funktionellen Relevanz von Koronarstenosen verändert hat. Insbesondere die CT-basierte FFR erscheint praktikabel für die

klinische Routine, da im Gegensatz zur CTMP auf eine zusätzliche Anwendung von Röntgenstrahlung, KM oder pharmakologische Belastung verzichtet werden kann. Bei Anwendung von ML-Algorithmen kann hierbei weitere Berechnungszeit eingespart werden.

8 Abstract in English

Coronary CT angiography is a noninvasive diagnostic procedure that is particularly well suited for excluding coronary artery disease in selected patient cohorts with low to intermediate risk profiles. The diagnostic accuracy of this modality decreases with higher disease prevalence due to the number of false positive findings. This is in part attributable to the limitations of subjective interpretation of anatomic CT datasets. Most notably, the assessment of stenosis degree in the case of calcified plaques underlies a trend towards overestimation. Meanwhile, invasive FFR has become the accepted reference standard for detecting lesion-specific ischemia. This new reference standard applies to coronary CT angiography as well. Based on a selection of the author's own publications, the present habilitation thesis aimed at expounding the progression of coronary CT angiography from a visual-anatomic diagnostic modality to usage of quantitative stenosis markers, contrast gradients and finally utilization of computational fluid dynamics as well as ML algorithms in order to assess the hemodynamic relevance of coronary artery stenosis.

Initially, the introduction of iterative CT reconstruction techniques showed increased image quality as well as reduced blooming artifacts in the presence of coronary artery stents and calcium compared with the traditional raw data reconstruction FBP. This translated into a significantly improved diagnostic accuracy mainly driven by a significant increase in specificity and positive predictive value. Different quantitative stenosis markers, such as LL, MLD, MLA, %APV, remodeling-index, LL/MLD^4 and CCO were subsequently examined from routine coronary CT angiography datasets. It was shown that these allowed for an improvement in diagnostic accuracy of coronary CT angiography. The morphologic index LL/MLD^4 and CCO were more suitable for this purpose than other markers. Furthermore, techniques of CTMP were discussed and their potential for detecting hemodynamically relevant stenosis was outlined. However, CTMP involves additional radiation dose, contrast material and pharmacologic stress agents. Moreover, the novel technique CT-based FFR was introduced. It is based on computational fluid dynamics and flow simulation. Two approaches

for CT-based FFR can be differentiated: the commercially available algorithm FFR_{CT} (requires external data transfer) and the prototype algorithm cFFR (allows for time-efficient intrahospital application on a regular workstation due to the integration of reduced-order models for fast flow computation). CT-based FFR showed favorable diagnostic accuracy compared with conventional coronary CT-angiography. This finding was chiefly attributable to a significantly improved specificity. The results of a meta-analysis suggested a systematic effect, as improved diagnostic accuracy was likewise present with FFR_{CT} and cFFR. In a subgroup analysis of intermediate stenoses as well, an improved diagnostic accuracy of CT-based FFR compared with coronary CT angiography was found. Most recently, a ML algorithm based on artificial intelligence for virtually instantaneous prediction of functional relevance of coronary artery stenoses was examined. Regardless of stenosis location, this algorithm allowed for significant improvements in diagnostic accuracy compared with coronary CT angiography alone.

In conclusion, the presented results demonstrate that coronary CT angiography has evolved from visual-anatomic diagnostic interpretation to a more comprehensive assessment of functional relevance of coronary artery stenosis in parallel to the development of invasive coronary angiography. CT-based FFR seems most qualified for implementation in clinical routine, as it does not require any additional radiation dose, contrast material or pharmacologic stress. In the context of CT-based FFR, use of ML algorithms promises further reductions in computing time.

9 Abkürzungsverzeichnis

% APV	Prozentuales aggregiertes Plaquevolumen
AUC	Fläche unter der Kurve (*Area Under the Curve*)
CCO	Coronary Contrast Opacification
CT	Computertomografie
CTMP	Computertomografie-basierte myokardiale Perfusionsbildgebung
EKG	Elektrokardiogramm
FBP	Gefilterte Rückprojektion (*Filtered Back Projection*)
FFR	Fraktionelle Flussreserve
HE	Hounsfield Einheit
IRIS	Iteratives Rekonstruktionsverfahren (*Iterative Reconstruction in Image Space*)
KHK	Koronare Herzerkrankung
KI	95 %-Konfidenzintervall
KM	Kontrastmittel
LL	Läsionslänge
MBF	Myokardialer Blutfluss
MDCT	Multidetektor-Computertomografie
ML	Maschinelle Lernenverfahren
MLA	Minimale Lumenfläche
MLD	Minimaler Lumendurchmesser
TAG	Transluminaler Abschwächungsgradient

10 Abbildungsverzeichnis

11 Literaturverzeichnis

11.1 Zitierte Literatur

1. Statistisches Bundesamt. Sterbefälle insgesamt nach der ICD-10 im Jahr 2019. Abgerufen am 19.10.2021 unter: https://www.destatis.de/DE/ZahlenFakten/GesellschaftStaat/Gesundheit/Todesursachen/Todesursachen.html.
2. Knuuti J, Wijns W, Saraste A, Capodanno D, Barbato E, Funck-Brentano C, et al. 2019 ESC Guidelines for the diagnosis and management of chronic coronary syndromes. Eur Heart J. 2020;41(3):407-77.
3. National Institute for Health and Clinical Excellence. Chest Pain of Recent Onset: Assessment and Diagnosis of Recent Onset Chest Pain or Discomfort of Suspected Cardiac Origin (update 2016). CG95. Abgerufen am 18.03.2019 unter: https://www.nice.org.uk/guidance/cg95.
4. Newby DE, Adamson PD, Berry C, Boon NA, Dweck MR, Flather M, et al. Coronary CT Angiography and 5-Year Risk of Myocardial Infarction. N Engl J Med. 2018;379(10):924-33.
5. Min JK, Dunning A, Lin FY, Achenbach S, Al-Mallah M, Budoff MJ, et al. Age- and sex-related differences in all-cause mortality risk based on coronary computed tomography angiography findings results from the International Multicenter CONFIRM (Coronary CT Angiography Evaluation for Clinical Outcomes: An International Multicenter Registry) of 23,854 patients without known coronary artery disease. J Am Coll Cardiol. 2011;58(8):849-60.
6. Ambrose JA, Winters SL, Arora RR, Haft JI, Goldstein J, Rentrop KP, et al. Coronary angiographic morphology in myocardial infarction: a link between the pathogenesis of unstable angina and myocardial infarction. J Am Coll Cardiol. 1985;6(6):1233-8.
7. Hachamovitch R, Hayes SW, Friedman JD, Cohen I, Berman DS. Comparison of the short-term survival benefit associated with revascularization compared with medical therapy in patients with no prior

coronary artery disease undergoing stress myocardial perfusion single photon emission computed tomography. Circulation. 2003;107(23):2900-7.

8. Shaw LJ, Berman DS, Maron DJ, Mancini GB, Hayes SW, Hartigan PM, et al. Optimal medical therapy with or without percutaneous coronary intervention to reduce ischemic burden: results from the Clinical Outcomes Utilizing Revascularization and Aggressive Drug Evaluation (COURAGE) trial nuclear substudy. Circulation. 2008;117(10):1283-91.
9. Pijls NH, Fearon WF, Tonino PA, Siebert U, Ikeno F, Bornschein B, et al. Fractional flow reserve versus angiography for guiding percutaneous coronary intervention in patients with multivessel coronary artery disease: 2-year follow-up of the FAME (Fractional Flow Reserve Versus Angiography for Multivessel Evaluation) study. J Am Coll Cardiol. 2010;56(3):177-84.
10. Tonino PA, De Bruyne B, Pijls NH, Siebert U, Ikeno F, van' t Veer M, et al. Fractional flow reserve versus angiography for guiding percutaneous coronary intervention. N Engl J Med. 2009;360(3):213-24.
11. Davies JE, Sen S, Dehbi HM, Al-Lamee R, Petraco R, Nijjer SS, et al. Use of the Instantaneous Wave-free Ratio or Fractional Flow Reserve in PCI. N Engl J Med. 2017;376(19):1824-34.
12. Götberg M, Christiansen EH, Gudmundsdottir IJ, Sandhall L, Danielewicz M, Jakobsen L, et al. Instantaneous Wave-free Ratio versus Fractional Flow Reserve to Guide PCI. N Engl J Med. 2017;376(19):1813-23.
13. Achenbach S, Marwan M, Schepis T, Pflederer T, Bruder H, Allmendinger T, et al. High-pitch spiral acquisition: a new scan mode for coronary CT angiography. J Cardiovasc Comput Tomogr. 2009;3(2):117-21.
14. Buzug TM. Computed Tomography: From Photon Statistics to Modern Cone-Beam CT. 1 ed: Springer-Verlag Berlin Heidelberg; 2008. 522 p.
15. Brenner DJ, Hall EJ. Computed tomography--an increasing source of radiation exposure. N Engl J Med. 2007;357(22):2277-84.
16. Brooks RA, Di Chiro G. Statistical limitations in x-ray reconstructive tomography. Med Phys. 1976;3(4):237-40.

17. Renker M, Geyer LL, Krazinski AW, Silverman JR, Ebersberger U, Schoepf UJ. Iterative image reconstruction: a realistic dose-saving method in cardiac CT imaging? Expert Rev Cardiovasc Ther. 2013;11(4):403-9.
18. Stocker TJ, Deseive S, Leipsic J, Hadamitzky M, Chen MY, Rubinshtein R, et al. Reduction in radiation exposure in cardiovascular computed tomography imaging: results from the PROspective multicenter registry on radiaTion dose Estimates of cardiac CT angIOgraphy iN daily practice in 2017 (PROTECTION VI). Eur Heart J. 2018;39(41):3715-23.
19. Budoff MJ, Dowe D, Jollis JG, Gitter M, Sutherland J, Halamert E, et al. Diagnostic performance of 64-multidetector row coronary computed tomographic angiography for evaluation of coronary artery stenosis in individuals without known coronary artery disease: results from the prospective multicenter ACCURACY (Assessment by Coronary Computed Tomographic Angiography of Individuals Undergoing Invasive Coronary Angiography) trial. J Am Coll Cardiol. 2008;52(21):1724-32.
20. Meijboom WB, Meijs MF, Schuijf JD, Cramer MJ, Mollet NR, van Mieghem CA, et al. Diagnostic accuracy of 64-slice computed tomography coronary angiography: a prospective, multicenter, multivendor study. J Am Coll Cardiol. 2008;52(25):2135-44.
21. Menke J, Kowalski J. Diagnostic accuracy and utility of coronary CT angiography with consideration of unevaluable results: A systematic review and multivariate Bayesian random-effects meta-analysis with intention to diagnose. Eur Radiol. 2016;26(2):451-8.
22. Miller JM, Rochitte CE, Dewey M, Arbab-Zadeh A, Niinuma H, Gottlieb I, et al. Diagnostic performance of coronary angiography by 64-row CT. N Engl J Med. 2008;359(22):2324-36.
23. Meijboom WB, van Mieghem CA, Mollet NR, Pugliese F, Weustink AC, van Pelt N, et al. 64-slice computed tomography coronary angiography in patients with high, intermediate, or low pretest probability of significant coronary artery disease. J Am Coll Cardiol. 2007;50(15):1469-75.
24. Sarwar A, Rieber J, Mooyaart EA, Seneviratne SK, Houser SL, Bamberg F, et al. Calcified plaque: measurement of area at thin-section flat-panel CT

and 64-section multidetector CT and comparison with histopathologic findings. Radiology. 2008;249(1):301-6.

25. Meijs MF, Meijboom WB, Prokop M, Mollet NR, van Mieghem CA, Doevendans PA, et al. Is there a role for CT coronary angiography in patients with symptomatic angina? Effect of coronary calcium score on identification of stenosis. Int J Cardiovasc Imaging. 2009;25(8):847-54.
26. Agatston AS, Janowitz WR, Hildner FJ, Zusmer NR, Viamonte M, Detrano R. Quantification of coronary artery calcium using ultrafast computed tomography. J Am Coll Cardiol. 1990;15(4):827-32.
27. Rixe J, Achenbach S, Ropers D, Baum U, Kuettner A, Ropers U, et al. Assessment of coronary artery stent restenosis by 64-slice multi-detector computed tomography. Eur Heart J. 2006;27(21):2567-72.
28. Ziegler A, Köhler T, Proksa R. Noise and resolution in images reconstructed with FBP and OSC algorithms for CT. Med Phys. 2007;34(2):585-98.
29. Brooks RA, Di Chiro G. Theory of image reconstruction in computed tomography. Radiology. 1975;117(3 Pt 1):561-72.
30. Min JK, Swaminathan RV, Vass M, Gallagher S, Weinsaft JW. High-definition multidetector computed tomography for evaluation of coronary artery stents: comparison to standard-definition 64-detector row computed tomography. J Cardiovasc Comput Tomogr. 2009;3(4):246-51.
31. Flicek KT, Hara AK, Silva AC, Wu Q, Peter MB, Johnson CD. Reducing the radiation dose for CT colonography using adaptive statistical iterative reconstruction: A pilot study. AJR Am J Roentgenol. 2010;195(1):126-31.
32. Gosling O, Loader R, Venables P, Roobottom C, Rowles N, Bellenger N, et al. A comparison of radiation doses between state-of-the-art multislice CT coronary angiography with iterative reconstruction, multislice CT coronary angiography with standard filtered back-projection and invasive diagnostic coronary angiography. Heart. 2010;96(12):922-6.
33. Leipsic J, Labounty TM, Heilbron B, Min JK, Mancini GB, Lin FY, et al. Estimated radiation dose reduction using adaptive statistical iterative reconstruction in coronary CT angiography: the ERASIR study. AJR Am J Roentgenol. 2010;195(3):655-60.

34. Prakash P, Kalra MK, Ackman JB, Digumarthy SR, Hsieh J, Do S, et al. Diffuse lung disease: CT of the chest with adaptive statistical iterative reconstruction technique. Radiology. 2010;256(1):261-9.
35. Prakash P, Kalra MK, Kambadakone AK, Pien H, Hsieh J, Blake MA, et al. Reducing abdominal CT radiation dose with adaptive statistical iterative reconstruction technique. Invest Radiol. 2010;45(4):202-10.
36. Renker M, Ramachandra A, Schoepf UJ, Raupach R, Apfaltrer P, Rowe GW, et al. Iterative image reconstruction techniques: Applications for cardiac CT. J Cardiovasc Comput Tomogr. 2011;5(4):225-30.
37. Min JK, Shaw LJ, Berman DS. The present state of coronary computed tomography angiography a process in evolution. J Am Coll Cardiol. 2010;55(10):957-65.
38. Hacker M, Jakobs T, Hack N, Nikolaou K, Becker C, von Ziegler F, et al. Sixty-four slice spiral CT angiography does not predict the functional relevance of coronary artery stenoses in patients with stable angina. Eur J Nucl Med Mol Imaging. 2007;34(1):4-10.
39. Rispler S, Keidar Z, Ghersin E, Roguin A, Soil A, Dragu R, et al. Integrated single-photon emission computed tomography and computed tomography coronary angiography for the assessment of hemodynamically significant coronary artery lesions. J Am Coll Cardiol. 2007;49(10):1059-67.
40. Di Carli MF, Dorbala S, Curillova Z, Kwong RJ, Goldhaber SZ, Rybicki FJ, et al. Relationship between CT coronary angiography and stress perfusion imaging in patients with suspected ischemic heart disease assessed by integrated PET-CT imaging. J Nucl Cardiol. 2007;14(6):799-809.
41. Schuijf JD, Wijns W, Jukema JW, Atsma DE, de Roos A, Lamb HJ, et al. Relationship between noninvasive coronary angiography with multi-slice computed tomography and myocardial perfusion imaging. J Am Coll Cardiol. 2006;48(12):2508-14.
42. Lin F, Shaw LJ, Berman DS, Callister TQ, Weinsaft JW, Wong FJ, et al. Multidetector computed tomography coronary artery plaque predictors of stress-induced myocardial ischemia by SPECT. Atherosclerosis. 2008;197(2):700-9.

43. Nakazato R, Shalev A, Doh JH, Koo BK, Gransar H, Gomez MJ, et al. Aggregate plaque volume by coronary computed tomography angiography is superior and incremental to luminal narrowing for diagnosis of ischemic lesions of intermediate stenosis severity. J Am Coll Cardiol. 2013;62(5):460-7.
44. Li M, Zhang J, Pan J, Lu Z. Coronary stenosis: Morphologic index characterized by using CT angiography correlates with fractional flow reserve and is associated with hemodynamic status. Radiology. 2013;269(3):713-21.
45. Voros S, Rinehart S, Vazquez-Figueroa JG, Kalynych A, Karmpaliotis D, Qian Z, et al. Prospective, head-to-head comparison of quantitative coronary angiography, quantitative computed tomography angiography, and intravascular ultrasound for the prediction of hemodynamic significance in intermediate and severe lesions, using fractional flow reserve as reference standard (from the ATLANTA I and II Study). Am J Cardiol. 2014;113(1):23-9.
46. Motoyama S, Sarai M, Harigaya H, Anno H, Inoue K, Hara T, et al. Computed tomographic angiography characteristics of atherosclerotic plaques subsequently resulting in acute coronary syndrome. J Am Coll Cardiol. 2009;54(1):49-57.
47. Park HB, Heo R, ó Hartaigh B, Cho I, Gransar H, Nakazato R, et al. Atherosclerotic plaque characteristics by CT angiography identify coronary lesions that cause ischemia: a direct comparison to fractional flow reserve. JACC Cardiovasc Imaging. 2015;8(1):1-10.
48. Lackner K, Bovenschulte H, Stützer H, Just T, Al-Hassani H, Krug B. In vitro measurements of flow using multislice computed tomography (MSCT). Int J Cardiovasc Imaging. 2011;27(6):795-804.
49. Choi JH, Min JK, Labounty TM, Lin FY, Mendoza DD, Shin DH, et al. Intracoronary transluminal attenuation gradient in coronary CT angiography for determining coronary artery stenosis. JACC Cardiovasc Imaging. 2011;4(11):1149-57.

50. Chow BJ, Kass M, Gagné O, Chen L, Yam Y, Dick A, et al. Can differences in corrected coronary opacification measured with computed tomography predict resting coronary artery flow? J Am Coll Cardiol. 2011;57(11):1280-8.
51. Rumberger JA, Feiring AJ, Lipton MJ, Higgins CB, Ell SR, Marcus ML. Use of ultrafast computed tomography to quantitate regional myocardial perfusion: a preliminary report. J Am Coll Cardiol. 1987;9(1):59-69.
52. Bastarrika G, Ramos-Duran L, Rosenblum MA, Kang DK, Rowe GW, Schoepf UJ. Adenosine-stress dynamic myocardial CT perfusion imaging: initial clinical experience. Invest Radiol. 2010;45(6):306-13.
53. Ko BS, Cameron JD, Meredith IT, Leung M, Antonis PR, Nasis A, et al. Computed tomography stress myocardial perfusion imaging in patients considered for revascularization: a comparison with fractional flow reserve. Eur Heart J. 2012;33(1):67-77.
54. Meinel FG, De Cecco CN, Schoepf UJ, Nance JW, Silverman JR, Flowers BA, et al. First-arterial-pass dual-energy CT for assessment of myocardial blood supply: do we need rest, stress, and delayed acquisition? Comparison with SPECT. Radiology. 2014;270(3):708-16.
55. Wang Y, Qin L, Shi X, Zeng Y, Jing H, Schoepf UJ, et al. Adenosine-stress dynamic myocardial perfusion imaging with second-generation dual-source CT: comparison with conventional catheter coronary angiography and SPECT nuclear myocardial perfusion imaging. AJR Am J Roentgenol. 2012;198(3):521-9.
56. Weininger M, Schoepf UJ, Ramachandra A, Fink C, Rowe GW, Costello P, et al. Adenosine-stress dynamic real-time myocardial perfusion CT and adenosine-stress first-pass dual-energy myocardial perfusion CT for the assessment of acute chest pain: initial results. Eur J Radiol. 2012;81(12):3703-10.
57. Rochitte CE, George RT, Chen MY, Arbab-Zadeh A, Dewey M, Miller JM, et al. Computed tomography angiography and perfusion to assess coronary artery stenosis causing perfusion defects by single photon emission

computed tomography: the CORE320 study. Eur Heart J. 2014;35(17):1120-30.

58. Rossi A, Merkus D, Klotz E, Mollet N, de Feyter PJ, Krestin GP. Stress myocardial perfusion: imaging with multidetector CT. Radiology. 2014;270(1):25-46.
59. Nesto RW, Kowalchuk GJ. The ischemic cascade: temporal sequence of hemodynamic, electrocardiographic and symptomatic expressions of ischemia. Am J Cardiol. 1987;59(7):23C-30C.
60. Taylor CA, Fonte TA, Min JK. Computational fluid dynamics applied to cardiac computed tomography for noninvasive quantification of fractional flow reserve: scientific basis. J Am Coll Cardiol. 2013;61(22):2233-41.
61. Zarins CK, Taylor CA, Min JK. Computed fractional flow reserve (FFTCT) derived from coronary CT angiography. J Cardiovasc Transl Res. 2013;6(5):708-14.
62. Kim HJ, Vignon-Clementel IE, Coogan JS, Figueroa CA, Jansen KE, Taylor CA. Patient-specific modeling of blood flow and pressure in human coronary arteries. Ann Biomed Eng. 2010;38(10):3195-209.
63. West GB, Brown JH, Enquist BJ. A general model for the origin of allometric scaling laws in biology. Science. 1997;276(5309):122-6.
64. Sharma P, Itu L, Zheng X, Kamen A, Bernhardt D, Suciu C, et al. A framework for personalization of coronary flow computations during rest and hyperemia. Conf Proc IEEE Eng Med Biol Soc. 2012;2012:6665-8.
65. Koo BK, Erglis A, Doh JH, Daniels DV, Jegere S, Kim HS, et al. Diagnosis of ischemia-causing coronary stenoses by noninvasive fractional flow reserve computed from coronary computed tomographic angiograms. Results from the prospective multicenter DISCOVER-FLOW (Diagnosis of Ischemia-Causing Stenoses Obtained Via Noninvasive Fractional Flow Reserve) study. J Am Coll Cardiol. 2011;58(19):1989-97.
66. Gaur S, Achenbach S, Leipsic J, Mauri L, Bezerra HG, Jensen JM, et al. Rationale and design of the HeartFlowNXT (HeartFlow analysis of coronary blood flow using CT angiography: NeXt sTeps) study. J Cardiovasc Comput Tomogr. 2013;7(5):279-88.

67. Min JK, Berman DS, Budoff MJ, Jaffer FA, Leipsic J, Leon MB, et al. Rationale and design of the DeFACTO (Determination of Fractional Flow Reserve by Anatomic Computed Tomographic AngiOgraphy) study. J Cardiovasc Comput Tomogr. 2011;5(5):301-9.
68. Grunau GL, Min JK, Leipsic J. Modeling of fractional flow reserve based on coronary CT angiography. Curr Cardiol Rep. 2013;15(1):336.
69. Nørgaard BL, Leipsic J, Gaur S, Seneviratne S, Ko BS, Ito H, et al. Diagnostic performance of noninvasive fractional flow reserve derived from coronary computed tomography angiography in suspected coronary artery disease: the NXT trial (Analysis of Coronary Blood Flow Using CT Angiography: Next Steps). J Am Coll Cardiol. 2014;63(12):1145-55.
70. Min JK, Leipsic J, Pencina MJ, Berman DS, Koo BK, van Mieghem C, et al. Diagnostic accuracy of fractional flow reserve from anatomic CT angiography. JAMA : the journal of the American Medical Association. 2012;308(12):1237-45.
71. Sianos G, Morel MA, Kappetein AP, Morice MC, Colombo A, Dawkins K, et al. The SYNTAX Score: an angiographic tool grading the complexity of coronary artery disease. EuroIntervention. 2005;1(2):219-27.
72. Norgaard BL, Leipsic J, Gaur S, Seneviratne S, Ko BS, Ito H, et al. Diagnostic performance of noninvasive fractional flow reserve derived from coronary computed tomography angiography in suspected coronary artery disease: the NXT trial (Analysis of Coronary Blood Flow Using CT Angiography: Next Steps). Journal of the American College of Cardiology. 2014;63(12):1145-55.
73. Renker M, Schoepf UJ, Wang R, Meinel FG, Rier JD, Bayer RR, et al. Comparison of diagnostic value of a novel noninvasive coronary computed tomography angiography method versus standard coronary angiography for assessing fractional flow reserve. Am J Cardiol. 2014;114(9):1303-8.
74. Coenen A, Lubbers MM, Kurata A, Kono A, Dedic A, Chelu RG, et al. Fractional flow reserve computed from noninvasive CT angiography data: diagnostic performance of an on-site clinician-operated computational fluid dynamics algorithm. Radiology. 2015;274(3):674-83.

75. Min JK, Koo BK, Erglis A, Doh JH, Daniels DV, Jegere S, et al. Usefulness of noninvasive fractional flow reserve computed from coronary computed tomographic angiograms for intermediate stenoses confirmed by quantitative coronary angiography. Am J Cardiol. 2012;110(7):971-6.
76. Nakazato R, Park HB, Berman DS, Gransar H, Koo BK, Erglis A, et al. Noninvasive fractional flow reserve derived from computed tomography angiography for coronary lesions of intermediate stenosis severity: results from the DeFACTO study. Circ Cardiovasc Imaging. 2013;6(6):881-9.
77. Scott IA. Demystifying machine learning: a primer for physicians. Intern Med J. 2021;51(9):1388-400.
78. Itu L, Rapaka S, Passerini T, Georgescu B, Schwemmer C, Schoebinger M, et al. A machine-learning approach for computation of fractional flow reserve from coronary computed tomography. J Appl Physiol (1985). 2016;121(1):42-52.
79. Obermeyer Z, Emanuel EJ. Predicting the Future - Big Data, Machine Learning, and Clinical Medicine. N Engl J Med. 2016;375(13):1216-9.
80. Parmar C, Grossmann P, Bussink J, Lambin P, Aerts HJWL. Machine Learning methods for Quantitative Radiomic Biomarkers. Sci Rep. 2015;5:13087.
81. Arsanjani R, Xu Y, Dey D, Vahistha V, Shalev A, Nakanishi R, et al. Improved accuracy of myocardial perfusion SPECT for detection of coronary artery disease by machine learning in a large population. J Nucl Cardiol. 2013;20(4):553-62.
82. van Engelen A, Wannarong T, Parraga G, Niessen WJ, Fenster A, Spence JD, et al. Three-dimensional carotid ultrasound plaque texture predicts vascular events. Stroke. 2014;45(9):2695-701.
83. Motwani M, Dey D, Berman DS, Germano G, Achenbach S, Al-Mallah MH, et al. Machine learning for prediction of all-cause mortality in patients with suspected coronary artery disease: a 5-year multicentre prospective registry analysis. Eur Heart J. 2017;38(7):500-7.
84. Coenen A, Kim YH, Kruk M, Tesche C, De Geer J, Kurata A, et al. Diagnostic Accuracy of a Machine-Learning Approach to Coronary

Computed Tomographic Angiography-Based Fractional Flow Reserve: Result From the MACHINE Consortium. Circ Cardiovasc Imaging. 2018;11(6):e007217.

85. Cury RC, Abbara S, Achenbach S, Agatston A, Berman DS, Budoff MJ, et al. CAD-RADS(TM) Coronary Artery Disease - Reporting and Data System. An expert consensus document of the Society of Cardiovascular Computed Tomography (SCCT), the American College of Radiology (ACR) and the North American Society for Cardiovascular Imaging (NASCI). Endorsed by the American College of Cardiology. J Cardiovasc Comput Tomogr. 2016;10(4):269-81.
86. Renker M, Nance JW, Schoepf UJ, O'Brien TX, Zwerner PL, Meyer M, et al. Evaluation of heavily calcified vessels with coronary CT angiography: comparison of iterative and filtered back projection image reconstruction. Radiology. 2011;260(2):390-9.
87. Wang R, Baumann S, Schoepf UJ, Meinel FG, Rier JD, Morris JZ, et al. Comparison of quantitative stenosis characteristics at routine coronary computed tomography angiography with invasive fractional flow reserve for assessing lesion-specific ischemia. J Cardiovasc Comput Tomogr. 2015;9(6):546-52.
88. Baumann S, Wang R, Schoepf UJ, Steinberg DH, Spearman JV, Bayer RR, 2nd, et al. Coronary CT angiography-derived fractional flow reserve correlated with invasive fractional flow reserve measurements--initial experience with a novel physician-driven algorithm. Eur Radiol. 2015;25(4):1201-7.
89. Baumann S, Renker M, Hetjens S, Fuller SR, Becher T, Loßnitzer D, et al. Comparison of Coronary Computed Tomography Angiography-Derived vs Invasive Fractional Flow Reserve Assessment: Meta-Analysis with Subgroup Evaluation of Intermediate Stenosis. Acad Radiol. 2016;23(11):1402-11.
90. Renker M, Baumann S, Hamm CW, Tesche C, Kim WK, Savage RH, et al. Influence of coronary stenosis location on diagnostic performance of

machine learning-based fractional flow reserve from CT angiography. J Cardiovasc Comput Tomogr. 2021;15(6):492-8.

91. Bittencourt MS, Schmidt B, Seltmann M, Muschiol G, Ropers D, Daniel WG, et al. Iterative reconstruction in image space (IRIS) in cardiac computed tomography: initial experience. Int J Cardiovasc Imaging. 2011;27(7):1081-7.
92. Baumann S, Renker M, Schoepf UJ, De Cecco CN, Coenen A, De Geer J, et al. Gender differences in the diagnostic performance of machine learning coronary CT angiography-derived fractional flow reserve -results from the MACHINE registry. Eur J Radiol. 2019;119:108657.
93. Nous FMA, Coenen A, Boersma E, Kim YH, Kruk MBP, Tesche C, et al. Comparison of the Diagnostic Performance of Coronary Computed Tomography Angiography-Derived Fractional Flow Reserve in Patients With Versus Without Diabetes Mellitus (from the MACHINE Consortium). Am J Cardiol. 2019;123(4):537-43.
94. Tesche C, Otani K, De Cecco CN, Coenen A, De Geer J, Kruk M, et al. Influence of Coronary Calcium on Diagnostic Performance of Machine Learning CT-FFR: Results From MACHINE Registry. JACC Cardiovasc Imaging. 2020;13(3):760-70.
95. Douglas PS, Pontone G, Hlatky MA, Patel MR, Norgaard BL, Byrne RA, et al. Clinical outcomes of fractional flow reserve by computed tomographic angiography-guided diagnostic strategies vs. usual care in patients with suspected coronary artery disease: the prospective longitudinal trial of FFR(CT): outcome and resource impacts study. Eur Heart J. 2015;36(47):3359-67.
96. Hlatky MA, De Bruyne B, Pontone G, Patel MR, Norgaard BL, Byrne RA, et al. Quality-of-Life and Economic Outcomes of Assessing Fractional Flow Reserve With Computed Tomography Angiography: PLATFORM. J Am Coll Cardiol. 2015;66(21):2315-23.

11.2 Verzeichnis der Originalarbeiten des Verfassers

Renker M, Ramachandra A, Schoepf UJ, Raupach R, Apfaltrer P, Rowe GW, Vogt S, Flohr TG, Kerl MJ, Bauer RW, Fink C, Henzler T. Iterative image reconstruction techniques: Applications for cardiac CT. J Cardiovasc Comput Tomogr 2011, 5:225-30.

Renker M, Nance JW, Schoepf UJ, O'Brien TX, Zwerner PL, Meyer M, Kerl JM, Bauer RW, Fink C, Vogl TJ, Henzler T. Evaluation of Heavily Calcified Vessels with Coronary CT Angiography: Comparison of Iterative and Filtered Back Projection Image Reconstruction. Radiology 2011, 260:390-9.

Kerl JM, Bauer RW, **Renker M**, Weber E, Weisser P, Korkusuz H, Schell B, Larsson MC, Kromen W, Jacobi V, Vogl TJ. Triphasic Contrast Injection Improves Evaluation of Dual-Energy Lung Perfusion in Pulmonary CT Angiography. Eur J Radiol. 2011 Dec;80(3):e483-7.

Bauer RW, Frellesen C, **Renker M**, Schell B, Lehnert T, Ackermann H, Schoepf UJ, Jacobi V, Vogl TJ, Kerl JM. Dual energy CT pulmonary blood volume assessment in acute pulmonary embolism - correlation with D-dimer level, right heart strain and clinical outcome. Eur Radiol 2011, 21(9):1914-21.

Moscariello A, Takx RA, Schoepf UJ, **Renker M**, Zwerner PL, O'Brien TX, Allmendinger T, Vogt S, Schmidt B, Savino G, Fink C, Bonomo L, Henzler T. Coronary CT angiography: image quality, diagnostic accuracy, and potential for radiation dose reduction using a novel iterative image reconstruction technique-comparison with traditional filtered back projection. Eur Radiol 2011, 21(10):2130-8.

Bauer RW, Kramer S, **Renker M**, Schell B, Larson MC, Beeres M, Lehnert T, Jacobi V, Vogl TJ, Kerl JM. Dose and image quality at CT pulmonary angiography-comparison of first and second generation dual-energy CT and 64-slice CT. Eur Radiol 2011, 21(10):2139-47.

Renker M, Schoepf UJ, Wang R, Meinel FG, Rier JD, Bayer RR 2nd, Moellmann H, Hamm CW, Steinberg DH, Baumann S. Comparison of diagnostic value of a novel noninvasive coronary computed tomography angiography method versus standard coronary angiography for assessing fractional flow reserve. Am J Cardiol 2014, 114:1303-8.

Baumann S, Wang R, Schoepf UJ, Steinberg DH, Spearman JV, Bayer RR 2nd, Hamm CW, **Renker M**. Coronary CT Angiography-Derived Fractional Flow Reserve Correlated with Invasive Fractional Flow Reserve Measurements - Initial Experience with a Novel Physician-Driven Algorithm. Eur Radiol 2015, 25:1201-7.

Wang R, Baumann S, Schoepf UJ, Meinel FG, Rier JD, Morris JZ, Moellmann H, Hamm CW, Steinberg DH, **Renker M**. Comparison of quantitative stenosis characteristics at routine coronary computed tomography angiography with invasive fractional flow reserve for assessing lesion-specific ischemia. J Cardiovasc Comput Tomogr 2015, 9(6):546-52.

Newallo D, Meinel FG, Schoepf UJ, Baumann S, Leddy RJ, Vliegenthart R, Moellmann H, Hamm CW, Morris PB, **Renker M**. Mammographic Detection of Breast Arterial Calcification as an Independent Predictor of Coronary Atherosclerotic Disease in a Single Ethnic Cohort of African American Women. Atherosclerosis 2015, 242:218-221.

Qi L, Zhao Y, Zhou CS, Spearman JV, **Renker M**, Schoepf UJ, Zhang LJ, Lu GM. Image quality and radiation dose of lower extremity CT angiography at 70 kVp on an integrated circuit detector dual-source computed tomography. Acta Radiol 2015, 56(6):659-65.

Opolski MP, Achenbach S, Schuhbäck A, Rolf A, Möllmann H, Nef H, Rixe J, **Renker M**, Witkowski A, Kepka C, Walther C, Schlundt C, Debski A, Jakubczyk

M, Hamm CW. Coronary computed tomographic prediction rule for time-efficient guidewire crossing through chronic total occlusion: insights from the CT-RECTOR multicenter registry (Computed Tomography Registry of Chronic Total Occlusion Revascularization). JACC Cardiovasc Interv 2015, 8(2):257-267.

Spearman JV, **Renker M**, Schoepf UJ, Krazinski AW, Herbert TL, De Cecco CN, Nietert PJ, Meinel FG. Prognostic value of epicardial fat volume measurements by computed tomography: a systematic review of the literature. Eur Radiol. 2015, 25(11):3372-81.

Wang R, **Renker M**, Schoepf UJ, Wichmann JL, Fuller SR, Rier JD, Bayer RR 2nd, Steinberg DH, De Cecco CN, Baumann S. Diagnostic value of quantitative stenosis predictors with coronary CT angiography compared to invasive fractional flow reserve. Eur J Radiol. 2015, 84(8):1509-1515.

Renker M, Varga-Szemes A, Schoepf UJ, Baumann S, Piccini D, Zenge MO, Rehwald WG, Müller E, Rier JD, Möllmann H, Hamm CW, Steinberg DH, De Cecco CN. A non-contrast, free-breathing, self-navigated 3-dimensional MR technique for aortic root and vascular access route assessment in the context of transcatheter aortic valve replacement. Eur Radiol 2016, 26(4):951-8.

Baumann S, **Renker M**, Hetjens S, Fuller SR, Becher T, Loßnitzer D, Lehmann R, Akin I, Borggrefe M, Lang S, Wichmann JL, Schoepf UJ.Comparison of Coronary Computed Tomography Angiography-Derived vs Invasive Fractional Flow Reserve Assessment: Meta-Analysis with Subgroup Evaluation of Intermediate Stenosis. Acad Radiol 2016, 23:1402-1411.

Baumann S, Huseynov A, Koepp J, Jabbour C, Behnes M, Becher T, **Renker M**, Lang S, Borggrefe M, Lehmann R, Akin I. Comparison of Serum Uric Acid, Bilirubin, and C-Reactive Protein as Prognostic Biomarkers of In-Hospital MACE Between Women and Men With ST-Segment Elevation Myocardial Infarction. Angiology 2016, 67(3):272-80.

Varga-Szemes A, Muscogiuri G, Schoepf UJ, Wichmann JL, Suranyi P, De Cecco CN, Cannaò PM, **Renker M**, Mangold S, Fox MA, Ruzsics B. Clinical feasibility of a myocardial signal intensity threshold-based semi-automated cardiac magnetic resonance segmentation method. Eur Radiol. 2016 May;26(5):1503-11.

Dörr O, Liebetrau C, Möllmann H, Gaede L, Troidl C, Wiebe J, **Renker M**, Bauer T, Hamm C, Nef H. Long-term verification of functional and structural renal damage after renal sympathetic denervation. Catheter Cardiovasc Interv. 2016, 87(7):1298-303.

Baumann S, Koepp J, Becher T, Huseynov A, Bosch K, Behnes M, Fastner C, El-Battrawy I, **Renker M**, Lang S, Weiß C, Borggrefe M, Lehmann R, Akin I. Biomarker evaluation as a potential cause of gender differences in obesity paradox among patients with STEMI. Cardiovasc Revasc Med 2016, 17(2):88-94.

Tesche C, De Cecco CN, Caruso D, Baumann S, **Renker M**, Mangold S, Dyer KT, Varga-Szemes A, Baquet M, Jochheim D, Ebersberger U, Bayer RR 2nd, Hoffmann E, Steinberg DH, Schoepf UJ. Coronary CT angiography derived morphological and functional quantitative plaque markers correlated with invasive fractional flow reserve for detecting hemodynamically significant stenosis. J Cardiovasc Comput Tomogr. 2016, 10(3):199-206.

McQuiston AD, Crawford C, Schoepf UJ, Varga-Szemes A, Canstein C, **Renker M**, De Cecco CN, Baumann S, Naylor GJP. Segmentations of the cartilaginous skeletons of chondrichthyan fishes by the use of state-of-the-art computed tomography. World J Radiol. 2017 Apr 28;9(4):191-198.

Kim WK, Liebetrau C, **Renker M**, Rolf A, Van Linden A, Arsalan M, Husser O, Möllmann H, Hamm C, Walther T. Transfemoral aortic valve implantation using a

self-expanding transcatheter heart valve without pre-dilation. Int J Cardiol 2017, 243:156-160.

Kim WK, **Renker M**, Rolf A, Liebetrau C, Van Linden A, Arsalan M, Doss M, Rieck J, Opolski MP, Möllmann H, Walther T, Hamm CW. Accuracy of device landing zone calcium volume measurement with contrast-enhanced multidetector computed tomography. Int J Cardiol 2018, 263:171-176.

Arsalan M, Weferling M, Hecker F, Filardo G, Kim WK, Pollock BD, Van Linden A, Arsalan-Werner A, **Renker M**, Doss M, Kalbas S, Hamm CW, Liebetrau C, Mack MJ, Walther T. TAVI risk scoring using established versus new scoring systems: role of the new STS/ACC model. EuroIntervention 2018, 13(13):1520-1526.

Kim WK, Gaede L, Husser O, Liebetrau C, **Renker M**, Rolf A, Fischer-Rasokat U, Möllmann S, Blumenstein J, Guenther E, Van Linden A, Arsalan M, Doss M, Loders S, Arnold M, Hamm CW, Walther T, Achenbach S, Möllmann H. Computed Tomography for Diagnosis and Classification of Bicuspid Aortic Valve Disease in Transcatheter Aortic Valve Replacement. JACC Cardiovasc Imaging. 2018, 11(10):1539-1540.

Arsalan M, Kim WK, Van Linden A, Liebetrau C, Pollock BD, Filardo G, **Renker M**, Möllmann H, Doss M, Fischer-Rasokat U, Skwara A, Hamm CW, Walther T. Predictors and outcome of conversion to cardiac surgery during transcatheter aortic valve implantation. Eur J Cardiothorac Surg 2018, 54(2):267-272.

Tesche C, De Cecco CN, Baumann S, **Renker M**, McLaurin TW, Duguay TM, Bayer RR 2nd, Steinberg DH, Grant KL, Canstein C, Schwemmer C, Schoebinger M, Itu LM, Rapaka S, Sharma P, Schoepf UJ. Coronary CT Angiography-derived Fractional Flow Reserve: Machine Learning Algorithm versus Computational Fluid Dynamics Modeling. Radiology 2018, 288(1):64-72.

Kim WK, Möllmann H, Liebetrau C, **Renker M**, Rolf A, Simon P, Van Linden A, Arsalan M, Doss M, Hamm CW, Walther T. The ACURATE neo Transcatheter Heart Valve: A Comprehensive Analysis of Predictors of Procedural Outcome. JACC Cardiovasc Interv. 2018, 11(17):1721-1729.

Baumann S, Kryeziu P, Tesche C, Shuler DC, Becher T, Rutsch M, Behnes M, Stach K, Jacobs BE, **Renker M**, Henzler T, Haubenreisser H, Schoenberg SO, Weiss C, Borggrefe M, Schwemmer C, Schoepf UJ, Akin I, Lossnitzer D. Association of Serum Lipid Profile With Coronary Computed Tomographic Angiography-derived Morphologic and Functional Quantitative Plaque Markers. J Thorac Imaging. 2019, 34(1):26-32.

Kim WK, Brinkert M, Mangner N, Gatto F, Husser O, **Renker M**, Liebetrau C, Gasior T, Doss M, Walther T, Hamm C, Linke A, Toggweiler S, Möllmann H. Transfemoral implantation of the ACURATE neo prosthesis using a low-profile expandable introducer system: A multicenter registry. Int J Cardiol. 2019, 281:76-81.

Fischer-Rasokat U, **Renker M**, Liebetrau C, van Linden A, Arsalan M, Weferling M, Rolf A, Doss M, Möllmann H, Walther T, Hamm CW, Kim WK. 1-Year Survival After TAVR of Patients With Low-Flow, Low-Gradient and High-Gradient Aortic Valve Stenosis in Matched Study Populations. JACC Cardiovasc Interv. 2019, 12(8):752-763.

Kim WK, **Renker M**, Rolf A, Fischer-Rasokat U, Wiedemeyer J, Doss M, Möllmann H, Walther T, Nef H, Hamm CW, Liebetrau C. Annular versus supra-annular sizing for TAVI in bicuspid aortic valve stenosis. EuroIntervention. 2019, 15(3):e231-e238.

Keranov S, Kim WK, Arsalan M, **Renker M**, Keller T, Bauer T, Dörr O, Nef HM, Gaede L, Möllmann H, Walther T, Hamm CW, Liebetrau C. Predictive value of

preprocedural procalcitonin for short- and long-term mortality after transfemoral transcatheter aortic valve implantation. Heart Vessels. 2019, 34(12):1993-2001.

Wichmann JL, Takx RAP, Nunez JH, Vliegenthart R, Otani K, Litwin SE, Morris PB, De Cecco CN, Rosenberg RD, Bayer RR 2nd, Baumann S, **Renker M**, Vogl TJ, Wenger NK, Schoepf UJ. Relationship Between Pregnancy Complications and Subsequent Coronary Artery Disease Assessed by Coronary Computed Tomographic Angiography in Black Women. Circ Cardiovasc Imaging. 2019, 12(7):e008754.

Baumann S, **Renker M**, Schoepf UJ, De Cecco CN, Coenen A, De Geer J, Kruk M, Kim YH, Albrecht MH, Duguay TM, Jacobs BE, Bayer RR, Litwin SE, Weiss C, Akin I, Borggrefe M, Yang DH, Kepka C, Persson A, Nieman K, Tesche C. Gender differences in the diagnostic performance of machine learning coronary CT angiography-derived fractional flow reserve -results from the MACHINE registry. Eur J Radiol. 2019, 119:108657.

Fischer-Rasokat U, **Renker M**, Liebetrau C, Weferling M, Rolf A, Doss M, Möllmann H, Walther T, Hamm CW, Kim WK. Outcome of patients with heart failure after transcatheter aortic valve implantation. PLoS One. 2019, 14(11):e0225473.

Baumann S, Hirt M, Schoepf UJ, Rutsch M, Tesche C, **Renker M**, Golden JW, Buss SJ, Becher T, Bojara W, Weiss C, Papavassiliu T, Akin I, Borggrefe M, Schoenberg SO, Haubenreisser H, Overhoff D, Lossnitzer D. Correlation of machine learning computed tomography-based fractional flow reserve with instantaneous wave free ratio to detect hemodynamically significant coronary stenosis. Clin Res Cardiol. 2020, 109(6):735-745.

Baumann S, Özdemir GH, Tesche C, Schoepf UJ, Golden JW, Becher T, Hirt M, Weiss C, **Renker M**, Akin I, Schoenberg SO, Borggrefe M, Haubenreisser H, Lossnitzer D, Overhoff D. Coronary CT angiography derived plaque markers

correlated with invasive instantaneous flow reserve for detecting hemodynamically significant coronary stenoses. Eur J Radiol. 2020, 122:108744.

Tesche C, Otani K, De Cecco CN, Coenen A, De Geer J, Kruk M, Kim YH, Albrecht MH, Baumann S, **Renker M**, Bayer RR, Duguay TM, Litwin SE, Varga-Szemes A, Steinberg DH, Yang DH, Kepka C, Persson A, Nieman K, Schoepf UJ. Influence of Coronary Calcium on Diagnostic Performance of Machine Learning CT-FFR: Results From MACHINE Registry. JACC Cardiovasc Imaging. 2020, 13(3):760-770.

Kim WK, Liebetrau C, Fischer-Rasokat U, **Renker M**, Rolf A, Doss M, Möllmann H, Nef H, Walther T, Hamm CW. Challenges of recognizing bicuspid aortic valve in elderly patients undergoing TAVR. Int J Cardiovasc Imaging. 2020, 36(2):251-256.

Baumann S, Kaeder F, Schoepf UJ, Golden JW, Kryeziu P, Tesche C, **Renker M**, Jannsen S, Weiss C, Hetjens S, Schoenberg SO, Borggrefe M, Akin I, Lossnitzer D, Overhoff D. Prognostic Value of Coronary Computed Tomography Angiography-derived Morphologic and Quantitative Plaque Markers Using Semiautomated Plaque Software. J Thorac Imaging. 2021 Mar 1;36(2):108-115.

Steinbach R, Schoepf UJ, Griffith LP, van Assen M, **Renker M**, Sahbaee P, Schwemmer C, Fischer AM, Varga-Szemes A, Martin SS, Bayer RR 2nd. A fully automated software platform for structural mitral valve analysis. Eur Radiol. 2020 Dec;30(12):6528-6536.

Kim WK, Möllmann H, Liebetrau C, **Renker M**, Walther T, Hamm CW. Effectiveness and Safety of the ACURATE Neo Prosthesis in 1,000 Patients With Aortic Stenosis. Am J Cardiol. 2020 Sep 15;131:12-16.

Fischer-Rasokat U, **Renker M**, Liebetrau C, Weferling M, Rolf A, Doss M, Möllmann H, Walther T, Hamm CW, Kim WK. Does the severity of low-gradient

aortic stenosis classified by computed tomography-derived aortic valve calcification determine the outcome of patients after transcatheter aortic valve implantation (TAVI)? Eur Radiol. 2021 Jan;31(1):549-558.

Yoon SH, Kim WK, Dhoble A, Milhorini Pio S, Babaliaros V, Jilaihawi H, Pilgrim T, De Backer O, Bleiziffer S, Vincent F, Shmidt T, Butter C, Kamioka N, Eschenbach L, **Renker M**, Asami M, Lazkani M, Fujita B, Birs A, Barbanti M, Pershad A, Landes U, Oldemeyer B, Kitamura M, Oakley L, Ochiai T, Chakravarty T, Nakamura M, Ruile P, Deuschl F, Berman D, Modine T, Ensminger S, Kornowski R, Lange R, McCabe JM, Williams MR, Whisenant B, Delgado V, Windecker S, Van Belle E, Sondergaard L, Chevalier B, Mack M, Bax JJ, Leon MB, Makkar RR; Bicuspid Aortic Valve Stenosis Transcatheter Aortic Valve Replacement Registry Investigators. Bicuspid Aortic Valve Morphology and Outcomes After Transcatheter Aortic Valve Replacement. J Am Coll Cardiol. 2020 Sep 1;76(9):1018-1030.

Fischer-Rasokat U, **Renker M**, Liebetrau C, Möllmann H, Hamm CW, Kim WK. Impact of Rapid Ventricular Pacing During Transcatheter Implantation of Self-Expanding Aortic Valve Prostheses in Patients at Highest Risk. J Invasive Cardiol. 2020 Dec;32(12):E355-E361.

Renker M, Kriechbaum SD, Schmidt SE, Larsen BS, Wolter JS, Dörr O, Fischer-Rasokat U, Kim WK, Liebetrau C, Bøttcher M, Nef H, Bauer T, Hamm CW. Prospective validation of an acoustic-based system for the detection of obstructive coronary artery disease in a high-prevalence population. Heart Vessels. 2021 Aug;36(8):1132-1140.

Renker M, Fischer-Rasokat U, Walther C, Kim W, Rixe J, Dörr O, Nef H, Rolf A, Möllmann H, Hamm CW. Evaluation of Patients for Percutaneous Edge-to-Edge Mitral Valve Repair – Comparison of Cardiac Computed Tomography Angiography with Transesophageal Echocardiography. J Thorac Imaging. 2021 Jul 7. doi: 10.1097/RTI.0000000000000602. Epub ahead of print.

Renker M, Baumann S, Hamm CW, Tesche C, Kim W, Savage RH Coenen A, Nieman K, De Geer J, Persson A, Kruk M, Kepka C, Yang DH, Schoepf UJ. Influence of Coronary Stenosis Location on Diagnostic Performance of Machine Learning-based Fractional Flow Reserve from CT Angiography. J Cardiovasc Comput Tomogr 2021, S1934-5925(21)00082-4.

Reifart J, Liebetrau C, Weferling M, Dörr O, **Renker M**, Bhumimuang K, Liakopoulos O, Choi YH, Nef H, Hamm CW, Kim WK. Single versus double use of a suture-based closure device for transfemoral aortic valve implantation. Int J Cardiol. 2021 May 15;331:183-188.

Kim WK, Bhumimuang K, **Renker M**, Fischer-Rasokat U, Möllmann H, Walther T, Choi YH, Nef H, Hamm CW. Determinants of paravalvular leakage following transcatheter aortic valve replacement in patients with bicuspid and tricuspid aortic stenosis. Eur Heart J Cardiovasc Imaging. 2021 Feb 14:jeab011. doi: 10.1093/ehjci/jeab011. Epub ahead of print.

Kim WK, Doerr O, **Renker M**, Choi YH, Liakopoulos O, Hamm CW, Nef H. Initial experience with a novel, modular, minimalistic approach for transfemoral aortic valve implantation. Int J Cardiol. 2021 Jun 1;332:54-59.

Weferling M, Liebetrau C, **Renker M**, Fischer-Rasokat U, Choi YH, Hamm CW, Kim WK. Right bundle branch block is not associated with worse short- and mid-term outcome after transcatheter aortic valve implantation. PLoS One. 2021 Jun 16;16(6):e0253332.

Fischer-Rasokat U, **Renker M**, Liebetrau C, Weferling M, Rolf A, Hain A, Sperzel J, Choi YH, Hamm CW, Kim WK. Long-Term Survival in Patients with or without Implantable Cardioverter Defibrillator after Transcatheter Aortic Valve Implantation. J Clin Med. 2021 Jun 30;10(13):2929.

Voigtländer L, Kim WK, Mauri V, Goßling A, **Renker M**, Sugiura A, Linder M, Schmidt T, Schofer N, Westermann D, Reichenspurner H, Nickenig G, Blankenberg S, Hamm C, Conradi L, Adam M, Sinning JM, Seiffert M. Transcatheter aortic valve implantation in patients with a small aortic annulus: performance of supra-, intra- and infra-annular transcatheter heart valves. Clin Res Cardiol. 2021 Aug 13. doi: 10.1007/s00392-021-01918-8. Epub ahead of print.

Kim WK, **Renker M**, Doerr O, Hofmann S, Nef H, Choi YH, Hamm CW. Impact of implantation depth on outcomes of new-generation balloon-expandable transcatheter heart valves. Clin Res Cardiol. 2021 Sep 2. doi: 10.1007/s00392-021-01932-w. Epub ahead of print.

Fischer-Rasokat U, **Renker M**, Liebetrau C, Weferling M, Rieth A, Rolf A, Choi YH, Hamm CW, Kim WK. Predictive value of overt and non-overt volume overload in patients with high- or low-gradient aortic stenosis undergoing transcatheter aortic valve implantation. Cardiovasc Diagn Ther. 2021 Oct;11(5):1080-1092.

Fischer-Rasokat U, **Renker M**, Bänsch C, Weferling M, Liebetrau C, Herrmann E, Liakopoulos O, Choi YH, Hamm CW, Kim WK. Effects of statins after transcatheter aortic valve implantation in key patient populations. J Cardiovasc Pharmacol. 2021 Nov 1;78(5):e669-e674.

Fischer-Rasokat U, **Renker M**, Liebetrau C, Weferling M, Rolf A, Doss M, Hamm CW, Kim WK. Prognostic impact of echocardiographic mean transvalvular gradients in patients with aortic stenosis and low flow undergoing transcatheter aortic valve implantation. Catheter Cardiovasc Interv. 2021 Nov 15;98(6):E922-E931.

12 Danksagung

Meinen klinischen und wissenschaftlichen Lehrern, Prof. Dr. med. Christian Hamm, Prof. Dr. med. Helge Möllmann, Prof. Dr. med. Christoph Liebetrau, Prof. Dr. med. Holger Nef, PD Dr. med. Andreas Rolf und PD Dr. med. Ulrich Fischer-Rasokat bin ich zu großem Dank verpflichtet. Sie begleiteten mich als Vorbilder und unterstützten mich fortwährend. An dieser Stelle möchte ich insbesondere auch PD Dr. med. Won-Keun Kim für die Zusammenarbeit und das tagtägliche Vertrauen in der Klinik danken.

Besonderer Dank gebührt auch Prof. Dr. med. Matthias Kerl und Prof. Dr. med. Ralf Bauer, die mir als Betreuer auf dem Weg zur Dissertation die ersten wissenschaftlichen Schritte ebneten und als Freunde erhalten geblieben sind. Durch sie kam der Kontakt zu Prof. Dr. med. U. Joseph Schoepf zustande, der mich wissenschaftlich sehr prägte. Ich danke ihm für das entgegengebrachte Vertrauen und die Möglichkeit, mich in seiner Arbeitsgruppe zu entfalten. In diesem Zusammenhang gilt mein Dank auch PD Dr. med. Stefan Baumann, mit dem ich über Klinikgrenzen hinweg zusammenarbeitete und den ich zum engeren Freundeskreis zählen kann.

Ohne meine Eltern und meinen Bruder wäre diese Arbeit schlicht nicht möglich gewesen, da sie mir Freude am Lernen und Lehren schenkten, mich mit Durchhaltevermögen ausstatteten, mir Forschungsaufenthalte ermöglichten, und immer mit Rat und Tat zur Seite standen.

Diese Arbeit ist letztlich meiner lieben Frau Lorraine gewidmet, die mir die Zeit und Kraft gibt, mich neben der Klinik auch noch wissenschaftlichen Vorhaben zu widmen. Mit größtmöglicher Geduld und liebevollem Verständnis hat sie maßgeblich dazu beigetragen, dass ich diese Zeilen vollenden konnte. Auch meinem Sohn Leonard und meiner Tochter Victoria widme ich diese Arbeit, da beide mein Leben ungemein bereichert haben und unsere Bindung trotz meiner Abwesenheiten so stark gewachsen ist.

13 Zugrunde liegende PUBLIKATIONEN 1-7

Journal of Cardiovascular Computed Tomography (2011) 5, 225–230

Journal of Cardiovascular Computed Tomography

Technical Notes

Iterative image reconstruction techniques: Applications for cardiac CT

Matthias Renker, BS[a], Ashok Ramachandra, BS[a], U. Joseph Schoepf, MD[a,*], Rainer Raupach, PhD[b], Paul Apfaltrer, MD[a,c], Garrett W. Rowe, BS[a], Sebastian Vogt, PhD[b], Thomas G. Flohr, PhD[b], J. Matthias Kerl, MD[d], Ralf W. Bauer, MD[d], Christian Fink, MD[c], Thomas Henzler, MD[a,c]

[a]Heart and Vascular Center, Medical University of South Carolina, Ashley River Tower, MSC 226, 25 Courtenay Dr, Charleston, SC 29401, USA; [b]Siemens Healthcare, CT Division, Forchheim, Germany; [c]Department of Clinical Radiology and Nuclear Medicine, University Medical Center Mannheim, Medical Faculty Mannheim, Heidelberg University, Mannheim, Germany and [d]Department of Diagnostic and Interventional Radiology, Goethe University, Frankfurt, Germany

KEYWORDS:
Iterative reconstruction;
Filtered back-projection;
Coronary CT angiography;
Image noise;
Radiation dose;
Cardiac CT

BACKGROUND: Traditional limitations of cardiac CT are related to image noise, blooming artifacts from calcifications and stents, and radiation exposure. We evaluated whether these limitations can be ameliorated by the use of iterative reconstruction in image space (IRIS) instead of traditional filtered back projection (FBP) image reconstruction techniques.

METHODS: We compared image reconstruction with the use of IRIS with traditional FBP for their effect on image quality, noise, volume of heavy coronary artery calcifications, and stents as a measure of "blooming" artifacts, and radiation dose at cardiac CT. The radiation dose comparison was performed as a matched pair analysis, whereas all other comparisons were performed within the same group of patients.

RESULTS: The subjective image quality of IRIS reconstructions was rated higher than FBP reconstructions. Image noise was lower with IRIS than with FBP. The volume of stents and heavy coronary artery calcifications measured lower in IRIS reconstructed series compared with FBP. Similar levels of image noise were achieved with 80/100 kVp of tube voltage with IRIS compared with 120 kVp and FBP, resulting in a 62% reduction in effective dose.

CONCLUSION: Our preliminary experiences suggest that IRIS incrementally improves the CT evaluation of coronary arteries, especially in challenging scenarios. Substantial radiation reduction seems feasible without associated increases in image noise.

Introduction

Obtaining diagnostic image quality while keeping radiation as low as reasonably achievable presents an important challenge in cardiac CT in which the need for high spatial and temporal resolutions has traditionally resulted in relatively high radiation exposure. CT image reconstruction has traditionally

Conflict of interest: U.J.S. receives research support from and is a consultant for Bayer, Bracco, General Electric, Medrad, and Siemens. S.V., R.R. and T.G.F. are employees of Siemens Healthcare. The remaining authors report no conflicts of interest.

* Corresponding author.
E-mail address: schoepf@musc.edu

Submitted December 20, 2010. Accepted for publication May 17, 2011.

1934-5925/$ - see front matter © 2011 Society of Cardiovascular Computed Tomography. All rights reserved.
doi:10.1016/j.jcct.2011.05.002

Table 1 Image acquisition parameters of patient studies used in the assessment of image quality and volumes of coronary artery calcifications and stents (n = 24)

	Values
Tube voltage	
120 kVp, n	19
100 kVp, n	4
80 kVp, n	1
Tube current, mean ± SD (mAs)	332.1 ± 8.9
CT dose index volume, mean ± SD (mGy)	36.3 ± 20.4
Dose-length product, mean ± SD (mGy)	631.4 ± 299.8
Scan length, mean ± SD (cm)	12.9 ± 1.7

used filtered back projection (FBP). However, with FBP, increased spatial resolution directly associates with increased image noise,[1] leading to compensation by application of higher x-ray tube settings and therefore higher radiation exposure. Moreover, FBP has limitations vis-à-vis 3-dimensional cone-beam geometry, data completeness, and low photon environments.[2] Some of these technical shortcomings contribute to well-known limitations of cardiac CT, such as beam-hardening or "blooming" artifacts arising from dense coronary calcifications and iatrogenic metallic hardware (eg, stents), which limits the evaluation of stent patency and of coronary stenosis, typically because of overestimation of stenosis.[3]

Iterative reconstruction techniques were introduced almost 4 decades ago[4] as an alternative approach for improving CT image quality by reducing quantum noise and artifacts associated with FBP. Recent progress in computing power now enables iterative image reconstruction, within a clinically acceptable time frame.

Advantages of iterative reconstruction for the in vitro evaluation of coronary artery stents have previously been described.[5] We aimed to explore the potential in vivo role and benefits of iterative reconstruction in image space (IRIS), a recently introduced iterative reconstruction technique, for cardiac CT applications.

Technical methods

Cardiac CT procedures

Since iterative reconstruction became available at our institution, all clinical and research cardiac CT studies were reconstructed with both traditional FBP and IRIS. All cardiac CT studies were performed on a second-generation dual-source CT system (SOMATOM Definition Flash; Siemens, Forchheim, Germany). Regardless of acquisition technique, all studies were reconstructed with 0.75-mm section thickness and 0.4-mm reconstruction increment, using 4 different algorithms ("kernels"), that is, the FBP algorithms "B26f" and "B46f", as well as the corresponding IRIS algorithms "I26" and "I46." The 46 algorithms were included because of the previously described beneficial effects of higher spatial frequency kernels on the evaluation of coronary artery stents and heavy calcifications.[5]

Potential of iterative image reconstruction to improve image quality

In 24 consecutive clinical patients (Table 1) subjective image quality rating was performed in a blinded fashion by 2 experienced observers with the use of a 5-point scale, according to the severity of image noise, beam-hardening artifacts, and blooming artifacts in FBP versus IRIS reconstructed image series. The following evaluation key was applied: 1, nondiagnostic because of excessive image noise and artifacts; 2, limited diagnostic value with substantial image noise and artifacts; 3, diagnostic, moderate image quality; 4, diagnostic, good image quality minimally limited by image noise and artifacts; and 5, excellent image quality without artifacts.

Image noise was defined as the standard deviation of the measured Hounsfield units within circular regions of interest (ROIs) in the ascending aorta, left ventricular myocardium, left ventricular cavity, and interventricular septum. We adapted the size of the ROIs to account for anatomical differences of the patients. However, within the same patient, the ROI size was kept constant for the different reconstruction approaches.

Image appearance of heavy calcifications and stents and effect on stenosis detection

Volumes of heavily calcified plaques and coronary artery stents were evaluated in the same 24 patients on FBP and IRIS reconstructed datasets with the use of a dedicated volume analysis tool (Volume analysis software, Version VE31A; Siemens). Coronary artery calcifications and stents were semiautomatically segmented by drawing ROIs around these structures, which were then automatically propagated to the neighboring sections and manually corrected, if necessary. To only include calcium and stents, voxels within these ROIs with attenuation values in the range of contrast medium were automatically excluded from the segmentation. Therefore, we measured the maximum contrast attenuation in Hounsfield units within the ascending aorta and added 20% to this value to define the minimum attenuation level of voxels to be included in the volumetric analysis. Between the different reconstruction techniques of individual patients this level was kept constant.

Potential of iterative image reconstruction for radiation dose reduction

To estimate the potential for radiation dose reduction with the use of IRIS instead of FBP, we performed a matched pair analysis of patients who had participated in our ongoing cardiac CT radiation dose-reduction studies approved by the institutional review board. Twelve patients

Table 2 Baseline demographic characteristics of the matched pair analysis group

	FBP group (n = 12)	IRIS group (n = 12)	*P* value
Age, mean ± SD (y)	56.9 ± 7.3	57.8 ± 8.0	NS
Male-to-female ratio, n:n	6:6	6:6	1
Height, mean ± SD (cm)	165.8 ± 12.6	167.5 ± 14.3	NS
Weight, mean ± SD (kg)	84.1 ± 12.5	84.7 ± 13.2	NS
Body mass index, mean ± SD (kg/m^2)	30.7 ± 5.3	30.2 ± 6.8	NS
Heart rate, mean ± SD (beats/min)	64.0 ± 6.9	63.3 ± 7.4	NS

FBP, filtered back projection; IRIS, iterative reconstruction in image space.

that were imaged with 120 kVp of tube voltage were matched according to body mass index and image acquisition protocol with 12 patients who had been studied with 80 or 100 kVp (Table 2). The tube current was adjusted individually according to body type. Image noise and radiation dose were compared between both groups.

Results

Subjective image quality and image noise

Cardiac CT studies that were reconstructed with IRIS showed higher image quality than studies reconstructed with FBP. The median image quality scores and corresponding interquartile ranges are displayed in Table 3. Image noise was lower on image datasets reconstructed with IRIS than with FBP (Fig. 1 and Fig. 2; Table 4).

Image appearance of heavy calcifications and stents and effect on stenosis detection

Severe coronary artery calcifications were present in 15 of the 24 patients. Coronary artery stents were present in 7 patients, including 2 patients with multiple stents. The volume of calcifications was significantly lower in studies that were reconstructed with IRIS than with FBP (29.1 ± 16.9 mm^3 vs 38.5 ± 18.9 mm^3, respectively; $P = 0.021$). Volumes of coronary artery stents were also significantly lower in studies that were reconstructed with IRIS than with FBP (205.9 ± 149.9 mm^3 vs 211.9 ± 150.3 mm^3, respectively; $P = 0.047$; Fig. 3).

Potential for radiation dose reduction

As shown in Table 5, similar levels of image noise were measured in 80/100-kVp IRIS-reconstructed series and 120-kVp FBP-reconstructed studies in our matched pair analysis (Fig. 3). No significant differences were observed in terms of tube current for our tube voltage groups (80/100 kVp IRIS, and 120 kVp FBP). The IRIS-reconstructed cardiac CT studies that used 80/100 kVp resulted in an average effective dose of 3.7 mSv compared with an average of 9.7 mSv from FBP-reconstructed studies that used 120 kVp. This corresponds to a radiation dose reduction of 62%.

Discussion

Our preliminary data suggest that the use of IRIS instead of traditional FBP for reconstructing coronary CT data results in substantial reduction in image noise and improved quality of the diagnostic image. Accordingly, our results are consistent with a recently published study by Bittencourt et al[6] concluding that IRIS improves objective image noise without impairment of diagnostic image quality. These effects may be helpful when studying patients with obesity in whom high levels of image noise ordinarily preclude the accurate evaluation of small vascular structures, such as the coronary arteries.

A recently published study investigated the effect of tube voltage reduction on the diagnostic performance of coronary CT.[7] Leipsic et al[8] showed radiation dose reduction by the use of iterative reconstruction techniques in comparison to FBP at comparable signal-to-noise ratios by decreased tube current. On the basis of a matched pair analysis, our observations indicate the potential for substantial reductions in effective radiation exposure by means of reduced tube voltage, without associated increases in image noise, if IRIS is used instead of FBP. The measured raw data are used inefficiently by FBP in the sense of neglecting the individual data noise. Iterative reconstruction overcomes this limitation by using statistical weighting and

Table 3 Subjective image quality rating for the different image reconstruction kernels

	FBP B26f, median (interquartile range)	IRIS I26f, median (interquartile range)	*P* value	FBP B46f, median (interquartile range)	IRIS I46f, median (interquartile range)	*P* value
Image quality score	4 (3–5)	5 (4–5)	<0.05	4 (4–5)	5 (4–5)	<0.05

FBP, filtered back projection; IRIS, iterative reconstruction in image space.

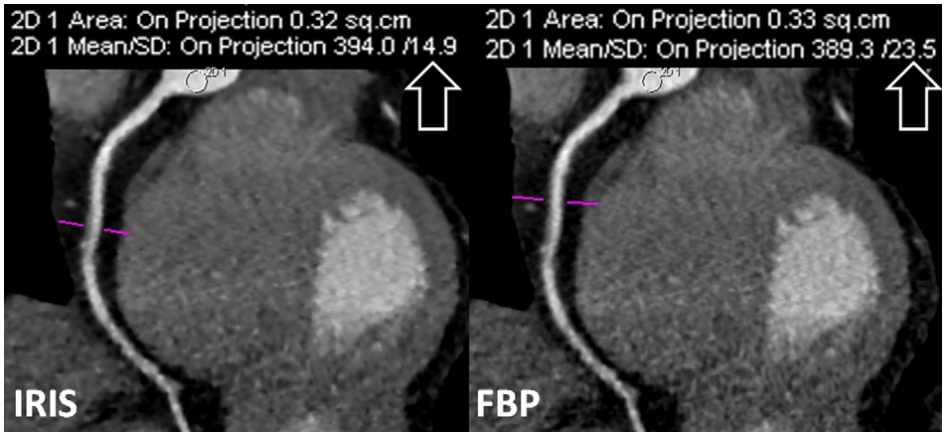

Figure 1 Two studies of a 55-year-old woman with a body mass index of 37 kg/m^2. Curved multiplanar reformations of the right coronary artery on the basis of IRIS (left) and FBP (right) reconstructions are shown. Image noise is significantly reduced with the use of IRIS instead of FBP.

regularization, which represents the essential mechanism for radiation dose reduction. It can be shown that all parts of iterative reconstruction that address data statistics can be translated into an equivalent optimization process in the image domain, implying that image-based iterative reconstruction will have an equal potential in terms of

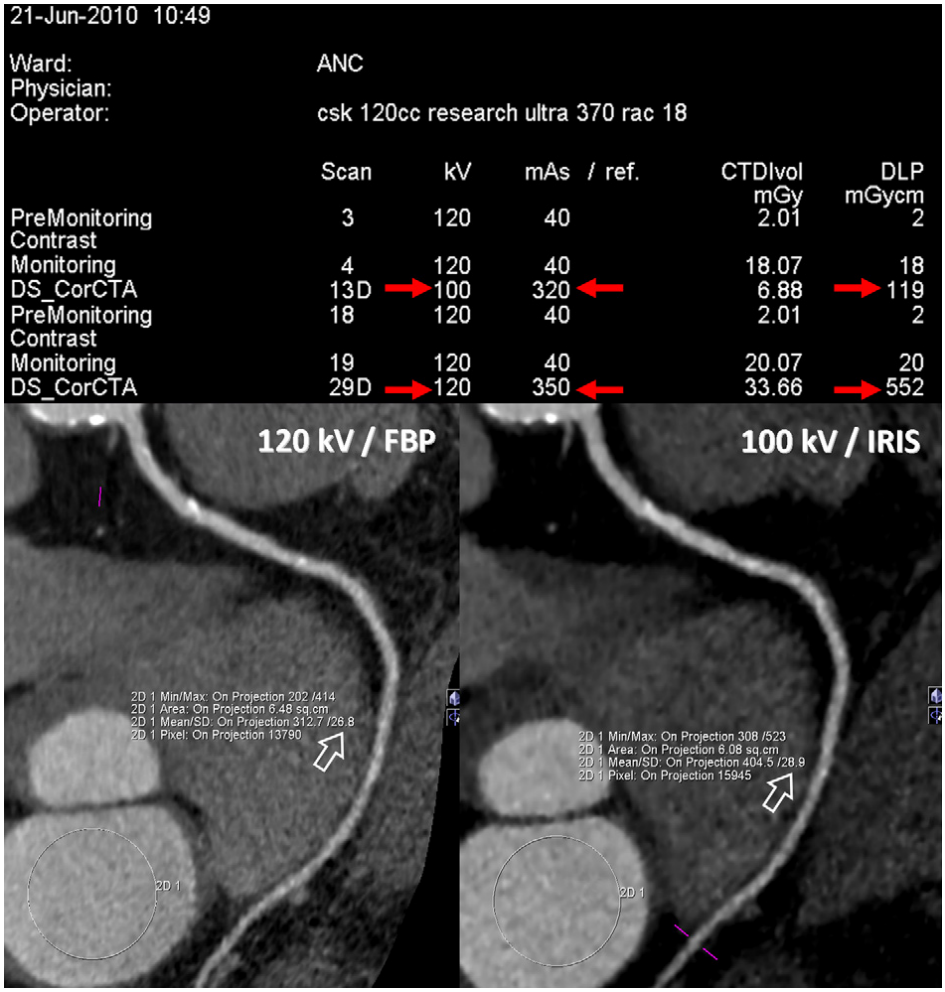

Figure 2 Two cardiac CT studies of a 72-year-old-male research subject are shown. The first study was performed with 100 kVp/320 mAs, resulting in a dose-length-product of 119 mGy · cm (≈1.7 mSv), whereas the second acquisition was performed with 120 kVp/350 mAs, resulting in a dose-length-product of 552 mGy · cm (≈7.7mSv). Image noise was similar in both studies with a standard deviation of 26.8 HU with FBP and of 28.9 HU with IRIS (*arrows*).

Table 4 Comparison of image noise between datasets reconstructed with filtered back projection (FBP) and iterative reconstruction in image space (IRIS)

Region of interest	Image noise FBP, mean ± SD	Image noise IRIS, mean ± SD	*P* value
Aortic root			
26 algorithm	36.6 ± 14	27.9 ± 14	0.012
46 algorithm	38.6 ± 17	28.4 ± 11	0.006
Left ventricular myocardium			
26 algorithm	35.1 ± 17	26.1 ± 14	0.010
46 algorithm	37.3 ± 17	28.2 ± 10	0.009
Interventricular septum			
26 algorithm	37.0 ± 18	27.5 ± 17	0.011
46 algorithm	38.3 ± 15	27.2 ± 14	0.012
Left ventricular cavity			
26 algorithm	40.6 ± 21	32.5 ± 17	0.005
46 algorithm	42.1 ± 19	34.2 ± 13	0.013

radiation dose reduction compared with iterative reconstruction with the use of repeated forward and back projection.[7,9]

A general, inherent limitation of all studies that compare iterative reconstruction with traditional FBP is that observers cannot be effectively blinded to the reconstruction technique because of the distinct differences in image characteristics between the 2 approaches. However, according to our initial results IRIS results in more effective suppression of beam-hardening and blooming artifacts than FBP at constant x-ray tube settings as suggested by the lower volumes of heavy coronary artery calcifications and metallic stents in IRIS-reconstructed series. Compared with FBP, this enables a more realistic appreciation of the true size of these high-density objects that are typically exaggerated by artifact. In our initial experience, these effects may allow better delineation of the vessel lumen adjacent to high-density structures and result in an incremental improvement in the CT evaluation of heavily calcified coronary artery segments as well as of coronary artery stents,

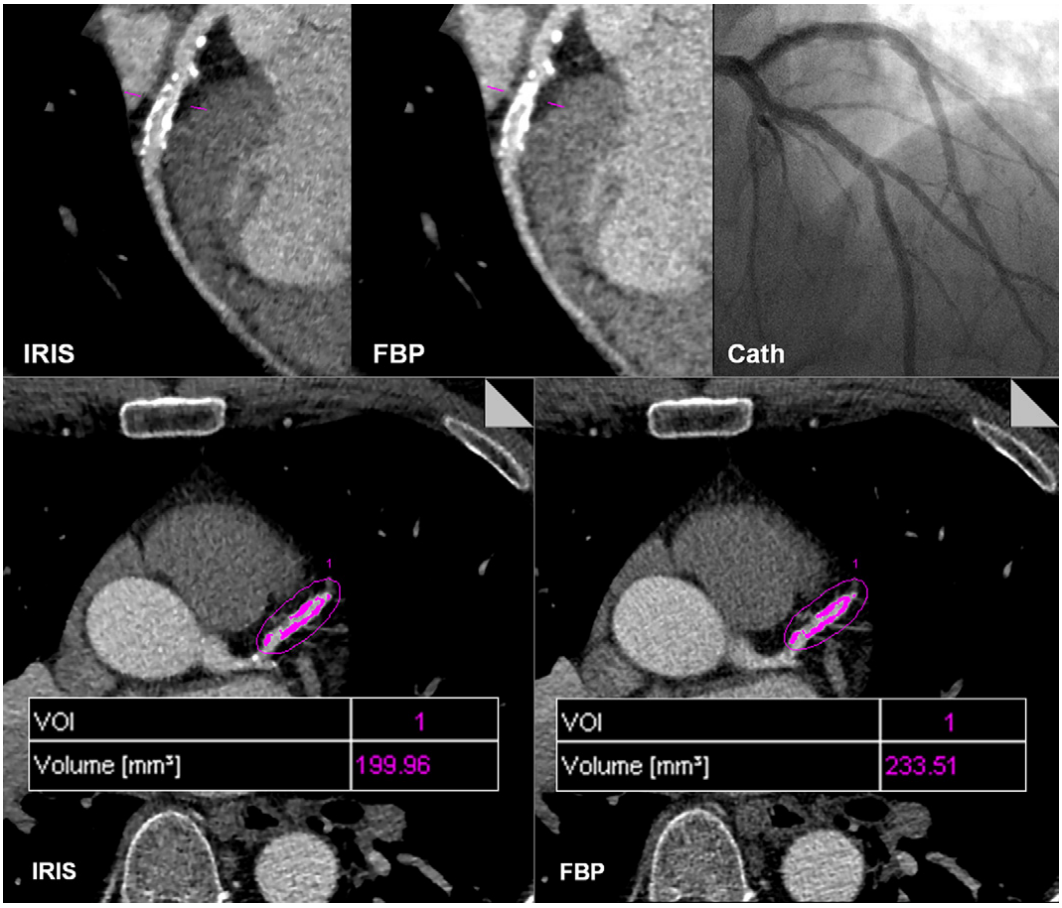

Figure 3 Contrast-enhanced, prospectively electrocardiographic-triggered coronary CT angiography study in a 63-year-old man with heavily calcified plaques in the left coronary artery. Curved multiplanar reformations show heavy calcifications. Blooming artifacts limit the evaluation of the adjacent vessel lumen in FBP reconstructions and suggest the presence of a significant stenosis. Blooming artifacts are reduced in iterative reconstructions, which improve visualization of the adjacent vessel lumen and enable correct classification of the degree of stenosis as not significant, as confirmed by coronary catheterization. Volume analysis of the calcifications shows a lower volume measurement with IRIS than with FBP, indicating reduced image blooming.

Table 5 Image acquisition parameters in the matched pair analysis group

	FBP group (n = 12)	IRIS group (n = 12)	*P* value
Tube voltage			
120 kVp, n	12		
100 kVp, n		9	
80 kVp, n		3	
Tube current, mean ± SD (mAs)	332.7 ± 9.1	336.0 ± 11.3	0.39
CT dose index volume, mean ± SD (mGy)	41.8 ± 17.8	19.7 ± 9.4	<0.001
Dose-length product, mean ± SD (mGy · cm)	685.6 ± 278.8	266.9 ± 160.0	<0.001
Scan length, mean ± SD (cm)	12.8 ± 1.6	12.9 ± 1.9	0.41
Image noise, mean ± SD (HU)	24.9 ± 6.0	26.0 ± 7.5	0.84
Effective dose, mean ± SD (mSv)	9.6 ± 3.9	3.7 ± 2.2	0.35

FBP, filtered back projection; IRIS, iterative reconstruction in image space.

both of which have traditionally been recognized as limitations of cardiac CT.

References

1. Ziegler A, Kohler T, Proksa R: Noise and resolution in images reconstructed with FBP and OSC algorithms for CT. Med Phys. 2007;34: 585–98.
2. Thibault JB, Sauer KD, Bouman CA, Hsieh J: A three-dimensional statistical approach to improved image quality for multislice helical CT. Med Phys. 2007;34:4526–44.
3. Sarwar A, Rieber J, Mooyaart EA, Seneviratne SK, Houser SL, Bamberg F, Raffel OC, Gupta R, Kalra MK, Pien H, Lee H, Brady TJ, Hoffmann U: Calcified plaque: measurement of area at thin-section flat-panel CT and 64-section multidetector CT and comparison with histopathologic findings. Radiology. 2008;249:301–6.
4. Brooks RA, Di Chiro G: Theory of image reconstruction in computed tomography. Radiology. 1975;117(3 Pt 1):561–72.
5. Min JK, Swaminathan RV, Vass M, Gallagher S, Weinsaft JW: High-definition multidetector computed tomography for evaluation of coronary artery stents: comparison to standard-definition 64-detector row computed tomography. J Cardiovasc Comput Tomogr. 2009;3:246–51.
6. Bittencourt MS, Schmidt B, Seltmann M, Muschiol G, Ropers D, Daniel WG, Achenbach S: Iterative reconstruction in image space (IRIS) in cardiac computed tomography: initial experience [published online ahead of print December 1, 2010]. Int J Cardiovasc Imaging. doi:10.1007/s10554-010-9756-3.
7. Leipsic J, Nguyen G, Brown J, Sin D, Mayo JR: A prospective evaluation of dose reduction and image quality in chest CT using adaptive statistical iterative reconstruction. AJR Am J Roentgenol. 2010;195:1095–9.
8. Leipsic J, Labounty TM, Heilbron B, Min JK, Mancini GB, Lin FY, Taylor C, Dunning A, Earls JP: Estimated radiation dose reduction using adaptive statistical iterative reconstruction in coronary CT angiography: the ERASIR study. AJR Am J Roentgenol. 2010;195: 655–60.
9. Bruder H, Raupach R, Sunnegardh J, Sedlmair M, Stierstorfer K, Flohr TG: Adaptive iterative reconstruction. Proc SPIE Medical Imaging. 2011; doi:10.1117/12.877953.

Evaluation of Heavily Calcified Vessels with Coronary CT Angiography: Comparison of Iterative and Filtered Back Projection Image Reconstruction[1]

Matthias Renker, BS
John W. Nance, Jr, MD
U. Joseph Schoepf, MD
Terrence X. O'Brien, MD, MS
Peter L. Zwerner, MD
Mathias Meyer, BS
J. Matthias Kerl, MD
Ralf W. Bauer, MD
Christian Fink, MD
Thomas J. Vogl, MD
Thomas Henzler, MD

Purpose: To prospectively compare traditional filtered back projection (FBP) and iterative image reconstruction for the evaluation of heavily calcified arteries with coronary computed tomography (CT) angiography.

Materials and Methods: The study had institutional review board approval and was HIPAA compliant. Written informed consent was obtained from all patients. Fifty-five consecutive patients (35 men, 20 women; mean age, 58 years ± 12 [standard deviation]) with Agatston scores of at least 400 underwent coronary CT angiography and cardiac catheterization. Image data were reconstructed with both FBP and iterative reconstruction techniques with corresponding cardiac algorithms. Image noise and subjective image quality were compared. To objectively assess the effect of FBP and iterative reconstruction on blooming artifacts, volumes of circumscribed calcifications were measured with dedicated volume analysis software. FBP and iterative reconstruction series were independently evaluated for coronary artery stenosis greater than 50%, and their diagnostic accuracy was compared, with cardiac catheterization as the reference standard. Statistical analyses included paired *t* tests, Kruskal-Wallis analysis of variance, and a modified McNemar test.

Results: Image noise measured significantly lower (P = .011–.035) with iterative reconstruction instead of FBP. Image quality was rated significantly higher (P = .031 and .042) with iterative reconstruction series than with FBP. Calcification volumes measured significantly lower (P = .019 and .026) with iterative reconstruction (44.3 mm^3 ± 64.7 and 46.2 mm^3 ± 68.8) than with FBP (54.5 mm^3 ± 69.5 and 56.3 mm^3 ± 72.5). Iterative reconstruction significantly improved some measures of per-segment diagnostic accuracy of coronary CT angiography for the detection of significant stenosis compared with FBP (accuracy: 95.9% vs 91.8%, P = .0001; specificity: 95.8% vs 91.2%, P = .0001; positive predictive value: 76.9% vs 61.1%, P = .0001).

Conclusion: Iterative reconstruction reduces image noise and blooming artifacts from calcifications, leading to improved diagnostic accuracy of coronary CT angiography in patients with heavily calcified coronary arteries.

[1] From the Heart and Vascular Center, Medical University of South Carolina, Ashley River Tower, 25 Courtenay Dr, Charleston, SC 29425-2260 (M.R., J.W.N., U.J.S., T.X.O., P.L.Z., M.M., J.M.K., R.W.B., C.F., T.H.); Department of Radiology, Johann Wolfgang Goethe University, Frankfurt, Germany (M.R., J.M.K., R.W.B., T.J.V.); Ralph H. Johnson Veterans Affairs Medical Center, Charleston, SC (T.X.O.); and Institute of Clinical Radiology and Nuclear Medicine, University Medical Center Mannheim, Heidelberg University, Mannheim, Germany (M.M., C.F., T.H.). Received December 30, 2010; revision requested February 28, 2011; revision received March 18; accepted April 2; final version accepted April 20. Supported in part by the Research and Development Program of the Department of Veterans Affairs. **Address correspondence to** U.J.S. (e-mail: *schoepf@musc.edu*).

The contents do not represent the views of the Department of Veterans Affairs or the United States Government.

A large body of literature has shown that coronary computed tomography (CT) angiography can be used to sensitively rule out coronary artery stenosis in patients with chest pain (1). Nevertheless, those studies also consistently demonstrate that, despite advances in CT technology, the specificity of this test frequently remains limited by heavy coronary artery calcifications, which are the most common reason for false-positive findings. Heavy calcifications cause blooming artifacts, which can lead to overestimation of lesions (2), often prompting unnecessary coronary catheterization or myocardial perfusion studies (3,4).

The current standard CT image reconstruction technique is filtered back projection (FBP). However, FBP has limitations vis-à-vis three-dimensional cone-beam geometry, data completeness, and low photon environments (5). To some extent, blooming artifacts arising from heavy calcifications are attributable to these technical shortcomings (6).

Iterative reconstruction techniques have been proposed for over 3 decades to improve CT image quality by reducing quantum noise and artifacts (7) but were used mainly in the context of emission tomography (8). Only recently has computer power evolved enough to enable iterative image reconstruction within a clinically acceptable time frame for general CT applications. Beneficial effects of iterative reconstruction techniques in CT applications throughout the body have since been reported (9–13). However, the potential of this approach to improve the diagnostic accuracy of coronary CT angiography, especially in problematic scenarios (eg, the presence of heavy calcifications), has not been explored.

Accordingly, the aim of our prospective study was to compare traditional FBP with iterative image reconstruction for the evaluation of heavily calcified arteries with coronary CT angiography.

Advances in Knowledge

- Heavy coronary artery calcifications show significantly lower volumes at coronary CT angiography when iterative image reconstruction is used compared with traditional filtered back projection (FBP), indicating decreased blooming artifacts from calcified coronary atherosclerotic plaques.
- Compared with FBP, iterative image reconstruction significantly improves accuracy, specificity, and positive predictive value (PPV) of coronary CT angiography for the evaluation of coronary artery stenosis in patients with heavy vessel calcifications.

Implication for Patient Care

- An increase in the specificity and PPV of coronary CT angiography with iterative reconstruction techniques could reduce the number of unnecessary follow-up studies performed as a result of false-positive findings at coronary CT angiography in patients with heavily calcified plaques.

Materials and Methods

U.J.S. is a consultant for Bayer Healthcare (Berlin, Germany), Medrad (Indianola, Pa), and Siemens Healthcare (Forchheim, Germany), whose products were used in this investigation. The authors who are not consultants for those companies had control of inclusion of any data and information that might present a conflict of interest.

Patients

This study was part of a larger investigation evaluating the accuracy of coronary CT angiography for detection of coronary artery stenosis in symptomatic patients referred for cardiac catheterization. The study was approved by the institutional review board of the Medical University of South Carolina and was conducted in accordance with Health Insurance Portability and Accountability Act regulations. Written informed consent was obtained from all patients. We prospectively included coronary CT angiograms of 55 consecutive patients (35 men, 20 women; mean age, 58 years ± 12 [standard deviation]) with an Agatston score of at least 400, which is indicative of substantial calcified plaque burden. Exclusion criteria were a history of contrast material reaction and impaired renal function (creatinine higher than 1.5 mg/dL and/or glomerular filtration rate lower than 60 mL/min).

Scanning Technique

Calcium scoring and coronary CT angiography were performed with a second-generation dual-source CT scanner (Somatom Definition Flash; Siemens Healthcare). Prior to contrast material–enhanced coronary CT angiography, calcium scoring was performed in all patients by using a prospective electrocardiographically (ECG)-triggered high-pitch spiral acquisition technique (14). Transverse images were reconstructed with a section thickness of 3 mm and 50% overlap. The coronary CT angiography technique was chosen individually for each patient depending on heart rate and/or rhythm and body mass index, with the goal of minimizing radiation exposure. Scan techniques included traditional retrospective ECG gating with default use of ECG-dependent tube current modulation, prospective ECG triggering, and prospective ECG-triggered high-pitch spiral acquisitions. Contrast enhancement was achieved by injecting 60–90 mL of iodinated contrast material (370 mg I/mL iopromide, Ultravist;

Published online before print
10.1148/radiol.11103574 **Content code:** CA

Radiology 2011; 260:390–399

Abbreviations:
ECG = electrocardiography
FBP = filtered back projection
PPV = positive predictive value
ROI = region of interest

Author contributions:
Guarantors of integrity of entire study, M.R., U.J.S., M.M., T.H.; study concepts/study design or data acquisition or data analysis/interpretation, all authors; manuscript drafting or manuscript revision for important intellectual content, all authors; approval of final version of submitted manuscript, all authors; literature research, M.R., J.W.N., U.J.S., T.X.O., M.M., J.M.K., R.W.B., C.F., T.H.; clinical studies, M.R., U.J.S., T.X.O., P.L.Z., J.M.K., R.W.B., C.F., T.J.V.; statistical analysis, M.R., U.J.S., M.M., R.W.B., T.J.V., T.H.; and manuscript editing, all authors

Potential conflicts of interest are listed at the end of this article.

Bayer Healthcare), injected at 6 mL/sec through an 18-gauge intravenous antecubital catheter by using a dual-syringe injector (Stellant D; Medrad). Acquisition parameters were as follows: detector collimation, 2 × 64 × 0.6 mm; gantry rotation time, 280 msec; and tube current–time product, 320 mAs per rotation. The tube potential used was 120 kV in patients with a body mass index of 25 kg/m^2 or greater, 100 kV in patients with a body mass index of less than 25 kg/m^2 but greater than or equal to 20 kg/m^2, and 80 kV in patients with a body mass index of less than 20 kg/m^2. Images were acquired in the craniocaudal direction from above the origin of the coronary arteries to below the dome of the diaphragm. Effective radiation dose was derived by multiplying the dose-length product by a chest-specific conversion coefficient (κ = 0.014 mSv/Gy/cm) (15).

Image Reconstruction

Images were reconstructed from the coronary CT angiography raw data with both FBP and iterative image reconstruction (Iterative Reconstruction in Image Space [IRIS]; Siemens Healthcare) (Fig 1). This iterative reconstruction approach is based on an initial master FBP reconstruction with a very sharp convolution algorithm, or kernel, still containing all frequencies and, therefore, all information of the initial raw data. Subsequent iterative processing loops are applied to the image volume with the goal of reducing image noise while preserving spatial resolution. During each iteration, general image properties (eg, edge information and contrast-to-noise ratio) are analyzed based on a noise model of the system, which is directly derived from the raw data. The Gaussian noise model is applied in a regularization step. Image noise is estimated from image volume data by locally computing the minimum noise variance. The strength of the regularization controls the effect of the edge-preserving low-pass filter in each update of the iteration procedure (5). The result of the regularization step is compared with the initial data to generate an update image, which is added to the previous data set before the next iteration is performed. Therefore, the iterative loops enable noise reduction while preserving edge information and low-contrast structures. Iterative and FBP reconstructions were performed at a section thickness of 0.75 mm and a position increment of 0.4 mm. Corresponding vascular and high-spatial-resolution kernels were applied for FBP (B26f and B46f, respectively) and iterative reconstructions (I26f and I46f, respectively). The B46f and I46f kernels, which are sharp edge-preserving convolution algorithms, were included because of the previously described beneficial effects of these higher-spatial-frequency algorithms on the evaluation of high density structures, such as heavy coronary artery calcifications and stents (16–19).

Image Noise, Attenuation, and Subjective Image Quality

All data sets were transferred to a standalone image processing workstation (Syngo MMWP VE 36A; Siemens). In each data set, one observer (M.R.) measured image noise, which was defined as the standard deviation of the measured attenuation (in Hounsfield units) within circular regions of interest (ROIs) in the ascending aorta, interventricular septum, and left ventricular cavity. The size of the ROIs was adapted to account for anatomic differences of our patients; however, between the different reconstruction approaches, the ROI size was kept constant within each patient. Subjective image quality was independently rated by two radiologists (U.J.S. and T.H., with 10 and 5 years experience in coronary CT angiography, respectively). FBP and iterative reconstructed images were reviewed in random order. Images were rated on a five-point Likert scale according to the severity of image noise, quality of contour delineation, and general image impression (1 = poor, 2 = fair, 3 = moderate, 4 = good, 5 = excellent).

Volumetric Analysis of Coronary Artery Calcifications

One observer (M.R.) used a threshold-based volumetry software tool (Volume Analysis, version VE31A; Siemens) to determine the volumes of fragmented and diffuse (20) coronary artery calcifications within FBP and iterative reconstruction data sets. Calcifications were semiautomatically segmented by defining ROIs around calcifications, which were then automatically propagated to the neighboring sections and manually corrected, if necessary. Voxels within these ROIs with attenuation values in the range of contrast material were automatically excluded from the segmentation, with the goal of only including calcium. To achieve this, we measured the maximum contrast attenuation within the ascending aorta and added 20% to this measurement to define the minimum attenuation level of voxels to be included in the volumetric analysis. This level was kept constant between the different reconstruction techniques in individual patients.

Coronary CT Angiography versus Coronary Catheterization

All data sets and reconstructions were jointly evaluated by two radiologists (U.J.S., T.H.) for the presence of stenotic (>50%) coronary artery disease using the American Heart Association 15-segment model (21). Readers were blinded to the reconstruction technique. For lesion detection, readers were provided with a combination of the vascular and high-spatial-resolution algorithm reconstruction series based on FBP (B26f plus B46f) and iterative (I26f plus I46f) reconstruction. FBP and iterative reconstruction image series were presented in random order at least 3 weeks apart in the same patient to minimize reader recall. The readers were permitted to adjust window and level settings individually for each study. Cardiac catheterization served as the reference standard for stenosis detection and was performed with the conventional Judkins technique on the same day as the coronary CT angiography. At least two views of the right coronary artery and four views of the left coronary artery were interpreted for greater than 50% stenosis by two cardiologists (T.X.O. and P.L.Z., both with more than 15 years experience) in consensus by using the same 15-segment American Heart Association model.

Table 1

Patient Demographics and Scan Parameters

Parameter	Datum
Age (y)	58.2 ± 12.0
Male-to-female ratio	35:20
Height (cm)	170.4 ± 10.3
Weight (kg)	92.2 ± 20.7
Body mass index (kg/m^2)	31.6 ± 5.8
Heart rate (beats per minute)*	63.1 ± 8.0 (53–72)
Agatston score*	710 ± 289 (466–2934)
No. of patients at each tube potential	
80 kVp	1
100 kVp	10
120 kVp	44
Tube current–time product (mAs)	331.4 ± 22.9
CT dose index volume (mGy)	35.0 ± 21.2
Dose-length product (mGy · cm)	609.1 ± 394.3
Scan length (cm)	12.9 ± 1.8
Effective dose (mSv)	
Retrospective ECG gated (n = 35)	10.5 ± 4.2
Prospective ECG triggered (n = 11)	6.6 ± 3.1
High pitch spiral (n = 9)	2.3 ± 1.4

Note.—Unless otherwise specified, data are means ± standard deviations.

* Data in parentheses are the range.

Figure 1

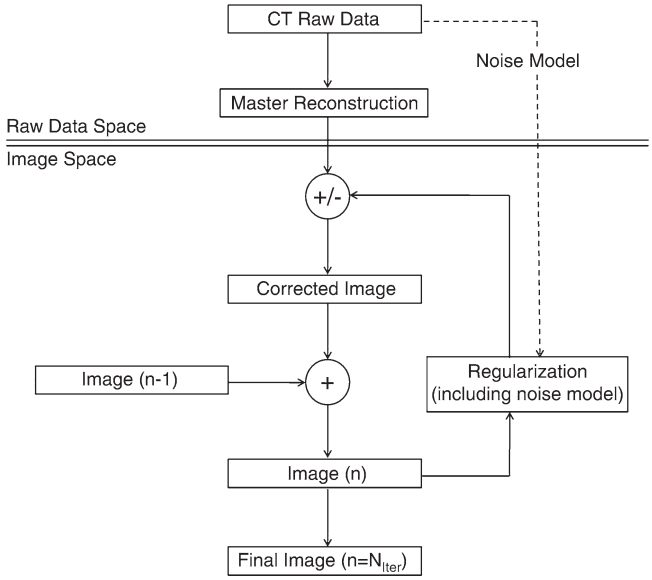

Figure 1: Schematic of the iterative reconstruction process (Iterative Reconstruction in Image Space [IRIS]; Siemens Healthcare). A single FBP image reconstruction initially takes place in the raw data domain to generate a master reconstruction. All further reconstruction steps take place in image space. Further steps include a regularization loop based on prior image information with the goal of suppressing artifacts and reducing image noise. − = subtraction of detected image noise, + = modeling of image noise and validation of corrections, n = image no. within iterative loop, n-1 = image of prior iterative loop, N_{Iter} = no. of iterations.

Statistical Analysis

Statistical analyses were performed by using dedicated statistical software (SPSS 12.0; SPSS, Chicago, Ill). The Shapiro-Wilk W test was used to identify normally distributed data. Significance was investigated with χ^2 statistics for categorical variables. Continuous variables are presented as means ± standard deviations and were compared by using one-on-one comparisons with either an independent t test for normally distributed data or a Mann-Whitney U test for nonnormally distributed data. Ordinal variables (ie, image quality) are presented as medians with interquartile ranges and were compared by using the Kruskal-Wallis analysis of variance. P values less than .05 were considered to indicate a significant difference. Interobserver agreement for subjective image quality was quantified by using κ statistics. The diagnostic accuracy (ie, accuracy, sensitivity, specificity, negative predictive value, and positive predictive value [PPV]) of each reconstruction technique for detection of large (>50%) stenoses was calculated with cardiac catheterization as the reference standard. Differences in diagnostic accuracy between the two reconstruction techniques were compared by creating matched sample tables and by using a modified McNemar test to calculate P values.

Results

All 55 coronary CT angiograms were successfully completed and considered to be of diagnostic image quality. Patient demographics and coronary CT angiogram characteristics are provided in Table 1. The average body mass index in our patient cohort was 31.6 kg/m^2, indicative of a high prevalence of obesity, and the average Agatston calcium score was 710, reflecting advanced atherosclerosis.

Image Noise, Attenuation, and Subjective Image Quality

In both image reconstructions using the vascular I26f and B26f as well as the high spatial resolution B46f and I46f convolution algorithms, mean image

Table 2

Mean Image Noise and Attenuation for the Four Different Reconstructions

Anatomic Region	Vascular Algorithm: FBP with B26f Kernel	Vascular Algorithm: Iterative Reconstruction with I26f Kernel	Vascular Algorithm: *P* Value	High-Spatial-Resolution Algorithm: FBP with B46f Kernel	High-Spatial-Resolution Algorithm: Iterative Reconstruction with I46f Kernel	High-Spatial-Resolution Algorithm: *P* Value
			Mean Image Noise			
Ascending aorta	33.4 ± 11.7	24.9 ± 10.8	.013	48.3 ± 15.2	35.9 ± 10.0	.025
Interventricular septum	30.5 ± 13.7	22.9 ± 12.5	.023	52.8 ± 16.6	38.0 ± 13.1	.011
Left ventricular cavity	38.6 ± 16.9	31.9 ± 16.3	.035	64.1 ± 28.2	47.8 ± 21.3	.017
			Mean Attenuation (HU)			
Ascending aorta	427.0 ± 131.8	430.7 ± 131.0	.085	431.7 ± 174.5	435.2 ± 176.9	.087
Interventricular septum	124.2 ± 42.2	119.1 ± 30.5	.069	128.7 ± 28.4	126.8 ± 35.2	.088
Left ventricular cavity	367.9 ± 133.0	372.1 ± 125.3	.075	373.1 ± 198.8	384.4 ± 216.4	.073

Note.—Unless otherwise specified, data are means ± standard deviations.

noise measured significantly lower using iterative reconstruction than FBP in all ROIs, while there was no significant difference in mean attenuation within the same anatomic regions (Table 2) (Fig 2).

Image quality of coronary CT angiograms reconstructed with iterative reconstruction was rated significantly higher than that of those reconstructed with FBP by both observers. With both iterative reconstructions (I26f and I46f kernels), the median image quality score was 5; whereas with both FBP reconstructions (B26f and B46f kernels), the median image quality score was 4. Pairwise Wilcoxon rank sum tests showed statistically higher ratings for iterative reconstruction than for FBP (I26f vs B26f, $P = .042$; I46f vs B46f, $P = .031$). Interobserver agreement was excellent for iterative and FBP reconstructions (I26f, $\kappa = 0.89$; I46f, $\kappa = 0.92$; B26f, $\kappa = 0.84$; B46f, $\kappa = 0.88$).

Volumetric Analysis of Coronary Artery Calcifications

A total of 142 circumscribed coronary artery calcifications were volumetrically analyzed among all four reconstructions. Coronary artery calcifications showed significantly lower volumes on iterative reconstruction images compared with FBP images (I26f vs B26f: 46.2 mm^3 ± 68.8 vs 56.3 mm^3 ± 72.5, $P = .026$; I46f vs B46f: 44.3 mm^3 ± 64.7 vs 54.5 mm^3 ± 69.5, $P = .019$) (Fig 3).

Figure 2

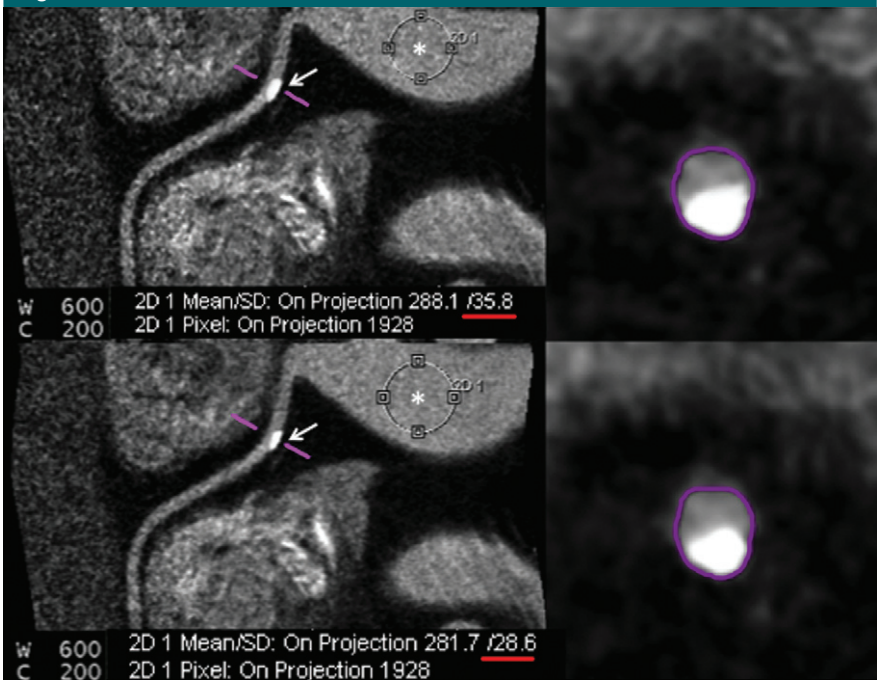

Figure 2: Contrast-enhanced retrospectively ECG-gated coronary CT angiographic images in a 63-year-old man (body mass index, 35.2 kg/m^2) referred for coronary catheterization because of chest pain on exertion. Left: Right coronary artery as curved multiplanar reformation along vessel centerline (purple). Right: Transverse sections through vessel (purple), orthogonal to centerline. Top: FBP reconstruction shows image noise in a circular aortic root ROI of 35.8 HU (red). Bottom: iterative reconstruction shows image noise in a circular aortic root ROI of 28.6 HU (red). Suppression of blooming artifacts in iterative reconstructions improves vessel lumen delineation adjacent to the calcified lesion (arrows) and facilitates estimation of the true degree of luminal narrowing.

Coronary CT Angiography versus Coronary Catheterization

A total of 825 coronary artery segments were analyzed with cardiac catheterization as well as with coronary CT angiography. Cardiac catheterization showed stenoses larger than 50% in 31 (56%) patients, with a total of 104 lesions. Six

patients had one-vessel disease, 18 patients had two-vessel disease, and seven patients had three-vessel disease. By using iterative reconstruction instead of FBP, there was a significant improvement in overall accuracy, specificity, and PPV on a per-segment level and in specificity and PPV on a per-patient level for the detection of significant stenosis with coronary CT angiography (Table 3). In 33 of 825 segments and three of 55 patients, iterative reconstruction enabled reclassification from false-positive to true-negative results (Figs 4, 5). In one patient, an isolated short but important stenosis in the distal posterior descending artery was missed in both iterative reconstruction and FBP series.

Discussion

Our findings show that the use of iterative reconstruction instead of traditional FBP significantly improves the specificity, PPV, and overall accuracy of coronary CT angiography for stenosis detection in patients with heavily calcified coronary arteries. These improvements are likely related to decreases in image noise, improved diagnostic image quality, and reduced blooming artifacts.

Advances in CT technology, with improvements in temporal and spatial resolution, have continuously increased the robustness and accuracy of coronary CT angiography for the noninvasive assessment of coronary artery disease (22,23). A multitude of studies have demonstrated the ability of this test to be used to reliably exclude coronary artery stenosis as compared with coronary catheterization (23–28) or as assessed through patient outcome (29–31). However, these studies have also identified several persistent limitations that remain considerable detractors from the diagnostic performance of coronary CT angiography. Among these are patient obesity, with associated high image noise, and the presence of heavy coronary artery calcifications (25,26,32). Blooming artifacts exaggerate the size of densely calcified plaques and limit the accurate evaluation of the adjacent coronary artery lumen, typically leading to overestimation of lesion severity. The resulting false-positive findings do not detract from this test's sensitivity; however, they decrease specificity, often leading to unnecessary subsequent layered testing to exclude stenotic coronary artery disease, which incurs additional cost, patient radiation exposure, and potential complications from coronary catheterization, thus limiting the clinical usefulness of coronary CT angiography (3,33).

Blooming artifacts from calcified plaques are partially attributed to the limited spatial and point-spread resolution of CT image reconstruction algorithms, which create a spillover effect from high-attenuation structures into adjacent lower-attenuation voxels, obscuring the coronary artery lumen (33–35). Blooming artifacts can be reduced by increasing spatial resolution through thinner collimated section widths and reconstruction thickness, as well as use of higher-resolution sharper reconstruction algorithms. However, these approaches come at the expense of higher image noise or higher radiation dose requirements for suppressing image noise when traditional FBP is used. Iterative reconstruction techniques, to a certain extent, allow decoupling of spatial resolution and image noise and offer the potential to selectively improve high-contrast resolution without affecting image noise in low-contrast areas (5,36).

Figure 3

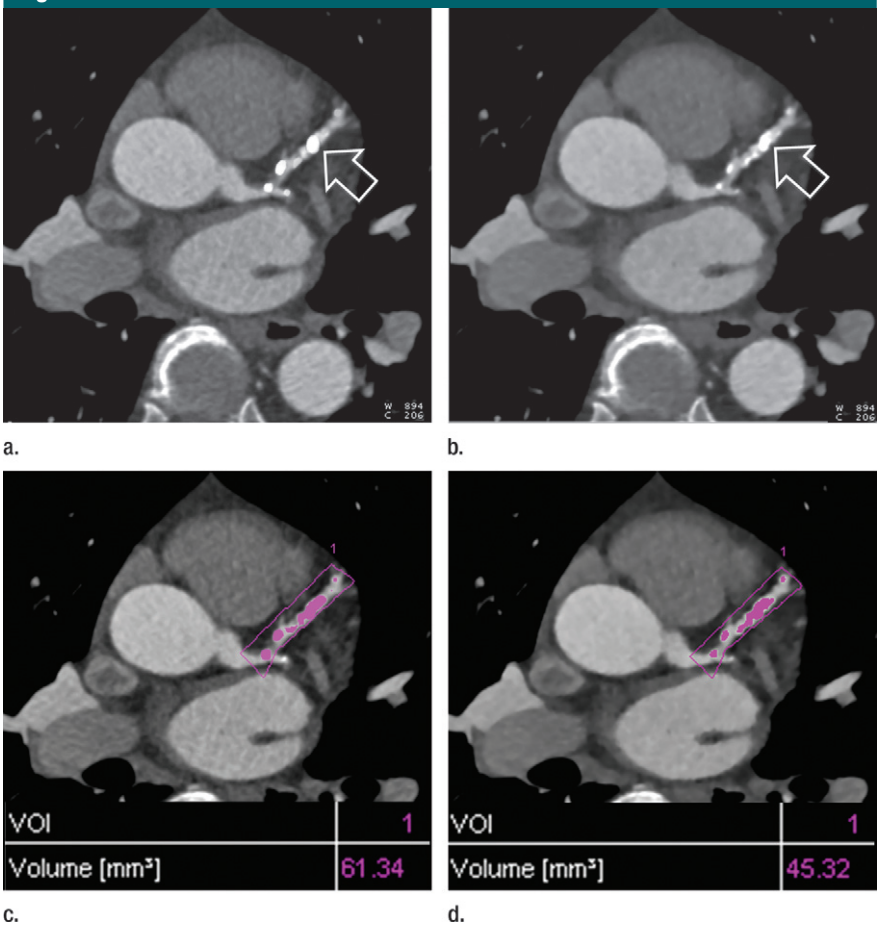

Figure 3: Contrast-enhanced prospectively ECG-triggered coronary CT angiographic images in a 76-year-old woman with chest pain and abnormal nuclear myocardial perfusion scan. Transverse **(a)** FBP and **(b)** iterative reconstruction images at the level of the aortic root show extensive calcified plaque burden (arrows) in the proximal left anterior descending coronary artery. Threshold-dependent volumetry of calcifications (purple) resulted in a measured volume of 61.34 mm^3 on **(c)** FBP reconstructions and of 45.32 mm^3 on **(d)** iterative reconstructions.

Table 3

Diagnostic Accuracy of FBP and Iterative Reconstruction for the Detection of Coronary Artery Stenoses Larger than 50% versus Reference Standard Cardiac Catheterization

	Per Segment			Per Patient		
Parameter	FBP	Iterative Reconstruction	*P* Value	FBP	Iterative Reconstruction	*P* Value
Accuracy (%)*	91.8 (71.7, 91.1)	95.9 (78.2, 94.9)	.0001	83.6 (89.7, 93.5)	89.1 (94.3, 97.0)	NS
Sensitivity (%)*	95.2 (83.8, 99.4)	96.2 (83.8, 99.4)	NS	96.7 (89.2, 97.9)	96.7 (90.5, 98.5)	NS
Specificity (%)	91.2 (46.7, 82.0)	95.8 (59.5, 90.8)	.0001	66.7 (89.0, 93.1)	79.2 (94.1, 97.1)	.0189
Negative predictive value (%)*	99.2 (69.2, 99.7)	99.4 (73.1, 99.7)	NS	94.1 (98.1, 99.7)	95.0 (98.4, 99.8)	NS
PPV (%)*	61.1 (62.2, 89.9)	76.9 (69.0, 94.6)	.0001	78.9 (53.1, 68.6)	85.7 (68.6, 83.7)	.0403
No. of true-positive findings	99	100	NS	30	30	NS
No. of false-positive findings	63	30	.0001	8	5	NS
No. of true-negative findings	658	691	.0001	16	19	NS
No. of false-negative findings	5	4	NS	1	1	NS

Note.—NS = not significant.

* Data in parentheses are 95% confidence intervals.

Accordingly, the properties of iterative reconstruction seem better suited than those of traditional FBP to address the requirements of coronary CT angiography, where both high spatial and contrast resolution are of importance for the evaluation of small target vessels containing both high-attenuation (calcifications, stents) and low-attenuation (noncalcified plaque) structures. As a postacquisition image reconstruction approach, the effects of iterative reconstruction should be largely independent of the image acquisition technique (eg, prospective ECG triggering vs retrospective ECG gating), although we did not subanalyze our results for this aspect.

The limitations of coronary CT angiography will not be completely overcome with iterative reconstruction techniques. However, the observed increase in specificity and PPV with use of this technique indicates the potential to reduce the need for unnecessary further testing in patients undergoing coronary CT angiography. We specifically selected for individuals with Agatston scores of at least 400, whereas the 2010 appropriate use criteria for cardiac computed tomography (37) consider the usefulness of coronary CT angiography in this scenario as uncertain. The more widespread implementation of iterative reconstruction techniques may hold potential for widening the scope of patients in whom

Figure 4

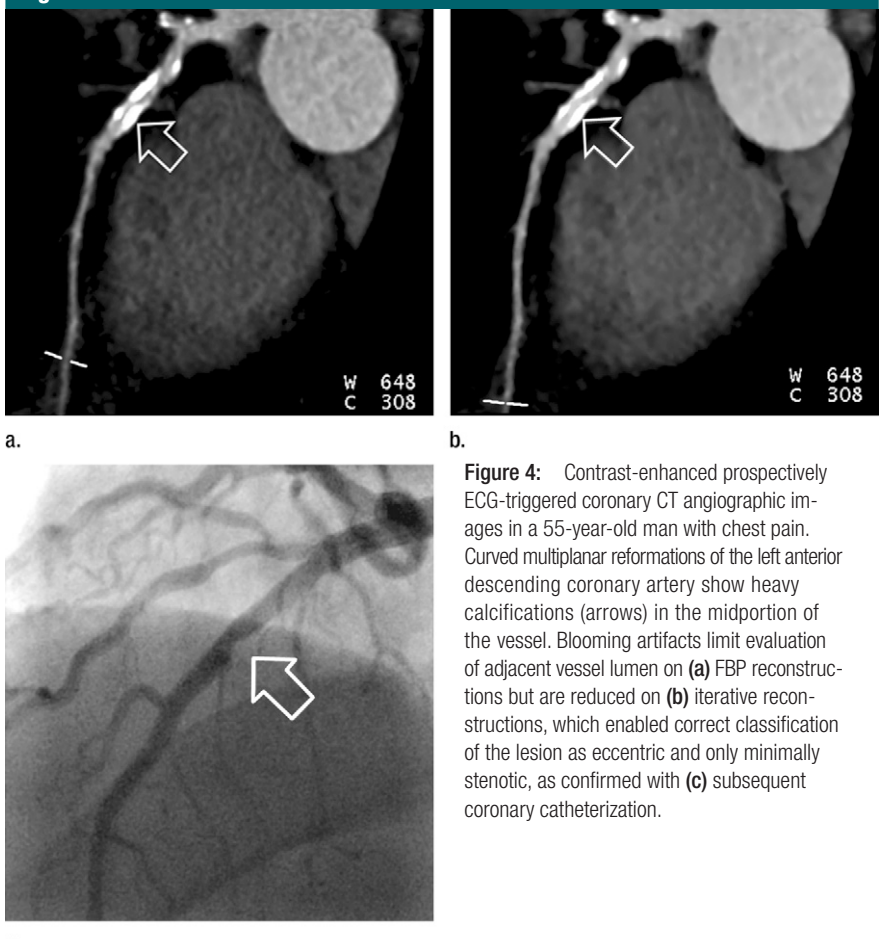

a. b. c.

Figure 4: Contrast-enhanced prospectively ECG-triggered coronary CT angiographic images in a 55-year-old man with chest pain. Curved multiplanar reformations of the left anterior descending coronary artery show heavy calcifications (arrows) in the midportion of the vessel. Blooming artifacts limit evaluation of adjacent vessel lumen on **(a)** FBP reconstructions but are reduced on **(b)** iterative reconstructions, which enabled correct classification of the lesion as eccentric and only minimally stenotic, as confirmed with **(c)** subsequent coronary catheterization.

Figure 5

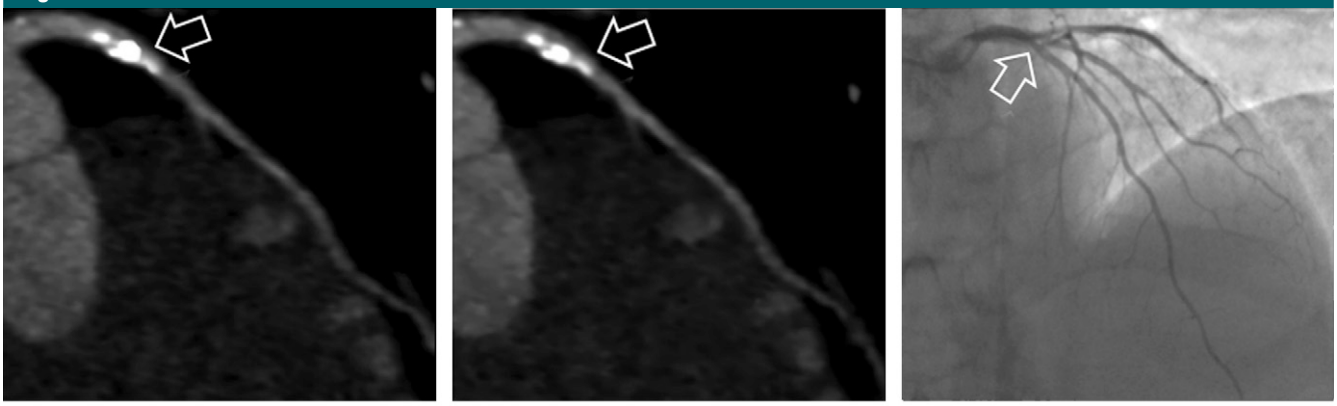

a. b. c.

Figure 5: Contrast-enhanced prospectively ECG-triggered coronary CT angiographic images in a 73-year-old man with chest pain. Curved multiplanar reformations of the left anterior descending coronary artery show heavy calcifications (arrows) in the proximal vessel. Blooming artifacts limit evaluation of adjacent vessel lumen on **(a)** FBP reconstructions, mimicking a substantial stenosis, but are reduced on **(b)** iterative reconstructions, which enabled correct classification of the lesion as not significantly stenotic, as confirmed with **(c)** subsequent coronary catheterization.

coronary CT angiography can be effectively and beneficially used.

In this investigation, we focused solely on possible improvements in diagnostic accuracy garnered by the use of iterative reconstruction over FBP in patients in whom heavily calcified coronary arteries pose a diagnostic challenge. Recent reports indicate the potential of radiation dose reduction through decreases in image noise with use of iterative reconstruction techniques (10,11). However, this was not the focus of our current study.

Due to the size of our cohort, only a limited number of patients were correctly reclassified as free of stenosis on the basis of iterative reconstruction, and the improvement in per-patient accuracy did not reach significance. However, the significant increases in specificity and PPV both on a per-segment and per-patient level hold promise to improve the relatively low performance (38) of this test for the evaluation of heavily calcified coronary arteries. In particular, when extrapolated to the overall number of patients undergoing coronary CT angiography, the benefits of reduced follow-up testing could be notable. A general inherent limitation of all studies that compare iterative reconstruction with traditional FBP is the fact that observers cannot be effectively blinded to the reconstruction technique because of the distinct differences in image characteristics between the two approaches. Moreover, in our study, all images were derived from the same raw data for each patient, leaving the possibility of some biases and inflated statistical significance owing to multireader effects that were not accounted for. The effect of interreader variation, which may have influenced the results on image quality, is likely small since the overall agreement between readers was excellent (>0.6), and the variance of κ statistics was lower than 10%. Based on the design of this study, intrareader variation was closely related to the choice of different kernels used and could be interpreted as a systematic influence across both reconstruction techniques. Another limitation is the absence of an outside reference standard, such as intravascular ultrasonography, to validate our volumetric measurements of coronary artery calcifications. Since we selected for patients with advanced atherosclerosis whose symptoms had indicated the need for coronary catheterization, the disease prevalence was high, exceeding 50%. Thus, the extrapolation of the general performance parameters of coronary CT angiography observed in our study to a population with a lower pretest likelihood of disease is limited by the well-known effects of disease prevalence on the predictive value of a test. However, this does not detract from the observation that a long-standing limitation of coronary CT angiography (ie, heavy calcifications) might be ameliorated by abandoning traditional FBP as the standard method for image reconstruction.

In summary, the results of our study suggest that accuracy, specificity, and PPV of stenosis detection with coronary CT angiography in heavily calcified vessels can be incrementally improved with use of iterative reconstruction instead of FBP. Accordingly, iterative reconstruction should be preferentially used in patients with advanced atherosclerosis to reduce the number of unnecessary follow-up studies.

Disclosures of Potential Conflicts of Interest: M.R. Financial activities related to the present article: none to disclose. Financial activities not related to the present article: receives travel/accommodations/meeting expenses from Siemens. Other relationships: none to disclose. **J.W.N.** No potential conflicts of interest to disclose. **U.J.S.** Financial activities related to the present article: none to disclose. Financial activities not related to the present article: is a consultant for and is on the speakers bureau of Bayer Healthcare, Bracco, GE Healthcare, Medrad, and Siemens Healthcare; institution has grants from Bayer Healthcare, Bracco, GE Healthcare, Medrad, and Siemens Healthcare. Other relationships: none to disclose. **T.X.O.** No potential conflicts of interest to disclose. **P.L.Z.** No potential conflicts of interest to disclose. **M.M.** No potential conflicts of interest to disclose. **J.M.K.** Financial activities related to the present article: none to disclose. Financial activities not related to the present

article: is a consultant for and on the speakers bureau of Siemens. Other relationships: none to disclose. **R.W.B.** Financial activities related to the present article: none to disclose. Financial activities not related to the present article: is on the speakers bureau of and receives travel/accommodations/meeting expenses from Siemens Healthcare. Other relationships: none to disclose. **C.F.** No potential conflicts of interest to disclose. **T.J.V.** No potential conflicts of interest to disclose. **T.H.** No potential conflicts of interest to disclose.

References

1. Vanhoenacker PK, Heijenbrok-Kal MH, Van Heste R, et al. Diagnostic performance of multidetector CT angiography for assessment of coronary artery disease: meta-analysis. Radiology 2007;244(2):419–428.
2. Meijs MF, Meijboom WB, Prokop M, et al. Is there a role for CT coronary angiography in patients with symptomatic angina? effect of coronary calcium score on identification of stenosis. Int J Cardiovasc Imaging 2009;25(8):847–854.
3. Raff GL, Gallagher MJ, O'Neill WW, Goldstein JA. Diagnostic accuracy of noninvasive coronary angiography using 64-slice spiral computed tomography. J Am Coll Cardiol 2005;46(3):552–557.
4. Zhang LJ, Wu SY, Wang J, et al. Diagnostic accuracy of dual-source CT coronary angiography: the effect of average heart rate, heart rate variability, and calcium score in a clinical perspective. Acta Radiol 2010;51(7):727–740.
5. Thibault JB, Sauer KD, Bouman CA, Hsieh J. A three-dimensional statistical approach to improved image quality for multislice helical CT. Med Phys 2007;34(11):4526–4544.
6. Zhang S, Levin DC, Halpern EJ, Fischman D, Savage M, Walinsky P. Accuracy of MDCT in assessing the degree of stenosis caused by calcified coronary artery plaques. AJR Am J Roentgenol 2008;191(6):1676–1683.
7. Brooks RA, Di Chiro G. Theory of image reconstruction in computed tomography. Radiology 1975;117(3 Pt 1):561–572.
8. Lange K, Carson R. EM reconstruction algorithms for emission and transmission tomography. J Comput Assist Tomogr 1984;8(2):306–316.
9. Flicek KT, Hara AK, Silva AC, Wu Q, Peter MB, Johnson CD. Reducing the radiation dose for CT colonography using adaptive statistical iterative reconstruction: a pilot study. AJR Am J Roentgenol 2010;195(1):126–131.
10. Gosling O, Loader R, Venables P, et al. A comparison of radiation doses between state-of-the-art multislice CT coronary angiography with iterative reconstruction, multislice CT coronary angiography with standard filtered back-projection and invasive diagnostic coronary angiography. Heart 2010;96(12):922–926.
11. Leipsic J, Labounty TM, Heilbron B, et al. Estimated radiation dose reduction using adaptive statistical iterative reconstruction in coronary CT angiography: the ERASIR study. AJR Am J Roentgenol 2010;195(3):655–660.
12. Prakash P, Kalra MK, Ackman JB, et al. Diffuse lung disease: CT of the chest with adaptive statistical iterative reconstruction technique. Radiology 2010;256(1):261–269.
13. Prakash P, Kalra MK, Kambadakone AK, et al. Reducing abdominal CT radiation dose with adaptive statistical iterative reconstruction technique. Invest Radiol 2010;45(4):202–210.
14. Achenbach S, Marwan M, Ropers D, et al. Coronary computed tomography angiography with a consistent dose below 1 mSv using prospectively electrocardiogram-triggered high-pitch spiral acquisition. Eur Heart J 2010;31(3):340–346.
15. Bongartz G, Golding SJ, Jurik AG, et al. 2004 CT quality criteria. Luxembourg: European Commission, 2004.
16. Achenbach S, Boehmer K, Pflederer T, et al. Influence of slice thickness and reconstruction kernel on the computed tomographic attenuation of coronary atherosclerotic plaque. J Cardiovasc Comput Tomogr 2010;4(2):110–115.
17. Cademartiri F, La Grutta L, Runza G, et al. Influence of convolution filtering on coronary plaque attenuation values: observations in an ex vivo model of multislice computed tomography coronary angiography. Eur Radiol 2007;17(7):1842–1849.
18. Cademartiri F, Runza G, Mollet NR, et al. Influence of increasing convolution kernel filtering on plaque imaging with multislice CT using an ex-vivo model of coronary angiography. Radiol Med (Torino) 2005;110(3):234–240.
19. Seifarth H, Raupach R, Schaller S, et al. Assessment of coronary artery stents using 16-slice MDCT angiography: evaluation of a dedicated reconstruction kernel and a noise reduction filter. Eur Radiol 2005;15(4):721–726.
20. Thilo C, Gebregziabher M, Mayer FB, Zwerner PL, Costello P, Schoepf UJ. Correlation of regional distribution and morphological pattern of calcification at CT coronary artery calcium scoring with noncalcified plaque formation and stenosis. Eur Radiol 2010;20(4):855–861.
21. Austen WG, Edwards JE, Frye RL, et al. A reporting system on patients evaluated for coronary artery disease: report of the Ad Hoc Committee for Grading of Coronary Artery Disease, Council on Cardiovascular Surgery, American Heart Association. Circulation 1975;51(4 Suppl):5–40.
22. Wang Y, Zhang Z, Kong L, et al. Dual-source CT coronary angiography in patients with atrial fibrillation: comparison with single-source CT. Eur J Radiol 2008;68(3):434–441.
23. Rist C, Johnson TR, Müller-Starck J, et al. Noninvasive coronary angiography using dual-source computed tomography in patients with atrial fibrillation. Invest Radiol 2009;44(3):159–167.
24. Hamon M, Biondi-Zoccai GG, Malagutti P, et al. Diagnostic performance of multislice spiral computed tomography of coronary arteries as compared with conventional invasive coronary angiography: a meta-analysis. J Am Coll Cardiol 2006;48(9):1896–1910.
25. Stein PD, Beemath A, Kayali F, Skaf E, Sanchez J, Olson RE. Multidetector computed tomography for the diagnosis of coronary artery disease: a systematic review. Am J Med 2006;119(3):203–216.
26. Scheffel H, Alkadhi H, Plass A, et al. Accuracy of dual-source CT coronary angiography: first experience in a high pre-test probability population without heart rate control. Eur Radiol 2006;16(12):2739–2747.
27. Martuscelli E, Romagnoli A, D'Eliseo A, et al. Accuracy of thin-slice computed tomography in the detection of coronary stenoses. Eur Heart J 2004;25(12):1043–1048.
28. Hoffmann MH, Shi H, Schmitz BL, et al. Noninvasive coronary angiography with multislice computed tomography. JAMA 2005;293(20):2471–2478.
29. Min JK, Shaw LJ, Devereux RB, et al. Prognostic value of multidetector coronary computed tomographic angiography for prediction of all-cause mortality. J Am Coll Cardiol 2007;50(12):1161–1170.
30. Gaemperli O, Valenta I, Schepis T, et al. Coronary 64-slice CT angiography predicts outcome in patients with known or suspected coronary artery disease. Eur Radiol 2008;18(6):1162–1173.
31. Ostrom MP, Gopal A, Ahmadi N, et al. Mortality incidence and the severity of coronary atherosclerosis assessed by computed tomography angiography. J Am Coll Cardiol 2008;52(16):1335–1343.
32. Catalán P, Leta R, Hidalgo A, et al. Ruling out coronary artery disease with noninvasive coronary multidetector CT angiography before noncoronary cardiovascular surgery. Radiology 2011;258(2):426–434.

33. Leber AW, Knez A, von Ziegler F, et al. Quantification of obstructive and nonobstructive coronary lesions by 64-slice computed tomography: a comparative study with quantitative coronary angiography and intravascular ultrasound. J Am Coll Cardiol 2005; 46(1):147–154.

34. Brodoefel H, Burgstahler C, Tsiflikas I, et al. Dual-source CT: effect of heart rate, heart rate variability, and calcification on image quality and diagnostic accuracy. Radiology 2008;247(2):346–355.

35. Cordeiro MA, Lima JA. Atherosclerotic plaque characterization by multidetector row computed tomography angiography. J Am Coll Cardiol 2006;47(8,Suppl):C40–C47.

36. Hara AK, Paden RG, Silva AC, Kujak JL, Lawder HJ, Pavlicek W. Iterative reconstruction technique for reducing body radiation dose at CT: feasibility study. AJR Am J Roentgenol 2009;193(3):764–771.

37. Taylor AJ, Cerqueira M, Hodgson JM, et al. ACCF/SCCT/ACR/AHA/ASE/ASNC/NASCI/SCAI/SCMR 2010 appropriate use criteria for cardiac computed tomography: a report of the American College of Cardiology Foundation Appropriate Use Criteria Task Force, the Society of Cardiovascular Computed Tomography, the American College of Radiology, the American Heart Association, the American Society of Echocardiography, the American Society of Nuclear Cardiology, the North American Society for Cardiovascular Imaging, the Society for Cardiovascular Angiography and Interventions, and the Society for Cardiovascular Magnetic Resonance. J Am Coll Cardiol 2010;56(22):1864–1894.

38. Brodoefel H, Tsiflikas I, Burgstahler C, et al. Cardiac dual-source computed tomography: effect of body mass index on image quality and diagnostic accuracy. Invest Radiol 2008;43(10):712–718.

Journal of Cardiovascular Computed Tomography 9 (2015) 546–552

Contents lists available at ScienceDirect

Journal of Cardiovascular Computed Tomography

journal homepage: www.JournalofCardiovascularCT.com

Research paper

Comparison of quantitative stenosis characteristics at routine coronary computed tomography angiography with invasive fractional flow reserve for assessing lesion-specific ischemia

Rui Wang, MD [a, b], Stefan Baumann, MD [a, c], U. Joseph Schoepf, MD [a, *], Felix G. Meinel, MD [a, d], Jeremy D. Rier, DO [a], Justin Z. Morris, BS [a], Helge Möllmann, MD [e], Christian W. Hamm, MD [f], Daniel H. Steinberg, MD [a], Matthias Renker, MD [a, f]

[a] Heart & Vascular Center, Medical University of South Carolina, Charleston, SC, USA
[b] Department of Radiology, Beijing Anzhen Hospital, Capital Medical University, Beijing, China
[c] First Department of Medicine, Faculty of Medicine Mannheim, University Medical Centre, Mannheim (UMM), University of Heidelberg, Mannheim, Germany
[d] Institute for Clinical Radiology, Ludwig-Maximilians-University Hospital, Munich, Germany
[e] Kerckhoff Heart and Thorax Center, Bad Nauheim, Germany
[f] Department of Medicine I, University Hospital Giessen and Marburg, Giessen, Germany

ARTICLE INFO

Article history:
Received 14 October 2014
Received in revised form
7 July 2015
Accepted 6 August 2015
Available online 12 August 2015

Keywords:
Coronary artery disease
Invasive coronary angiography
Coronary CT angiography
Fractional flow reserve

ABSTRACT

Objective: To comprehensively evaluate quantitative parameters derived from routine coronary CT angiography (cCTA) for predicting lesion-specific ischemia in comparison to invasive fractional flow reserve (FFR).

Background: The ability of cCTA to gauge lesion-specific ischemia is limited. Several quantitative parameters have been proposed to enhance the specificity of cCTA, such as morphologic indices (lesion length/minimal lumen diameter^4 [LL/MLD^4]; percentage aggregate plaque volume [%APV]) and a measure of intracoronary contrast gradients (corrected coronary opacification [CCO]).

Methods: Forty-nine patients who had undergone cCTA followed by FFR within 3 months were included. An experienced observer visually assessed all cCTA studies and derived multiple measures characterizing the lesion of interest, including LL, MLD, minimal lumen area (MLA), LL/MLD^4, remodeling index, %APV, and CCO. Lesion-specific ischemia was considered with FFR <0.8.

Results: Among 56 lesions, 13 were flow-obstructing by FFR. On univariate analysis, LL, MLD, LL/MLD^4, and CCO showed discriminatory power. The area under the curve of LL/MLD^4 (0.909) was significantly greater compared with MLD (0.802, $P = 0.014$), LL (0.739, $P = 0.041$), and CCO (0.809), although the latter did not reach statistical significance ($P = 0.175$). On multivariate regression, LL/MLD^4 was the only independent predictor of lesion-specific ischemia (odds ratio 2.021, $P = 0.001$). Moreover, LL/MLD^4 compared favorably to visual cCTA evaluation.

Conclusion: LL/MLD^4 derived from routine cCTA can enhance the detection of lesion-specific ischemia and may be superior to other described quantitative parameters.

Abbreviations: AUC, area under the receiver operating characteristic curve; CAD, coronary artery disease; CCO, corrected coronary opacification; cCTA, coronary CT angiography; FFR, fractional flow reserve; LL/MLD^4, lesion length/minimal lesion diameter^4; MLA, minimal luminal area; %APV, percentage aggregate plaque volume.

* Corresponding author. Heart & Vascular Center, Medical University of South Carolina, Ashley River Tower, 25 Courtenay Drive, Charleston, SC 29425-2260, USA.
E-mail addresses: rui_wang1979@hotmail.com (R. Wang), stefanbaumann@gmx.at (S. Baumann), schoepf@musc.edu (U.J. Schoepf), felix.meinel@med.uni-muenchen.de (F.G. Meinel), rier@musc.edu (J.D. Rier), jstn.morris821@gmail.com (J.Z. Morris), h.moellmann@kerckhoff-klinik.de (H. Möllmann), christian.hamm@innere.med.uni-giessen.de (C.W. Hamm), steinbe@musc.edu (D.H. Steinberg), matthias.renker@web.de (M. Renker).

http://dx.doi.org/10.1016/j.jcct.2015.08.003
1934-5925/

1. Introduction

Coronary computed tomographic angiography (cCTA) features robust diagnostic accuracy for coronary artery stenosis.[1,2] Although the high negative predictive value of cCTA allows for reliable exclusion of coronary artery disease, its moderate positive predictive value remains a limitation of this modality. Consequently, determining lesion-specific ischemia of anatomically identifiable coronary artery stenosis is regularly indeterminate by cCTA. Gauging the hemodynamic relevance of intermediate lesions is particularly unreliable.[3,4]

Invasive fractional flow reserve (FFR) demonstrably provides guidance for an improved patient care and is therefore suggested as the preferred test by the appropriate use criteria for diagnostic catheterization in order to assess the functional relevance of coronary lesions of stable patients with multivessel disease when evidence of ischemia is absent or previous findings are discrepant.[5–8] Aside from CT myocardial perfusion imaging and CT-based FFR derivation, ongoing, recent investigations have proposed several quantitative parameters for the characterization of coronary artery stenosis obtained at routine diagnostic cCTA that may have potential to increase the diagnostic performance of this test for the discrimination of hemodynamically relevant disease.[9–13] However, these parameters have largely been proposed and evaluated individually and to date their relative performance has never been compared in a systematic fashion and within the same patient population. Hence, the purpose of this study was to comprehensively evaluate and compare the diagnostic value of recently introduced quantitative characteristics of coronary artery stenoses, as derived from standard cCTA data, for the prediction of lesion-specific ischemia.

2. Material and methods

2.1. Patient population

The present study used a retrospective design; patients were eligible for inclusion if they had undergone cCTA followed by coronary catheter angiography with fractional flow reserve (FFR) interrogation from 01/2008 to 04/2014 because of suspected or known coronary artery disease. Patient data were excluded if the time interval between cCTA and invasive FFR exceeded 3 months. Baseline exclusion criteria further comprised previous revascularization (percutaneous coronary intervention with stent placement and coronary artery bypass graft surgery), occurrence of interprocedural complications (cardiac death, non-fatal myocardial infarction), and non-diagnostic cCTA image quality. Also, bifurcation lesions were excluded, because neither FFR nor quantitative cCTA-based parameters can be derived reliably. Our institutional review board approved the study and waived the need for written informed patient consent. This study was conducted in compliance with the Health Insurance Portability and Accountability Act.

2.2. Coronary catheter angiography with fractional flow reserve

Coronary catheter angiography was conducted as a standard procedure in our cardiac catheterization laboratory by an experienced interventional cardiologist per societal guidelines.[14] FFR was assessed intra-procedurally in intermediate lesions of patients without prior testing for myocardial ischemia, or with discrepancies of clinical presentation and non-invasive findings.[8] For this purpose, a dedicated pressure-monitoring guide wire was used. FFR was derived as the ratio of the mean coronary pressure distal to the stenosis over the mean aortic pressure at the time of pharmacologically-induced hyperemia (adenosine, 140 μg/kg/min). An FFR value < 0.80 was considered diagnostic for the presence of lesion-specific myocardial ischemia.

2.3. Coronary CT angiography acquisition

All cCTA examinations were performed on either first- or second-generation dual-source CT systems (Somatom Definition or Somatom Definition Flash, Siemens Healthcare, Forchheim, Germany). First, patients underwent a non-contrast medium enhanced calcium scoring scan (collimation, 32 × 1.2 mm; tube voltage 120 kV; tube current, 75 mA; slice thickness, 3 mm; increment, 1.5 mm).

Parameters of the cCTA protocol using first generation dual-source CT were as follows: gantry rotation time of 330 ms, 32 × 2 × 0.6 mm collimation with z-flying focal spot, tube voltage of 100 − 120 kV, and tube current of 320 to 650 mAs. With the second generation dual-source CT system the protocol involved a gantry rotation time of 280 ms, 2 × 64 × 0.6 mm collimation with z-flying focal spot, tube voltage of 80 − 120 kV, and tube current of 320 to 650 mAs. The acquisition techniques included retrospective electrocardiographic gating with default use of electrocardiography-dependent tube current modulation, prospective electrocardiographic triggering, and the high-pitch prospectively electrocardiography-triggered spiral mode. The acquisition technique was chosen individually for each patient with the goal of minimizing radiation exposure. Pharmacological rate control and nitroglycerin administration were available at the discretion of the attending physician of the day. The contrast agent was administered using a power injector (Stellant D, Medrad, Indianola, PA) at a rate of 4 − 6 mL/s for all phases through an 18 − 20 gauge antecubital intravenous line. A biphasic protocol was used with injection of 50 − 90 mL of contrast medium (Ultravist, 370 mgI/mL iopromide, Bayer, Wayne, NJ), followed by 30 mL of saline (0.9% sodium chloride) as a bolus chaser. Image reconstruction was performed for the cardiac phase with the least motion using the following parameters: 0.75 mm section thickness and 0.5 mm reconstruction increment using a vascular reconstruction algorithm (B26f).

2.4. Coronary CT angiography assessment

One observer used a 5-level Likert scale to grade the image quality of each cCTA dataset, with 0 = non-diagnostic; 1 = diagnostic despite impairment by image noise, artifacts and/or low vascular opacification; 2 = moderate image quality with sufficient intraluminal visibility, artifacts may be present; 3 = good vessel contrast in absence of major artifacts, low image noise; 4 = excellent image quality.

Axial images, cross-sectional views, and automatically generated curved planar reformations were used for evaluation. Lesion characterization was performed by one observer specialized in cardiovascular imaging (7 years of experience), who was blinded to the patients' clinical histories and the results of invasive angiography with FFR. The observer was only unblinded regarding the segmental location of the lesions of interest that had been interrogated by FFR. To obtain the vessel reference diameter and area, the average of non-diseased vessel dimensions proximal and distal to the lesion of interest were assessed at points where no atherosclerotic plaque could be detected.

Lesion length (LL) was measured on curved planar reformatted images and was measured as the maximum length between the proximal and distal extent of the lesion. Minimal lumen diameter (MLD) was determined as the smallest luminal diameter of a lesion of interest. Minimal lumen area (MLA) was measured manually at the narrowest level of the lesion on cross-sectional images. According to Li et al[11] LL divided by the fourth power of MLD resulted in an index (LL/MLD^4). Additionally, on cross-sectional vessel views,

the remodeling index was calculated as the ratio of the vessel area of the lesion over the proximal luminal reference area. In accordance with Nakazato et al[12] percentage aggregate plaque volume (% APV) was defined as the sum of the plaque volume divided by the sum of the vessel volume from the proximal to the distal extent of the lesion.[12]

Corrected coronary opacification (CCO) was defined as the ratio of the mean attenuation in the coronary artery distal to the lesion of interest relative to that of the aorta at the same axial section. Thus, the difference in CCO across a lesion of interest was equal to the lowest CCO proximal to a lesion minus the lowest CCO distal to the stenosis.[10] Coronary segments were visually classified, based on societal guidelines.[15]

2.5. Statistical analysis

All analyses were performed using dedicated statistical software (MedCalc for Windows, version 12.5, MedCalc Software, Ostend, Belgium). Continuous variables were presented as the mean ± standard deviation. The distribution of the data was assessed via the Kolmogorov-Smirnov test. Student t-test and Mann-Whitney U-test were used for normally and non-normally distributed data, respectively. In general, α was set at 0.05.

For the purpose of further statistical analyses, each lesion of interest was considered an independent observation. To report spatial distribution of lesions in the coronary artery system, lesions of interest affecting side branches were included in the descriptors of the corresponding major epicardial coronary artery. For visual gradation of lesions on cCTA, lesion-specific ischemia was defined as stenosis >50%. Using FFR as the reference standard, lesions were classified as non-obstructive or ischemia inducing. The presence of lesion-specific ischemia was considered, if the FFR interrogation resulted in a value of less than 0.80. Spearman's rank statistics were applied to analyze the degree of correlation between quantitative cCTA parameters and FFR. First, a univariate comparison of lesion-associated parameters between hemodynamically significant and non-obstructive lesions was performed. The area under the receiver operating characteristic curve (AUC) was determined to assess the overall diagnostic performance for each stenosis parameter that showed significant discriminatory power on univariate analysis. The AUCs were compared according to the method of DeLong.[16] Subsequently, multivariate logistic regression analysis was performed with block entry of all lesion-associated parameters found to be significant ($P < 0.05$) on univariate analyses. Finally, the AUC of parameters independently predicting lesion-specific ischemia was compared to the visual analysis of cCTA.

3. Results

3.1. Patient characteristics

In total, 75 patients had undergone both cCTA followed by invasive coronary angiography with FFR measurement. Fifteen patients (20.0%) were excluded due to an interprocedural time greater than three months or previous revascularization as defined above; four patients (5.3%) were excluded on account of non-evaluable cCTA datasets (severe motion artifacts), and seven patients (9.3%) were excluded due to the presence of bifurcation lesions. Thus, 49 patients with 56 lesions of interest with FFR interrogation available were included in the final analysis. Baseline characteristics are provided in Table 1.

3.2. Lesion characteristics

Among 56 lesions, 13 (23.2%) showed lesion-specific ischemia with FFR < 0.80. Of 49 patients, four had two lesions of interest, and one had three lesions of interest. Three patients had a sequential lesion. By visual grading of cCTA, 27 lesions were <50%, 20 were 50 − 69% and nine were ≥70%.

3.3. Diagnostic performance

The median subjective image quality score of cCTA was 3 (interquartile ranges, 2 − 3).

For the individual quantitative cCTA parameters, Spearman's rank coefficient showed the following correlation to FFR: LL ($r = -0.447$, $P = 0.001$), MLD ($r = 0.504$, $P < 0.001$), MLA ($r = 0.263$, $P = 0.051$), LL/MLD^4 ($r = -0.690$, $P < 0.001$), remodeling index ($r = -0.128$, $P = 0.347$), %APV ($r = -0.272$, $P = 0.043$), CCO ($r = -0.438$, $P = 0.001$).

Results of the univariate analysis of cCTA parameters are shown in Table 2. The AUC analyses of cCTA-based lesion descriptors that reached the level of significance on univariate statistics are demonstrated in Fig. 1 and Table 3. As a representative case example, Fig. 2 is provided. In direct comparison, the AUC of LL/MLD^4 was significantly greater than that of MLD ($P = 0.014$), and LL ($P = 0.041$). Although the AUC of LL/MLD^4 was greater than that of CCO (0.809), the difference was not statistically significant ($P = 0.175$). On multivariate logistic regression analysis only LL/MLD^4 remained as an independent predictor of lesion-specific ischemia (odds ratio 2.021, 95% confidence interval 1.331 − 3.069, $P = 0.001$). The AUC comparison of LL/MLD^4 with visual interpretation of cCTA is illustrated in Fig. 3.

4. Discussion

4.1. Context of the study results

We performed a comprehensive, comparative evaluation of quantitative lesion-associated parameters derived from routine clinical cCTA studies for the diagnosis of lesion-specific myocardial ischemia. Our results demonstrate that the morphologic index LL/

Table 1
Demographic data and procedural results.

Characteristic	Datum
No. of patients	49
Age, yrs	62.1 ± 11.4
No. of males[a]	33 (67%)
Height, cm	171.5 ± 11.9
Weight, kg	90.0 ± 21.3
Body-mass index, kg/m^2	30.8 ± 7.9
Left ventricular function, %	61.3 ± 10.6
Vital signs	
Systolic blood pressure, mmHg	132.6 ± 20.9
Diastolic blood pressure, mmHg	71.5 ± 11.1
Heart rate, beats per minute	72.4 ± 14.0
Cardiovascular risk factors[a]	
Diabetes mellitus	13 (26%)
Hypertension	24 (49%)
Dyslipidemia	23 (47%)
Smoking	5 (11%)
Agatston score[b]	810 ± 747
Range	0 − 2595
No. of patients ≥400	24 (49%)
No. of coronary artery stenoses	56
Spatial distribution of lesions of interest[a]	
Left anterior descending	38 (68%)
Left circumflex	8 (14%)
Right coronary artery	10 (18%)

Unless specified otherwise, data are presented as mean ± standard deviation.
[a] Data are frequencies with percentages in parentheses.
[b] Agatston score was obtained in 42 patients.

Table 2
Univariate analysis of coronary computed tomography angiography parameters for the prediction of the hemodynamic significance of stenoses according to the invasive reference standard fractional flow reserve (FFR).

Parameter	All lesions (N = 56)	Lesions with FFR ≥ 0.80 (N = 43)	Lesions with FFR < 0.80 (N = 13)	*P* Value	Odds ratio	95% Confidence interval of odds ratio
Lesion length, mm	25.5 ± 12.9	23.5 ± 12.7	32.4 ± 11.5	0.036	1.054	1.004 – 1.107
Minimal lumen diameter, mm	1.9 ± 0.5	2.1 ± 0.5	1.5 ± 0.2	0.004	0.026	0.002 – 0.322
Minimal lumen area, mm^2	5.4 ± 2.8	5.6 ± 2.8	5.0 ± 2.6	0.521	0.921	0.716 – 1.184
Lesion length/minimal lumen diameter^4	3.5 ± 4.5	2.1 ± 1.8	8.0 ± 7.2	0.001	2.021	1.331 – 3.069
Remodeling index	1.0 ± 0.3	1.0 ± 0.3	1.0 ± 0.3	0.893	1.152	0.146 – 9.114
Percentage aggregate plaque volume, %	41.0 ± 14.5	40.6 ± 13.4	42.1 ± 18.5	0.750	2.036	0.026 – 162.283
Coronary contrast opacification	0.1 ± 0.2	0.1 ± 0.1	0.2 ± 0.1	0.014	933.237	4.100 – 212436.233

Data are presented as mean ± standard deviation.

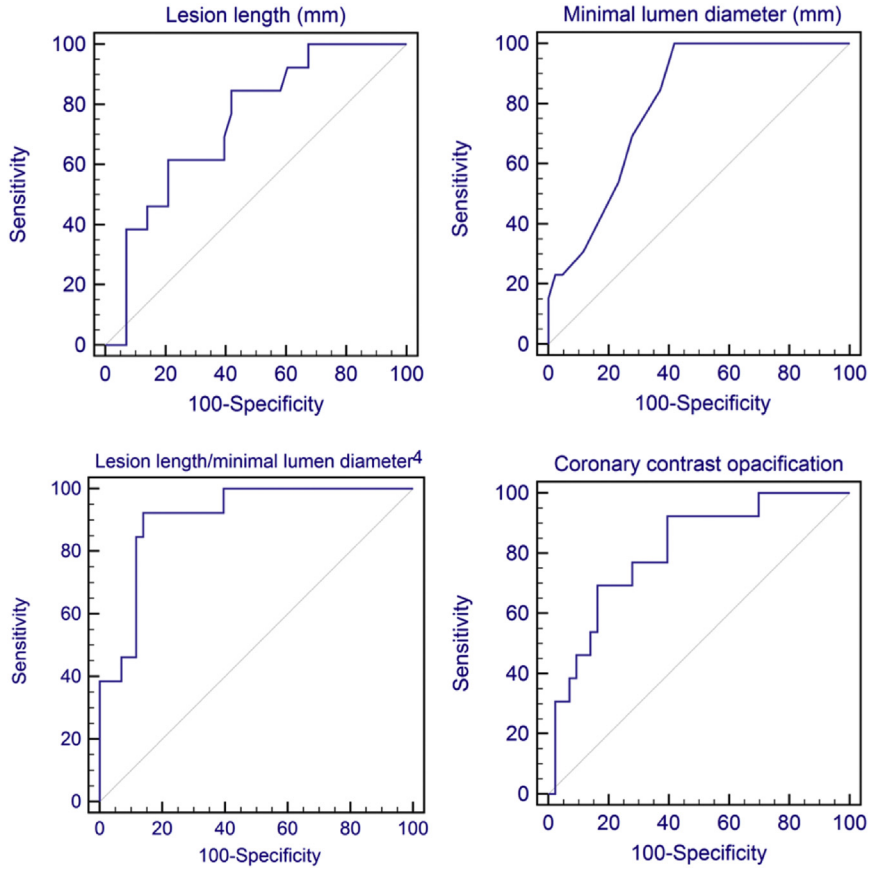

Fig. 1. Receiver operating characteristics curves are shown for lesion length, minimal lumen diameter, lesion length/minimal lumen diameter^4, and corrected coronary opacification.

Table 3
Area under the receiver operating characteristics curve (AUC) analyses of stenosis parameters reaching statistical significance for the detection of lesion-specific ischemia at univariate analysis.

Parameter	AUC (95% confidence interval)	*P* Value	Optimal cut-off value
Lesion length, mm	0.739 (0.604 – 0.847)	0.0012	20.4
Minimal lumen diameter, mm	0.802 (0.674 – 0.897)	<0.0001	1.8
Lesion length/minimal lumen diameter^4	0.909 (0.801 – 0.969)	<0.0001	3.54
Coronary contrast opacification	0.809 (0.681 – 0.901)	<0.0001	0.18

MLD^4 may be superior to other indicators of hemodynamically relevant coronary lesions, as determined by invasive FFR. This index, deduced from the Poiseuille equation, has been demonstrated to correlate well with invasive FFR results before.[11,17] The Poiseuille equation calculates the resistance of flow in the ideal state of laminar flow. Although stenoses cause turbulence instead of laminar flow, the diagnostic value of the simplified index LL/MLD^4 has been demonstrated.[11,17] Based on our investigation, the AUC of

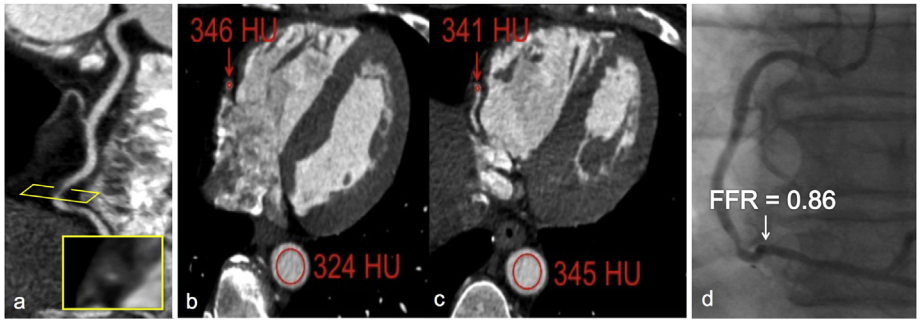

Fig. 2. Curved and axial multiplanar reformatted coronary computed tomography angiography views demonstrate non-calcified plaque within the right coronary artery causing >50% luminal narrowing (a). Calculation of the ratio lesion length/minimal lumen diameter^4 resulted in a value of 2.54, predicting the absence of lesion-specific ischemia (a). Axial thoracic views show derivation of corrected coronary opacification (CCO) as the ratio of the lowest mean attenuation in the coronary artery proximal to the lesion of interest relative to that of the aorta at the same axial section (b) minus the ratio of the lowest mean attenuation in the coronary artery distal to the lesion of interest relative to that of the aorta at the same axial section (c). The CCO difference of 0.079 suggests absence of lesion-specific ischemia. Use of fractional flow reserve as the invasive reference standard established the non-obstructive nature of the lesion by FFR = 0.86 (d).

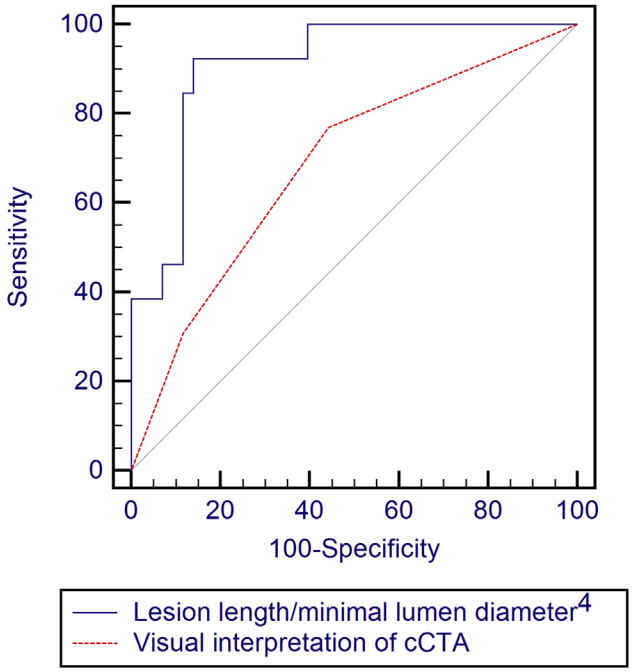

Fig. 3. Area under the receiver operating characteristics curve comparison between lesion length/minimal lumen diameter^4 (0.909) and visual evaluation of lesions at coronary computed tomography angiography (0.687). Lesion length/minimal lumen diameter^4 yields significantly ($P = 0.0036$) higher diagnostic performance.

the index LL/MLD^4 (0.909) suggests very good diagnostic performance. Furthermore, our results indicate that LL/MLD^4 may have incremental value over cCTA alone. However, as reflected by the range of the 95% confidence interval associated with the AUC value, the test variability is relatively high due to the size of our study population. Our results indicate an optimal cutoff value of 3.54, which is similar to previously reported results.[11] In a clinical context, application of this cutoff value would translate into the correct classification of an FFR-positive lesion with a sensitivity of 92.3% and a specificity of 86.1%.

In contrast to direct morphologic characterization of lesion geometry, CCO is an indirect cCTA parameter for the detection of lesion-specific ischemia depending on intraluminal attenuation values within the coronary arteries. CCO was introduced to overcome the influence of temporal uniformity by normalizing the contrast attenuation within coronary segments from different axial sections. In accordance with the literature,[10,18] our results demonstrate that CCO shows good diagnostic performance (AUC 0.809).

Furthermore, our results demonstrate that the remodeling index fails to predict lesion-specific ischemia, which is in agreement with previous investigations.[11] Different from previous results however, %APV failed to discriminate between flow-obstructing and non-obstructive lesions to a statistically significant extent.[12] The main reason for this observation may be found in different study design compared to the investigation by Nakazato et al[12] who for example excluded sequential lesions.

4.2. Clinical relevance

Comprehensive non-invasive anatomical and functional imaging would be desirable to identify patients who are likely to benefit from coronary catheter angiography and revascularization. Given its high sensitivity, cCTA has become an alternative imaging modality in the diagnostic algorithm to rule out coronary artery disease. However, the predictive value of visual cCTA analysis for ischemia-causing coronary lesions is poor.[19] It has been shown that hybrid imaging techniques (cCTA/single photon emission tomography and cCTA/CT myocardial perfusion imaging) integrate coronary anatomy and functional information for improved detection of coronary artery disease.[20–23] Unfavorably, these techniques result in increased radiation exposure and higher costs for the management of patients with suspected coronary artery disease.[24]

Applying the principles of computational fluid dynamics, CT-based derivation of FFR has been introduced for non-invasive detection of flow-limiting coronary artery stenoses based on routine anatomical cCTA datasets.[25] Several multi-center trials have reported that through the use of CT-based FFR, the number of false-positive test results can be reduced, which results in increased specificity and positive predictive value for assessing obstructive disease.[26–28] The off-site calculation of CT-based FFR requires supercomputational power and is time-consuming. Only recently, early experiences with a novel prototype algorithm for on-site computation of CT-based FFR within clinically viable time frames were described.[29]

Meanwhile, the morphologic indices and metrics of intracoronary contrast gradients comparatively evaluated here are currently available to be derived from regular anatomical cCTA datasets without the need for off-site data export, dedicated software, or altering the image acquisition protocol. While it is generally recognized that anatomic imaging tools, such as coronary

catheter angiography and cCTA, are poor predictors of the hemodynamic relevance of stenosis,[19,30] the study results suggest a correlation between selective cCTA-based anatomic measurements and FFR.

4.3. Limitations

Our study should be viewed in light of several limitations. First, this was a retrospective single center study with a relatively small sample size. Therefore, our investigation can serve as a proof of concept and the results should be validated by larger studies. Second, the assessment of cCTA and derivation of lesion-associated parameters were performed by a single reader. Third, we excluded some datasets due to the presence of substantial motion artifact, which interfered with obtaining the quantitative measures analyzed here. However, as indicated by the image quality scores, our sample was not overly selected to include only cCTA data of pristine image quality. Fourth, although the use of a filtered back projection algorithm was utilized for its universal applicability, it may have limited the accuracy of anatomic measurements due to blooming artifacts from calcified lesions. The predictive value of the cCTA parameters examined here may improve with the utilization of iterative reconstruction algorithms,[30] which are currently set to replace traditional filtered back projection reconstruction in clinical practice. Fifth, inconsistent nitroglycerin administration prior to cCTA acquisition may have influenced our results, as several lesion associated parameters are dependent on the vessel diameter.

5. Conclusions

In conclusion, quantitative parameters are available to be derived from routine coronary CT angiography datasets by regular workstations without additional radiation dose application and contrast material usage. Based on our findings, CT-derived parameters may enhance the diagnostic value for ischemia-inducing stenoses. The index LL/MLD[4] seems to be superior to other described quantitative parameters in the detection of lesion-specific ischemia.

Financial disclosure statement

U.J.S. is a consultant for and/or receives research support from Bayer (Wayne/NJ, USA), Bracco (Princeton/NJ, USA), GE Healthcare (Little Chalfont, UK), Medrad (Warrendale/PA, USA), and Siemens Healthcare (Malvern/PA, USA). Others authors declare that they have no financial disclosures.

Acknowledgments

None.

References

1. Miller JM, Rochitte CE, Dewey M, et al. Diagnostic performance of coronary angiography by 64-row CT. *N Engl J Med*. 2008;359:2324–2336.
2. De Cecco CN, Meinel FG, Chiaramida SA, Costello P, Bamberg F, Schoepf UJ. Coronary artery computed tomography scanning. *Circulation*. 2014;129:1341–1345.
3. Bech GJ, De Bruyne B, Pijls NH, et al. Fractional flow reserve to determine the appropriateness of angioplasty in moderate coronary stenosis: a randomized trial. *Circulation*. 2001;103:2928–2934.
4. Min JK, Koo BK, Erglis A, et al. Usefulness of noninvasive fractional flow reserve computed from coronary computed tomographic angiograms for intermediate stenoses confirmed by quantitative coronary angiography. *Am J Cardiol*. 2012;110:971–976.
5. Pijls NH, van Schaardenburgh P, Manoharan G, et al. Percutaneous coronary intervention of functionally nonsignificant stenosis: 5-year follow-up of the DEFER Study. *J Am Coll Cardiol*. 2007;49:2105–2111.
6. Tonino PA, De Bruyne B, Pijls NH, et al. Fractional flow reserve vs. angiography for guiding percutaneous coronary intervention. *N Engl J Med*. 2009;360:213–224.
7. De Bruyne B, Pijls NH, Kalesan B, et al. Fractional flow reserve-guided PCI vs. medical therapy in stable coronary disease. *N Engl J Med*. 2012;367:991–1001.
8. Patel MR, Bailey SR, Bonow RO, et al. ACCF/SCAI/AATS/AHA/ASE/ASNC/HFSA/HRS/SCCM/SCCT/SCMR/STS 2012 appropriate use criteria for diagnostic catheterization: a report of the American College of Cardiology Foundation appropriate use criteria task force, Society for Cardiovascular Angiography and Interventions, American Association for Thoracic Surgery, American Heart Association, American Society of Echocardiography, American Society of Nuclear Cardiology, Heart Failure Society of America, Heart Rhythm Society, Society of Critical Care Medicine, Society of Cardiovascular Computed Tomography, Society for Cardiovascular Magnetic Resonance, and Society of Thoracic Surgeons. *J Am Coll Cardiol*. 2012;59:1995–2027.
9. Choi JH, Min JK, Labounty TM, et al. Intracoronary transluminal attenuation gradient in coronary CT angiography for determining coronary artery stenosis. *JACC Cardiovasc Imaging*. 2011;4:1149–1157.
10. Chow BJ, Kass M, Gagne O, et al. Can differences in corrected coronary opacification measured with computed tomography predict resting coronary artery flow? *J Am Coll Cardiol*. 2011;57:1280–1288.
11. Li M, Zhang J, Pan J, Lu Z. Coronary stenosis: morphologic index characterized by using CT angiography correlates with fractional flow reserve and is associated with hemodynamic status. *Radiology*. 2013;269:713–721.
12. Nakazato R, Shalev A, Doh JH, et al. Aggregate plaque volume by coronary computed tomography angiography is superior and incremental to luminal narrowing for diagnosis of ischemic lesions of intermediate stenosis severity. *J Am Coll Cardiol*. 2013;62:460–467.
13. Voros S, Rinehart S, Vazquez-Figueroa JG, et al. Prospective, head-to-head comparison of quantitative coronary angiography, quantitative computed tomography angiography, and intravascular ultrasound for the prediction of hemodynamic significance in intermediate and severe lesions, using fractional flow reserve as reference standard (from the ATLANTA I and II Study). *Am J Cardiol*. 2014;113:23–29.
14. Scanlon PJ, Faxon DP, Audet AM, et al. ACC/AHA guidelines for coronary angiography: executive summary and recommendations. A report of the American College of Cardiology/American Heart Association task force on practice guidelines (Committee on Coronary Angiography) developed in collaboration with the Society for Cardiac Angiography and Interventions. *Circulation*. 1999;99:2345–2357.
15. Leipsic J, Abbara S, Achenbach S, et al. SCCT guidelines for the interpretation and reporting of coronary CT angiography: a report of the Society of Cardiovascular Computed Tomography Guidelines Committee. *J Cardiovasc Comput Tomogr*. 2014;8:342–358.
16. DeLong ER, DeLong DM, Clarke-Pearson DL. Comparing the areas under two or more correlated receiver operating characteristic curves: a nonparametric approach. *Biometrics*. 1988;44:837–845.
17. Jaffe R, Halon DA, Roguin A, Rubinshtein R, Lewis BSA. Poiseuille-based coronary angiographic index for prediction of fractional flow reserve. *Int J Cardiol*. 2013;167:862–865.
18. Stuijfzand WJ, Danad I, Raijmakers PG, et al. Additional value of transluminal attenuation gradient in CT angiography to predict hemodynamic significance of coronary artery stenosis. *JACC Cardiovasc Imaging*. 2014;7:374–386.
19. Gaemperli O, Schepis T, Valenta I, et al. Functionally relevant coronary artery disease: comparison of 64-section CT angiography with myocardial perfusion SPECT. *Radiology*. 2008;248:414–423.
20. Husmann L, Herzog BA, Gaemperli O, et al. Diagnostic accuracy of computed tomography coronary angiography and evaluation of stress-only single-photon emission computed tomography/computed tomography hybrid imaging: comparison of prospective electrocardiogram-triggering vs. retrospective gating. *Eur Heart J*. 2009;30:600–607.
21. Thilo C, Schoepf UJ, Gordon L, Chiaramida S, Serguson J, Costello P. Integrated assessment of coronary anatomy and myocardial perfusion using a retractable SPECT camera combined with 64-slice CT: initial experience. *Eur Radiol*. 2009;19:845–856.
22. Bastarrika G, Ramos-Duran L, Rosenblum MA, Kang DK, Rowe GW, Schoepf UJ. Adenosine-stress dynamic myocardial CT perfusion imaging: initial clinical experience. *Invest Radiol*. 2010;45:306–313.
23. Meinel FG, Ebersberger U, Schoepf UJ, et al. Global quantification of left ventricular myocardial perfusion at dynamic CT: feasibility in a multicenter patient population. *AJR Am J Roentgenol*. 2014.
24. Min JK, Koduru S, Dunning AM, et al. Coronary CT angiography versus myocardial perfusion imaging for near-term quality of life, cost and radiation exposure: a prospective multicenter randomized pilot trial. *J Cardiovasc Comput Tomogr*. 2012;6:274–283.
25. Min JK, Leipsic J, Pencina MJ, et al. Diagnostic accuracy of fractional flow reserve from anatomic CT angiography. *JAMA*. 2012;308:1237–1245.
26. Koo BK, Erglis A, Doh JH, et al. Diagnosis of ischemia-causing coronary stenoses by noninvasive fractional flow reserve computed from coronary computed tomographic angiograms. Results from the prospective multicenter DISCOVER-FLOW (diagnosis of ischemia-causing stenoses obtained via noninvasive fractional flow reserve) study. *J Am Coll Cardiol*. 2011;58:1989–1997.
27. Norgaard BL, Leipsic J, Gaur S, et al. Diagnostic performance of noninvasive fractional flow reserve derived from coronary computed tomography angiography in suspected coronary artery disease: the NXT trial (Analysis of coronary

blood flow using CT angiography: next steps). *J Am Coll Cardiol*. 2014;63:1145–1155.

28. Renker M, Schoepf UJ, Wang R, et al. Comparison of diagnostic value of a novel non-invasive coronary computed tomography angiography method versus standard coronary angiography for assessing fractional flow reserve. *Am J Cardiol*. 2014 Aug 12. http://dx.doi.org/10.1016/j.amjcard.2014.07.064 [Epub ahead of print].
29. Bauer RW, Thilo C, Chiaramida SA, Vogl TJ, Costello P, Schoepf UJ. Noncalcified atherosclerotic plaque burden at coronary CT angiography: a better predictor of ischemia at stress myocardial perfusion imaging than calcium score and stenosis severity. *AJR Am J Roentgenol*. 2009;193:410–418.
30. Renker M, Nance Jr JW, Schoepf UJ, et al. Evaluation of heavily calcified vessels with coronary CT angiography: comparison of iterative and filtered back projection image reconstruction. *Radiology*. 2011;260:390–399.

Eur Radiol
DOI 10.1007/s00330-014-3482-5

CARDIAC

Coronary CT angiography-derived fractional flow reserve correlated with invasive fractional flow reserve measurements – initial experience with a novel physician-driven algorithm

Stefan Baumann · Rui Wang · U. Joseph Schoepf · Daniel H. Steinberg · James V. Spearman · Richard R. Bayer II · Christian W. Hamm · Matthias Renker

Received: 17 April 2014 / Revised: 24 October 2014 / Accepted: 30 October 2014

Abstract
Objectives The present study aimed to determine the feasibility of a novel fractional flow reserve (FFR) algorithm based on coronary CT angiography (cCTA) that permits point-of-care assessment, without data transfer to core laboratories, for the evaluation of potentially ischemia-causing stenoses.
Methods To obtain CT-based FFR, anatomical coronary information and ventricular mass extracted from cCTA datasets were integrated with haemodynamic parameters. CT-based FFR was assessed for 36 coronary artery stenoses in 28 patients in a blinded fashion and compared to catheter-based FFR. Haemodynamically relevant stenoses were defined by an invasive FFR ≤0.80. Time was measured for the processing of each cCTA dataset and CT-based FFR computation. Assessment of cCTA image quality was performed using a 5-point scale.
Results Mean total time for CT-based FFR determination was 51.9±9.0 min. Per-vessel analysis for the identification of lesion-specific myocardial ischemia demonstrated good correlation (Pearson's product-moment $r=0.74$, $p<0.0001$) between the prototype CT-based FFR algorithm and invasive FFR. Subjective image quality analysis resulted in a median score of 4 (interquartile ranges, 3-4).
Conclusions Our initial data suggest that the CT-based FFR method for the detection of haemodynamically significant stenoses evaluated in the selected population correlates well with invasive FFR and renders time-efficient point-of-care assessment possible.
Key Points
- *CT-based FFR computation is a promising novel non-invasive application.*
- *A novel prototype algorithm permits time-efficient point-of-care CT-based FFR assessment.*
- *Initial results of the CT-based FFR prototype algorithm compare favourably with FFR.*

Keywords Coronary artery disease · Coronary CT angiography · Fractional flow reserve · Invasive coronary angiography · Myocardial ischemia

Abbreviations

CAD	Coronary artery disease
cCTA	Coronary computed tomographic angiography
FFR	Fractional flow reserve
CT-based FFR	Fractional flow reserve from coronary computed tomographic angiography
CCA	Invasive coronary catheter angiography

Introduction

Invasive coronary catheter angiography (CCA)-based measurement of fractional flow reserve (FFR) is the established reference standard for assessing the functional impact of a

S. Baumann · R. Wang · U. J. Schoepf (✉) · D. H. Steinberg · J. V. Spearman · R. R. Bayer II · M. Renker
Heart & Vascular Center, Medical University of South Carolina, Ashley River Tower, 25 Courtenay Drive, Charleston, SC 29425-2260, USA
e-mail: schoepf@musc.edu

S. Baumann
First Department of Medicine, Faculty of Medicine Mannheim, University Medical Centre Mannheim (UMM), University of Heidelberg, Mannheim, Germany

R. Wang
Department of Radiology, Beijing Anzhen Hospital, Capital Medical University, Beijing, China

C. W. Hamm · M. Renker
Department of Internal Medicine I, Cardiology/Angiology, Giessen University, Giessen, Germany

Published online: 18 November 2014

stenotic lesion on myocardial perfusion [1]. Invasive FFR measurement, therefore, plays a key role in borderline cases to determine whether revascularization is indicated [1, 2]. Furthermore, there is evidence that FFR-guided patient management can enhance survival free of major adverse cardiac events [3].

Developments within the field of image-based modelling and computational fluid dynamics allow for the simulation of coronary flow and pressure at rest as well as during hyperaemia based on 3-dimensional imaging [4, 5]. Via complex calculations, derivation of CT-based FFR is feasible in core laboratories utilizing parallel supercomputers. Importantly, CT-based FFR can be assessed without the need for additional imaging, modification of acquisition protocols, or administration of pharmacologic stressors. The DeFACTO trial [6] as well as the DISCOVER-FLOW trial [7] reported that by use of CT-based FFR, the number of false-positive test results could be reduced, thus, mitigating a traditional challenge to the diagnostic performance of coronary CT angiography (cCTA). More recently Norgaard et al. [8] also demonstrated increased specificity and positive predictive value for identifying obstructive disease. The ability to gauge the haemodynamic significance of lesions may be one of the more important steps of cCTA towards becoming a true gatekeeper to invasive CCA and directing treatment decisions.

A physician-driven, computational CT-based FFR algorithm that can be applied on-site, at the point-of-care and without data transfer, is currently being developed. Based on the coronary anatomy as well as left ventricular mass, both derived from cCTA along with basic haemodynamic parameters, CT-based FFR is computed via integration of reduced and/or more complex flow models, as appropriate. This non-invasive FFR algorithm aims to provide patient management guidance within clinically viable time frames. Here, we sought to evaluate the feasibility of this CT-based FFR prototype algorithm in patients with coronary artery disease (CAD) in correlation with invasive FFR.

Materials and methods

Study characteristics

We retrospectively included patients who had undergone both cCTA and non-emergent CCA with invasive FFR measurement within three months from September 2008 to November 2013. Baseline exclusion criteria were prior myocardial infarction, coronary artery bypass graft surgery, prior stent placement within the coronary artery of the lesion of interest, cardiac disease reducing the functional myocardial mass, bifurcation stenoses (type D, F, and G, according to the SYNTAX Score bifurcation classification [9]), severe proximal left main and/or right coronary artery stenosis, total coronary occlusion, collateralization, and non-diagnostic cCTA image quality. Moreover, patients with interprocedural complications, defined as cardiac death, non-fatal myocardial infarction, or revascularization were excluded. Among 39 eligible patients, six were excluded due to previous revascularization as defined above or because the time between procedures was greater than three months. Two patients were excluded on account of non-evaluable cCTA datasets (severe motion artefacts) while three patients were excluded due to the presence of bifurcation lesions. Finally, 28 patients were registered to the present study. The institutional review board approved this study and waived the need for written informed patient consent.

Coronary catheter angiography with FFR interrogation

CCA was performed as a standard procedure in our catheter laboratory. Each coronary segment was visually assessed for the degree of luminal stenosis by experienced interventional cardiologists. CCA quantification of the coronary artery lesions, which were subsequently evaluated with FFR, was recorded. If a luminal stenosis was suspected to be haemodynamically relevant, FFR interrogation was performed intraprocedurally. For this purpose, a dedicated pressure-monitoring guide wire was advanced distal to a stenosis. Hyperaemia was induced by administration of intravenous adenosine at a rate of 140 μg/kg per min. FFR was considered diagnostic of ischemia at a threshold of ≤0.80 and served as the reference standard for CT-based FFR measurements. If a patient had two or more lesions suspected to be haemodynamically relevant, FFR measurement was performed for each lesion of interest.

Coronary CT angiography technique

Clinically indicated cCTA examinations were performed by use of first and second generation dual-source CT systems (Somatom Definition and Somatom Definition Flash; Siemens Healthcare, Forchheim, Germany). The cCTA technique was chosen individually for each patient depending on the heart rate, heart rhythm, and body mass index, pursuing the goal of minimizing radiation exposure. Acquisition protocols included retrospective electrocardiographic (ECG) gating with default use of ECG-dependent tube current modulation, prospective ECG triggering, and a high-pitch prospectively ECG-triggered spiral mode. In accordance with previous studies [4, 10], if more than one cardiac phase was available by the image acquisition protocol, the reconstruction phase providing the best image quality with the lowest degree of motion artefacts was used for further post processing, including CT-based FFR derivation.

Briefly, cCTA parameters for the first generation dual-source CT system were as follows: tube potential, 100–120

kVp; tube current-time product, 350–650 mAs; gantry rotation time, 0.28 sec, detector collimation, 2×32×0.6 mm; section acquisition, and 2×64×0.6 mm with z-flying focal spot technique. A biphasic protocol was used with administration of 70–90 mL contrast medium (Ultravist, 370 mgI/mL iopromide, Bayer, Wayne, NJ, USA) at 4–6 mL/sec, followed by 30 mL saline as a bolus chaser. For the second generation dual-source CT system, protocol parameters were as follows: tube potential, 80–120 kVp; tube current-time product, 350–650 mAs; gantry rotation time, 0.28 sec; detector collimation, 2×64×0.6 mm; section acquisition, and 2×128×0.6 mm by means of a z-flying focal spot. Contrast enhancement was achieved by injecting 50–80 mL iopromide at 4–6 mL/sec followed by a 30 mL saline bolus. Pharmacological rate control and nitroglycerine administration were at the discretion of the attending physician of the day but were not used in this cohort. All data were reconstructed at a section thickness of 0.75 mm with 0.4 mm reconstruction increment using traditional filtered back projection and a vascular algorithm. Retrospective chart review was used to obtain the most recent resting blood pressure prior to the cCTA examination. The resting heart rate was obtained at the time of cCTA acquisition.

Image quality of cCTA

A subjective image quality rating of the cCTA datasets was independently conducted by two experienced observers on a per-patient basis using on a 5-level Likert item (1=non-diagnostic; 2=diagnostic despite impairment by image noise, artefacts and/or low vascular opacification; 3=moderate image noise with sufficient intraluminal visibility, artefacts may be present; 4=good vessel contrast in absence of major artefacts, low image noise; and 5=excellent image quality).

CT-based FFR assessment

Non-invasive FFR computation from cCTA was performed using a software research prototype (Siemens cFFR, Version 1.4; Siemens Healthcare, currently not commercially available) residing on a regular workstation (Intel Xeon E5630, 2.53GHz, 24 GB RAM). The software allows for the creation of a patient-specific model of the coronary arteries using a semiautomatic approach. The software extracts vessel centrelines automatically and allows for subsequent editing, before contours of the non-obstructed lumen are proposed to the user. Acceptance or correction of the luminal contour proposals and centreline editing were performed by consensus of two observers blinded to invasive results (Fig. 1). A 3-dimensional mesh representing the coronary artery tree was generated. A computational fluid dynamics approach was applied by the software to simulate the blood-flow from the 3-dimensional mesh and the patient-specific boundary conditions for a hyperaemic state. The boundary conditions are represented as lumped models for the heart and coronary microcirculation [11]. First, the boundary conditions are estimated from rest-state conditions such as systolic and diastolic cuff blood pressure, heart rate, and left ventricular mass, which are then appropriately modified to incorporate the effect of maximal hyperaemia by modelling the decrease in microvascular resistance as caused by the administration of adenosine [12, 13]. Based on the patient-specific mesh and boundary conditions, the blood flow simulation was performed by the software prototype manufacturer (Siemens Healthcare, Forchheim, Germany) using a hybrid approach [11], which couples reduced-order and full-order models for fast flow computation. Hereby, flow computation on a standard post-processing workstation in less than ten minutes is rendered possible. For any given point in the coronary tree, the CT-based FFR is computed by taking the ratio of the average of the local pressure over a cardiac cycle and the average aortic pressure. The results were displayed as colour-coded 3-dimensional meshes and allowed for the evaluation of the CT-based FFR value at arbitrary locations. CT-based FFR was assessed for those lesions of interest that had been evaluated invasively by FFR. In a blinded fashion, the CT-based FFR value of a coronary lesion of interest was obtained by interactively placing a measurement marker on the coronary model distal to the stenosis at the corresponding site of the invasive FFR measurement. As customary for invasive FFR, CT-based FFR values of ≤0.80 were considered haemodynamically relevant and diagnostic of lesion-specific ischemia. Stenoses of side branches were considered as lesions of the corresponding main coronary artery. For each cCTA dataset, we measured the CT-based FFR processing time including the time for the semiautomatic segmentation of the dataset and for the CT-based FFR computation.

Correlation of CT-based FFR to invasive FFR

Per societal guidelines, all stenoses were graded semiquantitatively [14]. A direct comparison of the CT-based FFR values associated with coronary artery stenoses that had been assessed invasively was performed on a per-vessel basis. We used statistics according to Pearson in order to analyse the degree of correlation.

Statistical analysis

All analyses were performed by use of dedicated statistical software (MedCalc for Windows, version 12.5, MedCalc Software, Ostend, Belgium). Normal distribution was assessed using the Kolmogorov-Smirnov test. Continuous variables are presented as means±standard deviations. Categorical variables are presented as medians with interquartile ranges in parentheses. *P* values of less than 0.05 were

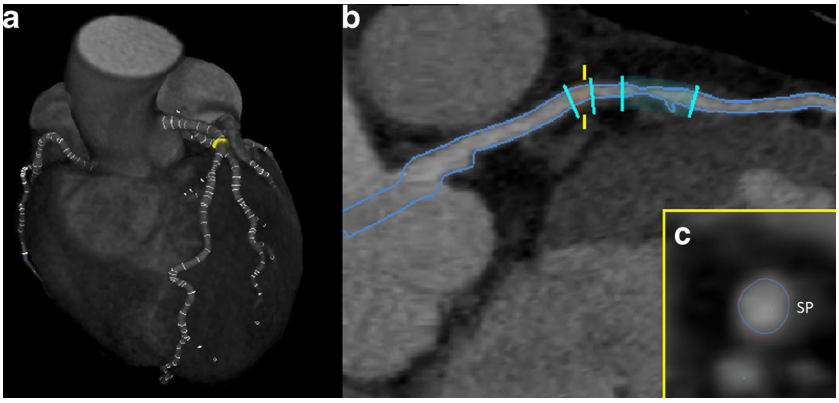

Fig. 1 **a** A 3-dimensional mesh representing a geometric model of the coronary artery tree is generated. **b** Multiplanar reconstruction with stenoses (highlighted in turquoise lines) as defined by the user. The blue lines represent the luminal borders. **c** Cross-sectional vessel view demonstrating a non-calcified plaque (SP). Luminal contour proposals (red dotted line) are automatically created by the software and accepted or corrected by the user. Marked in yellow are identical locations in the coronary tree

considered statistically significant. Pearson statistics were applied to analyze the degree of correlation between CT-based FFR and the invasive reference standard; Bland-Altman statistics were also performed. Interobserver agreement for subjective cCTA image quality rating between the two observers was quantified using linearly weighted κ-statistics (poor agreement, κ=0; slight agreement, κ=0.01–0.2; fair agreement, κ=0.21–0.4; moderate agreement, κ=0.41–0.6; good agreement, κ=0.61–0.8; and excellent agreement, κ=0.81–1).

Results

Patient characteristics

The study population consisted of 28 patients including 16 men (57.1 %), and 71.4 % of study patients were symptomatic with chest pain. The mean patient age was 62.2±10.4 years with a mean body mass index of 29.9±5.9 kg/m^2. The mean Agatston score within our cohort of study subjects was 539.2 ±601.6. This included eight patients with an Agatston score ≥400, indicative of heavily calcified coronary arteries. Vital signs, necessary for the CT-based FFR computation, demonstrated a mean systolic and diastolic blood pressure of 135.0± 16.8 mmHg and 71.4±9.5 mmHg, respectively, within the cohort. The mean heart rate was 71.5±12.2 beats per minute. A summary of relevant patient demographics and baseline characteristics is provided in Table 1.

Image quality of cCTA

The median subjective cCTA image quality score was 4 (interquartile ranges, 3–4) for both observers.

CT-based FFR assessment

For all patients, CT-based FFR computation was performed using the diastolic reconstruction. The mean total time for deriving CT-based FFR including dataset processing and flow computation was 51.9±9.0 min per study. The mean duration of the semiautomatic segmentation process of the coronary artery tree based on vessel centrelines as well as luminal contour proposals by the prototype software algorithm was 48.0±8.6 min. The final computational time to derive the flow metrics providing the CT-based FFR results, available at

Table 1 Patient characteristics

Parameter	Value
No. of patients	28
Age (y)	62.2±10.4
No. of males	16 (57.1 %)
Height (cm)	172.1±11.8
Weight (kg)	88.2±18.8
Body-mass index (kg/m^2)	29.9±5.9
Vital signs	
Systolic blood pressure (mmHg)	135.0±16.8
Diastolic blood pressure (mmHg)	71.4±9.5
Heart rate (beats per minute)	71.5±12.2
Agatston score	539.2±601.6
No. of patients ≥400	8 (28.6 %)
No. of coronary artery stenoses	36
No. of coronary artery stenoses per location	
Left anterior descending	23 (63.9 %)
Left circumflex	9 (25.0 %)
Right coronary artery	4 (11.1 %)

Note: Unless specified otherwise, data are presented as mean±standard deviation

arbitrary positions on the coronary artery tree, was measured at 3.9±0.8 min.

Correlation of CT-based FFR to invasive FFR

Comparison of invasively measured FFR and CT-based FFR was performed in 36 coronary artery stenoses. The CCA quantification of the coronary artery lesions that were subsequently evaluated with FFR revealed stenoses ranging from mild to severe (25-99 %). Within the left anterior descending, the left circumflex and the right coronary artery, 23 (63.9 %), nine (25.0 %) and four (11.1 %) stenoses were recorded. Stenoses were located proximally, medially and distally in the vessel in 19 cases (51.9 %), in 13 cases (36.5 %), and in four cases (11.5 %), respectively. Mean value of CT-based FFR was 0.85 for invasive FFR measurement and 0.87 for CT-based FFR, respectively. Figure 2 illustrates the results of the per-vessel analysis, which revealed good direct correlation between CT-based FFR values and invasively derived FFR measurements (Pearson's product-moment $r=0.74$, $p<0.0001$). Results of Bland-Altman analysis are provided in Fig. 3. Representative examples of anatomically obstructive lesions with and without haemodynamic significance are shown in Figs. 4 and 5.

Discussion

A large body of evidence demonstrates that cCTA alone is an effective diagnostic tool to rule out CAD based on the exceedingly high sensitivity approximating 98 % and negative predictive value of up to 100 % [15]. Traditionally, the specificity and positive predictive value have been somewhat lower. Therefore, there is the concern that more frequent use of this non-invasive imaging modality may incur increased invasive downstream testing, namely, unnecessary diagnostic CCA procedures. The limited discriminatory power of mere

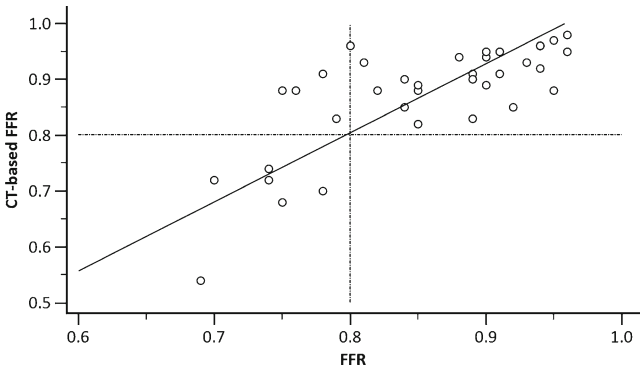

Fig. 2 Scatter plot demonstrating good correlation between CT-based FFR and invasively derived FFR (Pearson's correlation coefficient $r=0.74$; Regression equitation: $y=0.08197+0.9244\ x$)

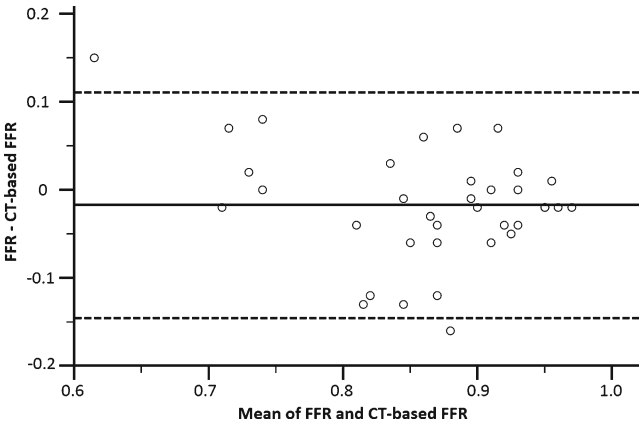

Fig. 3 Bland-Altman analysis plot comparing invasive fractional flow reserve and CT-based FFR on a per-lesion basis shows no systematic bias (95 % limits of agreement, -0.11 to 0.15)

anatomical imaging tests to identify haemodynamically relevant lesions constitutes a relevant issue in this context. Various methods have been proposed to derive more functional information from cCTA [16–19]. Recently, the addition of CT-based FFR to a mere quantitative cCTA interpretation has been described to integrate anatomical and physiological information on stenotic disease. CT-based FFR, thus, may be an attractive emergent approach to determine lesion-specific functional relevance more accurately than with cCTA alone.

In this preliminary report we discuss underlying technological principles and show initial results of a novel physician-driven prototype algorithm for the computation of FFR from cCTA. The thrust of this CT-based FFR algorithm aims at providing on-site, point-of-care availability of CT-based FFR evaluation within a clinically viable time frame. As it resides on a standard post-processing workstation, this prototype algorithm may rather seamlessly support practical utilization and patient management in routine clinical settings. Our very early experiences showed an evaluation time of less than 1 hour for deriving CT-based FFR, including the semiautomatic segmentation steps to extract a 3-dimensional coronary artery tree mesh from transverse grey scale images of a given cCTA dataset as well as the computational time for generating a patient-specific haemodynamic coronary artery model. Despite coupling of reduced-order and full-order models for a time-efficient simulation of coronary blood flow in patients with potentially significant stenoses, diagnostic performance does not seem to be meaningfully constrained. Our preliminary data demonstrates good correlation with invasive FFR measurements (Pearson's correlation coefficient $r=0.74$) and compares favourably to the results of previously published trials using a different CT-based FFR approach [6–8]. More specifically, the DISCOVER-FLOW [7], DeFACTO [6], and NXT [8] trials report Pearson correlation coefficients of $r=0.68$, $r=0.63$, and $r=0.82$, respectively. Therefore, our results suggest that the reduced order model for CT-based FFR derivation evaluated here may be capable of streamlining patient

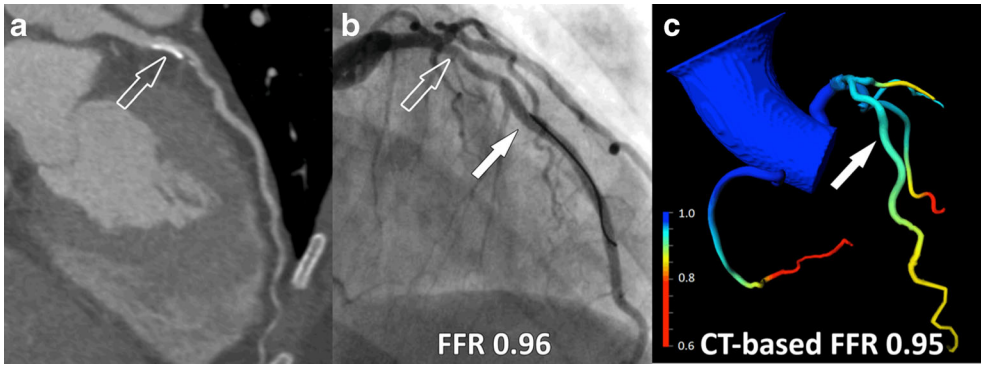

Fig. 4 A 53-year-old woman with atypical chest pain and an intermediate cardiovascular risk profile. **a** cCTA demonstrates a moderate (50-69 %) stenosis (open arrow) of the proximal segment of the left anterior descending coronary artery caused by mixed plaques. **b** Coronary catheter angiography shows mild stenosis (open arrow) with an invasive FFR measurement of 0.96 distal to the lesion (arrow) indicating a haemodynamically non-significant stenosis. **c** CT-based FFR derivation, displayed in a colour-coded 3-dimensional mesh, resulted in a value of 0.95 distal to the lesion (arrow)

management while preserving the good correlation with invasive FFR, which has been previously reported for remote, off-site CT-based FFR computation [6–8].

Our very preliminary experiences need to be gauged in light of several limitations, foremost the retrospective nature of our investigation in a small cohort. Furthermore, as in previous studies on this subject, our investigation is limited by selection bias as only patients with at least one invasively quantified stenosis were included, resulting in an unusually high prevalence of disease in the study population. Moreover, due to the small size of our exploratory cohort, we refrained from assessing the effect of this prototype algorithm on the overall indices of diagnostic accuracy and limited the performance analysis to correlation on a per-vessel basis. The investigation of a larger cohort of patients will be needed to provide more representative results. Similarly, future studies will have to investigate performance variables such as inter-observer reproducibility, which we did not yet explore in the course of this early algorithmic description.

As is true for quantitative cCTA, CT-based FFR requires reasonable diagnostic image quality for the generation of anatomically exact coronary artery tree models. Especially in a study population with a high prevalence of CAD, adequate image quality and accurate vessel lumen delineation are, thus, crucial [20]. Because severe degradation in image quality due to noise, low coronary artery contrast opacification, and artefacts critically limit conclusive cCTA interpretation, we excluded non-diagnostic datasets from this investigation. Thus, the subjective analysis revealed an overall good image quality, although the interquartile ranges indicate that the evaluated study cohort was not overly selected to only include excellent cases but was rather representative of clinical routine. Moreover, patients with complex bifurcation stenoses as well as with diseases reducing the functional myocardial mass were excluded because these are not amenable to the early prototype version examined here.

In conclusion, we introduce a newly developed CT-based FFR algorithm which, according to our early experience,

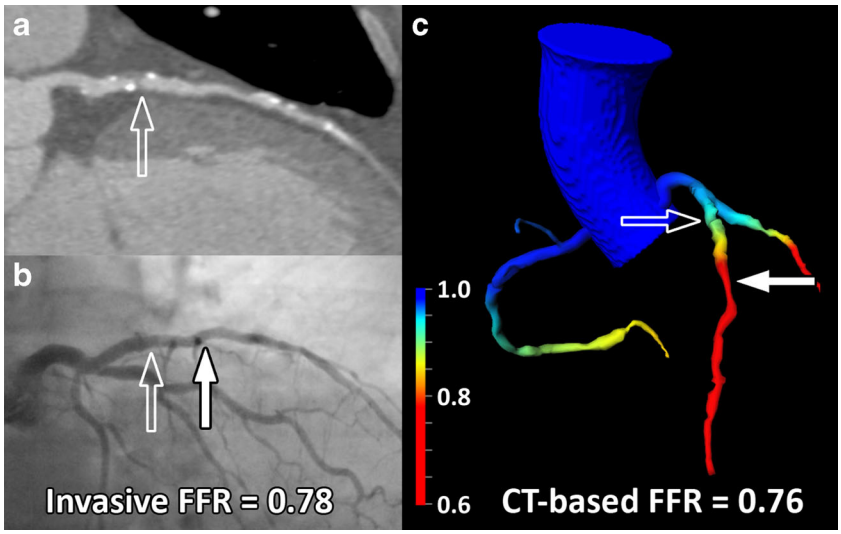

Fig. 5 **a** cCTA demonstrates a lesion (open arrow) in the proximal left anterior descending coronary artery caused by predominantly non-calcified plaque (**b**) Coronary catheter angiography shows moderate to severe stenosis (open arrow) of the mid-vessel with an invasive FFR measurement of 0.78 distal to the lesion (arrow) indicating a haemodynamically significant stenosis. **c** CT-based FFR derivation, displayed in a colour-coded 3-dimensional mesh, resulted in a value of 0.76 distal to the lesion (arrow)

holds promise to enable time-efficient, on-site evaluation of FFR from cCTA. Our preliminary data suggest high discriminatory power regarding haemodynamically relevant coronary artery stenoses, as CT-based FFR correlates well to the reference standard of invasive FFR. The assessment of lesion-specific ischemia at the point-of-care afforded in this manner may enhance patient management and guide rational therapeutic decision-making.

Acknowledgments The scientific guarantor of this publication is U. Joseph Schoepf. The authors of this manuscript declare relationships with the following companies: GE, Bracco, Siemens, Bayer and St. Jude. The authors state that this work has not received any funding. One of the authors has significant statistical expertise. Institutional Review Board approval was obtained. Written informed consent was waived by the Institutional Review Board. No animals were used in this study. No study subjects or cohorts have been previously reported. Methodology: retrospective, diagnostic or prognostic study, performed at one institution. Fast flow computations of coronary blood flow were not carried out in the United States.

References

1. Pijls NH, De Bruyne B, Peels K et al (1996) Measurement of fractional flow reserve to assess the functional severity of coronary-artery stenoses. N Engl J Med 334:1703–1708
2. Toth G, De Bruyne B, Casselman F et al (2013) Fractional flow reserve-guided versus angiography-guided coronary artery bypass graft surgery. Circulation 128:1405–1411
3. Tonino PA, De Bruyne B, Pijls NH et al (2009) Fractional flow reserve versus angiography for guiding percutaneous coronary intervention. N Engl J Med 360:213–224
4. Frauenfelder T, Boutsianis E, Schertler T et al (2007) In-vivo flow simulation in coronary arteries based on computed tomography datasets: feasibility and initial results. Eur Radiol 17:1291–1300
5. Grunau GL, Min JK, Leipsic J (2013) Modeling of fractional flow reserve based on coronary CT angiography. Curr Cardiol Rep 15:336
6. Min JK, Leipsic J, Pencina MJ et al (2012) Diagnostic accuracy of fractional flow reserve from anatomic CT angiography. JAMA 308: 1237–1245
7. Koo BK, Erglis A, Doh JH et al (2011) Diagnosis of ischemia-causing coronary stenoses by noninvasive fractional flow reserve computed from coronary computed tomographic angiograms. Results from the prospective multicenter DISCOVER-FLOW (diagnosis of ischemia-causing stenoses obtained Via noninvasive fractional flow reserve) study. J Am Coll Cardiol 58:1989–1997
8. Norgaard BL, Leipsic J, Gaur S et al (2014) Diagnostic performance of noninvasive fractional flow reserve derived from coronary computed tomography angiography in suspected coronary artery disease: the NXT trial (analysis of coronary blood flow using CT angiography: next steps). J Am Coll Cardiol 63:1145–1155
9. Sianos G, Morel MA, Kappetein AP et al (2005) The SYNTAX Score: an angiographic tool grading the complexity of coronary artery disease. EuroInterv 1:219–227
10. Husmann L, Alkadhi H, Boehm T et al (2006) Influence of cardiac hemodynamic parameters on coronary artery opacification with 64-slice computed tomography. Eur Radiol 16:1111–1116
11. Itu L, Sharma P, Mihalef V, Kamen A, Suciu C, Lomaniciu D (2012) A patient-specific reduced-order model for coronary circulationBiomedical Imaging (ISBI), 2012 9th IEEE International Symposium on, pp 832-835
12. Sharma P, Itu L, Zheng X et al (2012) A framework for personalization of coronary flow computations during rest and hyperemia. Conf Proc IEEE Eng Med Biol Soc 2012:6665–6668
13. Wilson RF, Wyche K, Christensen BV, Zimmer S, Laxson DD (1990) Effects of adenosine on human coronary arterial circulation. Circulation 82:1595–1606
14. Raff GL, Abidov A, Achenbach S et al (2009) SCCT guidelines for the interpretation and reporting of coronary computed tomographic angiography. J Cardiovasc Comput Tomogr 3:122–136
15. De Cecco CN, Meinel FG, Chiaramida SA, Costello P, Bamberg F, Schoepf UJ (2014) Coronary artery computed tomography scanning. Circulation 129:1341–1345
16. Ebersberger U, Marcus RP, Schoepf UJ et al (2014) Dynamic CT myocardial perfusion imaging: performance of 3D semi-automated evaluation software. Eur Radiol 24:191–199
17. Thilo C, Schoepf UJ, Gordon L, Chiaramida S, Serguson J, Costello P (2009) Integrated assessment of coronary anatomy and myocardial perfusion using a retractable SPECT camera combined with 64-slice CT: initial experience. Eur Radiol 19:845–856
18. Enrico B, Suranyi P, Thilo C, Bonomo L, Costello P, Schoepf UJ (2009) Coronary artery plaque formation at coronary CT angiography: morphological analysis and relationship to hemodynamics. Eur Radiol 19:837–844
19. Nasis A, Ko BS, Leung MC et al (2013) Diagnostic accuracy of combined coronary angiography and adenosine stress myocardial perfusion imaging using 320-detector computed tomography: pilot study. Eur Radiol 23:1812–1821
20. Moscariello A, Vliegenthart R, Schoepf UJ et al (2012) Coronary CT angiography versus conventional cardiac angiography for therapeutic decision making in patients with high likelihood of coronary artery disease. Radiology 265:385–392

Comparison of Diagnostic Value of a Novel Noninvasive Coronary Computed Tomography Angiography Method Versus Standard Coronary Angiography for Assessing Fractional Flow Reserve

Matthias Renker, MD[a,b], U. Joseph Schoepf, MD[a,*], Rui Wang, MD[a,c], Felix G. Meinel, MD[a,d], Jeremy D. Rier, DO[a], Richard R. Bayer II, MD[a], Helge Möllmann, MD[b], Christian W. Hamm, MD[b], Daniel H. Steinberg, MD[a], and Stefan Baumann, MD[a,e]

Noninvasive fractional flow reserve (FFR) from coronary computed tomography angiography (cCTA) correlates well with invasive FFR and substantially improves the detection of obstructive coronary artery disease. However, with current algorithms, computed tomography (CT)−based FFR is derived off-site in an involved time-consuming manner. We sought to investigate the diagnostic performance of a novel CT-based FFR algorithm, developed for time-efficient in-hospital evaluation of hemodynamically indeterminate coronary lesions. In a blinded fashion, CT-based FFR was assessed in 67 coronary lesions of 53 patients. Pressure guidewire−based FFR <0.80 served as the reference standard to define hemodynamically significant stenosis and assess the diagnostic performance of CT-based FFR compared with standard evaluation of cCTA (luminal diameter stenosis of ≥50%). We recorded the time needed for derivation of CT-based FFR. On a per-lesion and per-patient basis, CT-based FFR resulted in a sensitivity of 85% and 94%, a specificity of 85% and 84%, a positive predictive value of 71% and 71%, and a negative predictive value of 93% and 97%, respectively. The area under the receiver operating characteristic curve on a per-lesion basis was significantly greater for CT-based FFR compared with standard evaluation of cCTA (0.92 vs 0.72, p = 0.0049). A similar trend, albeit not statistically significant, was observed on per-patient analysis (0.91 vs 0.78, p = 0.078). Mean total time for CT-based FFR was 37.5 ± 13.8 minutes. In conclusion, the CT-based FFR algorithm evaluated here outperforms standard evaluation of cCTA for the detection of hemodynamically significant stenoses while allowing on-site application within clinically viable time frames. **(Am J Cardiol 2014;114:1303−1308)**

The diagnosis of coronary artery disease (CAD) is noninvasively accomplished with coronary computed tomography angiography (cCTA) by assessing coronary artery anatomy and direct visualization of atherosclerotic plaque.[1] This method also provides potential benefit via detection of nonobstructive coronary lesions before they develop hemodynamic significance and progression to clinical end points, chiefly major adverse cardiac events.[2] However, particularly with intermediate coronary artery lesions, the differentiation of flow-limiting stenoses remains a limitation of cCTA. To add physiological information to anatomic cCTA data, multiparametric imaging protocols are currently being developed, including computed tomography (CT) myocardial perfusion imaging and CT-based derivation of fractional flow reserve (FFR).[3,4] Initial approaches applied a CT-based FFR algorithm off-site using computations on a parallel supercomputer to solve complex Navier-Stokes equations for simulation of coronary hemodynamics.[5] We sought to investigate the diagnostic value of a novel CT-based FFR prototype algorithm, developed for time-efficient and in-hospital application without data transfer, to detect lesion-specific ischemia in coronary artery stenoses, as confirmed by invasive FFR.

Methods

Using a retrospective study design, we investigated patients with suspected or known coronary artery disease who had undergone clinically indicated cCTA, coronary catheter angiography (CCA), and FFR from September 2008 to February 2014 in a non-emergent setting. Exclusion criteria were defined as time between procedures exceeding 3 months, interprocedural major adverse cardiac events (cardiac death, nonfatal myocardial infarction, or revascularization), severely reduced left ventricular function, previous coronary artery bypass surgery, stent placement in the

[a]Heart & Vascular Center, Medical University of South Carolina, Charleston, South Carolina; [b]Kerckhoff Heart and Thorax Center, Bad Nauheim, Germany; [c]Department of Radiology, Beijing Anzhen Hospital, Capital Medical University, Beijing, China; [d]Institute for Clinical Radiology, Ludwig-Maximilians-University Hospital, Munich, Germany; and [e]First Department of Medicine, Faculty of Medicine Mannheim, University Medical Centre Mannheim (UMM), University of Heidelberg, Mannheim, Germany. Manuscript received May 30, 2014; revised manuscript received and accepted July 24, 2014.

See page 1308 for disclosure information.

*Corresponding author: Tel: (843) 792-2633; fax: (843) 792-0409.
E-mail address: schoepf@musc.edu (U.J. Schoepf).

0002-9149/14/$ - see front matter
http://dx.doi.org/10.1016/j.amjcard.2014.07.064

Table 1
Patient characteristics (n = 53)

Parameter	Mean ± Standard Deviation or Frequency (%)
Age (years)	61.2 ± 12.0
Men	34 (64%)
Height (cm)	173.2 ± 10.8
Weight (kg)	87.0 ± 21.2
Body-mass index (kg/m^2)	28.9 ± 6.5
Caucasian	44 (77%)
African American	13 (23%)
Hypertension*	31 (54%)
Diabetes mellitus	18 (32%)
Hyperlipidemia†	31 (54%)
Current smoker	8 (14%)
Prior percutaneous coronary intervention	9 (16%)
Prior coronary bypass surgery	0 (0%)
Left ventricular ejection fraction (%)	58.3 ± 9.3
Systolic blood pressure (mm Hg)	136.2 ± 15.7
Diastolic blood pressure (mm Hg)	71.8 ± 9.3
Heart rate (beats per minute)	70.2 ± 12.6
Aspirin	31 (54%)
Clopidogrel	10 (18%)
β blocker	30 (53%)
Statin	35 (61%)
Angiotensin converting enzyme inhibitor	23 (40%)
Calcium-channel blocker	10 (18%)

* Defined as blood pressure >140 mm Hg systolic, >90 mm Hg diastolic, or use of antihypertensive medication.
† Defined as a total cholesterol level of >200 mg/dl or use of antilipidemic medication.

Table 2
Procedural results (number of narrowing = 67)

Coronary Catheter Angiography	Frequency (%)
Luminal stenosis ≥50%	44 (66%)
Luminal stenosis ≥70%	21 (31%)
FFR <0.80	20 (30%)
No. of stenoses of interest per location	
Left anterior descending coronary artery	41 (61%)
Left circumflex coronary artery	15 (22%)
Right coronary artery	11 (16%)
Coronary Computed Tomography Angiography	**Value or Frequency (%)**
Agatston score, mean ± standard deviation*	778.4 ± 731.1
Range*	0–2547
No. of patients ≥400*	19 (36%)
Luminal stenosis ≥50%	55 (82%)
Luminal stenosis ≥70%	27 (40%)
Intermediate grade luminal stenosis (30%–70%)	39 (58%)
CT-based FFR <0.80	24 (36%)

* Agatston score was obtained in 46 patients.

vessel containing the lesion of interest, bifurcation stenosis types D to G (SYNTAX score classification[6]), severe stenosis of the proximal left main and/or the proximal right coronary artery, total chronic occlusion, and nondiagnostic quality of the cCTA data set. The responsible institutional review board for human research approved the present study. The need for written informed patient consent was waived for this retrospective study.

In all subjects, selective CCA had been performed in our cardiac catheterization laboratory as per current guidelines.[7] Multiple projections were obtained of each major coronary artery (left main, left anterior descending, left circumflex, and right coronary artery). CCA projection angles were adjusted on an individual patient basis depending on the cardiac orientation. Based on the CCA examination, luminal stenosis was visually graded by an experienced interventional cardiologist. FFR interrogation was conducted at the time of CCA if a stenosis was suspected to cause ischemia. As described previously,[8] a dedicated pressure-monitoring guidewire was advanced distal to a lesion of interest, and the exact position of the sensor was recorded before assessing FFR. Hyperemia was induced by intravenous administration of adenosine at a rate of 140 μg/kg per min. FFR was derived as the ratio of mean coronary pressure distal to the stenosis and mean aortic pressure at the time of pharmacologically induced hyperemia. A threshold of <0.80 was considered to indicate hemodynamic significance of stenoses.

All cCTA examinations were acquired using first- and second-generation dual-source CT scanners (Somatom Definition and Somatom Definition Flash; Siemens Healthcare, Forchheim, Germany) according to the guidelines of the Society of Cardiovascular Computed Tomography.[9] To minimize radiation exposure, the cCTA acquisition technique was selected on an individual basis with adaptation of the acquisition to heart rate, heart rhythm, and body mass index of each patient. Retrospective electrocardiographic gating with tube current modulation, prospective electrocardiographic triggering, and prospective high-pitch electrocardiographically triggered spiral acquisition were used. A volume of 50 to 80 ml of iodinated contrast material was injected at a rate of 4 to 6 ml/s, immediately followed by a 50-ml saline bolus. The parameters of the cCTA protocol were tube current-time product, 350 to 650 mAs; tube potential, 80 to 120 kVp; gantry rotation time, 0.28 to 0.33 seconds. All data sets were reconstructed at a section thickness of ≤0.75 mm, with an increment of 0.4 mm. Image reconstruction was performed using filtered back projection and a dedicated vascular kernel (B26f). Standard cCTA interpretation was performed by an observer with 7 years of experience in evaluating cCTA studies. The percent luminal diameter stenosis of each lesion of interest was visually determined using transverse CT sections and curved multiplanar reformats along the vessel centerline on a dedicated analysis platform (SyngoVia, Siemens). A qualitative image rating of the cCTA data sets was conducted by an experienced observer using a 5-point Likert scale (1 = nondiagnostic; 2 = diagnostic despite impairment by image noise, artifacts, and/or low contrast opacification; 3 = moderate image noise with sufficient intraluminal visibility, artifacts may be present; 4 = good vessel contrast in the absence of major artifacts, low image noise; and 5 = excellent, no diagnostic limitations).

CT-based FFR computation was performed on regular cCTA data sets without the need for additional imaging, modification of the acquisition protocol, or administration of pharmacologic stress agents. A software research prototype (Siemens cFFR, version 1.4; Siemens Healthcare, currently not commercially available) installed on a regular workstation

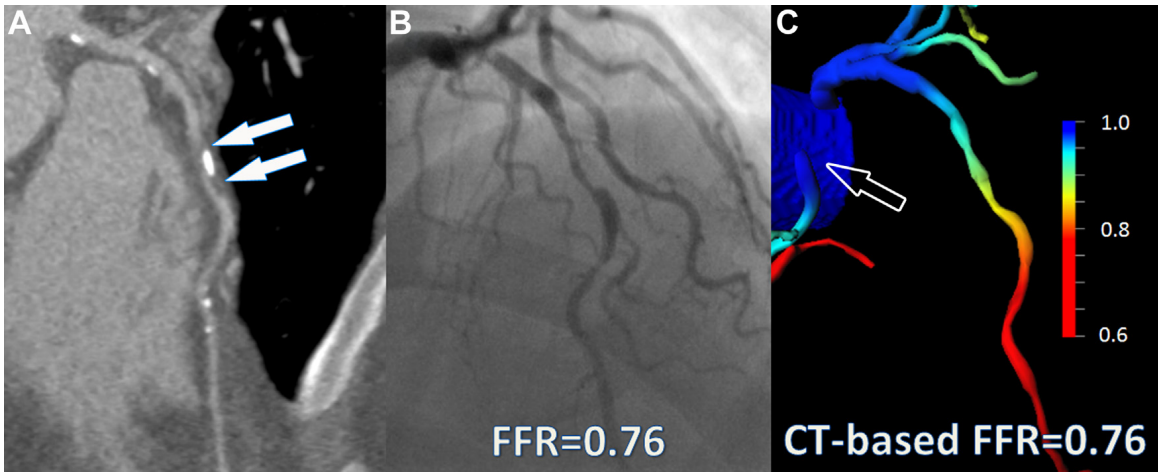

Figure 1. Multiplanar reformation of the left anterior descending coronary artery from a standard cCTA study demonstrates an intermediate to severe stenosis (*arrows*) *(A)*. CCA confirms the presence of a long irregular stenosis of the midvessel *(B)*. Invasive FFR was measured at 0.76, indicating lesion-specific ischemia. FFR derivation from cCTA of the lesion of interest revealed an identical value of 0.76 *(C)*. Incidentally, here is also an abnormal origin of the right coronary artery from the left coronary cusp (*open arrow*).

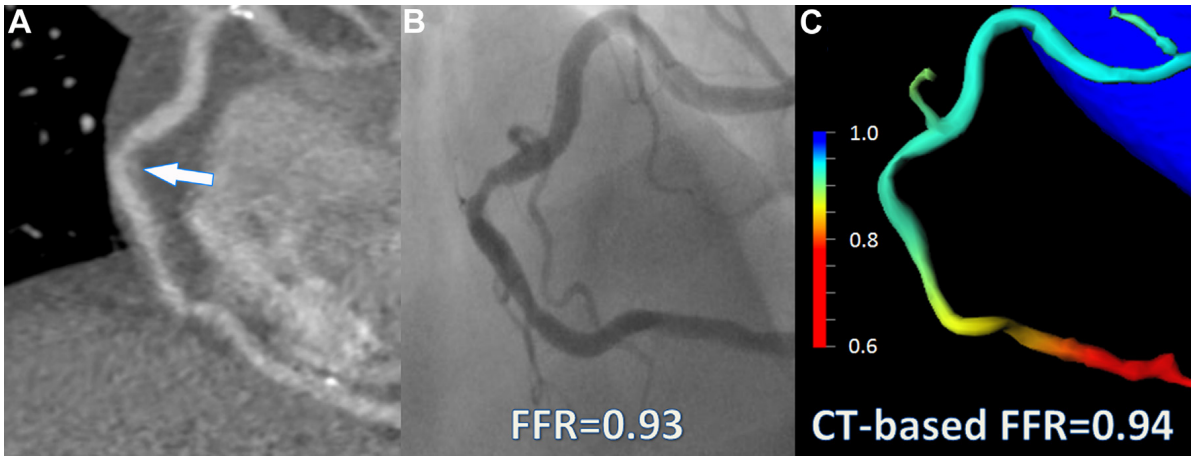

Figure 2. cCTA of the same patient seen in Figure 1, displayed as multiplanar reformation of the right coronary artery, shows an intermediate-degree luminal stenosis in the mid portion of the vessel (*arrow*) *(A)*. CCA confirms the lesion *(B)*. Catheter-based FFR was measured at 0.93, indicating a lack of hemodynamic significance of this lesion. Noninvasive FFR derivation from cCTA resulted in a value of 0.94, in good correlation with invasive measurement *(C)*.

was used to derive CT-based FFR. An experienced observer, who was blinded to the CCA and FFR results, accepted or corrected the luminal contour and centerline proposals offered by the software to generate a patient-specific 3-dimensional mesh of the coronary artery tree. Applying principles of computational fluid dynamics, the CT-based FFR algorithm simulates coronary blood flow from the 3-dimensional model and the patient-specific boundary conditions for a hyperemic state. Lumped cardiac and coronary microcirculatory models represent the individual boundary conditions. For this purpose, rest-state conditions including systolic and diastolic blood pressures, heart rate, and left ventricular mass are integrated and subsequently modified to incorporate the effect of maximal hyperemia by simulation of the decrease in microvascular resistance as induced by pharmacologic stressors.[10] Based on the patient-specific 3-dimensional mesh and the boundary conditions, fast flow computation of coronary blood flow was performed by the software prototype in a blinded fashion by coupling of reduced- and full-order models. Invasive FFR results served as the reference standard for the detection of lesion-specific ischemia. Emphasis was placed on assessing CT-based FFR from the coronary flow model at the same position as the invasive FFR, indicated by the recorded measurement position of the pressure guidewire sensor.

All statistical analyses were performed using dedicated statistical software (MedCalc for Windows, version 12.5; MedCalc Software, Ostend, Belgium). Continuous variables are presented as means ± SDs, and ordinal variables are presented as medians with interquartile ranges in parentheses. p Values <0.05 were considered to indicate statistical significance. Distribution of data was assessed using the Shapiro-Wilk test. Applying invasive FFR <0.80 as the reference standard, the diagnostic performance of $\geq 50\%$ diameter stenosis on cCTA and CT-based FFR <0.80 were evaluated on a per-lesion and per-patient level, including sensitivity, specificity, positive predictive value, and negative predictive value. Moreover, the area under the receiver

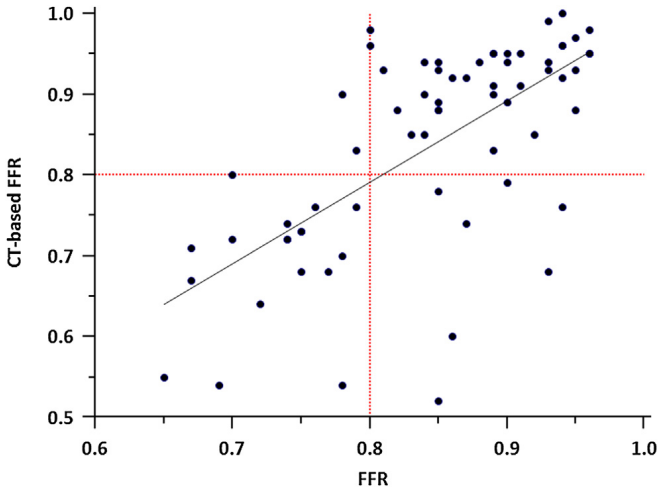

Figure 3. Performance on a per-lesion level for the identification of lesion-specific ischemia demonstrates good correlation between FFR derived from CT compared with the invasive reference standard (Spearman rank correlation coefficient $\rho = 0.66$, $p < 0.001$).

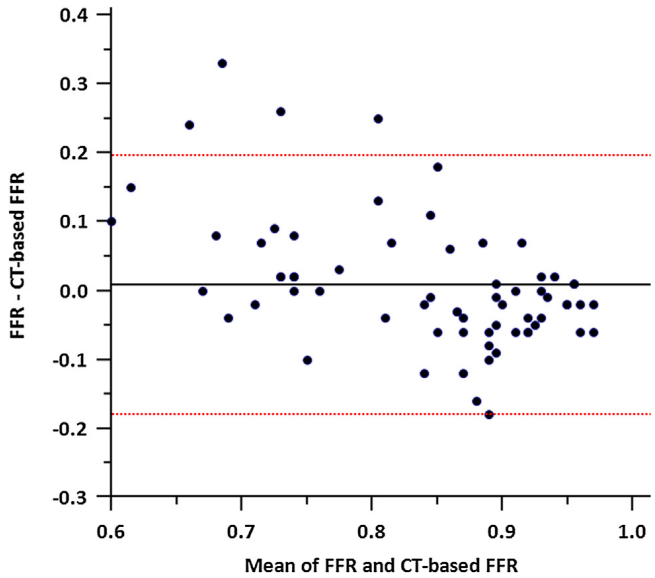

Figure 4. Bland-Altman analysis plot comparing invasive FFR and CT-derived FFR on a per-lesion basis shows no systematic bias (95% limits of agreement −0.18 to 0.20).

operating characteristics curve (AUC) was determined for cCTA and CT-based FFR as a metric of overall diagnostic performance. AUC comparisons were performed using the method of Hanley and McNeal.[11] For the per-patient analyses, a patient was considered positive for ischemia, if the FFR interrogation of any evaluable vessel resulted in a value of <0.80. Similarly, a patient was considered negative for ischemia if no vessel resulted in an FFR value of <0.80. The same rules were applied during the assessment of CT-based FFR. An analysis according to Bland-Altman was performed.[12] Spearman and Pearson statistics were applied to analyze the degree of correlation between CT-based FFR and the invasive reference standard.

Results

Eleven patients (21%) were excluded because of an interprocedural time >3 months or previous revascularization as defined previously, 3 patients (6%) were excluded on account of nonevaluable cCTA data sets (severe motion artifacts), and 5 patients (9%) were excluded because of bifurcation lesions. Patient demographics and baseline characteristics are provided in Table 1.

Coronary lesions evaluated by CCA and FFR ranged in severity from 30% to 90% luminal narrowing. FFR interrogation assessed the presence of hemodynamically relevant stenoses (FFR <0.80) in 20 vessels of 16 patients. Relevant results of cCTA and CCA with invasive FFR are illustrated in Table 2. Overall, a mean duration of 37.5 ± 13.8 minutes was recorded for the derivation of CT-based FFR including data set processing and coronary flow computation. The median subjective cCTA image quality score was 4 (interquartile range 3 to 4).

Representative case examples are shown in Figures 1 and 2. As illustrated in Figure 3, good correlation was observed between FFR and CT-based FFR (Spearman rank correlation coefficient $\rho = 0.66$, $p < 0.001$; Pearson product-moment $r = 0.66$, $p < 0.001$). No systematic bias was found on Bland-Altman analysis, as demonstrated in Figure 4. On both the per-patient and per-lesion level, the diagnostic performance of CT-based FFR <0.80 to detect flow-limiting stenoses was favorable in comparison with standard evaluation of cCTA (luminal stenosis ≥50%), as confirmed by the invasive reference standard FFR (Table 3).

In Figure 5, the AUCs demonstrate a substantial improvement of diagnostic performance with CT-based FFR compared with mere anatomic interpretation of cCTA for the detection of lesion-specific ischemia. This improvement in overall diagnostic performance was primarily driven by a dramatic increase in specificity from 34% to 85% on a per-lesion level and from 32% to 84% on a per-patient level with no significant change in sensitivity (Table 3).

Discussion

In this study, we examined the performance of a prototype algorithm for the computation of FFR from cCTA image data for the detection of hemodynamically significant coronary artery stenoses in comparison with invasively derived FFR. This algorithm aims at providing in-hospital availability of noninvasive FFR determination in a time-efficient manner. Our results demonstrate the potential of this CT-based FFR approach for the detection of obstructive coronary artery disease in a population with high disease prevalence. The overall correlation between CT-based FFR and the invasive reference standard FFR was good. More importantly, when measured against an FFR cut-off value of 0.80 to indicate hemodynamically significant stenoses, CT-based FFR yielded greater diagnostic performance to detect lesion-specific ischemia than anatomic interpretation of cCTA.

Increasing interest is placed on gauging the hemodynamic significance of coronary artery lesions, which has been demonstrated to provide superior guidance for patient management. Therefore, a variety of approaches are currently under investigation to add physiological information to the primarily anatomic imaging method of cCTA. Voros et al[13]

Table 3
Diagnostic performance of fractional flow reserve from coronary computed tomography angiography and standard evaluation of coronary computed tomography angiography, on a per-lesion and per-patient basis, using invasive fractional flow reserve as the reference standard

	Per-Lesion (n = 67)		Per-Patient (n = 53)	
	CT-Based FFR <0.80 (95% CI)	cCTA Stenosis ≥0.50 (95% CI)	CT-Based FFR <0.80 (95% CI)	cCTA Stenosis ≥0.50 (95% CI)
Sensitivity	85 (62–97)	90 (68–98)	94 (70–99)	94 (70–99)
Specificity	85 (72–94)	34 (21–49)	84 (68–94)	32 (18–50)
PPV	71 (49–87)	37 (23–52)	71 (48–89)	38 (23–54)
NPV	93 (81–98)	89 (65–98)	97 (84–99)	92 (64–99)

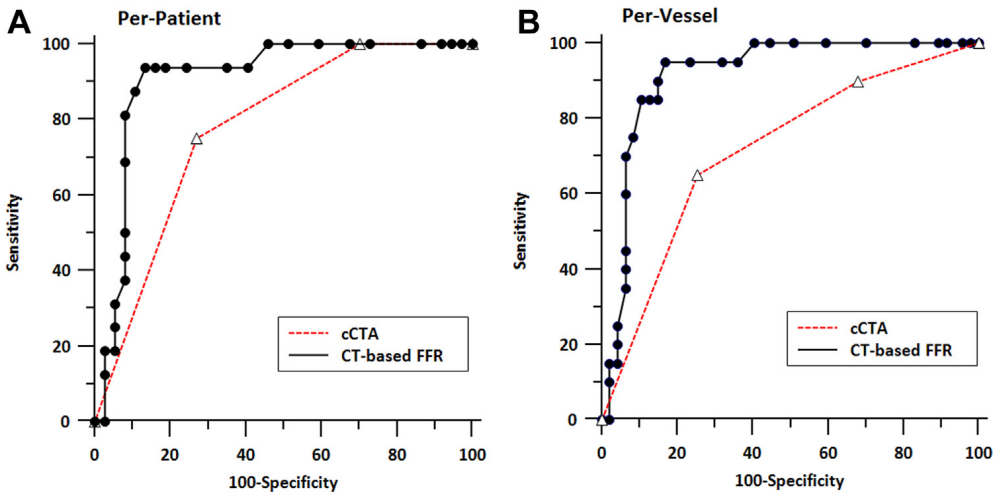

Figure 5. AUC comparison between cCTA and CT-based FFR on a per-patient *(A)* and per-lesion level *(B)*, using invasive FFR as the reference standard. On a per-patient and per-lesion level, the AUC for the detection of lesion-specific ischemia by CT-based FFR at the 0.80 threshold was 0.91 and 0.92, compared with 0.78 and 0.72, respectively, by cCTA at a 50% threshold. The AUC comparison reached statistical significance in the per-lesion analysis (p = 0.005, 95% confidence interval for difference 0.06 to 0.34) but not on a per-patient level (p = 0.078, 95% confidence interval for difference −0.01 to 0.28).

reported an improved diagnostic performance of quantitative anatomic cCTA measurements over intravascular ultrasound and over visual stenosis grading in correlation with FFR. Moreover, CT myocardial perfusion imaging is currently under evaluation for assessing the hemodynamic relevance of lesions.[14–17] However, approaches involving CT-based myocardial perfusion imaging ordinarily require an additional CT scan acquisition and typically involve the administration of a pharmacologic stressor, in analogy to nuclear-based techniques. The concept of deriving similar information from static cCTA acquisitions acquired at rest thus is attractive. Building on the principles of computational fluid dynamics, CT-based FFR was introduced as an add-on diagnostic approach for the simulation of coronary blood flow under rest conditions and in a hyperemic state without modifications of the cCTA acquisition protocol. Three larger trials have been completed to investigate the diagnostic performance of a previously introduced algorithm with data set evaluation in core laboratories using supercomputational power.[18–20] Despite the integration of less computationally demanding reduced-order models with full-order models for the simulation of coronary blood flow, the diagnostic performance of the presently studied CT-based FFR prototype algorithm for the computation of coronary hemodynamics remains high and largely reflects the results of these previous studies. However, previous CT-based FFR data set evaluation techniques required 1 to 4 hours per examination, whereas a mean duration of 38 minutes was recorded for the derivation of CT-based FFR using the novel algorithm. Similar to previous experiences, the marked improvement in diagnostic performance was mainly driven by an increased specificity and positive predictive value when comparing CT-based FFR with standard evaluation of cCTA. On a per-patient basis, the CT-based FFR approach evaluated here yielded an AUC comparable with the results of the Diagnosis of Ischemia-Causing Stenoses Obtained Via Noninvasive Fractional Flow Reserve (DISCOVER-FLOW) trial although certain differences in study design and patient characteristics have to be considered.[18]

Several limitations apply to our investigation. First, the number of subjects in this retrospective study was relatively small. This might explain why the AUC comparison between CT-based FFR and standard evaluation of cCTA for the detection of lesion-specific ischemia reached significance only on a per-lesion basis but not on a per-patient level. Furthermore, large-scale and preferably prospective studies will be needed to confirm our findings. Second, this study is subject to selection bias as only patients with ≥1 coronary artery lesions were included thus leading to an inevitably high prevalence of CAD. Third, only a selective spectrum of stenoses with indeterminate hemodynamic relevance was interrogated causing an artificially high prevalence of intermediate-degree

stenoses. Invasive assessment of FFR in patients with <30% luminal coronary artery stenosis on quantitative CCA is typically not performed at our institution as the presence of ischemia is infrequent in this group. However, this fact should render our patient cohort more representative of the intended clinical target population because CT-based FFR algorithms are most likely to be used to arbitrate the hemodynamic significance of intermediate stenoses. Fourth, a time frame of up to 3 months was allowed between cCTA and CCA with invasive FFR, which may affect the comparability.

Disclosures

Dr. Schoepf is a consultant for and/or receives research support from Bayer (Wayne, New Jersey), Bracco (Princeton, New Jersey), GE Healthcare (Little Chalfont, Buckinghamshire, United Kingdom), Medrad (Warrendale, Pennsylvania), and Siemens Healthcare (Malvern, Pennsylvania). Dr. Steinberg is a consultant for St. Jude Medical (St. Paul, Minnesota). Dr. Möllmann receives lecture fees from St. Jude Medical (St. Paul, Minnesota). The other authors have no conflicts of interest to disclose. Fast flow computations of coronary blood flow were not carried out in the United States.

1. De Cecco CN, Meinel FG, Chiaramida SA, Costello P, Bamberg F, Schoepf UJ. Coronary artery computed tomography scanning. *Circulation* 2014;129:1341−1345.
2. Ahmadi N, Nabavi V, Hajsadeghi F, Flores F, French WJ, Mao SS, Shavelle D, Ebrahimi R, Budoff M. Mortality incidence of patients with non-obstructive coronary artery disease diagnosed by computed tomography angiography. *Am J Cardiol* 2011;107:10−16.
3. Meinel FG, Ebersberger U, Schoepf UJ, Lo GG, Choe YH, Wang Y, Maivelett JA, Krazinski AW, Marcus RP, Bamberg F, De Cecco CN. Global quantification of left ventricular myocardial perfusion at dynamic CT: feasibility in a multicenter patient population. *AJR Am J Roentgenol* 2014;203:W174−80.
4. Min JK, Koo BK, Erglis A, Doh JH, Daniels DV, Jegere S, Kim HS, Dunning AM, Defrance T, Lansky A, Leipsic J. Usefulness of noninvasive fractional flow reserve computed from coronary computed tomographic angiograms for intermediate stenoses confirmed by quantitative coronary angiography. *Am J Cardiol* 2012;110:971−976.
5. Grunau GL, Min JK, Leipsic J. Modeling of fractional flow reserve based on coronary CT angiography. *Curr Cardiol Rep* 2013;15:336.
6. Sianos G, Morel MA, Kappetein AP, Morice MC, Colombo A, Dawkins K, van den Brand M, Van Dyck N, Russell ME, Mohr FW, Serruys PW. The SYNTAX score: an angiographic tool grading the complexity of coronary artery disease. *EuroIntervention* 2005;1:219−227.
7. Scanlon PJ, Faxon DP, Audet AM, Carabello B, Dehmer GJ, Eagle KA, Legako RD, Leon DF, Murray JA, Nissen SE, Pepine CJ, Watson RM, Ritchie JL, Gibbons RJ, Cheitlin MD, Gardner TJ, Garson A Jr, Russell RO Jr, Ryan TJ, Smith SC Jr. ACC/AHA guidelines for coronary angiography: executive summary and recommendations. A report of the American College of Cardiology/American Heart Association Task Force on Practice Guidelines (Committee on Coronary Angiography) developed in collaboration with the Society for Cardiac Angiography and Interventions. *Circulation* 1999;99:2345−2357.
8. Lopez-Palop R, Carrillo P, Frutos A, Cordero A, Agudo P, Mashlab S, Bertomeu-Martinez V. Comparison of effectiveness of high-dose intracoronary adenosine versus intravenous administration on the assessment of fractional flow reserve in patients with coronary heart disease. *Am J Cardiol* 2013;111:1277−1283.
9. Abbara S, Arbab-Zadeh A, Callister TQ, Desai MY, Mamuya W, Thomson L, Weigold WG. SCCT guidelines for performance of coronary computed tomographic angiography: a report of the Society of Cardiovascular Computed Tomography Guidelines Committee. *J Cardiovasc Comput Tomogr* 2009;3:190−204.
10. Sharma P, Itu L, Zheng X, Kamen A, Bernhardt D, Suciu C, Comaniciu D. A framework for personalization of coronary flow computations during rest and hyperemia. *Conf Proc IEEE Eng Med Biol Soc* 2012;2012:6665−6668.
11. Hanley JA, McNeil BJ. A method of comparing the areas under receiver operating characteristic curves derived from the same cases. *Radiology* 1983;148:839−843.
12. Bland JM, Altman DG. Statistical methods for assessing agreement between two methods of clinical measurement. *Lancet* 1986;1:307−310.
13. Voros S, Rinehart S, Vazquez-Figueroa JG, Kalynych A, Karmpaliotis D, Qian Z, Joshi PH, Anderson H, Murrieta L, Wilmer C, Carlson H, Ballard W, Brown C. Prospective, head-to-head comparison of quantitative coronary angiography, quantitative computed tomography angiography, and intravascular ultrasound for the prediction of hemodynamic significance in intermediate and severe lesions, using fractional flow reserve as reference standard (from the ATLANTA I and II Study). *Am J Cardiol* 2014;113:23−29.
14. Meinel FG, De Cecco CN, Schoepf UJ, Nance JW Jr, Silverman JR, Flowers BA, Henzler T. First-arterial-pass dual-energy CT for assessment of myocardial blood supply: do we need rest, stress, and delayed acquisition? Comparison with SPECT. *Radiology* 2014;270:708−716.
15. Wang Y, Qin L, Shi X, Zeng Y, Jing H, Schoepf UJ, Jin Z. Adenosine-stress dynamic myocardial perfusion imaging with second-generation dual-source CT: comparison with conventional catheter coronary angiography and SPECT nuclear myocardial perfusion imaging. *AJR Am J Roentgenol* 2012;198:521−529.
16. Weininger M, Schoepf UJ, Ramachandra A, Fink C, Rowe GW, Costello P, Henzler T. Adenosine-stress dynamic real-time myocardial perfusion CT and adenosine-stress first-pass dual-energy myocardial perfusion CT for the assessment of acute chest pain: initial results. *Eur J Radiol* 2012;81:3703−3710.
17. Bastarrika G, Ramos-Duran L, Schoepf UJ, Rosenblum MA, Abro JA, Brothers RL, Zubieta JL, Chiaramida SA, Kang DK. Adenosine-stress dynamic myocardial volume perfusion imaging with second generation dual-source computed tomography: concepts and first experiences. *J Cardiovasc Comput Tomogr* 2010;4:127−135.
18. Koo BK, Erglis A, Doh JH, Daniels DV, Jegere S, Kim HS, Dunning A, DeFrance T, Lansky A, Leipsic J, Min JK. Diagnosis of ischemia-causing coronary stenoses by noninvasive fractional flow reserve computed from coronary computed tomographic angiograms. Results from the prospective multicenter DISCOVER-FLOW (Diagnosis of Ischemia-Causing Stenoses Obtained Via Noninvasive Fractional Flow Reserve) study. *J Am Coll Cardiol* 2011;58:1989−1997.
19. Min JK, Leipsic J, Pencina MJ, Berman DS, Koo BK, van Mieghem C, Erglis A, Lin FY, Dunning AM, Apruzzese P, Budoff MJ, Cole JH, Jaffer FA, Leon MB, Malpeso J, Mancini GB, Park SJ, Schwartz RS, Shaw LJ, Mauri L. Diagnostic accuracy of fractional flow reserve from anatomic CT angiography. *JAMA* 2012;308:1237−1245.
20. Norgaard BL, Leipsic J, Gaur S, Seneviratne S, Ko BS, Ito H, Jensen JM, Mauri L, De Bruyne B, Bezerra H, Osawa K, Marwan M, Naber C, Erglis A, Park SJ, Christiansen EH, Kaltoft A, Lassen JF, Botker HE, Achenbach S; Group NXTTS. Diagnostic performance of noninvasive fractional flow reserve derived from coronary computed tomography angiography in suspected coronary artery disease: the NXT trial (Analysis of Coronary Blood Flow Using CT Angiography: Next Steps). *J Am Coll Cardiol* 2014;63:1145−1155.

Original Investigation

Comparison of Coronary Computed Tomography Angiography-Derived vs Invasive Fractional Flow Reserve Assessment: Meta-Analysis with Subgroup Evaluation of Intermediate Stenosis

Stefan Baumann, MD†, Matthias Renker, MD†, Svetlana Hetjens, PhD, Stephen R. Fuller, BSc, Tobias Becher, MD, Dirk Loßnitzer, MD, Ralf Lehmann, MD, Ibrahim Akin, MD, Martin Borggrefe, MD, Siegfried Lang, PhD, Julian L. Wichmann, MD, U. Joseph Schoepf, MD

Abbreviations

cCTA coronary computed tomography angiography

CI confidence interval

CT-FFR fractional flow reserve from coronary computed tomographic angiography

FFR fractional flow reserve

ICA invasive coronary angiography

sROC summary area under the receiver operating characteristic curve

Rationale and Objectives: Invasive coronary angiography (ICA) with fractional flow reserve (FFR) assessment is the reference standard for the detection of hemodynamically relevant coronary lesions. We have investigated whether coronary computed tomography angiography (cCTA)-derived FFR (fractional flow reserve from coronary computed tomographic angiography [CT-FFR]) measurement improves diagnostic accuracy over cCTA.

Methods and Results: A literature search was performed for studies comparing invasive FFR, cCTA, and CT-FFR. The analysis included three prospective multicenter trials and two retrospective single-center studies; a total of 765 patients and 1306 vessels were included in the meta-analysis. Compared to invasive FFR on a per-lesion basis, CT-FFR reached a pooled sensitivity, specificity, positive predictive value, and negative predictive value of 83.7% (95% confidence interval [CI]: 78.1–89.3), 74.7% (95% CI: 52.2–97.1), 64.8% (95% CI: 52.1–77.5), and 90.1% (95% CI: 80.8–99.3) compared to 84.6% (95% CI: 78.1–91.1), 49.7% (95% CI: 31.1–68.4), 39.0% (95% CI: 28.0–50.1), and 87.3% (95% CI: 72.5–100.0) for cCTA alone. In 634 vessels with intermediate stenosis (30%–70%), sensitivity, specificity, positive predictive value, and negative predictive value were 81.4% (95% CI: 70.4–92.9), 71.7% (95% CI: 54.5–89.0), 59.4% (95% CI: 35.5–83.4), and 89.9% (95% CI: 85.0–94.7) compared to 90.2% (95% CI: 80.6–99.9), 35.4% (95% CI: 23.5–47.3), 50.7% (95% CI: 30.6–70.8), and 82.5% (95% CI: 64.5–100.0) for cCTA alone. The summary area under the receiver operating characteristic curve of CT-FFR was superior to cCTA alone on a per-vessel (0.90 [95% CI: 0.82–0.98] vs 0.74 [95% CI: 0.63–0.86]; $P = .0047$) and for intermediate stenoses (0.76 [95% CI: 0.65–0.88] vs 0.57 [95% CI: 0.49–0.66]; $P = .0027$).

Conclusion: CT-FFR significantly improves specificity without noticeably altering the sensitivity of cCTA with invasive FFR as a reference standard for the detection of hemodynamically relevant stenosis.

Key Words: Coronary artery disease; coronary computed tomography angiography; fractional flow reserve; intermediate stenosis; meta-analysis.

Acad Radiol 2016; 23:1402–1411

From the Heart & Vascular Center, Medical University of South Carolina, Ashley River Tower, 25 Courtenay Drive, Charleston, SC 29425-2260, USA (S.B., M.R., S.R.F., J.L.W., U.J.S.); 1st Department of Medicine-Cardiology, University Medical Centre Mannheim, Mannheim, Germany and with DZHK (German Centre for Cardiovascular Research), partner site Heidelberg/Mannheim, Mannheim, Germany (S.B., T.B., D.L., R.L., I.A., M.B., S.L.); Kerckhoff Heart and Thorax Center, Department of Cardiology, Bad Nauheim (M.R.); Institute of Medical Statistics and Biometry, University Medical Centre Mannheim, Medical Faculty Mannheim, University of Heidelberg, Mannheim, Germany (S.H.); Department of Diagnostic and Interventional Radiology, University Hospital Frankfurt, Frankfurt, Germany (J.L.W.). Received April 8, 2016; revised July 20, 2016; accepted July 24, 2016. †Both first authors contributed equally. **Address correspondence to:** U.J.S. e-mail: schoepf@musc.edu.

http://dx.doi.org/10.1016/j.acra.2016.07.007

INTRODUCTION

Coronary computed tomography angiography (cCTA) is an established noninvasive method for the exclusion of obstructive coronary artery disease (CAD) in low to intermediate risk patient populations (1). Although it tends to overestimate lesion severity compared to invasive coronary angiography (ICA), cCTA allows for the noninvasive assessment of coronary artery anatomy. However, the hemodynamic significance of coronary stenoses cannot be sufficiently evaluated with cCTA alone (2). Fractional flow reserve (FFR) is an invasive technique performed during cardiac catheterization that evaluates the functional significance of indeterminate coronary stenoses and provides guidance for lesion-specific revascularization therapy (3).

At this time, three large prospective clinical trials have demonstrated the diagnostic value of a noninvasive FFR (fractional flow reserve from coronary computed tomographic angiography [CT-FFR]) algorithm (HeartFlow, Inc., Redwood City, CA) based on fluid-dynamic modeling of coronary flow using diagnostic cCTA data acquired at rest (4–6). Furthermore, an initial study presented results on the diagnostic performance of an alternative on-site algorithm (Siemens Healthcare, Forchheim, Germany), also based on fluid-dynamic modeling; these results were subsequently corroborated by a larger study (7,8). Taken together, these investigations have demonstrated that algorithm-based noninvasive FFR derivation from cCTA compares favorably to the diagnostic gold standard of invasive FFR.

METHODS

Study Design and Search Criteria

The present study was conducted in compliance with the Preferred Reporting Items for Systematic reviews and Meta-Analyses statement to establish standards to ensure the quality of meta-analyses (9). We performed a literature search on the Science Citation Index, EMBASE, Cochrane Library, Google Scholar, and PubMed databases until June 2015 using the following keywords: CT-based FFR, FFR CT, noninvasive FFR, noninvasive fractional flow reserve, non-invasive FFR, and non-invasive fractional flow reserve. Studies meeting the following inclusion criteria comprised the final meta-analysis: study design involving diagnostic accuracy assessment, age of all study subjects ≥18 years, subject presentation with suspected or known CAD, CT-FFR as the index test, invasive FFR as the diagnostic reference standard, CT-FFR and invasive FFR in at least 50 patients. Duplicate studies were excluded. The study selection process is diagrammed in Figure 1.

Three prospective multicenter trials were eligible for inclusion in the final meta-analysis: Diagnosis of Ischemia-Causing Stenoses Obtained via Noninvasive Fractional Flow Reserve, Determination of Fractional Flow Reserve by Anatomic Computed Tomographic Angiography, and Analysis of Coronary Blood Flow Using CT Angiography, Next Steps. Overall, 17 centers in 8 countries participated in these multicenter trials. In addition, we included two smaller retrospective

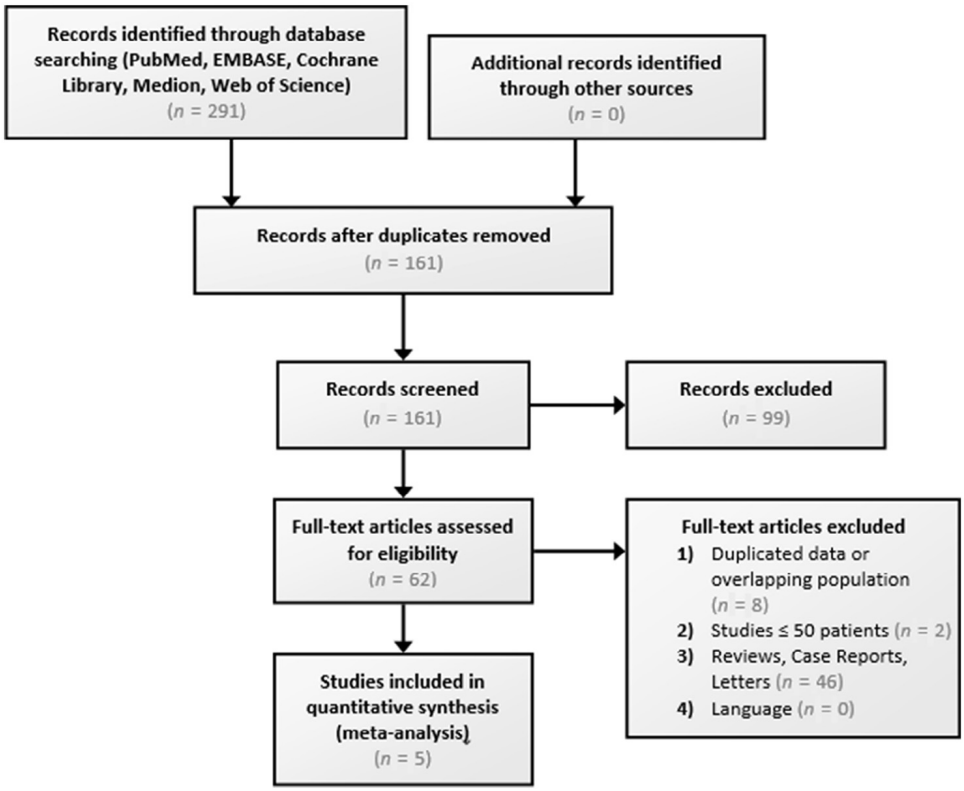

Figure 1. Flow diagram according to the PRISMA statement (9). PRISMA, Preferred Reporting Items for Systematic reviews and Meta-Analyses.

single-center studies by Renker et al. and Coenen et al. that used a novel on-site algorithm with a reduced order model application for rapid calculation (7,8).

Two reviewers with experience in cardiovascular imaging independently performed the data collection from all eligible studies. To calculate inter-reviewer variability, κ-statistics were applied. Of note, Institutional Review Board approval was waived for our study.

Study Population

All patients included in our analysis had known or suspected CAD and underwent cCTA and ICA with FFR measurement. Typical exclusion criteria were previous coronary intervention or bypass surgery, suspected acute coronary syndrome, and nondiagnostic cCTA image quality. Noteworthy differences among the included studies were exclusion of patients with significant arrhythmia, complex bifurcation stenosis, contraindications to beta-blocker, nitroglycerin, or adenosine administration, and body mass index >35 kg/m^2.

cCTA Protocol and Assessment

All included studies used a variety of different CT systems; however, a prerequisite for inclusion was the use of a 64- or higher detector CT system. The exact cCTA protocol was to the discretion of the center but adhered to the guidelines of the Society of Cardiovascular Computed Tomography for the performance of cCTA (10). Hemodynamically relevant coronary stenosis was defined as ≥50% luminal narrowing by visual estimation. Vessels with 30%–70% stenosis at cCTA by visual estimation were classified as intermediate (30%–70%), whereas in one study intermediate stenosis was defined as a quantitative maximal diameter stenosis from 40% to 69% at coronary angiography (11).

ICA with FFR Measurement

ICA with FFR measurement was performed according to the standard clinical protocol of each center, but all were conforming to societal guidelines (12). The position of the pressure wire during FFR measurement was recorded to enable CT-FFR calculation from the same position.

CT-FFR Computation

Three prospective multicenter studies used CT-FFR calculation in core laboratories using supercomputational power (HeartFlow, Inc., Redwood City, CA), as previously described (4–6). Two recent studies used a novel reduced order model for CT-FFR computation with a prototype software (Siemens Healthcare, Forchheim, Germany) designed for on-site CT-FFR assessment (7,8). In all studies, a three-dimensional blood flow and pressure simulation of the coronary artery tree was performed. Coronary blood flow was simulated for conditions of adenosine-induced hyperemia. CT-FFR was calculated at the same location as invasive FFR measurement and CT-FFR values ≤0.80 were considered to indicate lesion-specific ischemia.

Statistical Analyses

We pooled the diagnostic data of cCTA and CT-FFR from the five studies and compared them by forest plots. The diagnostic performance between cCTA and CT-FFR was analyzed by sensitivity, specificity, positive and negative predictive values, accuracy, and areas under the curve. The accuracy data were pooled and compared using summary area under the receiver operating characteristic curve (sROC) plots. For pooled values, the arithmetic means and 95% confidence interval (CI) of the five studies were weighted by patient numbers of the single studies. This resulted in the weighted arithmetic mean with 95% CI as pooled data of the five studies together. Absolute variables are reported as frequencies and percentages. Continuous variables are presented as means ± SD or 95% CI. Results were considered statistically significant at $P < .05$ (two-tailed). The calculations were performed with IBM SPSS 22 statistical software (IBM SPSS Statistics for Windows, Armonk, NY), InStat 3.00 (GraphPad Software Inc., San Diego, CA), SAS software, release 9.3 (SAS Institute Inc., Cary, NC) or RevMan 5.3 (The Cochrane Collaboration, Oxford, UK).

RESULTS

Patient Characteristics

In total, this meta-analysis included 765 patients who underwent ICA with FFR measurement and cCTA with CT-FFR. Average patient age was similar across all studies and ranged from 61.2 ± 12 to 64 ± 10 years. The exclusion rate varied from 11.6% to 30.4% and was mainly attributable to nonevaluable cCTA scans, for example, due to image artifacts. Among the 1306 vessels studied, 386 (29.6%) were considered ischemic with FFR ≤0.80. Baseline characteristics of the study cohorts are listed in Table 1, and vessel characteristics at cCTA and ICA are provided for each study in Table 2.

Diagnostic Accuracy of CT-FFR and cCTA for Diagnosing Ischemia

For detection of hemodynamic relevance on a per-vessel basis with an invasive FFR reference standard, pooled sensitivity, specificity, positive predictive value, and negative predictive value were 83.7% (95% CI: 78.1–89.3), 74.7% (95% CI: 52.2–97.1), 64.8% (95% CI: 52.1–77.5), and 90.1% (95% CI: 80.8–99.3) for CT-FFR, respectively, and were 84.6% (95% CI: 78.1–91.1), 49.7% (95% CI: 31.1–68.4), 39.0% (95% CI: 28.0–50.1), and 87.3% (95% CI: 72.5–100.0) for cCTA alone, respectively (Fig 2 and Table 3). On a per-patient basis, sensitivity, specificity, positive predictive value, and negative

TABLE 1. Study Design and Baseline Characteristics Presented as Mean ± Standard Deviation or Frequency (%)

	Koo et al. (DISCOVER-FLOW)	Min et al. (DeFACTO)	Nørgaard et al. (NXT Trial)	Renker et al.	Coenen et al.
Journal	J Am Coll Cardiol	JAMA	J Am Coll Cardiol	Am J Cardiol	Radiology
Year	2011	2012	2014	2014	2014
Study design	Multicenter, (4 centers in 3 countries), prospective	Multicenter (17 centers in 5 countries), prospective	Multicenter (10 centers in 8 countries), prospective	Single-center, retrospective	Single-center, retrospective
CT system	64- or 256-detector CT	64- or higher detector CT	64- or higher detector CT	64- or 128-section dual-source CT	64- or 128-section dual-source CT
CT-FFR software (manufacturer)	FFR_{CT} (HeartFlow, Inc., Redwood City, CA), V1.2	FFR_{CT} (HeartFlow, Inc., Redwood City, CA), V1.2	FFR_{CT} (HeartFlow, Inc., Redwood City, CA), V1.4	cFFR (Siemens Healthcare, Forchheim, Germany), $V1.4^{+}$	cFFR (Siemens Healthcare, Forchheim, Germany), $V1.4^{+}$
Number of included patients	103	252	251	53	106
Number of excluded patients	NA	33/285 (11.6%)	111/365 (30.4%)	19/64 (29.7%)	16/122 (13.1%)
Number of vessels	159	407	484	67	189
Age (years)	62.7 ± 8.5	62.9 ± 8.7	64 ± 10	61.2 ± 12.0	61.4 ± 9.2
Male (%)	74 (72%)	178 (70.6%)	162 (64%)	34 (64%)	82 (77%)
BMI (kg/m^2)	25.8 ± 3.5	NA	26 ± 3	28.9 ± 6.5	27.2 ± 4.0
Diabetes mellitus (%)	26 (26%)	53 (21.2%)	58 (23%)	18 (32%)	20 (19%)
Hypertension (%)	67 (65%)	179 (71.2%)	174 (69%)	31 (54%)	63 (59%)
Hyperlipidemia (%)	67 (65%)	201 (79.8%)	200 (79%)	21 (54%)	63 (59%)
Current smoker (%)	24 (36%)	44 (17.5%)	46 (18%)	8 (14%)	26 (25%)

BMI, body mass index; CT, computed tomography; CT-FFR, fractional flow reserve from coronary computed tomographic angiography; DeFACTO, Determination of Fractional Flow Reserve by Anatomic Computed Tomographic Angiography; DISCOVER-FLOW, Diagnosis of Ischemia-Causing Stenoses Obtained via Noninvasive Fractional Flow Reserve; FFR, fractional flow reserve; NA, not available; NXT, Analysis of Coronary Blood Flow Using CT Angiography, Next Steps.

TABLE 2. Vessel Characteristics According to cCTA, ICA, FFR, and CT-FFR

	Koo et al. (DISCOVER-FLOW)	Min et al. (DeFACTO)	Nørgaard et al. (NXT Trial)	Renker et al.	Coenen et al.
Invasive coronary angiography (ICA)					
ICA stenosis ≥50% (%)	NA	190 (46.5%)	81 (32%)	44 (66%)	87 (46.0%)
FFR ≤0.80 (%)	35 (23%)	151 (37.1%)	100 (21%)	20 (30%)	80 (42.3%)
Coronary computed tomography angiography (cCTA)					
Agatston score (±SD)	NA	381.5 ± 401.0	302 ± 468	778.4 ± 731.1	555 ± 542
cCTA stenosis ≥50% (%)	NA	216 (53.2%)	220 (87%)	55 (82%)	133 (70.4%)
CT-FFR ≤0.80 (%)	NA	216 (53.3%)	135 (28%)	24 (36%)	108 (57.1%)

CT-FFR, fractional flow reserve from coronary computed tomographic angiography; DeFACTO, Determination of Fractional Flow Reserve by Anatomic Computed Tomographic Angiography; DISCOVER-FLOW, Diagnosis of Ischemia-Causing Stenoses Obtained via Noninvasive Fractional Flow Reserve; FFR, fractional flow reserve; NA, not available; NXT, Analysis of Coronary Blood Flow Using CT Angiography, Next Steps; SD, standard deviation.

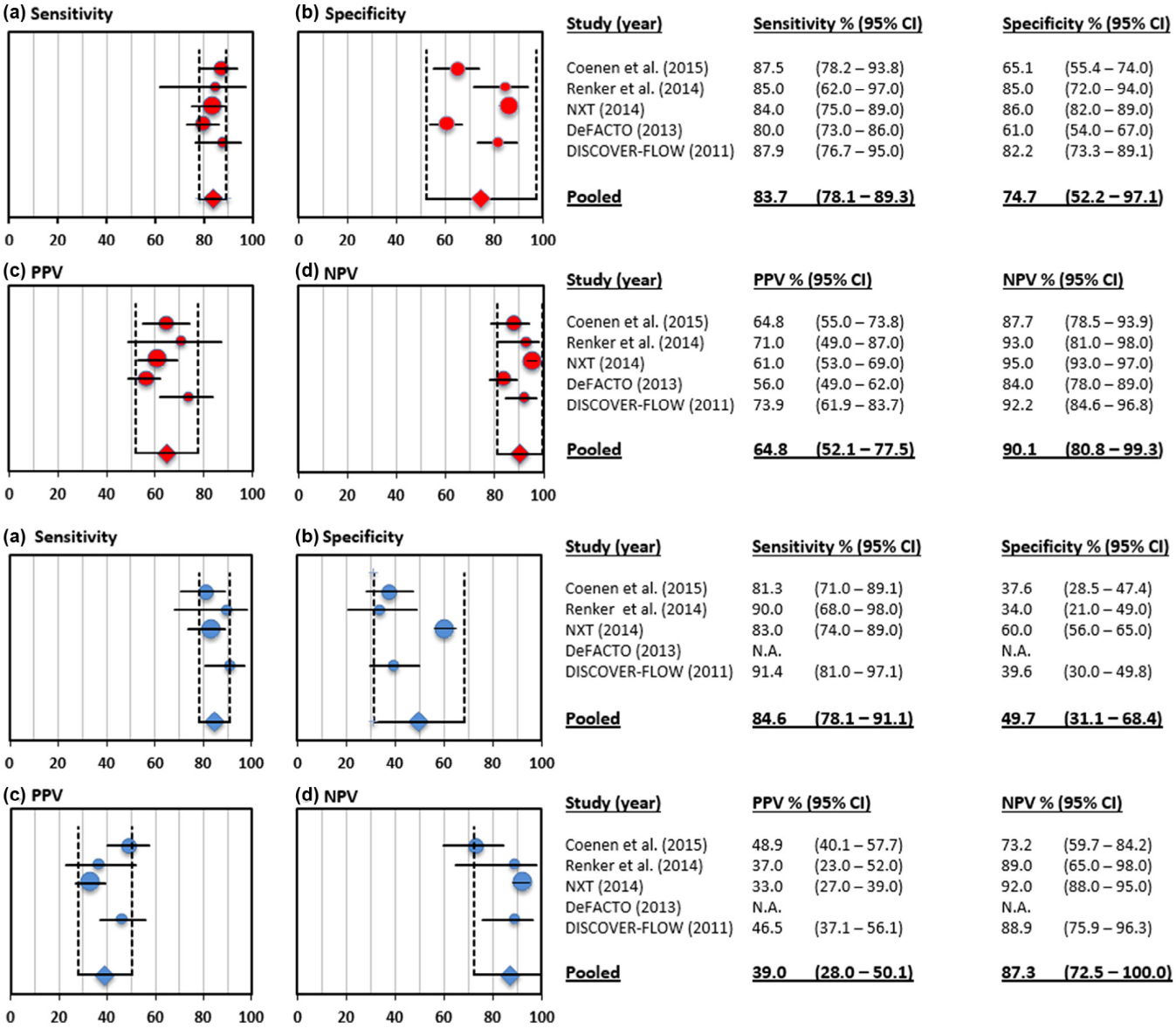

Figure 2. Forest plots of the sensitivity, specificity, PPV, NPV, and pooled diagnostic accuracy of CT-FFR (*red dots*) and cCTA (*blue dots*) for detection of hemodynamically significant coronary stenosis on a per-vessel basis compared to invasive FFR as a reference standard. cCTA, coronary computed tomographic angiography; CT-FFR, fractional flow reserve from coronary computed tomographic angiography; FFR, fractional flow reserve; NPV, negative predictive value; PPV, positive predictive value. (Color version of figure is available online.)

TABLE 3. Diagnostic Accuracy of CT-FFR and cCTA Compared to Invasive FFR as the Reference Standard on a Per-Vessel Level

	Koo et al. (DISCOVER-FLOW)	Min et al. (DeFACTO)	Nørgaard et al. (NXT Trial)	Renker et al.	Coenen et al.	Pooled
Per-vessel (n = 1306) diagnostic performance of CT-FFR <0.80 (95% CI) and cCTA ≥50% (95% CI) [in brackets]						
Number of vessels	159	407	484	67	189	1306
Sensitivity (%)	87.9 (76.7–95.0) [91.4 (81.0–97.1)]	80 (73–86) [NA]	84 (75–89) [83 (74–89)]	85 (62–97) [90 (68–98)]	87.5 (78.2–93.8) [81.3 (71.0–89.1)]	83.7 (78.1–89.3) [84.6 (78.1–91.1)]
Specificity (%)	82.2 (73.3–89.1) [39.6 (30.0–49.8)]	61 (54–67) [NA]	86 (82–89) [60 (56–65)]	85 (72–94) [34 (21–49)]	65.1 (55.4–74.0] [37.6 (28.5–47.4)]	74.7 (52.2–97.1) [49.7 (31.1–68.4)]
PPV (%)	73.9 (61.9–83.7) [46.5 (37.1–56.1)]	56 (49–62) [NA]	61 (53–69) [33 (27–39)]	71 (49–87) [37 (23–52)]	64.8 (55.0–73.8)] [48.9 (40.1–57.7)]	64.8 (52.1–77.5) [39.0 (28.0–50.1)]
NPV (%)	92.2 (84.6–96.8] [88.9 (75.9–96.3)]	84 (78–89) [NA]	95 (93–97) [92 (88–95)]	93 (81–98) [89 (65–98)]	87.7 (78.5–93.9) [73.2 (59.7–84.2)]	90.1 (80.8–99.3) [87.3 (72.5–100.0)]
Accuracy (%)	84.3 (77.7–90.0) [58.5 (50.4–66.2)]	NA [NA]	86 (83–89) [65 (61–69)]	NA [NA]	74.6 (68.4–80.8) [56.1 (49.0–63.2)]	83.1 (74.0–92.2) [61.7 (56.6–66.9)]
AUC	0.90 (NA) [0.75 (NA)] (P = .001)	NA [NA]	0.93 (0.91–0.95) [0.79 (0.74–0.84)] (P < .001)	0.92 (NA) [0.72(NA)] (P < .005)	0.83 (NA) [0.64 (NA)] (P < .001)	0.90 (0.82–0.98) [0.74 (0.63–0.86)] (P = .0047)
Correlation between CT-FFR and FFR						
Per-vessel correlation	Pearson's correlation coefficient = 0.678 (p < 0.0001)	Pearson correlation coefficient = 0.63 (P = NA)	Pearson correlation coefficient = 0.82 (P < .001)	NA	Pearson correlation coefficient = 0.59 (P = NA)	NA
	Spearman's rank correlation coefficient = 0.717 (p < 0.0001)	NA	NA	Spearman rank correlation coefficient = 0.66 (P < .001)	NA	NA

AUC, area under the receiver operating characteristic curve; cCTA, coronary computed tomographic angiography; CI, confidence interval; CT-FFR, fractional flow reserve from coronary computed tomographic angiography; DeFACTO, Determination of Fractional Flow Reserve by Anatomic Computed Tomographic Angiography; DISCOVER-FLOW, Diagnosis of Ischemia-Causing Stenoses Obtained via Noninvasive Fractional Flow Reserve; FFR, fractional flow reserve; NA, not available; NPV, negative predictive value; NXT, Analysis of Coronary Blood Flow Using CT Angiography, Next Steps; PPV, positive predictive value.

TABLE 4. Diagnostic Accuracy of CT-FFR and cCTA Compared to Invasive FFR as the Reference Standard on a Per-Patient Level

Per-Patient (n = 765) Diagnostic Performance of CT-FFR <0.80 (95% CI) and cCTA ≥50% (95% CI) [in brackets]						
Number of included patients	103	252	251	53	106	765
Sensitivity (%)	92.6 (82.1–97.9) [94.4 (84.6–98.8)]	90 (83–95) [84 (77–90)]	86 (77–92) [94 (86–97)]	94 (70–99) [94 (70–99)]	NA [NA]	89.2 (83.7–94.7) [90.2 (80.6–99.9)]
Specificity (%)	81.6 (68.0–91.2) [24.5 (13.3–38.9)]	54 (45–63) [42 (34–51)]	79 (72–84] [34 (27–41)]	84 (68–94) [32 (18–50)]	NA [NA]	70.2 (45.0–95.5) [(35.4 (23.5–47.3)]
PPV (%)	84.7 (73.0–92.8) [58.0 (47.0–68.4)]	67 (60–74) [61 (53–67)]	65 (56–74) [40 (33–47)]	71 (48–89) [38 (23–54)]	NA [NA]	69.3 (56.0–82.7) [50.7 (30.6–70.8)]
NPV (%)	90.9 (78.3–97.5) [80.0 (51.9–95.7)]	84 (0.74–0.91) [72 (61–81)]	93 (87–96] [92 (83–97)]	97 (84–99) [92 (64–99)]	NA [NA]	89.6 (80.6–98.5) [82.5 (64.4–100.0)]
Accuracy (%)	87.4 (79.4–93.1) [61.2 (51.1–70.6)]	NA [NA]	81 (76–85) [53 (47–57)]	NA [NA]	NA [NA]	82.9 (77.2–88.6) [55.4 (48.1–62.7)]
AUC	0.92 (NA) [0.70 (NA)] (P = .0001)	0.81 (0.75–0.86) [0.68 (0.62–0.74)] (P < .001)	0.90 (0.87–0.94) [0.81 (0.76–0.87)] (P = .0008)	0.91 [0.78 (NA)] (P = .078)	NA [NA]	0.87 (0.77–0.96) [0.74 (0.62–0.85)] (P = .0121)

AUC, area under the receiver operating characteristic curve; cCTA, coronary computed tomographic angiography; CI, confidence interval; CT-FFR, fractional flow reserve from coronary computed tomographic angiography; FFR, fractional flow reserve; NA, not available; NPV, negative predictive value; PPV, positive predictive value.

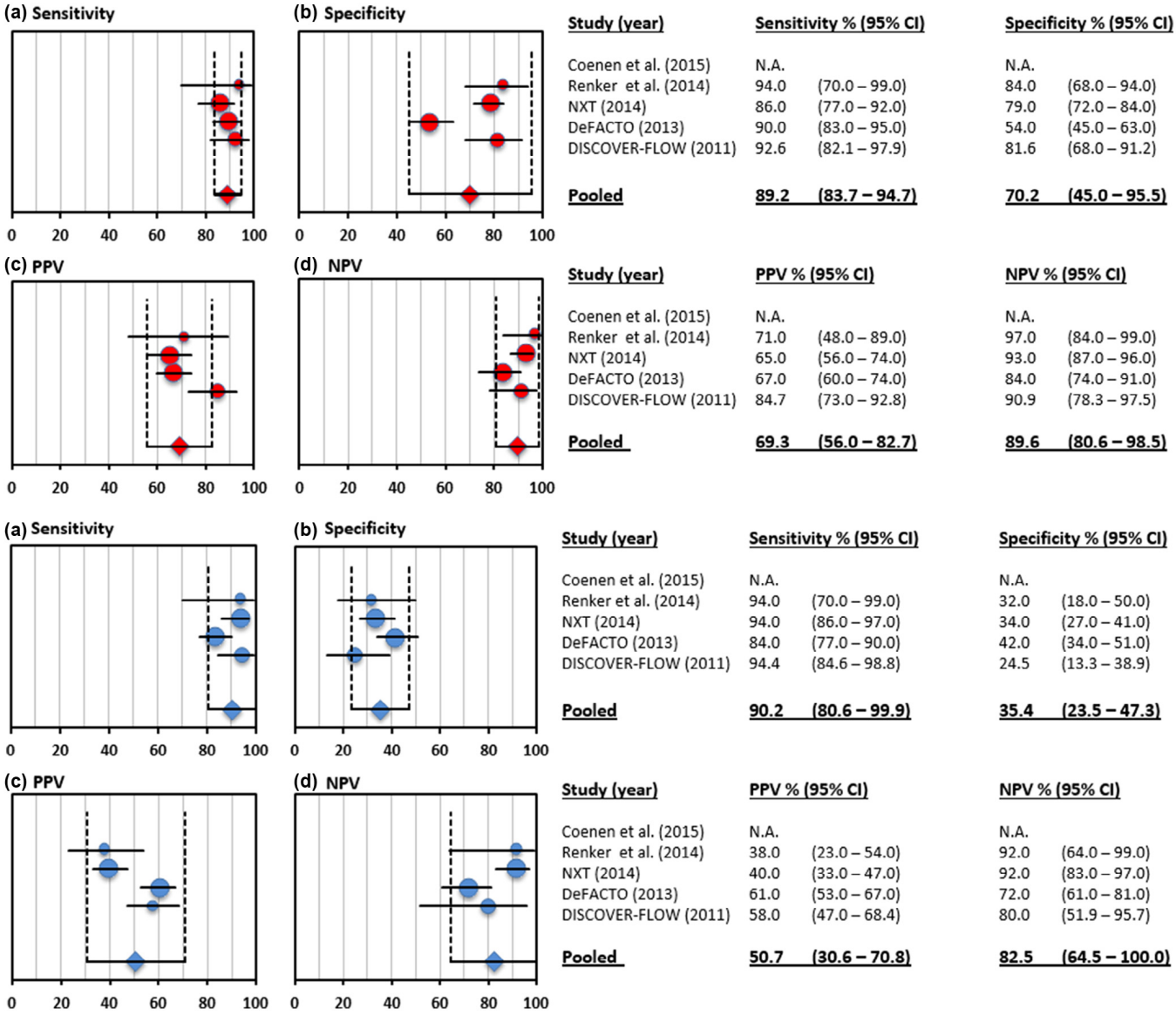

Figure 3. Forest plots of the sensitivity, specificity, PPV, NPV, and pooled diagnostic accuracy of CT-FFR (*red dots*) and cCTA (*blue dots*) for detection of hemodynamically significant coronary stenosis on a per-patient basis compared to invasive FFR as a reference standard. cCTA, coronary computed tomographic angiography; CT-FFR, fractional flow reserve from coronary computed tomographic angiography; FFR, fractional flow reserve; NPV, negative predictive value; PPV, positive predictive value. (Color version of figure is available online.)

predictive value were 89.2% (95% CI: 83.7–94.7), 70.2% (95% CI: 45.0–95.5), 69.3% (95% CI: 56.0–82.7), and 89.6% (95% CI: 80.6–98.5) for CT-FFR, respectively, and were 90.2% (95% CI: 80.6–99.9), 35.4% (95% CI: 23.5–47.3), 50.7% (95% CI: 30.6–70.8), and 82.5% (95% CI: 64.4–100.0) for cCTA alone, respectively (Fig 3 and Table 4). The sROC of CT-FFR was superior to cCTA alone on a per-vessel (0.90 [95% CI: 0.82–0.98] vs 0.74 [95% CI: 0.63–0.86], respectively; $P = .0047$) and per-patient level (0.87 [95% CI: 0.77–0.96] vs 0.74 [95% CI: 0.62–0.85], respectively; $P = .0121$] (Fig 4a and b). Inter-reviewer variability assessment resulted in $\kappa = 0.851$ and $\kappa = 0.775$ on a per-vessel and per-patient level, respectively, indicating substantial agreement.

Intermediate Stenosis

Of the 1306 vessels included in the meta-analysis, 634 vessels (48.5%) had lesions with intermediate luminal stenosis. For detection of lesion-specific ischemia for intermediate stenoses, the sensitivity, specificity, positive predictive value, and negative predictive value of CT-FFR were 81.4% (95% CI: 70.4–92.9), 71.7% (95% CI: 54.5–89.0), 59.4% (95% CI: 35.5–83.4), and 89.9% (95% CI: 85.0–94.7), respectively, compared to invasive FFR (Fig 5 and Table 5). As shown in Figure 4c, sROC of CT-FFR was significantly greater than that of cCTA alone also for intermediate stenoses (0.76 [95% CI: 0.65–0.88] vs 0.57 [95% CI: 0.49–0.66], respectively; $P = .0027$).

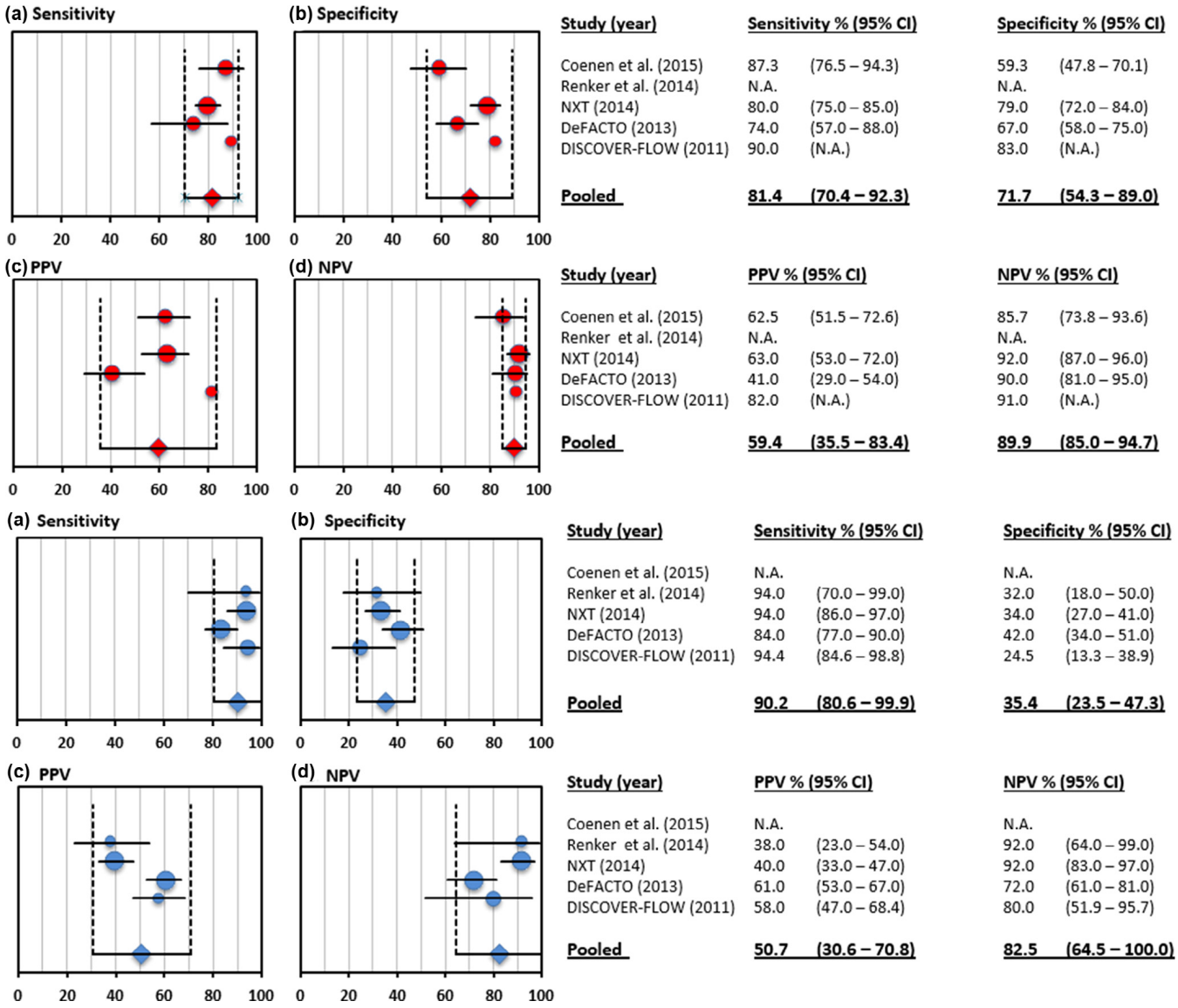

Figure 4. Summary receiver operating characteristic curves (sROC) of CT-FFR (*black line*) and cCTA (*orange line*) on a per-lesion **(a)**, per-patient **(b)**, and per-intermediate-lesion **(c)** bases for detecting ischemic lesions using FFR ≤0.80 as the reference standard. cCTA, coronary computed tomographic angiography; CT-FFR, fractional flow reserve from coronary computed tomographic angiography; FFR, fractional flow reserve. (Color version of figure is available online.)

Correlation of CT-FFR with FFR

On a per-vessel basis, there was a moderate to good correlation between CT-FFR and invasive FFR in all studies, with Pearson correlation coefficients ranging from 0.63 to 0.82 (4–6,8), and Spearman rank correlation coefficients ranging from 0.66 to 0.72 (4,7), mostly indicating a slight underestimation of hemodynamically relevant stenosis by CT-FFR (Table 3).

DISCUSSION

cCTA is a well-established noninvasive imaging technique for the exclusion of obstructive CAD in patients with a low to intermediate cardiovascular risk profile. However, this approach is based on the visual assessment of coronary anatomy to detect stenosis and is less conclusive in addressing the hemodynamic significance of lesions. This limitation is particularly true for the functional assessment of intermediate grade stenosis. Several different approaches have been developed for the noninvasive functional analysis of coronary artery lesions. CT myocardial perfusion imaging merges the anatomic information of cCTA with functional analysis, and this approach has been made increasingly feasible with recent technological advancements (13). Although results are promising, this technique comes at the price of additional radiation exposure and contrast media along with the need for pharmacologic stress agents (14).

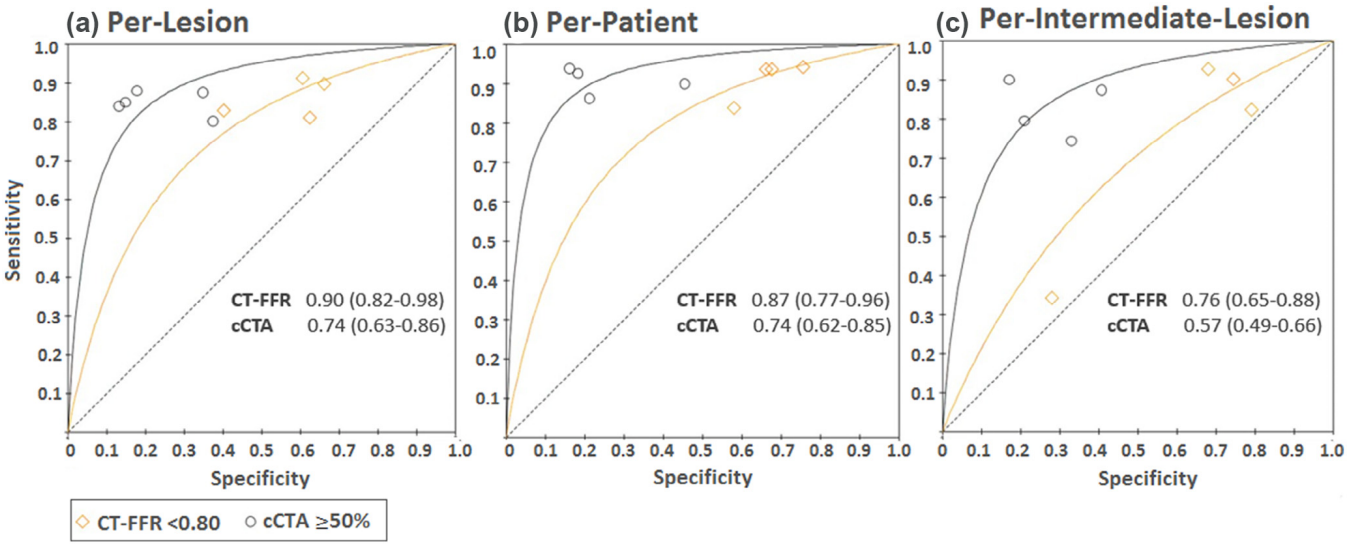

Figure 5. Forest plots of the sensitivity, specificity, PPV, NPV, and pooled diagnostic accuracy of CT-FFR (*red dots*) and cCTA (*blue dots*) for detection of hemodynamically significant coronary stenosis in vessels with intermediate luminal stenosis (30–70%). cCTA, coronary computed tomographic angiography; CT-FFR, fractional flow reserve from coronary computed tomographic angiography; NPV, negative predictive value; PPV, positive predictive value. (Color version of figure is available online.)

TABLE 5. Per-Vessel Diagnostic Performance of CT-FFR in Patients with Intermediate Luminal Stenosis (30%–70%) According to cCTA (*n* = 634)

	Koo et al. (DISCOVER-FLOW)	Min et al. (DeFACTO)	Nørgaard et al. (NXT Trial)	Renker et al.	Coenen et al.	Pooled
Substudy	Min et al. Am J Cardiol 2012	Nakazato Circ Imaging 2013				
Number of vessels with intermediate stenosis (30%–70%)	66/159* (11) (41.5%)	150/407 (15) (36.9%)	235/484 (48.6%)	39/67 (58.2%)	144/189 (76.2%)	634/1306 (48.5%)
Sensitivity (%)	90 (28–31) [90 (28–31)]	74 (57–88) [34 (19–52)]	80 (75–85) [93 (85–97)]	NA	87.3 (76.5–94.3) [82.5 (70.9–90.9)]	81.4 (70.4–92.3) [75.3 (27.6–100.0)]
Specificity (%)	83 (29–35) [26 (9–35)]	67 (58–75) [72 (63–80)]	79 (72–84) [32 (26–40)]	NA	59.3 (47.8–70.1) [21.0 (12.7–31.5)]	71.7 (54.3–89.0) [38.8 (25.6–77.5)]
PPV (%)	82 (28–34) [52 (28–54)]	41 (29–54) [27 (15–43)]	63 (53–72) [37 (31–44)]	NA	62.5 (51.5–72.6) [44.8 (35.6–54.3)]	59.4 (35.5–83.4) [38.0 (22.4–53.7)]
NPV (%)	91 (29–32) [75 (9–12)]	90 (81–95) [78 (69–86)]	92 (87–96) [91 (81–96)]	NA	85.7 (73.8–93.6) [60.7 [40.6–78.5]]	89.9 (85.0–94.7) [78.6 (55.4–100.0)]
Accuracy (%)	86 (57–66) [56 (43–68)]	69 (61–76) [63 (55–71)]	80 (75–85) [51 (44–57)]	NA	71.5 (64.2–78.9) [47.9 (39.8–56.1)]	75.9 (62.5–89.2) [55.1 (43.9–66.4)]
AUC	0.86 (0.78–0.95) [0.58 (0.49–0.67)] (*P* < .0001)	0.71 (0.62–0.79) [0.53 (0.44–0.62)] (*P* = .0063)	0.79 (0.74–0.85) [0.63 (0.58–0.67)] (*P* < .0001)	NA NA	0.73 (0.66–0.80) [0.52 (0.45–0.58)] (*P* < .0001)	0.76 (0.65–0.88) [0.57 (0.49–0.66)] (*P* = .0027)

AUC, area under the receiver operating characteristic curve; cCTA, coronary computed tomographic angiography; CT-FFR, fractional flow reserve from coronary computed tomographic angiography; DeFACTO, Determination of Fractional Flow Reserve by Anatomic Computed Tomographic Angiography; DISCOVER-FLOW, Diagnosis of Ischemia-Causing Stenoses Obtained via Noninvasive Fractional Flow Reserve; NA, not available; NPV, negative predictive value; NXT, Analysis of Coronary Blood Flow Using CT Angiography, Next Steps; PPV, positive predictive value.

* Intermediate stenosis was defined as quantitative coronary angiography confirmed maximal diameter stenosis 40%–69%.

CT-based FFR measurement is a recently introduced noninvasive technique with the potential to improve the diagnostic accuracy of cCTA for the detection of hemodynamically relevant stenosis. CT-FFR builds on recent advances in computational fluid dynamics that respect physical concepts, such as mass-flow correlation. Myocardial mass is approximated from three-dimensional imaging data and the CT-FFR algorithm then uses this and other information to simulate coronary flow under different boundary conditions, model pressure variations along the vessel course, and correct for stenosis overestimation. Thus, CT-FFR adds functional aspects to stenosis assessment and reduces false-positive test results, which leads to improved specificity. As an alternative to invasive FFR measurement, it may become particularly relevant for the difficult evaluation of intermediate stenosis to guide the indication for revascularization.

Because CT-FFR is derived from routine cCTA imaging data, significant artifacts including patient motion, low contrast enhancement, or blooming artifacts from coronary calcification may impair its diagnostic performance. The need with some algorithms for cCTA datasets to be transferred to an external core laboratory for analysis limits their practicality for clinical application. However, reduced order models have been developed to allow on-site application in a clinically relevant time frame.

Our study has several limitations that should be addressed. To date, only five published studies comparing CT-FFR to invasive FFR for the detection of lesion-specific ischemia matched our inclusion criteria; thus, our study is limited by a relatively small number of patients. Second, the included studies used two different approaches for assessing CT-FFR, and further differences in study design including patient inclusion and exclusion criteria may affect homogeneity.

The results of this meta-analysis suggest that noninvasive CT-FFR offers improved specificity without noticeably altering the sensitivity of cCTA in detecting hemodynamically relevant lesions in patients with suspected or known coronary artery disease over anatomic interpretation by cCTA alone. The increased diagnostic accuracy remained when only intermediate stenoses were analyzed as a pooled subgroup. Further results of current prospective trials (Prospective Longitudinal Trial of CT-FFR: Outcome and Resource Impacts, PLATFORM; NCT01943903) with integration into clinical practice and evaluation of resource use are expected to confirm the promising results of CT-FFR and may solidify the role of cCTA as a gatekeeper for invasive downstream testing.

REFERENCES

1. De Cecco CN, Meinel FG, Chiaramida SA, et al. Coronary artery computed tomography scanning. Circulation 2014; 129:1341–1345.
2. Moscariello A, Vliegenthart R, Schoepf UJ, et al. Coronary CT angiography versus conventional cardiac angiography for therapeutic decision making in patients with high likelihood of coronary artery disease. Radiology 2012; 265:385–392.
3. De Bruyne B, Fearon WF, Pijls NH, et al. Fractional flow reserve-guided PCI for stable coronary artery disease. N Engl J Med 2014; 371:1208–1217.
4. Koo BK, Erglis A, Doh JH, et al. Diagnosis of ischemia-causing coronary stenoses by noninvasive fractional flow reserve computed from coronary computed tomographic angiograms. Results from the prospective multicenter DISCOVER-FLOW (Diagnosis of Ischemia-Causing Stenoses Obtained Via Noninvasive Fractional Flow Reserve) study. J Am Coll Cardiol 2011; 58:1989–1997.
5. Min JK, Leipsic J, Pencina MJ, et al. Diagnostic accuracy of fractional flow reserve from anatomic CT angiography. JAMA 2012; 308:1237–1245.
6. Norgaard BL, Leipsic J, Gaur S, et al. Diagnostic performance of noninvasive fractional flow reserve derived from coronary computed tomography angiography in suspected coronary artery disease: the NXT trial (Analysis of Coronary Blood Flow Using CT Angiography: Next Steps). J Am Coll Cardiol 2014; 63:1145–1155.
7. Renker M, Schoepf UJ, Wang R, et al. Comparison of diagnostic value of a novel noninvasive coronary computed tomography angiography method versus standard coronary angiography for assessing fractional flow reserve. Am J Cardiol 2014; 114:1303–1308.
8. Coenen A, Lubbers MM, Kurata A, et al. Fractional flow reserve computed from noninvasive CT angiography data: diagnostic performance of an on-site clinician-operated computational fluid dynamics algorithm. Radiology 2014; 140992.
9. Moher D, Liberati A, Tetzlaff J, et al. Preferred reporting items for systematic reviews and meta-analyses: the PRISMA statement. BMJ 2009; 339:b2535.
10. Leipsic J, Abbara S, Achenbach S, et al. SCCT guidelines for the interpretation and reporting of coronary CT angiography: a report of the Society of Cardiovascular Computed Tomography Guidelines Committee. J Cardiovasc Comput Tomogr 2014; 8:342–358.
11. Min JK, Koo BK, Erglis A, et al. Usefulness of noninvasive fractional flow reserve computed from coronary computed tomographic angiograms for intermediate stenoses confirmed by quantitative coronary angiography. Am J Cardiol 2012; 110:971–976.
12. Levine GN, Bates ER, Blankenship JC, et al. 2011 ACCF/AHA/SCAI Guideline for Percutaneous Coronary Intervention. A report of the American College of Cardiology Foundation/American Heart Association Task Force on Practice Guidelines and the Society for Cardiovascular Angiography and Interventions. J Am Coll Cardiol 2011; 58:e44–e122.
13. Cury RC, Magalhaes TA, Borges AC, et al. Dipyridamole stress and rest myocardial perfusion by 64-detector row computed tomography in patients with suspected coronary artery disease. Am J Cardiol 2010; 106:310–315.
14. Techasith T, Cury RC. Stress myocardial CT perfusion: an update and future perspective. JACC Cardiovasc Imaging 2011; 4:905–916.
15. Nakazato R, Park HB, Berman DS, et al. Noninvasive fractional flow reserve derived from computed tomography angiography for coronary lesions of intermediate stenosis severity: results from the DeFACTO study. Circ Cardiovasc Imaging 2013; 6:881–889.

Journal of Cardiovascular Computed Tomography 15 (2021) 492–498

Contents lists available at ScienceDirect

Journal of Cardiovascular Computed Tomography

journal homepage: www.JournalofCardiovascularCT.com

Research paper

Influence of coronary stenosis location on diagnostic performance of machine learning-based fractional flow reserve from CT angiography

Matthias Renker [a,b], Stefan Baumann [a,c], Christian W. Hamm [b], Christian Tesche [a,d], Won-Keun Kim [b], Rock H. Savage [a], Adriaan Coenen [e], Koen Nieman [e], Jakob De Geer [f], Anders Persson [f], Mariusz Kruk [g], Cezary Kepka [g], Dong Hyun Yang [h], U. Joseph Schoepf [a,*]

[a] Heart & Vascular Center, Medical University of South Carolina, Charleston, SC, USA
[b] Department of Cardiology, Campus Kerckhoff of Justus-Liebig-University Giessen, Bad Nauheim, Germany
[c] First Department of Medicine-Cardiology, University Medical Centre Mannheim, Mannheim, Germany
[d] Department of Internal Medicine I, St.-Johannes-Hospital, Dortmund, Germany
[e] Department of Radiology, Erasmus University Medical Center, Rotterdam, the Netherlands
[f] Department of Radiology and Department of Medical and Health Sciences, Center for Medical Image Science and Visualization, CMIV, Linköping University, Linköping, Sweden
[g] Coronary Disease and Structural Heart Diseases Department, Invasive Cardiology and Angiology Department, Institute of Cardiology, Warsaw, Poland
[h] Department of Radiology, Asan Medical Center, University of Ulsan College of Medicine, Seoul, South Korea

ARTICLE INFO

Keywords:
Atherosclerosis
Coronary artery disease
Coronary computed tomography angiography
Fractional flow reserve
Machine learning

ABSTRACT

Background: Compared with invasive fractional flow reserve (FFR), coronary CT angiography (cCTA) is limited in detecting hemodynamically relevant lesions. cCTA-based FFR (CT-FFR) is an approach to overcome this insufficiency by use of computational fluid dynamics. Applying recent innovations in computer science, a machine learning (ML) method for CT-FFR derivation was introduced and showed improved diagnostic performance compared to cCTA alone. We sought to investigate the influence of stenosis location in the coronary artery system on the performance of ML-CT-FFR in a large, multicenter cohort.

Methods: Three hundred and thirty patients (75.2% male, median age 63 years) with 502 coronary artery stenoses were included in this substudy of the MACHINE (Machine Learning Based CT Angiography Derived FFR: A Multi-Center Registry) registry. Correlation of ML-CT-FFR with the invasive reference standard FFR was assessed and pooled diagnostic performance of ML-CT-FFR and cCTA was determined separately for the following stenosis locations: RCA, LAD, LCX, proximal, middle, and distal vessel segments.

Results: ML-CT-FFR correlated well with invasive FFR across the different stenosis locations. Per-lesion analysis revealed improved diagnostic accuracy of ML-CT-FFR compared with conventional cCTA for stenoses in the RCA (71.8% [95% confidence interval, 63.0%–79.5%] vs. 54.8% [45.7%–63.8%]), LAD (79.3 [73.9–84.0] vs. 59.6 [53.5–65.6]), LCX (84.1 [76.0–90.3] vs. 63.7 [54.1–72.6]), proximal (81.5 [74.6–87.1] vs. 63.8 [55.9–71.2]), middle (81.2 [75.7–85.9] vs. 59.4 [53.0–65.6]) and distal stenosis location (67.4 [57.0–76.6] vs. 51.6 [41.1–62.0]).

Conclusion: In a multicenter cohort with high disease prevalence, ML-CT-FFR offered improved diagnostic performance over cCTA for detecting hemodynamically relevant stenoses regardless of their location.

1. Introduction

To overcome the limited ability of coronary CT angiography (cCTA) for detecting hemodynamically relevant lesions, recent innovations within the field of computational fluid dynamics were adopted and noninvasive cCTA-based fractional flow reserve (CT-FFR) was developed.

Abbreviations: AUC, area under the receiver operating characteristics curve; cCTA, coronary CT angiography; CI, 95% confidence interval; CT-FFR, fractional flow reserve from coronary CT angiography; FFR, fractional flow reserve; LAD, left anterior descending coronary artery; LCX, left circumflex coronary artery; ML, machine learning; NPV, negative predictive value; PPV, positive predictive value; RCA, right coronary artery.

* Corresponding author. Heart & Vascular Center Medical University of South Carolina Ashley River Tower, 25 Courtenay Drive, Charleston, SC, 29425-2260, USA.
E-mail address: schoepf@musc.edu (U.J. Schoepf).

https://doi.org/10.1016/j.jcct.2021.05.005
Received 17 March 2021; Received in revised form 13 May 2021; Accepted 31 May 2021
Available online 4 June 2021

A mathematically demanding method for CT-FFR calculation using off-site supercomputational power showed improved diagnostic performance compared with traditional cCTA interpretation.[1–3] Via integration of reduced-order models, an alternative CT-FFR approach has been developed for more time-efficient use on in-hospital workstations and likewise showed improved diagnostic results over cCTA.[4,5] As a promising next step towards suitability for clinical decision-making, advancements in knowledge from computer science were applied and an artificial intelligence deep machine learning (ML) method for virtually instantaneous CT-FFR derivation was introduced.[6]

At present, the accuracy of ML-CT-FFR subject to lesion location within the coronary artery tree remains unknown. To address this unresolved question, we sought to investigate the influence of lesion location on the diagnostic capacity of ML-CT-FFR and traditional cCTA as measured by invasive FFR within a large multicenter population.

2. Methods

2.1. Study design and population

This was a post hoc substudy of the global, multicenter registry MACHINE (clinicaltrials.gov identifier: 02805621) with study details, rationale, and overall results as previously described.[7] Briefly, patients with clinically indicated cCTA and invasive coronary angiography with FFR measurement were included at five centers in five countries (the Netherlands, South Korea, Poland, United States, and Sweden). Patients with prior stent implantation in the vessel of interest or coronary bypass surgery, contraindications to beta-blockers, nitrates or adenosine, suspicion of acute coronary syndrome, significant arrhythmia, and body mass index >35 kg/m^2 were excluded. The study protocol was approved by the respective ethics committees and complied with the Declaration of Helsinki.

2.2. Acquisition and analysis of images from cCTA

The participating centers used dual-source CT technology (Somatom Definition or Somatom Definition Flash; Siemens Healthineers, Forchheim, Germany). Sublingual nitrates were used routinely at 4 of the medical centers (in 277 patients). All cCTA scans were post-processed using a medium-smooth reconstruction kernel and a slice thickness of $\leq$0.75 mm with 0.4 mm increments. The cCTA protocol and technique was chosen individually by the respective centers. cCTA interpretation was performed by observers at expert level with hemodynamically relevant coronary artery stenosis being defined as $\geq$70% luminal narrowing according to visual estimation.[8] Subjective image quality was rated on a per-patient basis using a 4-point Likert scale (1: poor; 2: satisfactory; 3: good; 4: excellent).

2.3. Invasive coronary angiography and FFR

Invasive coronary angiography and FFR was performed according to the standard clinical protocol of each center. The assessment of invasive FFR was either clinically indicated or due to research purposes. Hyperemia was induced by intravenous or intracoronary adenosine administration at a rate of 140 μg/kg/min. FFR values $\leq$0.80 were considered to indicate hemodynamic relevance of stenoses and served as the reference standard for lesion-specific ischemia. The position of the pressure wire during the FFR measurement was recorded.

2.4. Analysis of ML-CT-FFR

The most current version of a workstation-based research prototype for CT-FFR computation (cFFR version 1.4, Siemens Healthineers, Forchheim, Germany; currently not commercially available) was initially used for all cCTA datasets by each participating study center of the MACHINE consortium. Applying principles of computational fluid dynamics and integrating knowledge about patient-specific anatomical features derived from the corresponding cCTA datasets, the CT-FFR algorithm realized three-dimensional blood flow and pressure simulations of the coronary artery tree via coupling of reduced- and full-order models, as detailed previously.[9] Beyond CT-FFR, the workstation-based ML-CT-FFR research software application (cFFR version 2.1, Siemens Healthineers, Forchheim, Germany; currently not commercially available) allows for virtually instantaneous specification of FFR from standard cCTA.[6] ML-CT-FFR builds on a supervised learning approach, whereas previous experience with a framework of input and recognition of patterns is used to predict outcomes for new cases.[6] First, relevant patient and lesion-specific parameters were included in a neural network to simulate the interaction of these features. The deep artificial learning approach of this study used a large data pool of synthetic coronary artery trees that trained the software application. ML-CT-FFR was obtained at the same location as invasive FFR measurement and values $\leq$0.80 were considered to indicate lesion-specific ischemia.

2.5. Statistical analyses

Continuous variables are presented as mean $\pm$ standard deviation, or medians with interquartile ranges, according to their distribution. Absolute variables are reported as frequencies and percentages.

The location of all lesions of interest was categorized into either right coronary artery (RCA), left anterior descending coronary artery (LAD), or left circumflex coronary artery (LCX). In the case of a location within a side branch, lesions were assigned to the corresponding segment of the main coronary artery, based on a 15-segment model.[10] All lesions were furthermore categorized into either proximal, middle, or distal location. Specifically, lesions located in segments 3 and 4 of the RCA were defined distal. Lesions in segment 5 (i.e. left main; $n = 2$) were assigned to the proximal LAD. Lesions located in the diagonal branches (segments 9 and 10) were assigned to the LAD depending on the anatomy of the septal branches, and lesions located in segment 12 of the LCX were referred to as proximal, while those in segment 14 were defined middle.

Invasive FFR served as the reference standard for further testing. Pearson's correlation coefficient was calculated to determine the level of agreement of ML-CT-FFR and invasive FFR. Agreement analysis was performed by plotting the difference between ML-CT-FFR and invasive FFR measurements against the average of these parameters. The limits of agreement were calculated to establish a range of values within which 95% of the differences between the values would fall. Beyond accuracy, sensitivity, specificity, positive and negative predictive value, the area under the receiver operating characteristics curve (AUC) of ML-CT-FFR for detecting hemodynamic relevance of stenoses was assessed in comparison with conventional cCTA.[11] Two-sided p-values <0.05 were considered statistically significant.

MedCalc (version 19.4.1, MedCalc Software, Ostend, Belgium) was used for comparing AUCs. All other statistical analyses were performed with SPSS (Version 22.0, IBM Corp., Armonk, NY, USA).

3. Results

3.1. Patient characteristics

All relevant information for this substudy was present in 330 (94%) of in total 351 patients included in the MACHINE registry. Within the substudy cohort, 502 lesions of interest were present.

Within the RCA, LAD, and LCX, hemodynamic relevance was revealed by invasive FFR in 29/124 (23.4%), 138/265 (52.1%), and 39/113 (34.5%) lesions, respectively.

In the proximal, middle, and distal coronary artery segments, hemodynamic relevance was revealed in 75/163 (46.0%), 95/244 (38.9%), and 36/95 (37.9%) lesions, respectively. The segment with the lowest rate of hemodynamic relevance by invasive FFR was the middle segment of the RCA (18.9%). Further demographic and procedural findings are

provided in Table 1.

3.2. Correlation of ML-CT-FFR and invasive FFR

Pearson's correlation coefficients of ML-CT-FFR and invasive FFR showed significant associations: r = 0.49 for the RCA (p <0.001), r = 0.63 for the LAD (p <0.001), r = 0.71 for the LCX (p <0.001), r = 0.70 for the proximal vessel segments (p <0.001), r = 0.61 for the middle vessel segments (p <0.001), and r = 0.53 for the distal vessel segments (p <0.001). Corresponding scatter plots are displayed in Fig. 1.

The Bland-Altman analyses comparing ML-CT-FFR and invasive FFR showed the following mean differences: 0.05 (95% limits of agreement: 0.32 to 0.21) in the RCA, −0.02 (−0.27 to 0.22) in the LAD, −0.03 (−0.26 to 0.20) in the LCX, −0.02 (−0.25 to 0.21) in the proximal vessel segments, −0.03 (−0.27 to 0.21) in the middle vessel segments, and −0.07 (−0.33 to 0.20) in the distal vessel segments (Fig. 2).

3.3. Diagnostic performance of ML-CT-FFR compared with cCTA

In terms of accuracy, specificity, positive and negative predictive value, ML-CT-FFR showed improved performance in comparison with conventional cCTA to detect hemodynamically significant coronary artery stenoses in the RCA, LAD, LCX, proximal, middle, and distal vessel segments. The supporting data is presented in Tables 2 and 3. A patient example is given in Fig. 3.

The AUC analysis showed good discriminatory power of ML-CT-FFR with significant improvement compared with cCTA in the LAD (0.84 [95% confidence interval (CI): 0.79 to 0.88)] vs. 0.65 [CI: 0.59 to 0.71], p <0.001), LCX (0.90 [CI: 0.83 to 0.95)] vs. 0.72 [CI: 0.63 to 0.80], p = 0.001), proximal (0.89 [CI: 0.83 to 0.93)] vs. 0.78 [CI: 0.70 to 0.84], p = 0.003), middle (0.83 [CI: 0.78 to 0.88] vs. 0.66 [CI: 0.60 to 0.72], p <0.001), and distal vessel segments (0.78 [CI: 0.69 to 0.86] vs. 0.62 [CI: 0.52 to 0.72], p = 0.008). Only in the RCA, the discriminatory power of ML-CT-FFR and cCTA was comparable (0.73 [CI: 0.64 to 0.81] vs. 0.74 [CI: 0.65 to 0.81], p = 0.930). These results of the AUC analysis are displayed in Fig. 4. Further comparisons of the AUCs of ML-CT-FFR and cCTA for the proximal, middle, and distal segment of each coronary artery are shown in Supplementary Fig. 1.

Table 1
Clinical baseline characteristics and procedural results from 330 patients with 502 vessels.

Parameter	Result
Demographic data	
Age [y]	63 (56–69)
Female	82 (24.8%)
Body mass index [kg/m^2][a]	26.8 (24.5–29.1)
Heart rate during cCTA [bpm]	63 (57–70)
Cardiovascular risk factors	
Hypertension	216 (65.5%)
Hyperlipidemia	196 (59.4%)
Family history of coronary artery disease	107 (32.4%)
Current smoker	117 (35.5%)
Diabetes mellitus	72 (21.8%)
Coronary CT angiography	
Image quality, 1–4[b]	3 (3–4)
Tube voltage [kV]	100 (100–120)
Tube current [mA]	246 (165–341)
Dose length product [mGy x cm]	529 (360–784)
Left ventricular mass [g]	163 (144–181)
Agatston-Score[c]	238 (39–676)
Agatston-Score 0	28 (8.9%)
Agatston-Score >400	128 (40.7%)
Patients with cCTA stenosis ≥50%	323 (97.9%)
Patients with cCTA stenosis ≥70%	287 (87.0%)
Vessels with cCTA stenosis ≥50%	435 (86.7%)
Vessels with cCTA stenosis ≥70%	364 (72.5%)
Patients with ML-CT-FFR ≤0.80	237 (71.8%)
Vessels with ML-CT-FFR ≤0.80	236 (47.0%)
Invasive coronary angiography	
Patients with invasive FFR ≤0.80	241 (73.0%)
Vessels with invasive FFR ≤0.80	206 (41.0%)

Values are median (interquartile range) or n (%).
[a] Data was not available in 9 patients.
[b] 1, poor; 2, satisfactory; 3; good; 4, excellent.
[c] Data was not available in 16 patients.

3.4. ML-CT-FFR subgroup comparisons

The diagnostic performance of ML-CT-FFR as characterized by the AUC was neither statistically different for the vessel subgroups LAD and RCA (p = 0.066), nor for the LAD and LCX (p = 0.140), nor for the proximal and middle segments (p = 0.132), nor for the middle and distal segments (p = 0.394), nor for the comparison between proximal and distal vessel segments (p = 0.056). Only the AUC comparison between the subgroups RCA and LCX (p = 0.008) reached statistical significance.

4. Discussion

Based on an international multicenter registry of patients that underwent clinically indicated cCTA and invasive FFR interrogation, we examined the diagnostic value of a novel ML-CT-FFR algorithm focusing on the influence of lesion location. Previous reports on automated cCTA risk stratification as well as on knowledge-based detection of coronary artery stenosis severity indicate the importance of lesion location for the correct identification of significant coronary artery disease.[12,13] However, the relevance of lesion location within the coronary artery tree has not been assessed for the performance of ML-CT-FFR before.

Our results show an overall robust diagnostic performance of ML-CT-FFR in identifying hemodynamic relevance of stenoses with incremental value over traditional cCTA. Diagnostic accuracy was improved by ML-CT-FFR in comparison with cCTA, regardless of stenosis location. The favorable effect of ML-CT-FFR was present across all three epicardial coronary vessels and from the proximal to distal vessel segments. The improved diagnostic performance of ML-CT-FFR translated into significantly increased values for all stenosis locations, except for the RCA where ML-CT-FFR and cCTA were comparable.

The RCA is most often affected by CT motion artifacts due to its course and velocity.[14] Therefore, the RCA is commonly considered difficult to image by cCTA. However, our analysis revealed reduced improvement in the diagnostic performance of ML-CT-FFR compared with cCTA in the RCA. Interestingly, this was mainly due to the middle segment of the RCA (Supplementary Fig. 1), where the AUC of ML-CT-FFR showed a diagnostic yield numerically inferior (p = 0.051) to that of cCTA. The reason for this observation may be found in a tendency of ML-CT-FFR to overestimate disease in the RCA more often than in the other coronary arteries. We speculated calcium burden or disease prevalence in the RCA to be attributable and examined these factors. The mean coronary calcium score of the RCA (195) was comparable with that of the LAD (204) and higher than that in the LCX (124). As shown in the result section, the prevalence of hemodynamically relevant stenosis was lowest in the middle segment of the RCA and therefore appears most relevant to the diagnostic performance of cCTA and ML-CT-FFR in the RCA. However, in our vessel subgroup comparisons of the diagnostic performance of ML-CT-FFR alone, a significant difference was found merely among the LCX and RCA.

Not only the RCA, also small vessel diameters of the distal coronary artery segments remain diagnostically challenging for cCTA. Yan et al. reported smaller vessel diameter to be an independent predictor of inaccuracy, based on their results from a prospective, multicenter investigation examining the diagnostic accuracy of cCTA in 291 patients.[15] Furthermore, it is recognized that the invasive or noninvasive FFR-values in the distal segment of any given vessel may include effects unrelated to the stenosis of interest. Distal vessel FFR and CT-FFR were previously shown to include the cumulative loss of pressure and the impact of all disease proximal to the measurement location.[16] Based on this

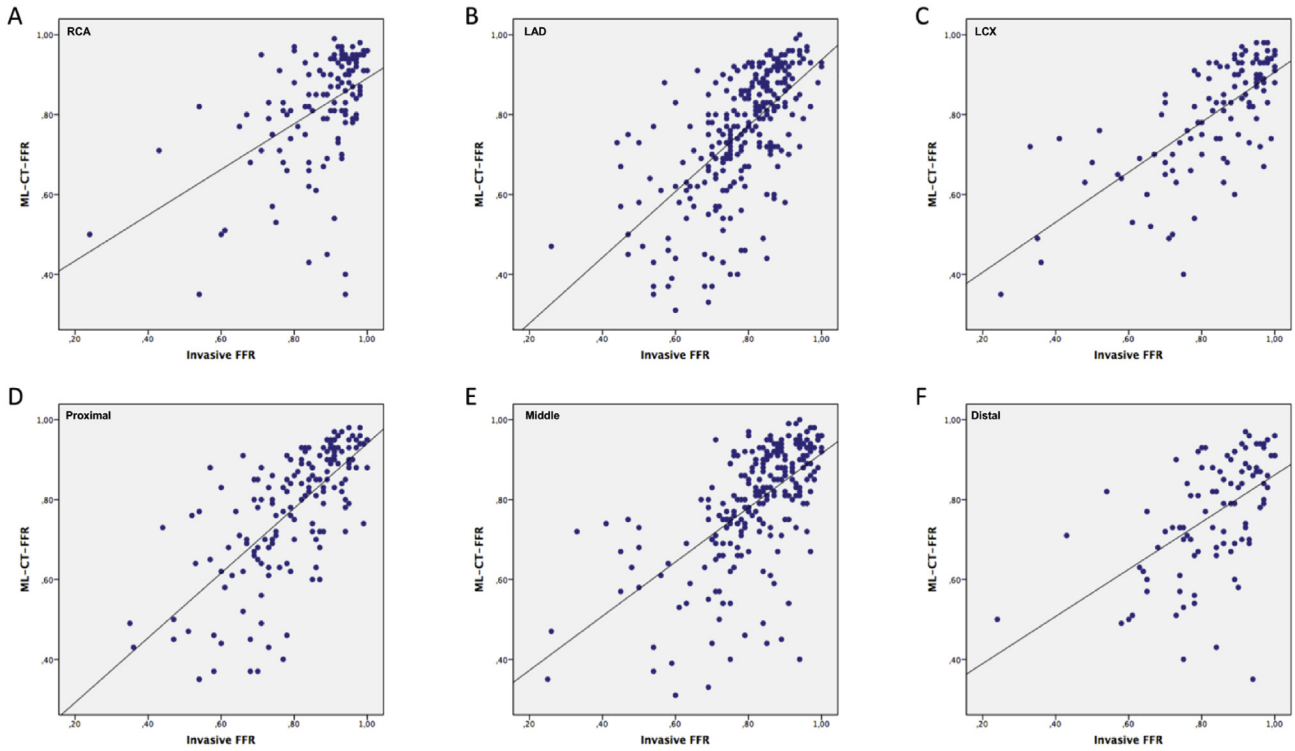

Fig. 1. Scatter plot showing the association of ML-CT-FFR with invasive FFR for the main epicardial vessels RCA (A), LAD (B), LCX (C) as well as for the proximal (D), middle (E), and distal vessel segments (F).

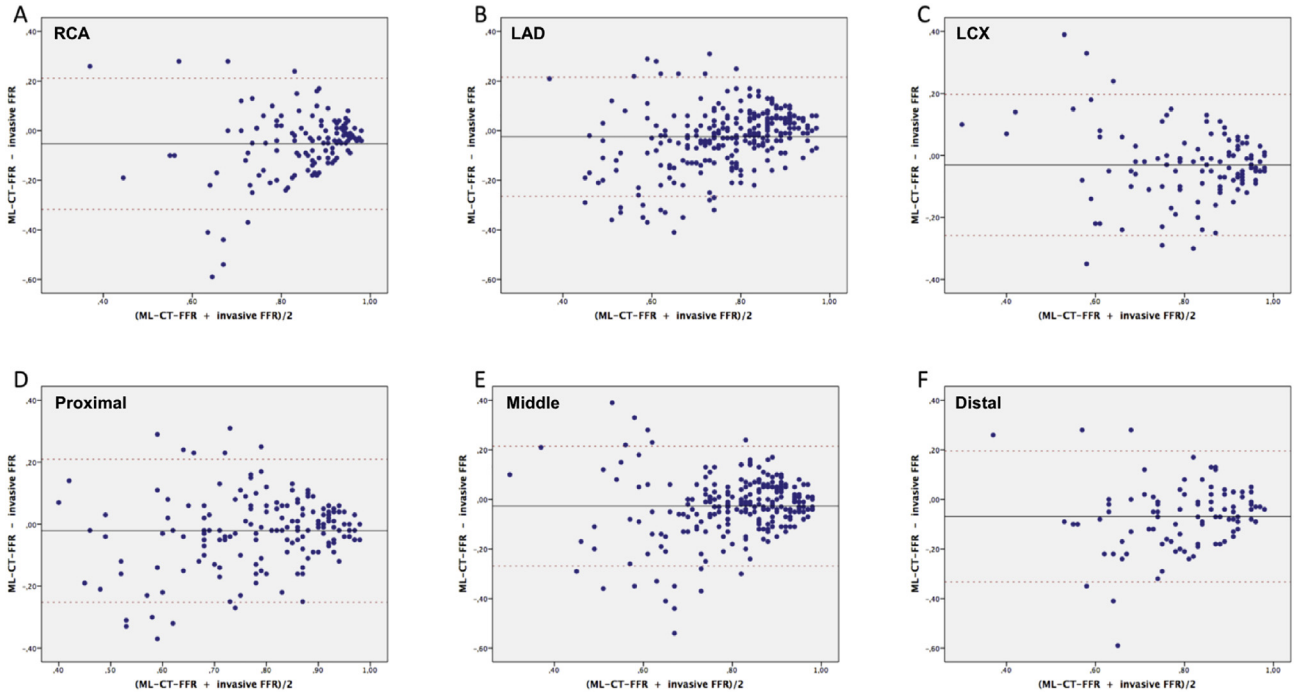

Fig. 2. Bland-Altman plot comparing ML-CT-FFR with invasive FFR for the main epicardial vessels RCA (A), LAD (B), LCX (C) as well as for the proximal (D), middle (E), and distal vessel segments (F).

knowledge, measurements routinely exclude vessel diameters <2 mm. Therefore, the diagnostic performance of ML-CT-FFR may have been unrestricted in the distal vessel segments. In fact, ML-CT-FFR improved accuracy, specificity, positive predictive value, and negative predictive value of cCTA in lesions located distally in the coronary arteries. Furthermore, the subgroup analysis of ML-CT-FFR did not reveal any significant difference when comparing the AUC for detecting hemodynamically relevant disease in the proximal, middle, and distal vessel segments.

To mitigate the limitation of cumulative pressure loss from the proximal to distal coronary segments, affirmation strategies for CT-FFR values have been studied in recent literature. Takagi et al.

Table 2
Per-vessel diagnostic performance of cCTA and ML-CT-FFR for the detection of hemodynamically relevant stenosis in RCA, LAD, and LCX (n = 502).

	RCA			LAD			LCX		
	cCTA (≥50%)	cCTA (≥70%)	ML-CT-FFR	cCTA (≥50%)	cCTA (≥70%)	ML-CT-FFR	cCTA (≥50%)	cCTA (≥70%)	ML-CT-FFR
Accuracy	45.2 (36.2–54.4)	54.8 (45.7–63.8)	71.8 (63.0–79.5)	54.7 (48.5–60.8)	59.6 (53.5–65.6)	79.3 (73.9–84.0)	54.9 (45.2–64.2)	63.7 (54.1–72.6)	84.1 (76.0–90.3)
Sensitivity	96.6 (82.2–99.9)	89.7 (72.7–97.8)	65.5 (45.7–82.1)	97.8 (93.7–99.6)	90.6 (84.4–94.9)	82.6 (75.2–88.5)	97.4 (86.5–99.9)	82.1 (66.5–92.5)	87.2 (72.6–95.7)
Specificity	29.5 (20.6–39.7)	44.2 (34.0–54.8)	73.7 (63.7–82.2)	8.6 (4.4–14.9)	26.0 (18.6–34.5)	75.6 (67.2–82.8)	32.4 (22.0–44.3)	54.1 (42.1–65.7)	82.4 (71.8–90.3)
PPV	29.5 (26.5–32.6)	32.9 (28.3–37.9)	43.2 (33.1–53.8)	53.4 (51.9–54.9)	57.1 (54.2–59.9)	78.6 (72.8–85.4)	43.2 (39.2–47.3)	48.5 (41.4–55.7)	72.3 (61.1–81.3)
NPV	96.6 (79.9–99.5)	93.3 (82.4–97.7)	87.5 (80.7–92.1)	78.6 (51.1–92.8)	71.7 (58.3–82.2)	80.0 (73.3–85.4)	96.0 (77.1–99.4)	85.1 (73.9–92.0)	92.4 (84.2–96.5)

Values are % (CI). Positive test results are defined as stenosis ≥50% or ≥70% on cCTA, and ML-CT-FFR ≤0.80.

Table 3
Per-vessel diagnostic performance of cCTA and ML-CT-FFR for the detection of hemodynamically relevant stenosis in proximal, middle, and distal vessel segments (n = 502).

	Proximal			Middle			Distal		
	cCTA (≥50%)	cCTA (≥70%)	ML-CT-FFR	cCTA (≥50%)	cCTA (≥70%)	ML-CT-FFR	cCTA (≥50%)	cCTA (≥70%)	ML-CT-FFR
Accuracy	58.3 (50.3–65.9)	63.8 (55.9–71.2)	81.5 (74.6–87.1)	50.8 (44.4–57.3)	59.4 (53.0–65.6)	81.2 (75.7–85.9)	46.3 (36.0–56.9)	51.6 (41.1–62.0)	67.4 (57.0–76.6)
Sensitivity	100.0 (95.1–100.0)	93.3 (85.1–97.8)	80.0 (69.2–88.4)	96.8 (91.1–99.3)	86.3 (77.7–92.5)	83.2 (74.1–90.1)	94.4 (81.3–99.3)	86.1 (70.5–95.3)	77.8 (60.9–89.9)
Specificity	23.6 (15.2–33.8)	38.6 (28.4–49.6)	82.8 (73.2–90.0)	21.5 (15.2–28.9)	42.3 (34.2–50.6)	79.9 (72.5–86.0)	17.0 (8.4–29.0)	30.5 (19.2–43.9)	61.0 (47.4–73.5)
PPV	45.4 (37.6–53.4)	56.5 (52.1–60.7)	80.0 (71.4–86.5)	38.9 (32.8–45.4)	48.8 (44.9–52.8)	72.5 (65.4–78.6)	41.0 (37.6–44.4)	43.1 (37.9–48.4)	54.9 (45.8–63.7)
NPV	52.1 (49.2–55.0)	87.2 (73.7–94.3)	82.8 (75.1–88.4)	91.4 (77.1–97.1)	82.9 (73.9–89.3)	88.2 (82.5–92.1)	83.3 (53.7–95.6)	78.3 (59.4–89.9)	81.8 (70.3–89.6)

Values are % (CI). Positive test results are defined as stenosis ≥50% or ≥70% on cCTA, and ML-CT-FFR ≤0.80.

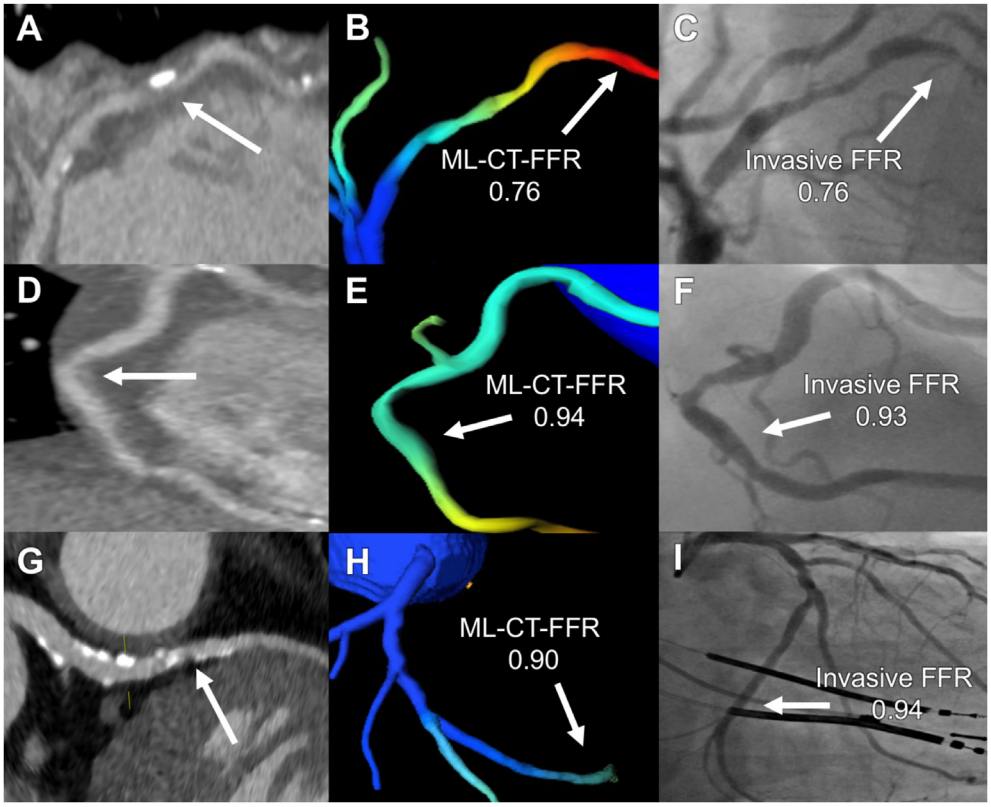

Fig. 3. Patient example with conventional cCTA (A) showing a severe (≥70%) stenosis of the LAD (arrow). ML-CT-FFR (B) resulted in a value of 0.76, denoting hemodynamic relevance and thereby reaching perfect agreement with the reference standard, invasive FFR (C). The cCTA (D) of the RCA shows a moderate (50–69%) stenosis in the middle segment (arrow). In this case, ML-CT-FFR (E) and invasive FFR (F) both resulted in a non-significant value. The cCTA (G) of a different patient shows a severe (≥70%) stenosis of the distal LCX (arrow), while ML-CT-FFR (H) and invasive FFR (I) demonstrated the stenosis to be not hemodynamically relevant.

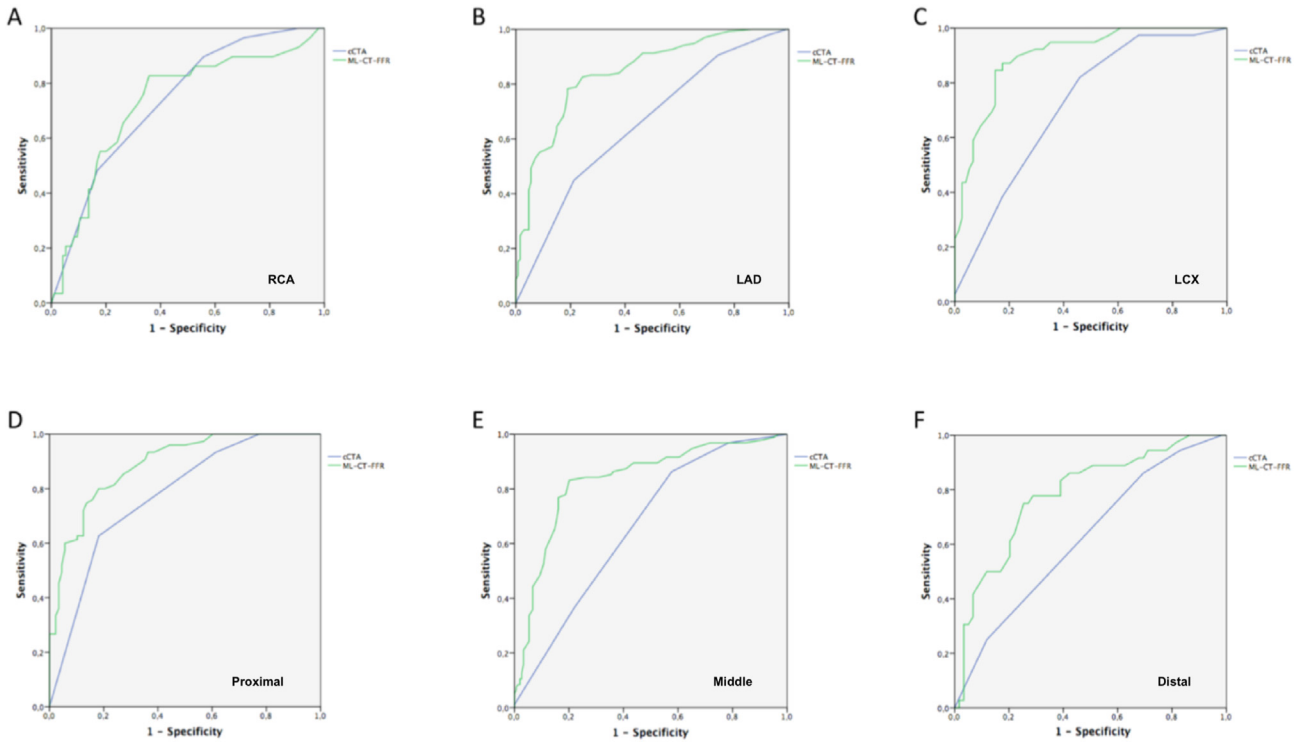

Fig. 4. Receiver operating characteristics curves displaying the diagnostic performance of conventional cCTA (blue) and ML-CT-FFR (green) for the main epicardial vessels RCA (A), LAD (B), LCX (C) as well as for the proximal (D), middle (E), and distal vessel segments (F). (For interpretation of the references to colour in this figure legend, the reader is referred to the Web version of this article.)

demonstrated a translesional CT-FFR gradient (ΔFFR_{CT}) to be superior in identifying and discriminating ischemia compared with regular CT-FFR and other measures.[17] However, this technique was not applied in our cohort of patients. As FFR and CT-FFR are both potentially affected by a cumulative loss of pressure, we did not observe any negative effects on our comparative analyses. As expected, ML-CT-FFR showed a significant correlation with invasive FFR, even in the distal coronary artery segments.

Although the clinical use of CT-FFR has recently been evaluated positively against cCTA in the triage-setting of patients with chest pain in an emergency department, the commercially available option for CT-FFR computation still requires image data transfer to external supercomputers and remains time consuming.[18] Further clinical application of this approach is therefore limited to date. For more rapid CT-FFR derivation, simplified on-site workstation-based prototype algorithms have been developed with promising results.[4,5] The approach of virtually instantaneous computation of FFR from cCTA used in the present investigation is yet another step towards clinical utility. Via recognition of subtle pattern combinations in large data amounts, transformation into readily available results is enabled by ML-CT-FFR and may be a future direction for noninvasive coronary imaging in daily practice. Previous substudies of the MACHINE registry did not show any constraints in the diagnostic performance of ML-CT-FFR by gender,[19] presence of diabetes,[20] or degree of coronary calcium.[21] Our results corroborate this trend and emphasize the diagnostic value of ML-CT-FFR for all stenosis locations.

This study has several limitations. First, selection and referral bias cannot be excluded for this registry-based research. Second, the location of stenoses within the coronary artery tree is not equally distributed in our study. Therefore, comparability of group sizes may be affected. However, this represents a real-world situation with patients referred for clinically indicated cCTA. Third, we did not compare ML-CT-FFR with other non-invasive methods. Further research is warranted to assess the diagnostic value of ML-CT-FFR against myocardial perfusion scintigraphy, stress magnetic resonance imaging, or stress echocardiography.

In conclusion, ML-CT-FFR correlated well with the invasive reference FFR and showed significantly improved diagnostic accuracy over cCTA for detecting hemodynamically relevant coronary artery stenosis regardless of location.

Declaration of competing interest

Dr. Renker has received speaker fees from Abbott. Dr. Baumann has received consulting fees from Phillips Volcano. Dr. Tesche has received research support and honoraria for speaking from Siemens. Dr. Kim received proctor/speaker fees from Abbott, Boston Scientific, Edwards Lifesciences, Medtronic, Meril. Dr. Nieman reports unrestricted institutional support from Siemens Healthineers, Bayer, GE, and Heartflow Inc., and consultancy honoraria from Siemens Medical Solutions USA. Dr. Persson reports on institutional support from Siemens Healthineers. Dr. Schoepf has received grants and/or personal fees from Bayer, Bracco, Elucid BioImaging, GE, Guerbet, HeartFlow Inc., Keya Medical, and Siemens. All other authors declare that they have no financial disclosures.

Appendix A. Supplementary data

Supplementary data to this article can be found online at https://doi.org/10.1016/j.jcct.2021.05.005.

References

1. Koo BK, Erglis A, Doh JH, et al. Diagnosis of ischemia-causing coronary stenoses by noninvasive fractional flow reserve computed from coronary computed tomographic angiograms. Results from the prospective multicenter DISCOVER-FLOW (Diagnosis of Ischemia-Causing Stenoses Obtained via Noninvasive Fractional Flow Reserve) study. *J Am Coll Cardiol.* 2011;58(19):1989–1997.
2. Min JK, Leipsic J, Pencina MJ, et al. Diagnostic accuracy of fractional flow reserve from anatomic CT angiography. *J Am Med Assoc.* 2012;308(12):1237–1245.
3. Norgaard BL, Leipsic J, Gaur S, et al. Diagnostic performance of noninvasive fractional flow reserve derived from coronary computed tomography angiography in

suspected coronary artery disease: the NXT trial (Analysis of Coronary Blood Flow Using CT Angiography: next Steps). *J Am Coll Cardiol*. 2014;63(12):1145–1155.
4. Coenen A, Lubbers MM, Kurata A, et al. Fractional flow reserve computed from noninvasive CT angiography data: diagnostic performance of an on-site clinician-operated computational fluid dynamics algorithm. *Radiology*. 2015;274(3):674–683.
5. Renker M, Schoepf UJ, Wang R, et al. Comparison of diagnostic value of a novel noninvasive coronary computed tomography angiography method versus standard coronary angiography for assessing fractional flow reserve. *Am J Cardiol*. 2014;114(9):1303–1308.
6. Itu L, Rapaka S, Passerini T, et al. A machine-learning approach for computation of fractional flow reserve from coronary computed tomography. *J Appl Physiol*. 1985;121(1):42–52, 2016.
7. Coenen A, Kim YH, Kruk M, et al. Diagnostic accuracy of a machine-learning approach to coronary computed tomographic angiography-based fractional flow reserve: result from the MACHINE consortium. *Circ Cardiovasc Imaging*. 2018;11(6), e007217.
8. Cury RC, Abbara S, Achenbach S, et al. CAD-RADS(TM) coronary artery disease - reporting and data system. An expert consensus document of the society of cardiovascular computed tomography (SCCT), the American college of radiology (ACR) and the north American society for cardiovascular imaging (NASCI). Endorsed by the American college of cardiology. *J Cardiovasc Comput Tomogr*. 2016;10(4):269–281.
9. Coenen A, Lubbers MM, Kurata A, et al. Coronary CT angiography derived fractional flow reserve: methodology and evaluation of a point of care algorithm. *J Cardiovasc Comput Tomogr*. 2016;10(2):105–113.
10. Austen WG, Edwards JE, Frye RL, et al. A reporting system on patients evaluated for coronary artery disease. Report of the ad hoc committee for grading of coronary artery disease, council on cardiovascular surgery, American heart association. *Circulation*. 1975;51(4 Suppl):5–40.
11. DeLong ER, DeLong DM, Clarke-Pearson DL. Comparing the areas under two or more correlated receiver operating characteristic curves: a nonparametric approach. *Biometrics*. 1988;44(3):837–845.
12. Ferencik M, Nomura CH, Maurovich-Horvat P, et al. Quantitative parameters of image quality in 64-slice computed tomography angiography of the coronary arteries. *Eur J Radiol*. 2006;57(3):373–379.
13. Kang D, Slomka PJ, Nakazato R, et al. Automated knowledge-based detection of nonobstructive and obstructive arterial lesions from coronary CT angiography. *Med Phys*. 2013;40(4), 041912.
14. de Graaf MA, Broersen A, Ahmed W, et al. Feasibility of an automated quantitative computed tomography angiography-derived risk score for risk stratification of patients with suspected coronary artery disease. *Am J Cardiol*. 2014;113(12):1947–1955.
15. Yan RT, Miller JM, Rochitte CE, et al. Predictors of inaccurate coronary arterial stenosis assessment by CT angiography. *JACC Cardiovasc Imaging*. 2013;6(9):963–972.
16. Cami E, Tagami T, Raff G, et al. Assessment of lesion-specific ischemia using fractional flow reserve (FFR) profiles derived from coronary computed tomography angiography (FFRCT) and invasive pressure measurements (FFRINV): importance of the site of measurement and implications for patient referral for invasive coronary angiography and percutaneous coronary intervention. *J Cardiovasc Comput Tomogr*. 2018;12(6):480–492.
17. Takagi H, Ishikawa Y, Orii M, et al. Optimized interpretation of fractional flow reserve derived from computed tomography: comparison of three interpretation methods. *J Cardiovasc Comput Tomogr*. 2019;13(2):134–141.
18. Chinnaiyan KM, Safian RD, Gallagher ML, et al. Clinical use of CT-derived fractional flow reserve in the emergency department. *JACC Cardiovasc Imaging*. 2020;13(2 Pt 1):452–461.
19. Baumann S, Renker M, Schoepf UJ, et al. Gender differences in the diagnostic performance of machine learning coronary CT angiography-derived fractional flow reserve -results from the MACHINE registry. *Eur J Radiol*. 2019;119, 108657.
20. Nous FMA, Coenen A, Boersma E, et al. Comparison of the diagnostic performance of coronary computed tomography angiography-derived fractional flow reserve in patients with versus without diabetes mellitus (from the MACHINE consortium). *Am J Cardiol*. 2019;123(4):537–543.
21. Tesche C, Otani K, De Cecco CN, et al. Influence of coronary calcium on diagnostic performance of machine learning CT-FFR: results from MACHINE registry. *JACC Cardiovasc Imaging*. 2020;13(3):760–770.